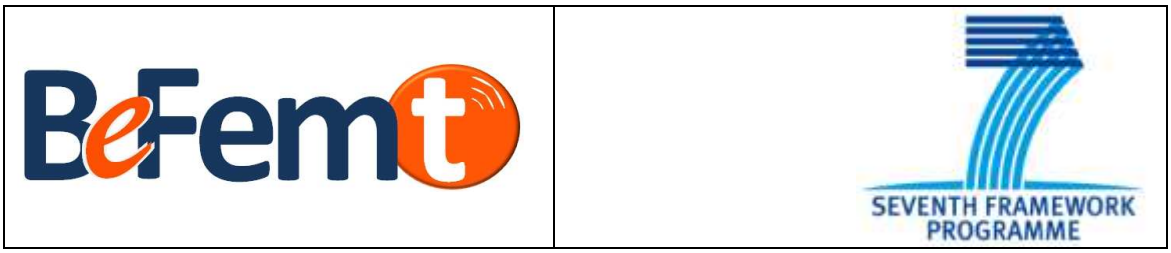

INFSO-ICT-248523 BeFEMTO

D4.4

Integrated SON Techniques For Femtocells Radio Access

Contractual Date of Delivery to the CEC:	M30
Actual Date of Delivery to the CEC:	M30
Author(s):	Sylvie Mayrargue, Antonio de Domenico, Emilio Calvanese Strinati, Ana Galindo Serrano, Lorenza Giupponi, Mischa Dohler, Serkan Uygungelen, Zubin Bharucha, Dimity Marandin, Stefan Brueck, Andrea Garavaglia, Masood Maqbool, Massinissa Lalam, Carmen Palacios, Mariano Lopez, Atta ul Quddus, Youngwook Ko, Ali Imran, Mehrdad Shariat, Mehdi Bennis, Hari Pennanen, Carlos H.Lima, Francesco Pantisano
Participant(s):	*CEA, CTTC, DOCOMO, MIMOON, QC, SCET, TTI, UNIS, UOULU*
Workpackage:	WP4 (Self-Organizing Radio Access for Networked, Mobile and Fixed Relay Femtocells)
Estimated person months:	*42*
Security:	**PU**
Nature:	**R**
Version:	FINAL
Total number of pages:	138

Abstract: The focus of BeFEMTO WP4 "Self-Organising Radio Access for Networked, Mobile and Fixed Relay Femtocells" is on Self-Organized Networks (SON). This is the final deliverable covering and positioning all the work performed within WP4 since the beginning of the project. This deliverable summarizes work which has already been presented in greater detail in prior deliverables D4.1, D4.2 and D4.3; and also contains entirely novel contributions which have not been documented to date. The emphasis of this deliverable is to present an overarching vision of WP4 SON's contribution to the academic and industrial landscape at large. To this end, we present the SON enablers and a large plethora of local, distributed and central SON approaches. We position it w.r.t. BeFEMTO's challenges and performance targets. The developed SON framework is understood to have made a significant step forward for facilitating large scale networked femtocell rollouts. Latest standardisation activities also indicate that said work has and will have a significant impact onto the standardisation landscape, notably 3GPP.

Keyword List: femtocells, SON, interference management, architecture, X2 interface, distributed, centralised, localised, RRM, energy saving, 3GPP, NGMN

Executive Summary

The focus of BeFEMTO WP4 "Self-Organising Radio Access for Networked, Mobile and Fixed Relay Femtocells" is on Self-Organized Networks (SON). This is the final deliverable covering and positioning all the work performed within WP4 since the beginning of the project. Part of this work has already been presented in D4.1 [34], D4.2 [16] and D4.3 [40] but it also contains entirely novel contributions which have not been documented to date. The emphasis of this deliverable is to present an overarching vision of WP4's contribution to the academic and industrial SON landscape at large.

SON is mandated by the expected high number and density of femtocells and their unplanned deployment, in order to keep deployment and management costs low. Self-optimization of the radio access allows reduction of interference, optimization of radio resource allocation and reduction of energy requirements, while at the same time minimizing the complexity of network management. This deliverable thus pays particular emphasis to these elements and coherently presents WP4's SON vision and contributions, which are summarized in the following paragraphs.

The industry community's and BeFEMTO's SON vision as well as WP4's positioning w.r.t said visions is dealt with in Section 2. First, the SON concept as defined by 3GPP and NGMN is recalled; then, the BeFEMTO architecture for SON introduced in [68] is described. BeFEMTO's innovative algorithms are mapped onto this architecture, including an exposure on SON enablers and SON sub-functions. Following NGMN/3GPP terminology, the SON algorithms in WP4 have been classified according to "*local algorithms*", "*distributed algorithms between eNBs and HeNBs*", "*distributed algorithms between HeNBs*", and "*centralized algorithms*" [2], [10]. The "local" category does not require an air interface coordination; the two "distributed" categories make use of an interface for exchanging information between BSs, extending the role of the X2 interface, as defined in 3GPP LTE Release 10; and the "centralized" category makes use of another BeFEMTO architecture innovation: the Local Femto Gateway (LFGW) which enables powerful interference management schemes for networked femto-cells

The SON enablers and their functional characteristics are detailed in Section 3. More specifically, Section 3 describes the previously introduced femto-cell automatic location determination, automatic coverage estimation, biologically inspired network synchronization, RF front-end functionalities for self-optimization such as power control, and Network Listen Module (NLM) enablers, which are revised to facilitate a complete picture of the SON work conducted within WP4.

The localised, distributed and centralised SON algorithms are then detailed in Section 4. Most of these SON methods address the issue of intercell interference coordination (ICIC) in femtocell networks, where the aggressors usually are the small cells and the victims are the macro user equipments (MUEs). Some methods also address co-tier interference between femto-cells and femto-cell users. The following SON algorithms classification has been used, which is also in-line with 3GPP notation:

- In Section 4.1, **local** algorithms are proposed. Several algorithms deal with automatic coverage control, and another one inspired from reinforcement learning (RL) addresses the problem of cross-tier ICIC in femtocell networks.
- Section 4.2 describes the BeFEMTO **distributed** algorithms with coordination between HeNBs and eNBs via an extended X2 interface. They addresses mainly cross tier interference as well as interference originating from relays, fixed or mobile femtos considered as small cells.

  Section 4.3 describes BeFEMTO **distributed** algorithms with coordination between HeNBs via an X2 interface.

- Section 4.4 describes the **centralized** algorithms.

The SON framework developed in BeFEMTO has made a significant step forward for facilitating large scale networked femtocell rollouts. Latest standardisation activities also indicate that said work has and will have a significant impact onto the standardisation landscape, in particular onto 3GPP.

Authors

Partner	Name	Phone / Fax / e-mail
CEA		
	Antonio de Domenico	Phone: +33 4 38 78 18 17
		e-mail: antonio.de-domenico@cea.fr
	Emilio Calvanese Strinati	Phone: +33 4 38 78 17 34
		e-mail: emilio.calvanese-strinati@cea.fr
	Sylvie Mayrargue	Phone: +33 4 38 78 62 42
		e-mail: sylvie.mayrargue@cea.fr
CTTC		
	Ana Galindo	e-mail: amgalindo@cttc.es
	Lorenza Giupponi	e-mail: lgiupponi@cttc.es
	Mischa Dohler	Phone: +34 679 094 *007*
		e-mail: mischa.dohler@cttc.es
DOCOMO		
	Serkan Uygungelen	Phone: +49 89 56824 226
		e-mail: uygungelen@docomolab-euro.com
	Zubin Bharucha	Phone: +49 89 56824 231
		e-mail: bharucha@docomolab-euro.com
mimoOn		
	Dimitry Marandin	e-mail: dimitri.marandin@mimoon.de
Sagemcom Energy & Telecom		
	Masood Maqbool	Phone: +33 1 57 61 13 63
		e-mail: masood.maqbool@sagemcom.com
	Massinissa Lalam	Phone: +33 1 57 61 13 41
		e-mail: massinissa.lalam@sagemcom.com
Qualcomm		
	Stefan Brueck	Phone: +49 911 54013-270
		e-mail: sbrueck@qualcomm.com
	Andrea Garavaglia	Phone: +49 911 54013-530
		e-mail: andreag@qualcomm.com
TTI		
	Mariano López	Phone: +34 942291212
		e-mail: mlopez@ttinorte.es
	Carmen Palacios	Phone: +34 942291212
		e-mail: mcpalacios@ttinorte.es
University of Surrey		
	Atta ul Quddus	Phone: +44 1483 683787
		e-mail: a.quddus@surrey.ac.uk
	Youngwook Ko	Phone: +44 1483 683883
		e-mail: y.ko@surrey.ac.uk
	Mehrdad Shariat	e-mail: m.shariat@surrey.ac.uk

UOulu		
	Mehdi Bennis	Phone: +358 40 8241 742 e-mail: bennis@ee.oulu.fi
	Harri Pennanen	Phone: +358408241742 e-mail: hpenna@ee.oulu.fi
	Carlos H. Lima	Phone: +358 40 7489 5974 e-mail: carlosl@ee.oulu.fi
	Francesco Pantisano	Phone: +358408241742 e-mail: fpantisano@ee.oulu.fi

Table of Content

List of Acronyms and Abbreviations

Acronym	Meaning
3GPP	3rd Generation Partnership Project
ABE	Automatic Boundary Estimation
AGC	Automatic Gain Control
AM	Amplitude Modulation
AMMP	Active Macro Mobile Protection
AP	Access Point
AWGN	Additive White Gaussian Noise
BSCBS	Base Station Coordinated Beam Selection
BB	Baseband
BCH	Broadcast Channel
BER	Bit Error Rate
BS	Base Station
BW	BandWidth
CA	Carrier Aggregation
CCRS	Coordinated and Cooperative Relay System
CCDF	Complementary Cumulative Distribution Function
CDF	Cumulative Distribution Function
CQI	Channel Quality Indicator
CRS	Cell-specific reference signals
CSG	Closed Subscriber Group
DAS	Distributed Antenna System
DASA	Dynamic and Autonomous Subband Assignment
DeNB	Donor eNB
DF	Decode and Forward
DL	Downlink
DM	Device Management
eGB DFR	Extended Graph-Based Dynamic Frequency Reuse
EGT	Evolutionary Game Theory
EM	Edge Matrix
eNB	Extended Node B
EPS	Evolved Packet System
EVM	Error Vector Magnitude
FBS	Femto Base Station
FDD	Frequency Division Duplex
FFR	Fractional Frequency Reuse
FUE	Femtocell User Equipment
GB DFR	Graph-Based Dynamic Frequency Reuse
GNSS	Global Navigation Satellite System
GW	Gateway
HeMS	HeNB Management System
HeNB	Home eNB
HetNet	Heterogeneous Network
HPA	High Power Amplifier
ICI	Intercell Interference
ICIC	Intercell Interference Control
IE	Interpolation Error
ISR	Interference to Signal Ratio
JFI	Jain Fairness Index
KPI	Key Performance Indicator
LTE	Long-Term Evolution
LFGW	Local Femto Gateway
LIPA	Local IP Access
LMA	Local Mobility Anchor
LOS	Line-Of-Sight
LP	Linear Programming

MAG	Mobile Access Gateway
MART	Mobile Assisted Range Tuning
MUE	Macrocell User Equipment
MBS	Macrocell Base Station
MCS	Modulation and Coding Scheme
MIMO	Multiple Input Multiple Output
ML	Machine Learning
MME	Mobility Management Entity
MRN	Mobile Relay Network/ Mobile Relay Node
NL	Network Listen
NM	Network Management
NMM	Network Monitor Module
OFDMA	Orthogonal Frequency Division Multiple Access
OFR	Outdoor Fixed Relay femtocells
OP	Optimisation Problem
OpAmp	Operational Amplifier
OTA	Over the Air
PA	Power Amplifier
PC	Power Control
PDN	Packet Data Network
PF	Proportionally Fair
PFBS	Power of Femto Base Station
PGW	PDN Gateway
PM	Perturbation Matrix
PMI	Precoding Matrix Indicator
PMIP	Proxy Mobile IP
POMDP	Partially Observable Markov Decision Process
PRB	Physical Resource Block
PRS	Positioning Reference Signals
PS	Power Setting, Primary Subband
PSAP	Public-Safety Answering Point
QAM	Quadrature Amplitude Modulation
QoS	Quality of Service
QPSK	Quadrature Phase Shift Keying
RACE	RSRP-based Autonomous Coverage Estimation
RB	Resource Block
REM	Radio Environment Measurement/ Radio Environment Map
RI	Rank Indicator
RF	Radio Frequency
RL	Reinforcement Learning
RNTP	Relative Narrow-band Transmit Power
RR	Restriction Request
RRM	Radio Resource Management
RSRP	Reference Signal Received Power
RSRQ	Reference Signal Received Quality
RSSI	Received Signal Strength Indicator
RTT	Round-Trip Time
SE	Spectral Efficiency
SGW	Serving Gateway
SIC	Successive Interference Cancellation
SINR	Signal to Interference plus Noise Ratio
SIPTO	Selected IP Traffic Offload
SO	Self Organized
SON	Self-Organising Network
SOR	Successive Over-Relaxation
SO-RRIM	Self-Organising Radio Resource and Interference Management
SS	Secondary Subband
TDOA	Time Difference-Of-Arrival
TO BSOF	Tilt Optimization through bio-mimetic SO Framework

TOA	Time-Of-Arrival
Tx	Transmitter
UAA	Uplink Adaptive Attenuation
UE	User Equipment
UL	Uplink
VCA	Voltage Controlled Amplifier
VMUE	Virtual MUE
WSN	Wireless sensor networks

1. Introduction

This final deliverable introduces the latest technical contributions to the SON framework and also positions BeFEMTO WP4's work w.r.t. other cutting-edge SON developments. The most promising component and scenario agnostic developments related to advanced RRM schemes and self-organised and self-optimised femto solutions are described here, in order to offer the community a viable and complete self-organised technology suite. It includes integrated and optimised SON techniques for networked, mobile and fixed relay femtos. In the following sections, we summarize the overall BeFEMTO philosophy and how WP4's SON developments contribute to meeting the project's milestones and performance criteria.

1.1 Meeting BeFEMTO's WP4 Vision & Goals

The core motivation of the BeFEMTO project is to pursue investigation into development and optimisation of *indoor* and *outdoor* broadband femtocell technologies. The designed femtocell technologies have to be **autonomously self-managing** and provide **open and shared access**. As illustrated in Figure 1-1, BeFEMTO's WP4 vision comprises three major themes, i.e. indoor networked femtocells, outdoor fixed relay femtocell and outdoor mobile femtocell. All these themes are considered in this document.

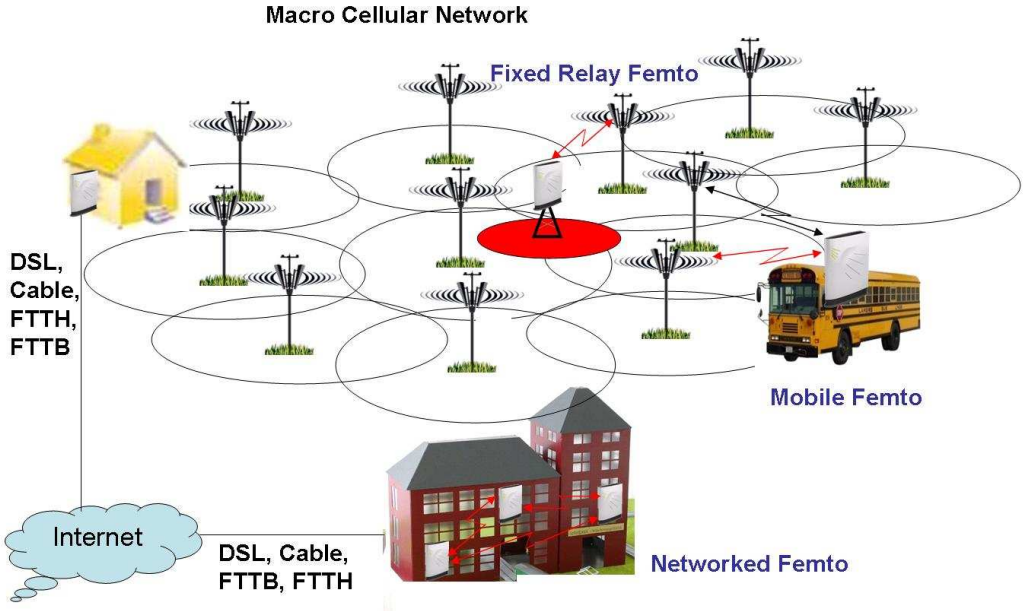

Figure 1-1: BeFEMTO WP4's vision of broadband evolved femtocells.

With the **indoor networked femtocells,** BeFEMTO WP4 investigated advanced cooperative schemes between femtocells installed in buildings such as hospitals, offices or shopping malls. This approach has gone far beyond any state-of-art femto technology and offers new service provisioning for home, office and enterprise environments, and, consequently, new market and business opportunities for service providers. From a technical perspective, networked femtocells require novel concepts and algorithms with special focus on resource and interference management, network synchronization, and architectural design facilitating a tight integration into macro and other infrastructure networks. The networks of femtocells could be formed by wired or wireless connections.

Mobile & relay outdoor femtocells are also novel and they provide broadband connectivity to people outdoors, walking or on the move using e.g. public transports. Consequently, we have to cope with a wireless backhaul link as opposed to the wireline link used for fixed or indoor stand-alone femto nodes. Moreover, moving and relay femtocells have to be tightly integrated into an overall heterogeneous network deployment without jeopardizing macro network capacity and quality. This again requires to pay special attention for instance to radio resource management, interference management, group-handover and admission control techniques.

From a technical point of view, the goal has been to achieve a high **system spectral efficiency of at least 8bps/Hz/cell** (at a certain outage level) and a **maximum mean transmit power of less than 10mW for indoors femtos**. Figure 1-2 illustrates these objectives in comparison to GSM and UMTS/LTE-based cellular systems where spectral efficiency and base station output power values have been taken from [21][85][86][87][88]. Furthermore, we have added an indicative range where most BeFEMTO WP4 contributions position themselves. The majority of SON algorithms which are introduced and/or reviewed in this document, clearly meet the requirements. All contributions strictly respect the power cap of 10dBm and – for those where a spectral efficiency translation and appropriate performance scaling has been possible – meet the target of 8bps/Hz/cell at given outage levels.

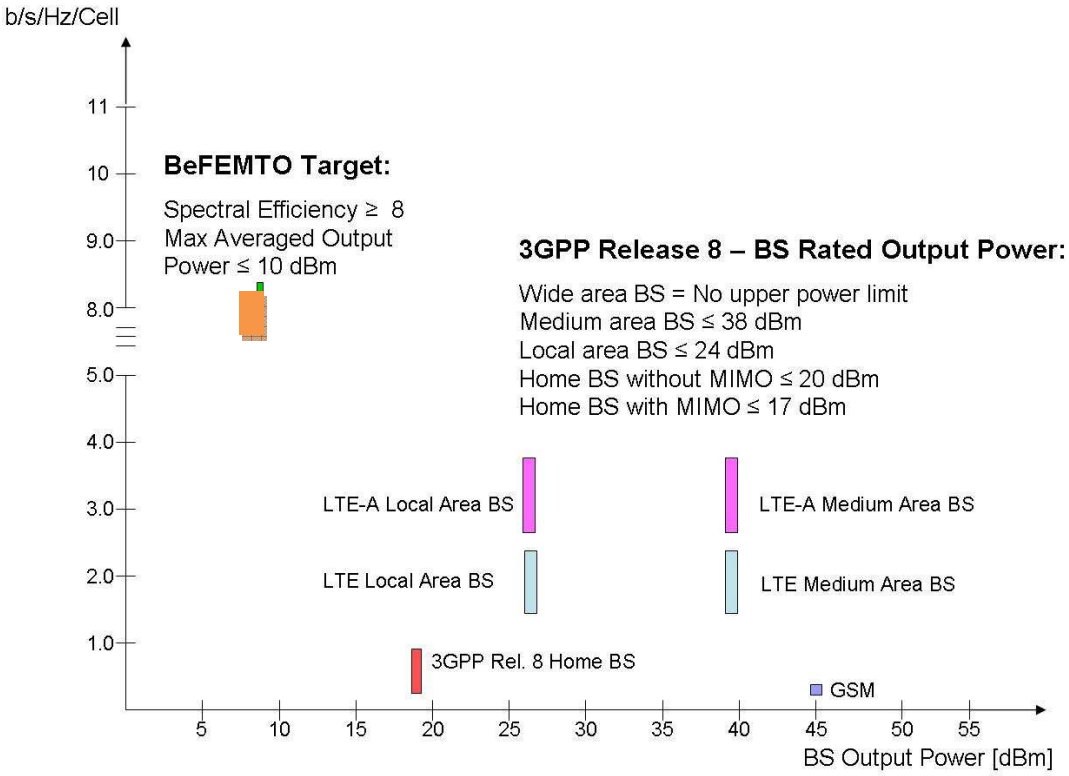

Figure 1-2: Illustration of BeFEMTO's targets in relation to 3GPP based cellular systems, as well as the finally achieved efficiency of the example SON contribution of RL-SON.

1.2 Meeting BeFEMTO's WP4 Objectives & Challenges

To achieve the project's vision and goals, the following objectives have been successfully addressed over the project duration:

- **O4.1:** Development of new algorithms to allow for accurate real-time estimation of geographic location of femtocells and autonomous coverage estimation for all the scenarios – successfully accomplished.
- **O4.2:** Development of radio context aware learning mechanisms, in centralized and decentralized fashion, and of network synchronization schemes, together with evaluation of implications on system stability and on the time-scales of different parameters involved in self-organisation – successfully accomplished.
- **O4.3:** Research on novel RRM solutions (interference management, resource allocation, scheduling, handover, admission control, flow control) tailored to the emerging paradigm of networked femtocells – successfully accomplished (except for flow control which has not directly been dealt with).
- **O4.4:** Enable integrated self-optimisation of radio access schemes and parameters taking into account the required signalling on the control plane as well as the associated energy requirements – successfully accomplished.
- **O4.5:** Adaptation and further improvement of above algorithms to the needs of fixed relay and mobile femtocells – successfully accomplished.

To meet these objectives, the following challenges have been dealt with:

- **Interference Management.** Assume that femto nodes operate in the same frequency band as overlay networks such as macro or micro nodes. Then, a major challenge is to cope with the caused mutual interference. This is a serious problem because femtocells are likely to be rolled out in an unplanned manner, and, hence, without pre-determined network layout. In order to ensure a successful future deployment of femtocells, no matter which theme is considered, efficient interference management by coordination between femto and overlay systems with less control signalling overhead is of utmost importance. In this context, self-organizing and self-optimizing concepts play a significant role aiming for an easy and fast network deployment and operation. BeFEMTO envisages indoor positioning schemes and femtocell coverage estimation techniques as well as other related information to be incorporated in self-optimisation algorithms to improve performance and, more importantly, stability of operation. By further including flexible transceiver technologies with interference cancellation properties and coordinated multi-point technologies into a cross-layer interference management, BeFEMTO envisages a high scalability and flexibility to handle efficiently wireless signals with very diverse Quality of Service (QoS) requirements in order to meet the high spectrum efficiency target of 8bps/Hz/cell (at a given outage level).
- **Link and Access Management.** Handover, admission control and, resource management algorithms such as load balancing and flow control have to be designed to allow for a tight interworking of femto nodes with overlay systems. Especially the flat architecture of 3GPP LTE/LTE-A mandates the implementation of distributed management concepts, e.g. across femto and macro nodes, and it is a challenge to come up with optimal solutions requiring less control signalling effort whilst meeting power efficiency, high and diverse QoS constraints, as well as the different time-variant channel conditions.
- **Dynamic Bandwidth Allocation and Sharing.** Multi-operator band sharing for indoor standalone femtocells is a challenging task to be addressed as an approach to allow for efficient macro-femto coexistence and enhance capacity. For instance, a flexible allocation of a user being served by a femto node which supports frequency bands in a multi-operator shared fashion allows for assigning the user to the band that jeopardizes macro network transmissions at a minimum. This also includes handling backhaul (aggregated traffic) and user-specific signals simultaneously in case of fixed/mobile relay femto nodes and networked femtocells, but also takes into account the broader scope of jointly managing non-adjacent frequency bands allocated to mobile communication systems by regulatory bodies.

A further tabulated summary of above challenges w.r.t. the SON algorithms exposed in this document, is given in the conclusion of Section 5.

1.3 Organization of D4.4

The remainder of the document is organized as follows.

The industry community's and BeFEMTO's SON vision as well as WP4's positioning w.r.t said visions is dealt with in Section 2. First, the SON concept as defined by 3GPP and NGMN is recalled; then, the BeFEMTO architecture for SON [68] is described. BeFEMTO's innovative algorithms are mapped onto this architecture, including a distinction between SON enablers and SON sub-functions. Following NGMN/3GPP terminology, the SON algorithms in WP4 have been classified according to "*local algorithms*", "*distributed algorithms between eNBs and HeNBs*", "*distributed algorithms between HeNBs*", and "*centralized algorithms*" [2], [10]. The "local" category does not require an air interface coordination; the two "distributed" categories make use of an interface for exchanging information between BSs, extending the role of the X2 interface, as defined in 3GPP LTE Release 10; and the "centralized" category makes use of another BeFEMTO architecture innovation: the Local Femto Gateway, which enables powerful interference management schemes for networked femto-cells

Section 3 details SON enablers and their functional characteristics. Notably, the previously introduced femto-cell automatic location determination, automatic coverage estimation, biologically inspired network synchronization, RF front-end functionalities for self-optimization such as power control, and Network Listen Module enablers are revised to facilitate a complete picture of the SON work conducted within WP4.

The localised, distributed and centralised SON algorithms are then detailed in Section 4. Most of these algorithmic SON methods address the issue of intercell interference coordination (ICIC) in femtocell networks, the aggressors generally being the small cells and the victims the macro user equipments (MUEs); some methods also address co-tier interference, between femto-cells and femto-cell users. In what follows is a more detailed description of the different SON algorithms according to their classification.

- In Section 4.1, **local** algorithms are proposed. Several algorithms deal with automatic coverage control, and another one inspired from reinforcement learning (RL) addresses the problem of cross-tier ICIC in femtocell networks.

- Section 4.2 describes the BeFEMTO **distributed** algorithms, with coordination between HeNBs and eNBs, via an extended X2 interface. It addresses mainly cross tier interference, and also the specific issue of relays, fixed or mobile femtos viewed as small cells.
  Notably, Section 4.2.1 presents a coordinated beam selection scheme: a victim MUE sends its serving cell a request to be forwarded over X2 to an interfering HeNB, asking it not to use a certain precoding matrix, thus reducing its interference level. The same scheme can actually be also used in a cross tier scenario. In section 4.2.2, cell edge MUEs leverage on the neighbouring small cells, establishing a device-to-device connection whereby MUEs forward their traffic to the FUEs. In return for its cooperation, each macrocell user grants the FUE a fraction of its super-frame as a reward mechanism. Section 4.2.3 presents a cross-tier ICIC based on a learning approach. Femtocells first independently learn a policy which allows them to control their interference at potentially close MUEs. Since the learning task takes time, as a second step femtocells can take advantage of the policies already learnt by other more expert nodes (docitive approach). Femtocells rely on some information from the macrocell system; assumed to be conveyed over X2: In a scenario where an Outdoor Fixed Relay (OFR) is interfered by neighbouring macro cells, it is shown in Section 4.2.4 that a SO optimization of eNB antennas tilt leads to a Spectral Efficiency enhancement of the OFR access link. Section 4.2.5 deals with the issue of heterogeneous (wired/wireless) backhaul capacity, in which backhaul-aware cell selection is of utmost importance, through which UEs autonomously associate to the best cell taking account both access and backhaul links. LTE Rel-10 is focusing on fixed relays, while advanced relay scenarios like high speed train can become quite popular. Thus, a mobile relay architecture is first defined, enhancing that of LTE Rel 10 (Section 4.2.6, and a contribution on cooperative moving relays, coping with a limited capacity backhaul, is presented in Section 4.2.7).

- Section 4.3 describes BeFEMTO **distributed** algorithms, with coordination between HeNBs via an X2 interface.
  Notably, in Section 4.3.1, it is shown that femtocells can converge much faster to the optimal network operating point, at the cost of exchanging information with neighbouring femtocells. This is done through the X2 interface. In both replication by dynamics and fictitious play procedures, there is a need for an X2 interface within the femtocell tier, in addition to an X2 interface to gauge the interference caused on the macrocell tier. In Section 4.3.2, dealing with TDD mode, a downlink beamformer design is proposed for minimizing the total transmitted power of HeNBs subject to fixed cross-tier interference constraints and femto-UE specific SINR constraints. A limited backhaul information exchange is needed between HeNBs which can take place over X2 interface. In Section 4.3.3, co tier interference is managed by a novel dynamic and autonomous subband assignment method based on a modified graph colouring algorithm. HeNBs send measurements from their users to the interfering neighbours by an indicator on an X2 interface. Section 4.3.4 is focused on a new collaborative power usage among the femtocell users that aims at enhancing the energy efficiency of the SON operation in a distributed manner. Unlike conventional schemes addressing only the power usage for the data, power usage for the channel information feedbacks has been also taken into account. For this achievable benefit, the X2 interface between femtocells is used. Section 4.3.5 considers a two–tier co–channel femtocells network, where each femtocell shares the radio spectrum with the overlaid macrocell. Given an orthogonal channel deployment between femtocells, achievable by low signalling over the X2 interface, a new distributed method for admission control and radio resource scheduling (RSS) that aims at enhancing the ergodic sum capacity on the uplink of the femtocells is proposed. The key of the method is that it takes into account the energy usage for both the signalling and the data transmission. The solution for the aggregated interference problem from femtocells to macrocells introduced in Section 4.3.6, is based on a learning approach. A completely autonomous solution based on Partially Observable Markov Decision Process (POMDP) is proposed, where femtocells estimate their impact in the macro user through interpolation techniques.

- Section 4.4 describes the **centralized** algorithms.
  Notably, in Section 4.4.1, a centralized co tier interference mitigation algorithm is presented. Similar to Section 4.3.3, HeNBs define its interfering neighbours with the help of the measurement reports from the users. Here, a central controller, (LFGW) collects the measurements. Then, the controller assigns subbands by using a modified graph colouring algorithm. In order to protect primary subbands, HeNBs send the assignment information to the interfering neighbours via an X2 interface. Section 4.4.2 proposes a novel graph-based multi-cell scheduling framework to efficiently mitigate downlink inter-cell interference in small cell OFDMA networks. This framework incorporates adaptive graph-partitioning and utility optimization concepts to address inter-cell interference in two phases: both phases rely on sharing the channel state information in centralized manner via a Local femto Gateway (LFGW). Section 4.4.3 presents a comparison between two interference mitigation algorithms, based on the concept of "Ghost" femtocells. "Ghost" is a resource allocation paradigm that takes advantage of the large amount of available spectrum vs. the low number of users in a femto cell. It is both a co-tier interference and a cross-tier interference scheme. For standalone femtos, HeNBs selfishly attempt to maximize the spectrum reuse. In networked femtos, first a distributed method for estimating how neighbouring HeNBs affect each other transmission reliability is introduced. Then, the LFGW uses this information to locally coordinate the access of neighbouring femtocells and manage the frequency reuse amongst nearby HeNBs. A distributed version of $Ghost_{NF}$, where signalling and computation costs are shared amongst neighbouring HeNBs over the X2 interface is made feasible. However, this solution results in higher overhead and latency. In Section 4.4.4, a HetNet-based centralized power setting algorithm for femtocell clusters is introduced, which makes use of a linear programming framework. The method exploits the LFGW, which coordinates co-located femtocell measurements/actions and perform the linear programming resolution. An iterative distributed implementation is also possible. This algorithm encompasses the possibility to automatically switch-off the most disturbing femtocells under SON operation.

In summary, the SON framework developed in BeFEMTO has made a significant step forward for facilitating large scale networked femtocell rollouts. Latest standardisation activities also indicate that said work has and will have a significant impact onto the standardisation landscape, notably 3GPP.

2. Classification of SON Algorithms

This section is dedicated to a sufficiently detailed classification of SON algorithms. It commences with a review of the SON architecture in general as well as BeFEMTO's elaboration thereupon. We then summarize the current status of SON developments, mainly in NGMN and 3GPP, and assess the impact BeFEMTO (notably WP4) has on said standards bodies.

2.1 SON Taxonomy and Architecture

2.1.1 3GPP & NGMN SON Taxonomy

Self-organizing networks (SON) refer to an operational principle in which various elements of a network configure and adapt themselves to meet given operating conditions. SON is carving out an important operational niche in two directions: First, it is automating what used to be purely manual processes, where it aims to reduce manual intervention for deployment savings and automate repetitive processes. Typical examples are automatic planning & self-configuration. Second, it is able to execute actions which were previously too fast or too complex to be handled by a human. The aim is to improve run-time operation based on real-time data and automate optimization of critical network elements. Typical examples are self-optimization & self-healing.

SON is clearly within the realm of automation, however, is not new but rather a further evolution of previous automation efforts. It is based on the following important elements: "autonomous", "distributed", "intelligent/cognitive" and "optimality". Hence, SON approaches may differ substantially and network engineering should be striving for a (close to) optimal solution. The important constituents of a SON cycle are depicted in the figure below, where we can clearly distinguish elements of automated planning, self configuration, self optimization and self healing.

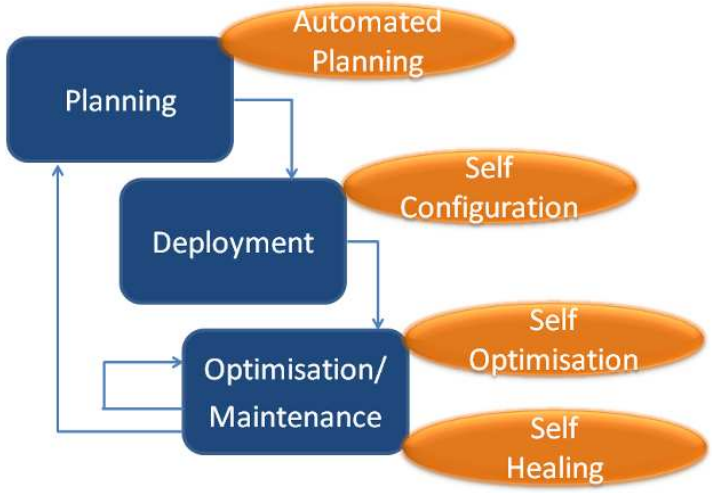

Figure 2-1: SON functional overview, composed of automated planning, configuration, optimization and healing.

As per NGNM and 3GPP, SON has the following levels of execution:

- **localised**: autonomous SON execution based on purely local information at (H)eNB & UE;
- **distributed**: autonomous SON execution based on information exchanged with neighbouring (H)eNB (eg via X2 interface);
- **centralized**: decision taking based on (fairly complete) system information (eg at NM/DM levels); and
- *hybrid*: any mixture of above.

The different execution levels are visually depicted in Figure 2-2, where the left figure shows them from a management point of view and the right one from an operational point of view.

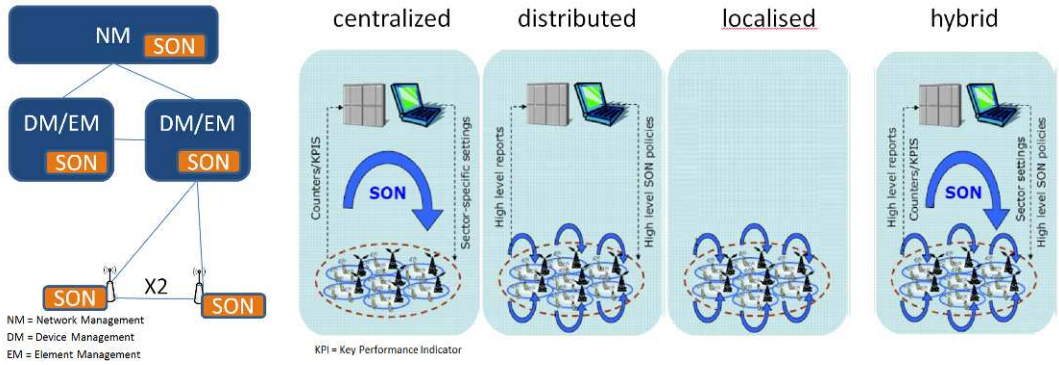

Figure 2-2: Different SON execution levels: management point of view (left) and operational point of view (right).

A Key Performance Indicator (KPI) for centralized SON algorithms is the timing, in 3GPP language referred to as collection interval. The following cases can be distinguished:

- **Collection Interval:** time period during which statistics and data are collected, which is limited by vendor's OAM bandwidth; typical 5min (i.e. not at scheduling level!)
- **Analysis Interval:** time period needed to draw decision; typically several collection intervals (filtering effect by considering also prior data history)
- **Change Interval:** time period between executing the changes in the network; typically limited by system's operational constraints

Centralized, distributed and localized approaches trade important performance indicators. For instance, a centralized approach requires an enormous amount of information to be exchanged and is very prone to "single point of failure". Therefore, it is typically only used for trans-network issues, such as self-configuration, global load balancing, etc. On the other end of the spectrum, there is the localized approach which only takes and acts upon local information and is thus very fast. It is typically used for schedulers. In between both, there is the distributed approach, where information exchange is only with neighbouring stations. This approach trades both centralized and purely localized approaches and is often used for local load balancing. This is depicted in Figure 2-3.

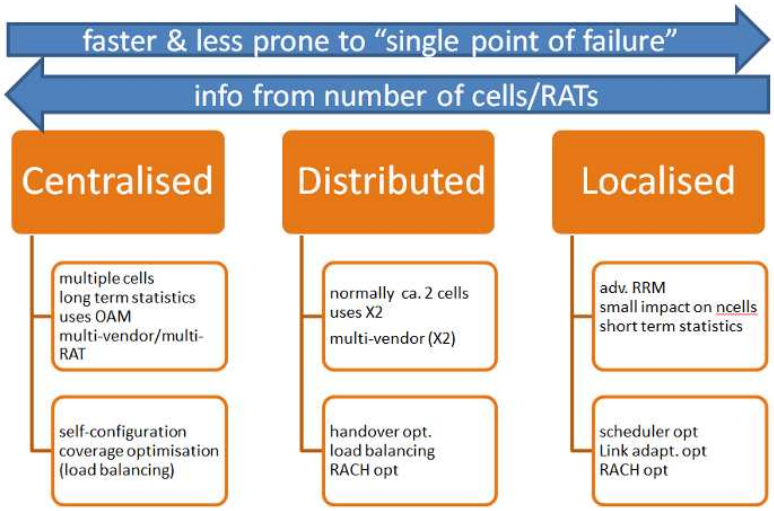

Figure 2-3: Important trade-off between centralized, distributed and localized SON approaches.

2.1.2 BeFEMTO SON Architecture

BeFEMTO has had a major contribution to the SON framework at large, as well as to that initiated by 3GPP. Reference [68] highlights the various contributions made by the project.

A first enhancement can be found in the BeFEMTO Evolved Packet System (EPS) architecture, which builds upon 3GPP's Rel-10 EPS architecture and extends it in several aspects. Figure 2-4 provides a graphical overview of the functional entities of this architecture as well as the interfaces between them.

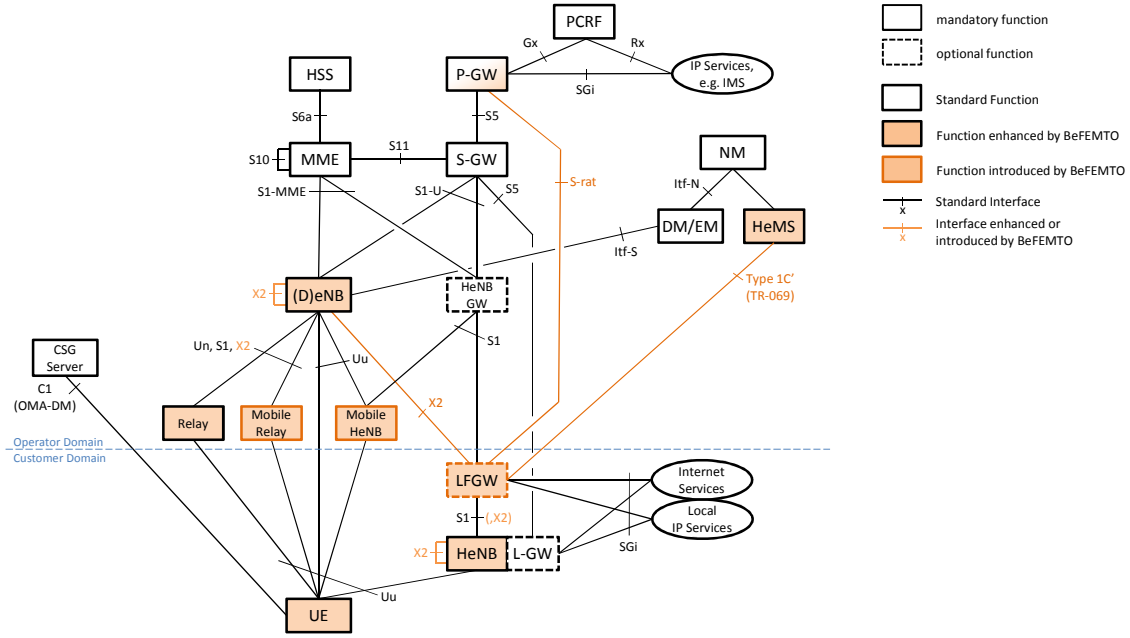

Figure 2-4: BeFEMTO EPS Architecture with functional entities and interfaces enhanced or newly introduced by BeFEMTO highlighted.

The full description of all functionalities can be found in [68]. In the sequel are given only those that are relevant to BeFEMTO SON algorithms. **Donor eNB** is a key component for outdoor **fixed and moving relays** femto cells, so is **Local Femtocell GateWay** for centralized algorithms, and enhanced X2 interface, for distributed algorithms.

- **(Donor) evolved NodeB ((D)eNB) (enhanced):** This functional entity is part of the E-UTRAN and terminates the radio interface from the UE (the Uu interface) on the mobile network side. It includes radio bearer control, radio admission control and scheduling and radio resource allocation for both uplink and downlink. The eNB is also responsible for the transfer of paging messages to the UEs and header compression and encryption of the user data. eNBs are interconnected by the X2 interface and connected to the MME and the S-GW by the S1-MME and the S1-U interface, respectively. An eNB is called a Donor eNB if it controls one or more relays: in this case S1/X2 proxy functionalities, PGW/SGW functions for relay node and Un interface are supported in addition [43]. In the BeFEMTO architecture, (D)eNBs exchange additional information with other network entities ((D)eNBs, HeNBs, etc.) to improve radio-resource and interference management and self-optimization.
- **Local Femtocell GateWay (LFGW) (new):** The LFGW is a functional entity deployed optionally within a femtocell network, specifically within a customer premise. Similar to a HeNB GW, it can serve as a concentrator for S1 interfaces and can also serve as a local mobility anchor, a local mobility control entity and central local breakout point for Local IP Access (LIPA) and Selected IP Traffic Offload (SIPTO) with support for femto⇔femto and femto⇔macro mobility. It further supports local routing and load balancing and may act as a HeNB controller for centralized Radio Resource and Interference Management support.
- **HeNB Management System (HeMS) (enhanced):** The HeMS assumes either the role of an initial HeMS (optional) or of a serving HeMS. The initial HeMS may be used to perform identity and location verification of a HeNB and assigns the appropriate serving HeMS, security gateway and HeNB-GW or MME to the HeNB. The serving HeMS supports identity verification of the HeNB and may also support HeNB-GW or MME discovery. Typically, the serving HeMS is located inside the operator's secure network domain and the address of the serving HeMS is provided to the HeNB via the initial HeMS. In the BeFEMTO EPS, the HeMS needs enhancements for supporting the new LFGW element, e.g. for providing the key material allowing the LFGW to be inserted into the S1 interface and the local management policies.

- **Relay (enhanced):** A relay is a node that is wirelessly connected to a DeNB and relays traffic from UEs to and from that DeNB. The relay can be a cell on its own as is the case in LTE Rel-10 or a node that only supports a reduced protocol stack of an eNB. Femtocell relays have been enhanced by a full duplexing transmission scheme in which they can transmit and receive simultaneously [40].
- **Mobile Relay (new):** A mobile relay is a relay that additionally supports mobility between DeNBs (see [40] for details).
- **X2 (enhanced):** The X2 interface logically connects eNB↔eNB, open access HeNB⇔HeNB and closed access HeNB⇔HeNB with the same access group to each other. It is a point-to-point interface that supports seamless mobility, load and interference management as defined in LTE Rel-10 and **enhancements thereof introduced by BeFEMTO, e.g. for the use with novel SON algorithms or between mobile relays mounted on trains (i.e. moving in a group)**

A second contribution to architecture is described in Figure 2-5 (see [68])., of which. the right hand side describes the radio part.

BeFEMTO has introduced functions (SON enablers),-which are understood to enable SON functionalities and which are dealt with in some greater details in subsequent sections. These functionalities, along with real-time and non-real-time information from the system, aid the core SON functionalities for improved radio resource and interference management. These latter functionalities are included in the Self-Optimising Radio Resource and Interference Management (SO-RRIM) functional block that optimizes the radio resource usage within and between (H)eNBs.

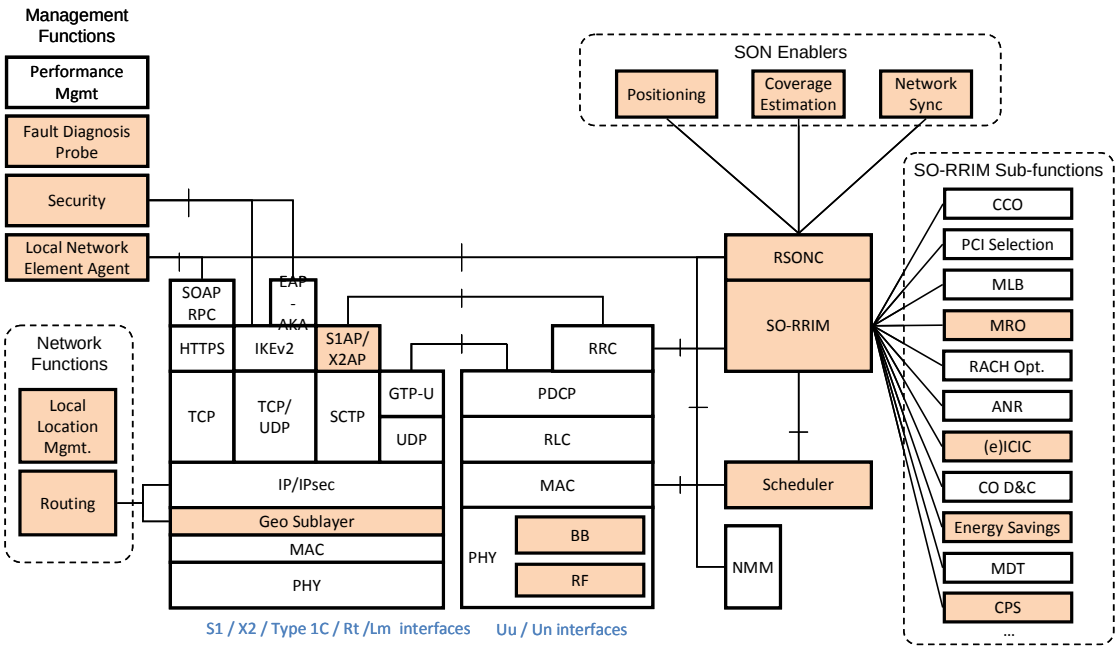

Figure 2-5: BeFEMTO's layered architecture with the additions and SON building blocks clearly highlighted.

.

Above described layered and protocol architecture is important for understanding the operational functionalities of the developed SON enablers and functions.

2.1.2.1 BeFEMTO SON Enablers

As for the SON enablers, BeFEMTO has made significant contributions, with more information given in Section 3. As shown in Figure 2-5, the Network Monitor Module (NMM) supported by advanced RF functionalities plays a central role since it facilitates both the SON enablers as well as SON sub-functions.

2.1.2.1.1 Canonical Basis Elements

Therefore, the basis for below enablers and subfunctions as well as SON functions dealt with throughout this document is the NMM which in turn is dependent on advanced RF functionalities:

- **NMM (Network Monitor Module)** also called NLM (Network Listen Module), or Sniffer. The Sniffer Module is a real-time system that continuously captures/monitors data or signals passing through the network. It is a useful tool whose measurements can be used in SON techniques to adapt the transmitting power taking into account interference to other users and systems.
- **RF Front-End Functionalities for Self-Optimization.** The power control in the transmitter's RF chain, using an open/closed power loop block scheme, allows to follow changes of the desired transmitted power as well as to recover from possible power failures of other components in the RF transmitter chain.

2.1.2.1.2 SON Enablers

The enablers are functions which facilitate subsequent SON functions and sub-functions:

- **Automatic Location Determination of Femto BS & MS.** The main problem and motivator is that HeNBs are placed by customers and that Femto User Equipments (FUEs) move, yielding to uncertainty & dynamicity. In addition, the real-time location of HeNBs and associated FUEs is needed for
  a. emergency situations (E911/E112),
  b. verification of licensed spectrum use,
  c. enabler for Radio Resource Management (RRM) & SON algorithms. .
- **Automatic Coverage Estimation.** The main problem and motivator for this enabler is that current radio network planning is mainly static based on drive-tests. Furthermore, to limit interference to the macro cell and optimize femto RRM, autonomous coverage estimation is vital. Finally, currently used methods are inefficient (Downlink (DL) → macro interference, UpLink (UL) → femto dynamic range limit).
- **Biologically Inspired Network Synchronization.**. The main problem is that accurate femto-femto & femto-macro network synchronization is needed for RRM and interference. Known algorithms (IEEE1588, NTP, sniffing, GPS) all have shortcomings in the context of femto cell.

2.1.2.2 SON Sub-Functions

The sub-functions, understood to be SON sub-algorithms which are common to numerous SON algorithms in the system, are as follows:

- **(enhanced) Inter-Cell Interference Coordination ((e)ICIC):** ICIC has the task to manage radio resources such that inter-cell interference is kept under control. ICIC is inherently a multi-cell RRM function that needs to take into account information from multiple cells. Enhanced ICIC extends this to heterogeneous networks, e.g. in Rel-10 initially for non-carrier aggregation (CA) based LTE deployments only.
- **Energy Saving (ES):** This function allows optimising the energy consumption enabling the possibility for a cell providing additional capacity, to be switched off when its capacity is no longer needed and to be re-activated when needed.
- **Centralised Power Setting (CPS)** (new): This function enables the possibility for a cell to be switched off which creates too much interference among a set of cells controlled by the Local Femto Gateway (LFGW). This is done as per LFGW indication until the LFGW requests the cell to re-evaluate its contribution based on measurements performed by the cell's NMM or until the LFGW re-evaluates itself the interference situation based on the feedback of measurements performed by the NMM of all or a set of controlled cells. LFGW is a new entity, introduced by BeFEMTO, as a part of EPS Architecture, described Erreur ! Source du renvoi introuvable..
- **Automatic Neighbour Relation (ANR) Function:** The ANR Function detects, adds and removes neighbour cells and manages a neighbour relation table automatically. This can then be used to establish X2 connections to peer (H)eNBs, execute handovers over X2 and update the UE measurement configuration.

- **Mobility Control (MC):** controls mobility of users in connected and idle mode. Idle mode is controlled by setting cell reselection parameters to the correct values (thresholds etc.). In connected mode this function is responsible for deciding when and to which cell the handover procedure should be triggered. Handover decisions may be based on UE and (H)eNB measurements, neighbour cell load (see MLB), cell load (traffic distribution, transport and hardware resources) and operator defined policies. The actual handover execution is handled in RRC and S1/X2.
- **QoS Parameter Optimisation (QOS_F):** The QOS_F covers different optimisation targets which affect the efficient support of QoS in RRM. The optimisation can include (but is not restricted to) admission control parameters, scheduler parameters, other MAC/RRM parameters, like retransmission configuration and congestion control optimisation.
- **Minimization of Drive Testing (MDT):** MDT includes the automatic collection of UE measurements and the logging of data that can be used to replace manual drive testing to evaluate the network performance per physical location Erreur ! Source du renvoi introuvable.Erreur ! Source du renvoi introuvable.. One distinguishes between Immediate MDT by UEs in CONNECTED state and Logged MDT by UEs in IDLE mode. In the latter case, measurements are collected and reported in a batch manner to the eNB at a later point in time
- **Capacity and Coverage Optimisation (CCO):** This function handles the coverage and capacity optimization. It enables automatic/intelligent adjustment of the coverage based on inputs from Coverage Estimation, UE, PHY and NMM and optimises capacity, for example of control channels, based on UE measurement feedback and locally available information
- **Mobility Load Balancing (MLB) / Load Balancing (LB_F) Optimization:** The objective of load balancing is to distribute cell load evenly among cells or to transfer part of the traffic to other cells such that radio resources remain highly utilized and the QoS of in-progress sessions are maintained and call dropping is kept sufficiently small. This is done by means of self-optimisation of mobility parameters or handover actions. It also includes setting of cell reselection mode for idle mode load balancing

With the SON architecture and its enablers clarified, we are now able to introduce the BeFEMTO WP4 SON enablers and algorithms.

2.2 WP4 SON enablers

The following SON enablers have been introduced by BeFEMTO, and are described in detail in Section 3.

Automatic Location Determination of Femto BS & MS.

Traditional location techniques via GNSS or macrocell triangulation do not work for all HeNBs, especially those located in deep indoor. Therefore, we have worked on a maximum likelihood relative positioning algorithm w.r.t. prior localised HeNBs with access to GNSS/macrocell (Section 3.1). It has the following characteristics: medium complexity, scalable in number of reference as well as query points, mean error = 1.4m, no use of X2 interface.

Automatic Coverage Estimation.

To obtain an accurate coverage estimation, we have introduced in Section 3.2, the Autonomous Coverage Estimation (RACE) algorithm which is based on Received Signal Received Power (RSRP) and geographic location, yielding the desired coverage bins. Furthermore, we introduced the Automatic Boundary Estimation (ABE) algorithm, which is a smoothing of the RACE bins, using a best cell classification method. It yields the following characteristics: low complexity, scalable, mean error = f(bin size & positioning algorithm).

Biologically Inspired Network Synchronization., Distributed biologically inspired firefly algorithms have been known but not applied to sparse femto cells. BeFEMTO has developed a mathematical description by the theory of coupled oscillators, which is based on fire-flies. We have facilitated the exchange of synchronization words between femto-cell entities, such that the internal clocks are adjusted based on the timing of received synchronization words. It yields the following technical characteristics (which had been dealt with in much greater details in [34]): low complexity, scalable, quick convergence, no X2 required (downlink synchronization).

2.3 Classification of WP4 SON Algorithms

As explained in Section 2.1, 3GPP and NGMN classify SON algorithms according to their level of coordination. they imply:

- those which do not need any coordination, are coined "local" or "stand-alone";
- those coined "distributed" need some information to be exchanged between HeNBs and eNB (in a yet non-standardised fashion), or between HeNBs on the X2 interface; in this latter case, as mentioned in Section 2.1, the X2 interface is enhanced in order to allow for exchange of information beyond what is presently standardised;
- those algorithms coined "centralized" rely on the existence of a gateway, which has access to parameters or even data, concerning an entire cluster of HeNBs.

Following 3GPP's and NGMN's taxonomy [2], [10], we now proceed by introducing the SON algorithms developed within WP4 for each of the categories.

2.3.1 Local SON Algorithms

Local SON algorithms refer to the case of no X2 or air interface coordination. Femtocell networks are poised to take the overall network spectral efficiency to a whole new level. This requires that low-power radio access points must be equipped with self-organization capabilities, in which they constantly sense the environment, and take autonomous decisions relying on simple feedback (from the environment). The emphasis is on decentralized and location-aware self-organized femtocell networks, which do not use the X2 interface to exchange information or coordinate transmissions.

Automatic Coverage Control

Three main methods for downlink coverage control, based on the control of the transmitted power transmitted by the femtocell are presented in Section 4.1.1, namely

- **Network Listen**, The femtocell power is configured to produce a minimum received power for a potential user at a distance r placed between the macrocell and femtocell. Calculations are based on simple path loss ,models
- **Mobile Assisted Range Tuning** is based on satistics of registrations with the femtocell performed by alien users over a certain period, and downlink channel quality reports obtained from home mobiles.
- **Active Macro Mobile Protection**. This method gives better results than always transmitting with low power because it only sacrifices femtocell coverage when a macro user is detected

As to the uplink coverage, it may be paradoxically impacted when the mobile is very close to the HeNB, because the power control reaches its minimum value, while the HeNB receiver gets saturated. A solution is to activate a signal attenuator at the receiver whenever it gets saturated.

Coverages for all these methods are compared via simulations. Note that none of these methods necessitate vcommunications with other femto or macro cells.

Self-Organizing Interference Management Techniques for Femtocell Networks

The local algorithm proposed in Section 4.1.2 is inspired from reinforcement learning (RL) which has been gaining a significant momentum with the advent of small cells and heterogeneous networks. RL is seen as a practical, robust and local solution allowing femtocells to self-organize in a decentralized manner. In addition, RL has a number of properties that allow operators to gauge the network performance gains in a proactive manner rather than reacting to the capacity crunch. Therefore, RL is well-suited to investigate the problem of intercell interference coordination (ICIC) under all its forms (time-domain, frequency-domain and spatial domains). The focus is on user-deployed femtocell networks, where the aggressors are the femtocells and the victims are macro UEs. During the sensing phase, femtocells need to learn their long-term performance by testing a number of transmission strategies (power level, frequency carrier etc). This is an iterative process, which is repeated until convergence is reached. In addition, a femtocell can simultaneously learn its own utility metric (which is a function of other femtocells in the network), and optimize its transmission strategy. The question at stake is "how to optimally self-organize in dense small cells?" In the sensing phase, the femtocells learn their long-term performance by testing a number of transmission strategies (power level, frequency carrier etc), where at every time instant *t*, femtocells build a probability distribution function which is based on the history of the applied actions/strategies up to *t-T*. Using a decision making function and history accumulation, femtocells can infer on what is the best strategy at time *t+1*. This process continues until reaching convergence. There are a number of nice properties that are worth noting: by chosing a long sensing phase, femtocells will learn their long-term

performance that is robust in nature to channel uncertainties and network dynamics (the femtocells are oblivious to who is present in the network). As said above, a femtocell can also simultaneously learn its own utility metric and optimize its transmission strategy thanks to the so-called two-time scale dynamics where the utility estimation process is faster than the probability distribution optimization.

2.3.2 Distributed SON Algorithms (global)

Distributed SON refers to the case of X2 and/or air interface coordination between BeFemto APs and eNB. The global notion indicates that exchange is between FeNBs and MeNBs. As explained in Section 2.1, the X2 interface, according to LTE Release 10, allows some information exchange between eNBs, between open access HeNBs and between closed access HeNBs with the same access group. BeFEMTO has extended its scope in order to allow information exchange between eNBs and HeNBS. New algorithms protecting macro users from interference generated by femto cells/femto users can thus be developed.

The **Spatial Domain based Interference Coordination** scheme of Section 4.2.1 aims to coordinate beams in neighbour cells so that beam collisions between nearby cell-edge users can be avoided and, hence, Signal to Interference plus Noise Ratio (SINR) for cell edge user can be improved. The coordination is based on feedback from UEs including not only CQI, Rank Indicator (RI) and Precoding Matrix Indicator (PMI), but also different types of additional messages to support the cooperation. These messages are exchanged between base stations (here HeNBs and eNB) over an X2 interface. This algorithm is an extension of eICIC in LTE Rel-10 since it applies time-domain restrictions in a frequency-domain subband and not for the entire bandwidth as eICIC does.

In **Spectrum Leasing as an Incentive for Macro-Femtocell cooperation in the UL,** proposed in Section 4.2.2, cell edge MUEs leverage on the neighbouring small cells in which a device-to-device connection is established whereby MUEs forward their traffic to the FUEs, who serve as an aggregator. Since the proposed solution is based on mutual cooperation, FUEs will not systematically help the MUEs, unless the macrocell rewards them in the form of a free resource. This is akin to the time-domain ICIC solution in 3GPP. In terms of implementation, the X2 interface is used to coordinate the transmissions from MUEs to FUEs. In addition, the coordination among the femtocell and the macrocells can be carried out using the X2 interface.

Interference control based on decentralized online learning is a solution for the aggregated interference problem from femtocells to macrocells based on a learning approach and is presented in Section 4.2.3. It is first shown that femtocells are able to independently learn a policy which allows them to control their interference at potentially close MUEs. Since the learning task takes time, as a second step the **docitive** approach is introduced where femtocells can take advantage of the policies already learnt by other more expert nodes. For the femtocells to be aware of the situation at the macrocell system, they rely on information from the macrocell system which is assumed to be conveyed through an X2 interface between macrocells and femtocells

The scope of Section 4.2.4 is focused on Spectral Efficiency (SE) enhancement on the access link of Outdoor Fixed Relay femtocells (OFR) through **Self-Organization (SO) of eNB antennas tilt**. Here, a Tilt Optimization through bio-mimetic SO Framework (TO-BSOF) is proposed in a distributed and self-organizing manner that provides near-optimal performance. The main advantage of TO-BSOF is that it does not have heavy signalling overheads associated with it. A negligible amount of signalling among the sectors is required to determine the location of OFRs. This signalling can be done through X2 interface and needs to be done only when the location of an OFR is changed.

Section 4.2.5 is dedicated to **Relays and Backhauling**. A decentralized algorithm is proposed that allows MUEs to optimize their cell edge performance through coordination between macro and femtocells, through an X2 interface. Backhaul-aware cell selection is of utmost importance, in which the backhaul part is instrumental in designing an optimal cell association at the UE side. In detail, the MUE splits its transmitted signal into a coarse and a fine messages, in which the coarse is intended to the macro base stations whereas the fine is to be decoded by a nearby small cell. Subsequently, the small cell decodes the signal and relays it to the macrocell over a heterogeneous backhaul. Since wired and wireless backhauls exhibit a number of tradeoffs, it is important that the decentralized algorithm is backhaul-aware. The proposed approach is shown to outperform the classical and uncoordinated approach in which the small cell and the macrocell operate independently.

Another stream of innovation in BeFEMTO deals with **mobile relays**, viewed as small cells needing over-the-air coordination with the macro base station. A mobile relay architecture is first defined, enhancing that of LTE Rel 10, then, a contribution on cooperative moving relays, coping with a limited capacity backhaul,

is presented. The **mobile relay architecture** extends the static work to the mobile case. LTE Rel-10 is focusing on fixed relays introduced mainly for coverage purposes, whereby the coverage of an eNB is extended by the introduction of a relay node, which represents an eNB with wireless backhaul. In order to support advanced relay scenarios, e.g. high speed trains, it is important to extend the existing LTE Rel-10 relay architecture towards mobility. Efficient support of group handover is also required. Several enhancements of the LTE Rel-10 relay architecture are investigated in Section 4.2.6 including the selection of the mobility anchor point for the relay and for the UE. Also handover procedures for moving relays are investigated.

System level simulations results for moving relay nodes, in which the backhaul is the bottleneck, are presented in Section 4.2.7. An enhanced version of X2 is needed to coordinate the various distributed transceivers on top of the train. This work is preliminary in that it provides results for the case where coordination is assumed to be perfect inside the train compartments. For future work, prediction-based RRM schemes will be developed in which leveraging on history and context information, UEs will seamlessly receive their QoS requirements.

2.3.3 Distributed SON Algorithms (local)

Distributed SON refers to the case of X2 and/or air interface coordination between BeFemto access points (APs). The local notion indicates that exchange is only between HeNBs. BeFEMTO has also envisioned enhancements on X2 in order to allow smooth information exchange between BeFemto HeNBs.

In Section 4.3.1, a tradeoff is analysed between **learning** with local information and with information exchange among femtocells. In other words, femtocells can converge much faster to the optimal network operating point at the cost of exchanging information with neighbouring femtocells. This is done through the X2 interface. In the case of Q-learning there is a need for an X2 interface between the macro and the femtocell tier in which the femtocell knows how much interference it causes onto the macrocell tier.

In Section 4.3.2, a **decentralized downlink beamformer** design is proposed for minimizing the total transmitted power of coordinated HeNBs subject to fixed cross-tier interference constraints and femto-UE specific SINR constraints. The proposed minimum power beamformer design relies on limited backhaul information exchange between coordinated HeNBs where real valued HeNB specific co-tier interference terms are solely exchanged. Coordination between HeNBs can be handled via X2.

In Section 4.3.3, a novel **dynamic and autonomous subband assignment** (DASA) method is investigated that is particularly well suited for decentralized wireless networks where subbands are assigned only by HeNBs in a distributed way, using a modified graph colouring algorithm. HeNBs send measurements from their users to the interfering neighbours by an indicator on an X2 interface. The proposed method is designed such that the interference protection does not coincide with an intolerable reduction in the attainable spatial reuse of radio resources.

Section 4.3.4, is focussed on a collaborative power usage that aims at enhancing the effective energy cost by the self-organization networking (SON) operation applied to femtocell users. Here, the aggregate power usage of the OFDMA based femtocell is developed by analyzing the **effective battery power usage** before the power amplifier by the users. Unlike conventional schemes addressing only the power usage for the data, effective battery power usage for the channel information feedbacks has been taken into account. Given this additional power usage, the effective power requirement for the self-organization of the interference requirement has been analyzed. Accordingly, it has been identified that in the context of the SON interference management, the proper signalling on the effective power control between femtocell users can enhance the energy efficiency. For this achievable benefit, the X2 interface between femtocells can be used to ensure that the concerned femtocells manage the interference towards the known incumbent receiver.

In Section 4.3.5, we consider a co-channel femto cell sharing the spectrum with the overlaid macrocell. We design a generic energy usage model in such a way that **energy usage** by femto cell users **at both the signalling and the data phases** is taken into consideration. We consider the orthogonal channel deployment between femtocells, each having the X2 interface with neighbouring femtocells. Over the X2 interface, it is assumed that medium or large-scale context information including the range of the spectrum per FBS, the number of FUEs available, and the sum energy budget can been exchanged. Thus, the ergodic sum capacity is enhanced.

The solution for the **aggregated interference problem from femtocells to macrocells** introduced in Section 4.3.6 is based on a learning approach. However, it relies on information from the macrocell system which is assumed to be conveyed through an X2 interface between macrocells and femtocells. Since this X2 interface has not been yet standardized by 3GPP, we propose here a completely autonomous solution

based on partially observable Markov decision process (POMDP**)**, where femtocells (exchanging information only among each other) estimate their impact in the macro user through interpolation techniques.

2.3.4 Centralized SON Algorithms

In Section 4.4.1 a centralized interference mitigation algorithm between femtocells is presented. In this algorithm, we assume that there is a central controller (a Local femto gateway (LFGW)). HeNBs define the interfering neighbours with the help of the measurement reports from the users. Then, the HeNBs send the IDs of the interfering neighbours to the central controller and the controller assigns subbands by using a modified graph colouring algorithm. The central controller sends the updated subband assignment (primary subbands) to the HeNBs. In order to protect primary subbands, HeNBs send the assignment information to the interfering neighbours via an X2 interface.

In Section 4.4.2, a novel **graph-based multi-cell scheduling framework to efficiently mitigate downlink inter-cell interference** in small cell OFDMA networks is proposed. This framework incorporates adaptive graph-partitioning and utility optimization concepts to address inter-cell interference in two phases: the first phase involves a locally-centralized graph-based Inter-cell Interference Coordination (ICIC) mechanism to mitigate ICI in dense small-cell deployments. Subsequently, the second phase provides a channel-aware resource allocation policy targeting the optimization of the system performance. Both phases rely on sharing the channel state information in centralized manner via a LFGW.

Section 4.4.3 presents a comparison between two algorithms, which rely on the concept of **"Ghost" femtocells**. The "Ghost" paradigm focuses on interference mitigation techniques based on resource allocation management. More precisely, it concentrates on both co-tier interference and cross-tier interference in LTE downlink scenarios. The two schemes exploit such an approach in residential Stand-Alone and Networked enterprise Femtocell deployments respectively. In the first algorithm, referred to as $Ghost_{SAF}$, HeNBs are not able to cooperatively mitigate the generated interference and they selfishly attempt to maximize the spectrum reuse. In the second scheme, named as $Ghost_{NF}$, a distributed method for estimating how neighbouring HeNBs affect each other transmission reliability is first introduced. Then, the LFGW uses this information to locally coordinate the access of neighbouring femtocells and manage the frequency reuse amongst nearby HeNBs. A distributed version of $Ghost_{NF}$, where signalling and computation costs are shared amongst neighbouring HeNBs over the X2 interface, is feasible. However, this solution would result in higher overhead and latency.

In Section 4.4.4, a HetNet-based centralized power setting algorithm for femtocell clusters is introduced, which makes use of a linear programming framework. The method is supported by the BeFEMTO architecture and specifically exploits the LFGW, which will coordinate co-located femtocell measurements/actions and perform the linear programming resolution. Compared to the traditional distributed approach, this centralized power setting algorithm allows significant macrocell and femtocell outage reductions which are more pronounced in heavy femtocell deployments. The algorithm in its centralised (LFGW as coordinator and solver) or iterative distributed (LFGW as coordinator only) implementation encompasses the possibility to automatically switch-off the most disturbing femtocells in a pure SON fashion enabling an easier deployment and an overall network performance.

2.3.5 Summary of SON Algorithms

Table 2-1 summarises above taxonomy and classification. It is evident that BeFEMTO WP4 has significantly advanced the state of the art in the various embodiments of distributed SON algorithms. Within this category of distributed SON, most algorithms are applicable to the case of networked femtos, but algorithms for the relay and mobile femto case have also been proposed.

Table 2-1: BeFEMTO algorithms classification.

	Local	**Distributed HeNB/eNB**	**Distributed HeNB**	**Centralized**
Reinforcement learning	X			
Spatial Domain based Interference Coordination		X		
Spectrum leasing		X		
Decentralized online learning		X		
Self-Optimization of Antenna Tilt		X		

Moving Relays		X		
Relay and backhauling		X		
Replication dynamics, fictitious play (FP) and classical Q-learning			X	
Decentralized Femto Base Station (HeNB) Coordination for Downlink Minimum Power Beamforming			X	
Dynamic and Autonomous Subband Assignment			X	
Battery Power Requirements for SON operation from the terminal perspective			X	
Energy-Aware Self-Organized Networking Enabled Co-Channel Femtocell			X	
Managing Femto to Macro Interference without X2 Interface Support Through POMDP			X	
Central Interference Mitigation between Femtocells				X
Graph colouring/Graph partitioning				X
Ghost femto cells distributed			X	
Ghost femto cells centralized				X
Power control				X

2.4 NGMN & 3GPP Impact

In this section, we gauge the impact of BeFEMTO's WP4 SON developments on two related standards bodies, i.e. NGMN and 3GPP, and vice versa, i.e. some design choices become evident with below exposure.

2.4.1 Impact on/of NGMN

NGMN issued two important deliverables regarding to SON:

1) "NGMN Recommendation on SON and O&M Requirements" [10] published in early 2009 that guides the implementation of SON for the future.

2) "NGMN TOP OPE Recommendations" [11] published in Autumn 2010 that is a result of NGMN project "Operational Efficiency" addressing SON and O&M aspects of next generation networks.

The latter document described the envisioned SON Use Cases (Figure 2-6) from the operator perspective and indeed had a strong impact on 3GPP work on SON.

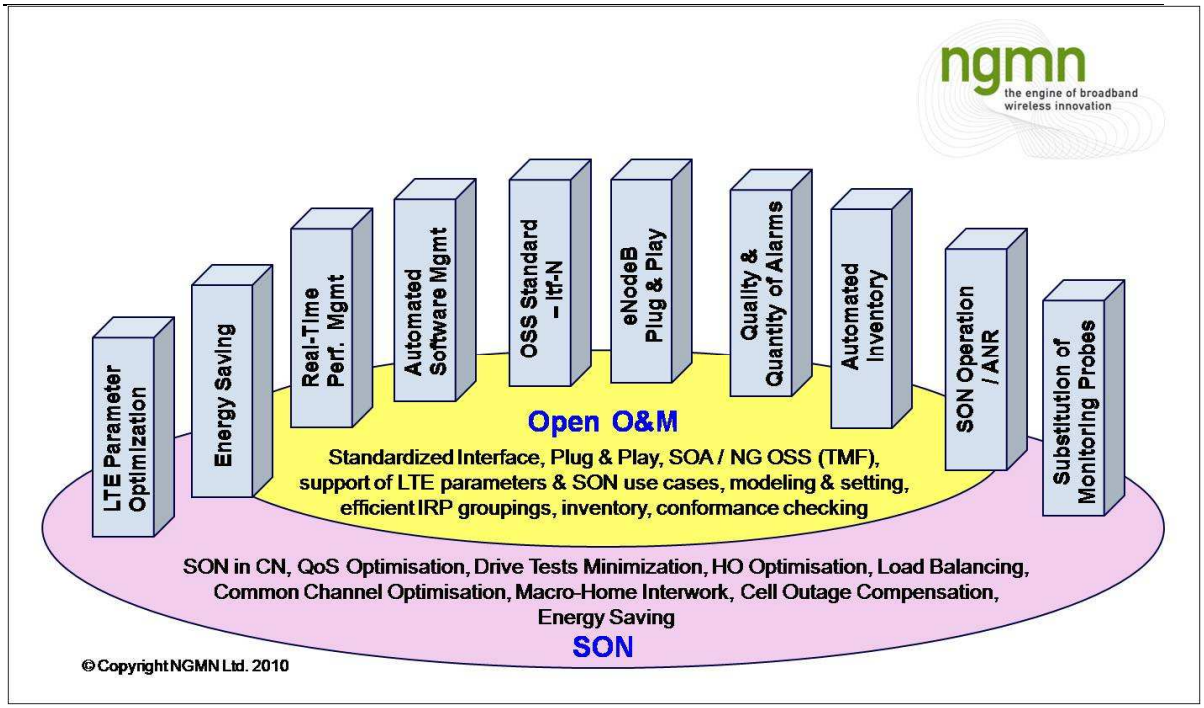

Figure 2-6: SON Use Cases [11].

BeFEMTO has addressed SON use cases of NGMN as shown in Table 2-2. Evidently, only the core network (CN) SON, common channel optimisation and macro-home interwork have not been addressed in WP4 because it was out of scope.

Table 2-2: Addressing NGMN SON Use Cases.

NGMN use case / **WP4 SON Algorithm**	SON in CN	QoS Optimisation	Drive Tests Minimization	HO Optimisation	Load Balancing	Common Channel Optimisation	Macro-Home Interwork	Cell Outage Compensation	Energy Saving
Reinforcement learning		x			x			x	x
Spatial Domain based Interference Coordination		x			x			x	x
Spectrum leasing		x			x			x	
Decentralized online learning		x		x	x			x	x
Self-Optimization of Antenna Tilt					x			x	x
Moving Relays			x	x	x				
Relay and backhauling				x	x			x	
Replication dynamics, fictitious play (FP) and classical Q-learning		x			x			x	x
Decentralized Femto Base Station (HeNB) Coordination for					x			x	x

Downlink Minimum Power Beamforming									
Dynamic and Autonomous Subband Assignment		x			x			x	
Battery Power Requirements for SON operation from the terminal perspective									x
Energy-Aware Self-Organized Networking Enabled Co-Channel Femtocell									x
Managing Femto to Macro Interference without X2 Interface Support Through POMDP		x			x			x	x
Central Interference Mitigation between Femtocells		x							
Graph colouring/Graph partitioning		x							
Ghost femto cells		x							x
Power control		x							

To address inter-operability between SON algorithms from different vendors, mimoOn of WP4 presented 2 proposals for standardizing SON interface and RRM algorithms **in multivendor LTE overlay networks** at the NGMN Partner Forum March 2012:

1) Standardisation of an Open *coordinated* SON interface for the eNB, pseudo real-time (100ms), covering a small set of key parameters, safeguarding multivendor overlay network stability, but leaving room for vendor-specific innovation on top.

2) Standardisation of a basic set of eNB RRM algorithms, setting a basic level of eNB behaviour predictability, safeguarding multivendor overlay network stability, and also leaving room for vendor-specific innovation on top.

The value of the proposals has been recognised by operators and vendors in NGMN forum and the ideas have been supported. However, the proposals can be successful only with a broad industry support. In fact, all major vendors will bring their own (proprietary) solutions for multilayer HetNets. This activity will be continued when a broad industry support will be obtained.

2.4.2 Impact on/of 3GPP

SON functionalities are very difficult to standardize for the following reasons: first, there are a lot of different ways to implement a SON function and second, these functions often contradict each other. For instance, load balancing is done at Network Management (NM) level but handover optimization done at eNB level and both want to adjust the same parameter at the eNB. A practical way to avoid this situation has been to standardize everything which is “configured” at NM level and do not standardize anything at eNB level. Furthermore, primary and secondary targets are defined.

As per Figure 2-7, which is based on 3GPP S5-102029, the approach has been to clearly separate between management, decision taking, executing and feedback functionalities. Also, certain policies with priority levels are used to decide on (possibly conflicting) decisions at all instances in the network. The featured 3GPP SON functions are grouped in four different classes:

- local algorithms,
- decentralized algorithms with coordination between femto eNBs,
- decentralized algorithms with coordination between femto eNBs and macro eNBs, and

- centralised algorithms.

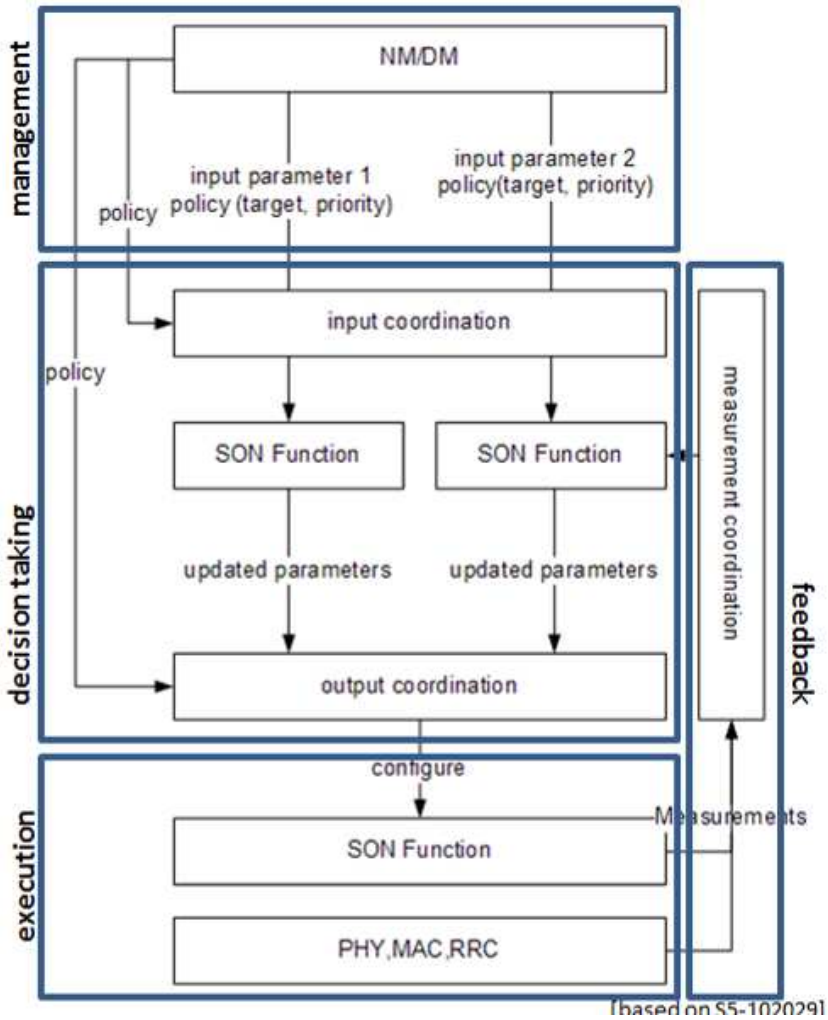

Figure 2-7: Standardization approach related to SON, there management, decision taking, execution and feedback are clearly split and prioritized.

In this classification, coordination refers to coordination over the X2 interface and/or directly the air interface. The individual algorithm classes have different impact on 3GPP standardisation taking LTE Rel-10 as the baseline. Standardisation impact is needed in general if additional messages between nodes need to be exchanged in order to support the coordination and/or if additional measurements need to be provided by the terminal. Exchange of messages between nodes typically impacts the X2 interface, whereas additional measurements provided by the terminal require enhancements of the air interface (Uu interface). In case that these air interface measurements are required by SON algorithms not running in the serving cell, the X2 interface can be impacted as well.

In Rel-8/9, no X2 interface between femtos (HeNBs) is supported. In Rel-10, X2 interface between femto nodes with open access and between femtos with closed/hybrid access has been introduced if the closed subscriber group (CSG) of the femtos has the same identifier. An X2 interface is not supported in LTE Rel-10 in case of femtos with different CSG IDs and between femtos and eNBs. Coordination directly over the air interface is not supported in LTE Rel-10 between any nodes.

Local SON algorithms do not require coordination between different nodes, neither over the air interface nor over the X2 interface. Since the algorithms run solely in one node, no standardisation impact requiring interface changes is expected. SON Algorithms belonging to the second class requiring coordination between femtos could make use of the existing X2 interface assuming the femtos have the same CSG ID. This class of algorithms requires extension of the existing X2 interface functionality in LTE Rel-10. Hence,

3GPP impact for this can be regarded as moderate in general. The third class of SON algorithms applying coordination between femtos and eNBs require the introduction of an X2 interface between femtos and eNBs. This interface is not yet supported in LTE Rel-10, its introduction is left for further discussion in Rel-11. The fourth class of SON algorithm relies on a central node. Standardisation impact depends on the location of the centralized SON algorithm. Assuming that no tight latency requirements are needed, the centralized SON algorithm could be located in the Operation and Maintenance (OAM) centre. In this case, extensions of the Itf-N interface are expected.

Moving relays have been identified as another field where standardization impact on top of LTE Rel-10 is needed. Relays have been introduced in Rel-10 for LTE as so-called Type 1 relays, which implies that they appear as regular eNBs to the UEs. The relay is connected over a LTE wireless backhaul to its donor eNB. However, in Rel-10 the relay does not support mobility for the backhaul link in the sense that the donor eNB cell cannot be changed in a seamless way. Moving relays are currently under discussion in LTE Rel-11 but completion of standardization work is probably shifted to Rel-12.

Table 2-3: Mapping of BeFEMTO algorithms on 3GPP sub functions

3GPP use case / **WP4 SON Algorithm**	e ICIC	QoS Parameter Optimisation	Drive Tests Minimization	Mobility Control	Load Balancing	Capacity and Coverage OpOptimisation	Centralised Power	Automatic Neighbour	Energy Saving
Reinforcement learning	■	■			■	■			■
Spatial Domain based Interference Coordination	■	■			■				■
Spectrum leasing	■	■			■				■
Decentralized online learning	■	■			■				■
Self-Optimization of Antenna Tilt		■			■				■
Moving Relays		■		■	■				
Relay and backhauling		■			■				
Replication dynamics, fictitious play (FP) and classical Q-learning	■	■			■	■			■
Decentralized Femto Base Station (HeNB) Coordination for Downlink Minimum Power Beamforming		■			■				■
Dynamic and Autonomous Subband Assignment	■	■			■				
Battery Power Requirements for SON operation from the terminal perspective									■
Energy-Aware Self-Organized Networking Enabled Co-Channel Femtocell									■
Managing Femto to Macro	■	■			■	■			■

Interference without X2 Interface Support Through POMDP									
Central Interference Mitigation between Femtocells									
Graph colouring/Graph partitioning									
Ghost femto cells									
Power control									

3. SON-Enabler Descriptions

This section summarizes previous findings on the SON enablers and introduces previously undocumented contributions.

3.1 Automatic Location Determination

3.1.1 Problem Statement

Unlike macro base stations that are deployed by network operators at known locations after careful cell planning, femtocells are deployed by users in their home or office premises. Determining the location of user-deployed femtocells is important due to the following main reasons:

- **Network management**
  - Disjoint or non-overlapping allocation of resources in the time and/or frequency domains among femtocells operating close to each other should be done in a way to reduce interference at user terminals. Information about femtocell locations may help in clustering neighbouring femtos together and allocating resources appropriately among them.
  - Position information may be used as an input to self-organizing network (SON) algorithms to properly initialize and update network/base station parameters.
  - Operators may need to identify the geographic region where a femto is being used for functions such as billing, network monitoring, and statistics gathering.
- **Regulatory requirement**
  - In some countries, operators need to roughly determine the location of a femtocell before it is put into operation in order to satisfy regulatory requirements.
- **Emergency positioning**
  - Enhanced emergency response services require that the location of a user terminal that initiates an emergency call is reported within a certain time window to a nearby Public-Safety Answering Point (PSAP). If no estimate of the exact location of the user terminal is available, the location of the serving cell is reported as a rough guess of the user terminal's location. In this context, the location of a serving femtocell needs to be determined. As femtocells have small coverage areas, a femtocell's location serves as a reasonable guess of the locations of the users it is serving.

3.1.2 Description of Scheme

A standalone Femto with a built-in GNSS module can be located using assisted Global Navigation Satellite System (GNSS), where the assistance data is calculated based on its rough position estimate, e.g., the location of the macro base station in whose coverage area the femtocell is located. Assisted-GNSS may not work when the femtocell is located deep indoors because the satellite signals are very weak and not enough satellites are visible to compute a position solution.

In a cluster of femtocells located, e.g., in an office building in an enterprise deployment, relative positioning is proposed as a viable positioning method. Femtocells that are placed close to windows can be located using, e.g., Assisted-GNSS or macrocell signals. These 'reference' femtocells then have known positions and are synchronized to common base time. Other femtocells, which are located deep indoors or see strong interference from nearby neighbours, may not be positioned using weak satellite or macrocell signals. These femtocells that have unknown positions and asynchronous transmit times are termed as 'blind' femtocells. In relative positioning method, each blind femtocell makes measurements (e.g., round-trip time (RTT), time of arrival (TOA) or time difference of arrival (TDOA)) with respect to not only the reference femtocells but also the other blind femtocells. Macro base stations whose signals are received indoors by one or more blind femtocells also serve as reference base stations and are considered as a part of the cluster for relative positioning.

Measurement of RTT between a pair of femtocells requires implementation of a trigger-response mechanism, where a packet is sent by one femtocell to the other which then responds by sending a packet back. The first femtocell then measures the time that elapsed between the transmission of the outgoing trigger packet and reception of the incoming response packet. The estimated range between the two is directly related to one half of the measured RTT. Measuring TOA of a packet transmitted by a neighbour femtocell requires perfect synchronization between all femtocells/macro base stations. It is not possible to

measure either RTT or TOA using the existing radio interface defined for 3GPP cellular communication systems, e.g., LTE. It is, therefore, proposed to make TDOA measurements at blind femtocells with respect to pairs of neighbour femtocells. TDOA measurements may be made using signals broadcasted by neighbour femtocells, e.g., cell-specific reference signal (CRS) or positioning reference signal (PRS) in LTE Rel. 9. Measuring TDOAs at a femtocell requires some limited user terminal functionality to be built-in the device, as the femtocell needs to process downlink broadcast signals that are meant for user terminals. Such functionality may be added to an already existing module like the one for radio environment monitoring.

The task of determining positions of blind femtocells can be formulated in the form of a least-squares joint estimator. This estimation problem can be solved by different methods, e.g., gradient search or genetic algorithm. Note that the transmit times of the blind femtocells need to be estimated in addition to positions as an LTE network is inherently asynchronous.

3.1.3 Simulation Results

System level simulations are conducted to determine positioning performance of TDOA estimation. The system simulator models a heterogeneous network with femtocells deployed within the coverage area of a hexagonal macrocell layout. For the femtocell deployment the dual-stripe model [12] is adopted, and each dual-stripe layout constitutes a femtocell cluster. TDOA measurements are generated at each blind femtocell, based on received Positioning Reference Signals (PRS) [13]. TDOA estimation is done for two different channel models: One Peak and Pedestrian A [14]. The One Peak channel exhibits a single non-fading line of sight (LOS) path, whereas Pedestrian A is a multipath channel with one LOS and 3 non-LOS paths. The RTDOA estimates collected at all blind femtocells in a cluster are fed into the position/transmit time calculation function to compute positions (and possibly transmit times) of all blind femtocells.

The Cumulative Distribution Functions (CDFs) of the position errors are depicted in Figure 3-1 for two deployment ratios in an asynchronous femtocell cluster. The deployment ratio is the probability that an apartment in a dual-stripe layout contains a femtocell. This ratio controls the density of femtocell deployment.

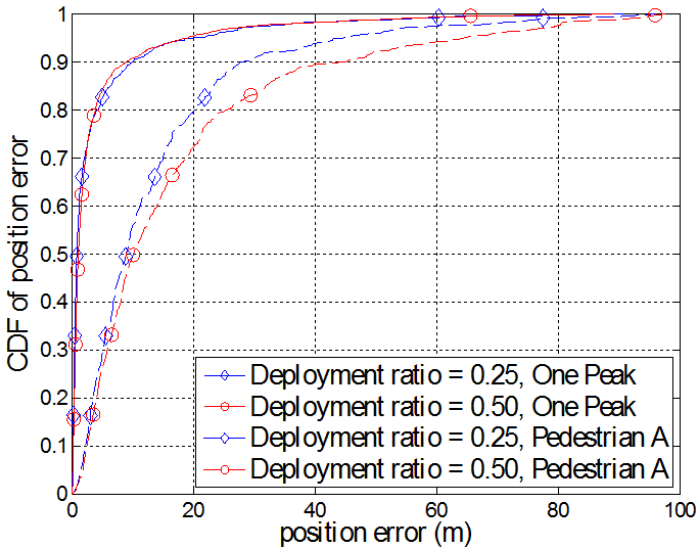

Figure 3-1 CDF of position errors

The position error at 67-percentile is below 2 m in case One Peak channel model is assumed. As the multipath profile of Pedestrian A channel results in larger errors in TDOA estimates, position error at 67-percentile is around 15 m.

3.2 Automatic Coverage Estimation

3.2.1 Problem Statement

In order to enable self-organisation, cellular systems need to have a framework to estimate their performance and diagnose specific performance related problems to trigger appropriate self-organising

mechanisms. While much work is ongoing on self-organization in cellular networks, work on *enabling self-organization* is still scarce.

3.2.2 Algorithm Description: RACE

Here, we propose a novel algorithm for autonomous coverage estimation of an access point, which could subsequently be used for triggering various self-organising functions and hence acts as an enabler for self-optimisation and self-healing. The algorithm is named as RSRP (Received Signal Received Power) based Autonomous Coverage Estimation (RACE). RACE can be used to estimate the coverage of a node based on the user RSRP reports and their position information in an autonomous manner. This coverage estimation is carried out by dividing the coverage area into virtual bins and estimating expected coverage in each bin by averaging the RSRP reports of users whenever they are located in that bin. The steps that need to be executed at each access point in order to obtain the coverage map autonomously are explained below:

- Entire coverage area is divided in virtual bins.
- Each UE's location is determined at the access point and based on its location it is allocated to the respective bin. It should be noted that location estimation is not part of coverage estimation algorithm. It is assumed that knowledge of the UE location (with some inaccuracy) is available at the access point by any of the existing technologies like GPS or other methods available in literature.
- Each UE reports its RSRP to the access point, which in turn logs these RSRP measurements together with the bin in which the UE lies.
- These reports are collected over a long period such that all the bins in the potential coverage area have been reported from by at least one UE.

The access point determines whether or not a given bin is covered by comparing the average RSRP reported from that bin with a threshold RSRP that indicates minimum level of coverage, e.g. -124 dBm in 3GPP LTE [15].

3.2.3 Simulation Results

Figure 3-2 shows the coverage map obtained through the RACE algorithm. Bin size of 50m × 50m is used. Total 80000 users are dropped in the whole cellular network of 19 cells with total area of around $\pi (1200\times2.5)^2$ m^2. It can be seen in the figure that other than the overall characterization of coverage, the coverage map can be used to identify the location and intensity of dead zones as well.

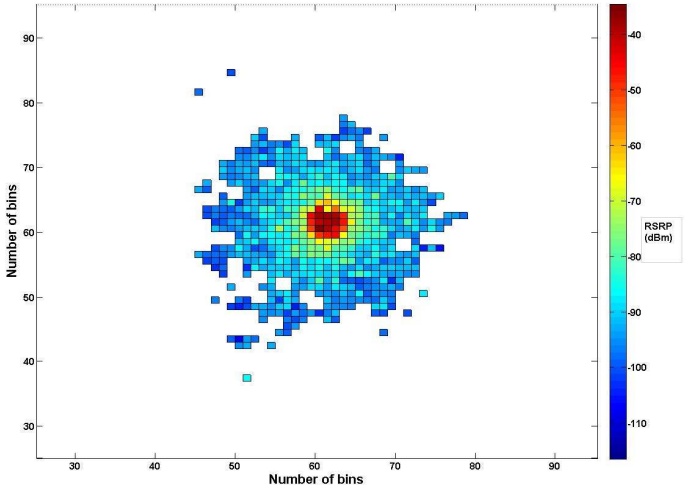

Figure 3-2: Autonomously generated coverage map at central eNB

Effect of Bin size and positioning error on RACE: In order to quantify the effect that the bin size can have on RACE, the actual coverage is first determined and the estimated coverage is compared against it using it as benchmark. Figure 3-3 shows the error in estimated coverage calculated for a range of bin sizes. As expected, it can be seen that the bin size has noticeable impact on the accuracy of the estimated coverage. The smaller the bin size, the more accurate is the coverage map. However, the accuracy achievable with small bin size comes at the cost of the increased processing complexity and storage space required for implementing RACE with smaller bin size. Furthermore, implementation of RACE with

smaller bin size also require more accurate user positioning algorithm to identify the exact location and thus the exact bin in which each user lies.

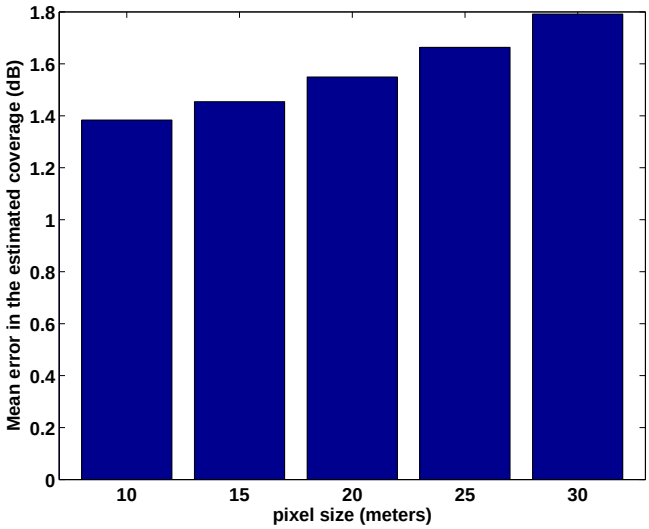

Figure 3-3: Error in the estimated coverage with reference to the actual benchmark coverage for range of bin size

RACE relies on the positioning information of the user to calculate the coverage maps. The state of the art positioning algorithms suffer from certain amount of error in their estimation of the position. Therefore it is important to investigate the effect of positioning error on the performance of RACE. To this end extensive simulation based analysis has been carried out to evaluate the impact positioning can have on the coverage level estimated by RACE as outlined in [16]. It can be seen that as expected the mean error in the estimated coverage increases as the positioning error increases. The trend is the same for different bin sizes. However, the smaller the bin size, the more sensitive the RACE is to the positioning error. Thus, the tolerance of RACE to large bins is particularly advantageous because larger bins size not only allows for low implementation complexity of RACE but it also decreases the sensitivity of RACE to positioning error.

3.2.4 Algorithm Description: ABE

Although RACE is a very useful mechanism in identifying the location of coverage dead zones, for some SON algorithms, e.g. handover parameter optimization, knowing the definitive boundary of the coverage area autonomously at the access point is vital. Automatic Boundary Estimation (ABE) algorithm proposed here provides a simple method to estimate the boundary of coverage area autonomously and is inspired by a boundary estimation suggested method in [17] and used for estimation of geographical spread of population of various species in the field of ecology. The procedure for algorithm is explained as follows.

The coverage map obtained through RACE is divided into M virtual angular strips. For a given strip, an arbitrary temporary value of radius is assumed that represents the temporary boundary of that strip. The bins in that strip are then petitioned into *rightly classified* and *misclassified bins*, for that temporary boundary. Misclassified bins are the bins outside the boundary that have required level of coverage, or bins inside the boundary that do not have required level of coverage. The temporary boundary is then optimised to minimise the number of misclassified bins in that strip. Using this procedure for each strip, the optimal radius is obtained for the each strip. The boundary of the coverage area of each access point can be obtained by joining the radii of all strips as shown in Figure 3-4.

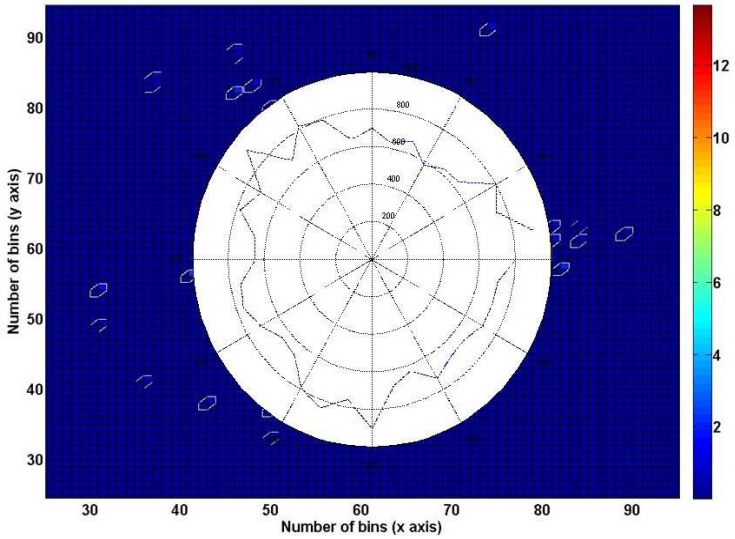

Figure 3-4: Automatically predicted coverage boundary for central eNB

3.2.5 Conclusions

The spectral efficiency metric is not directly applicable to RACE and ABE algorithms. However, the RACE algorithm can be used to determine the dead zones autonomously. Thus, RACE can be used to trigger SO techniques and thus boost system performance in terms of spectral efficiency. Similarly, the autonomously estimated boundaries of coverage area determined through the proposed ABE algorithm can also be used to trigger a number of SO techniques that aim at capacity, fairness and coverage optimization such as handover parameters optimization, etc. All these can substantially increase system spectral efficiency and also the call drop rate as another important measure..

3.3 Biologically Inspired Network Synchronization

This synchronization method proposes to achieve slot synchronization, i.e. agreement on a common transmission start and slot duration, by exchanging a synchronization word between femtocell entities. The synchronization word is common to all nodes, and is already included in the standard in the form of the PSS and SSS (Primary and Secondary Synchronization Sequences). The update rules for adjusting local clocks both in time and frequency are inspired from the natural phenomenon of firefly synchronization. This way, synchronization emerges over time, and also adapts to changes in the network topology.

Compared to existing solutions, the proposed method has a number of advantages, namely frequency synchronization is performed simultaneously with time synchronization; no additional overhead is required, as the existing PSS and SSS sequences; synchronization is reached for any initial timing and frequency offsets. As a limitation, scalability becomes an issue in very large networks, e.g. more than 100 femtocells synchronizing simultaneously. This issue may be circumvented when the timing reference from a macrocell can be accessed within the considered femtocell network.

The interested reader is referred to [68] for further details.

3.4 RF Front-End Functionalities for Self-Optimization

The power control and the sniffer capabilities in the RF are used by some algorithms in WP4. In this section a power control is described and simulations with results are presented. The sniffer capability, also known as Network Listen Module (NLM), is described.

3.4.1 Power Control

The High Power amplifier (HPA) is the element that feeds the antenna in the transmitter part and provides the desired levels of the output signal. Femtocell requirements include both absolute and relative accuracy for transmit power requirements [21]. The absolute requirements define a lower and an upper transmit power limit relative to a nominal transmit power. The relative requirements define a minimum and maximum transmit power difference between two transmitted slots, not necessarily adjacent time slots, as well as an aggregated transmit power difference over several time slots. There are two types of loops to implement the power control: closed-loop and open-loop.

Closed-loop power control represents one method for controlling the transmit power within the wireless communication device to comply with the relative and absolute transmit power requirements. Using a sample of the transmitted power, an error signal with respect to a reference is calculated and with this signal, the transmitted power signal is corrected. This type of control loop has the limitation of the power detector dynamic range. Another type of power control loop is the open-loop power control. It adjusts the transmitted power in response to power control commands produced by operational parameters and/or environmental conditions. These commands can be described as power commands produced by the Network Management, the own unit detection of low traffic load (dormant state) or user pushing a save energy mode. The combination of open-loop with closed-loop avoids [20] the transmit power to drift away from the desired transmit power.

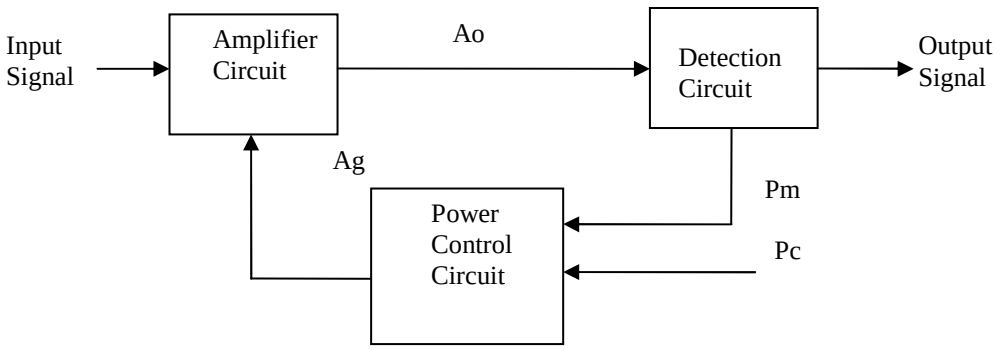

Figure 3-5: Power control.

3.4.1.1 Block scheme

A way to obtain both an open and closed loop for the power control is to introduce an automatic control gain loop that has a reference like shown in Figure 3-6. This figure shows a first approach using a monotone source and an ideal AM (Amplitude Modulation) detector.

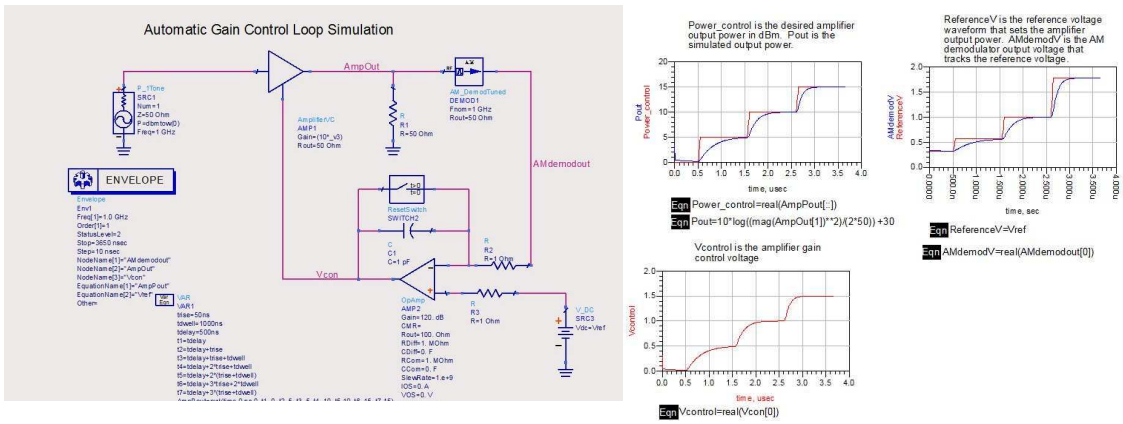

Figure 3-6: Gain control loop.

This type of loop uses a detected power provided by an AM detector and an error integrator controls a VCA (Voltage Controlled Amplifier) with the signal obtained from subtraction between a reference and the detected power.

A directional coupler at the output from the VCA allows that output signal suffers no distortion (only about 1 dB loss) and avoids mismatch due to the feedback loop in real implementation, Figure 3-7. This directional coupler also reduces the level of the detected signal in approximately 20 dB, changing the maximum level of the sample used in the control loop from 10 dBm to -10 dBm when max Pout for the LTE transmitter is required.

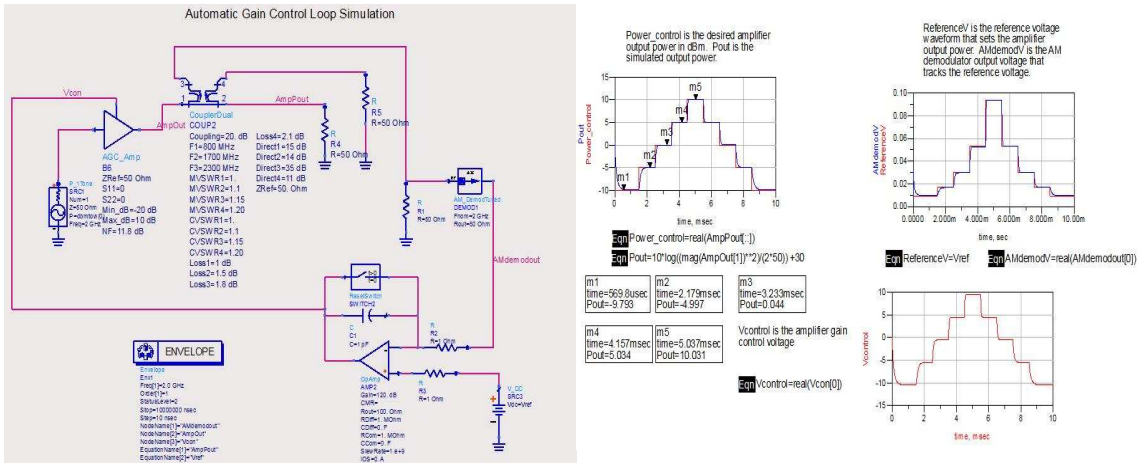

Figure 3-7: Gain control loop with directional coupler.

In a more real implementation the AM detector need to be changed to a log detector that allows to get info down to -80 dBm. Some manufacturers describe the logdetector as a cascade of amplifiers and detectors made with pin diodes that allow obtaining a more linear detected power. See Figure 3-8 and Figure 3-9.

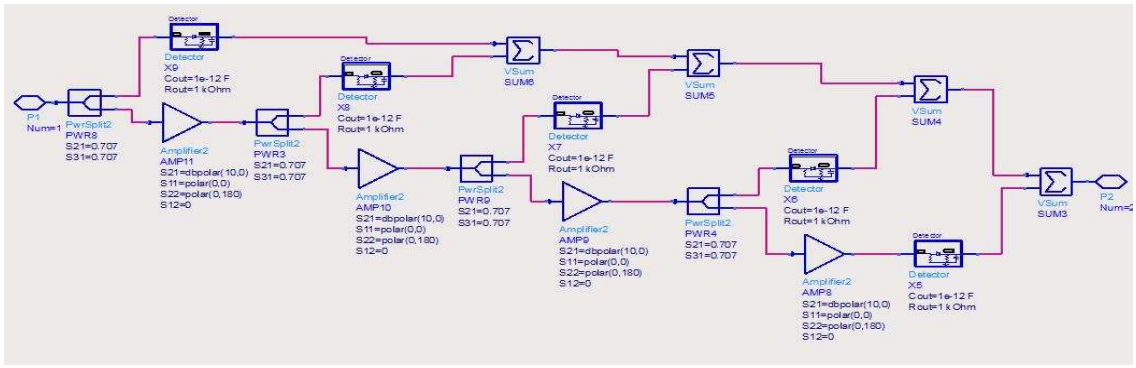

Figure 3-8: Logdetector module.

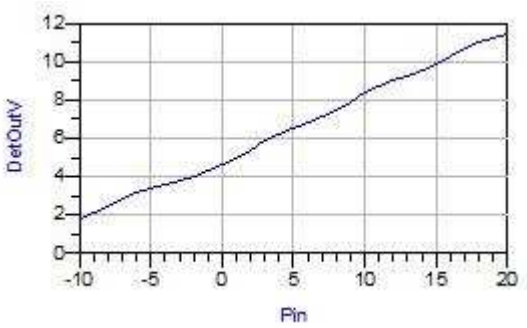

Figure 3-9: Logdetector detected power to Pin.

The detector that appears in Figure 3-8 has a non linear response in the detected power, see Figure 3-10 Using the above described logdetector, that internally is the cascade of detectors, followed each of them by an amplifier, less error and noise are introduced in detected power for low input power level.

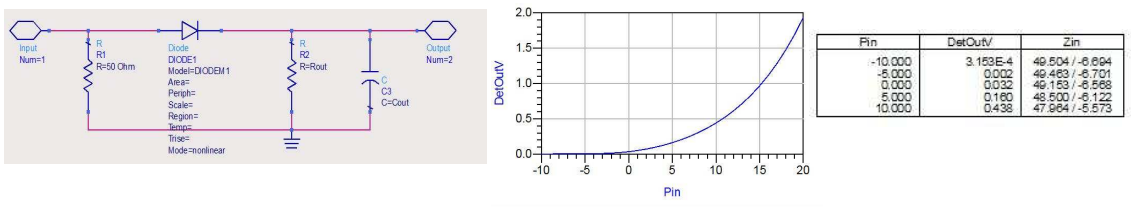

Figure 3-10: Detector scheme and its response.

3.4.1.2 LTE Simulations

For simulation results in this section, the LTE source is FDD, the loop filter used is an AGC (Automatic Gain Control) filter and the VCA is VcGainRF. These last two elements are described below.
The LTE signal is generated with 0 dBm at 2.1 GHz and its level for all the following simulation results is reduced in 22.5 dB to show how the end part of the RF front module works to obtain a desired output power passed to the antenna (-10 dBm to 10 dBm levels). The amplifier chain that simulated the end RF part is composed by a fixed amplifier of 10 dB followed by a VCA controlled by the AGC filter and an end fixed amplifier of 12.5 dB. With these three amplifiers the signal goes up to the desired level. The full scheme is shown in Figure 3-11.

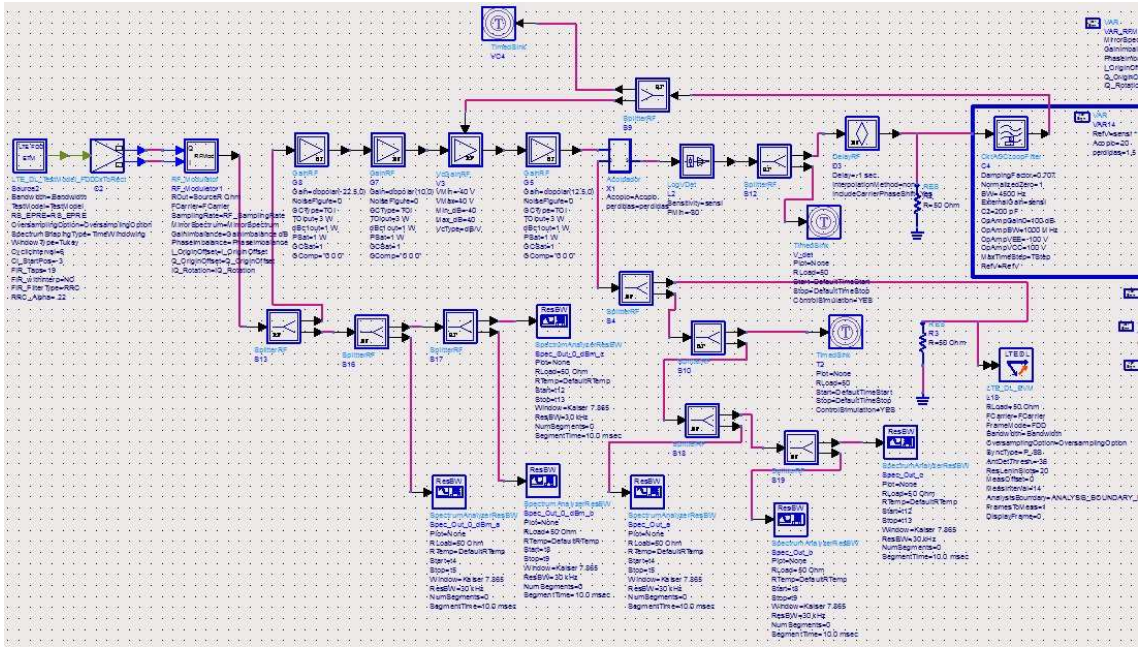

Figure 3-11: Scheme used in LTE simulations.

The model used for the logdetector has lineal response down to -80 dBm and sensitivity of 0.005V/dB.

3.4.1.2.1 AGC filter

The AGC filter used to obtain the voltage that controls the VCA is shown in Figure 3-12 and is described in [90].

It is composed by a voltage-controlled voltage source followed by an OpAmp (Operational Amplifier) component that forms the loop filter to work with the AGC loop. A second-order feedback loop is formed based on the DampingFactor and NormalizedZero parameters that must be specified.

The ExternalGain specifies gain external to this filter and the internal filter gain will be automatically set to achieve the specified second-order loop characteristics.
VrefV is the reference voltage for control loop OpAmp, proportional to the desired output power and that can be variable.

Scheme of the AGC filter is shown Figure 3-12.

The values used for the simulations are: ExternalGain=0.05 and DampingFactor=0.707.

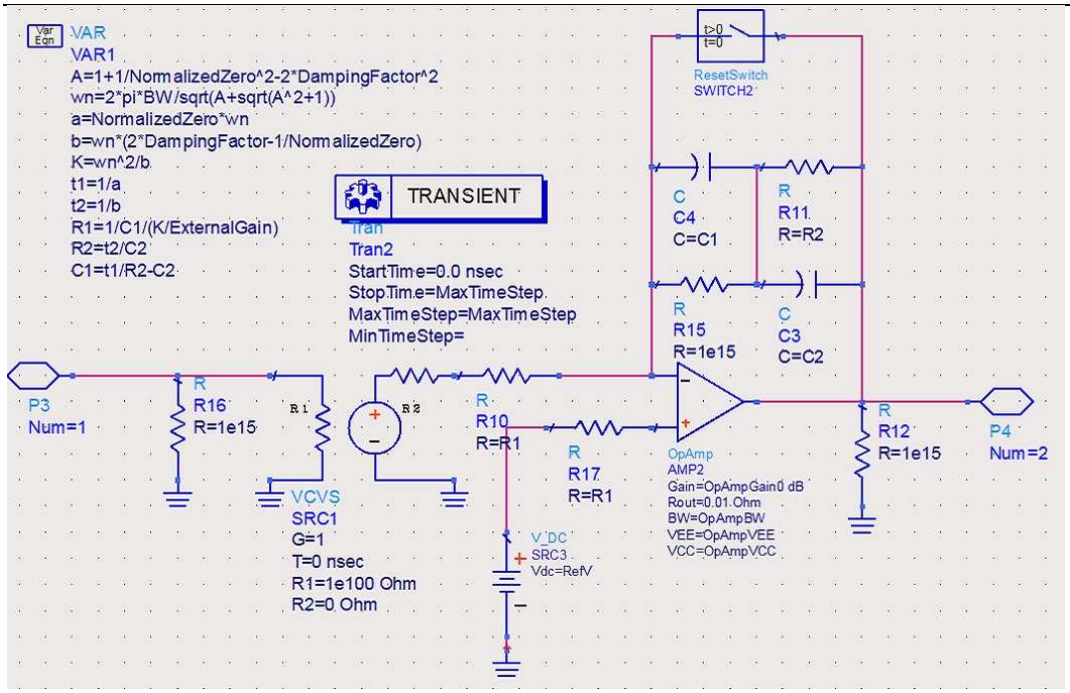

Figure 3-12: AGC filter.

3.4.1.2.2 VcGainRF

The VcGainRF used as VCA is a voltage controlled amplifier model that may include nonlinear gain compression.

The small signal gain is controlled by
- the voltage at pin 2, V2(t), above terminal in VCA module from Figure 3-13,
- the parameters Vmin, Vmax, Min_dB, Max_dB and VcType.

VcType is used to choose between two conversion types to obtain the power gain of the VCA, linear or dB/V (the different formulas are shown below).

V2(t) is limited by a lower limit of Vmin and a maximum limit of Vmax. The minimum gain, Min_dB, occurs for V 2 (t)=Vmin. The maximum gain, Max_dB, occurs at V2(t)=Vmax.
The gain characteristic for V2(t) between VMin and VMax is set by VcType to be either a dB/V characteristic or a linear characteristic.

For VcType=dB/V, the small signal power gain

$$PowerGain(dB) = Min\_dB + \frac{(V2(t) - V\min) \times (Max\_dB - Min\_dB)}{V\max - V\min} \quad (3.1)$$

For VcType=linear, the small signal power gain

$$PowerGain(dB) = 20 \times \log_{10}(VoltageGain) \quad (3.2)$$

where

$$VoltageGain(dB) = \frac{V2(t) - V\min}{V\max - V\min} \times 10^{\frac{Max\_dB}{20}} + \frac{V\max - V2(t)}{V\max - V\min} \times 10^{\frac{Min\_dB}{20}} \quad (3.3)$$

For the simulations, whose results are shown in this section, the following values had been used: VcType= dB/V, VMin=-40V, VMax=40V, Min_dB=-40 and Max_dB=40

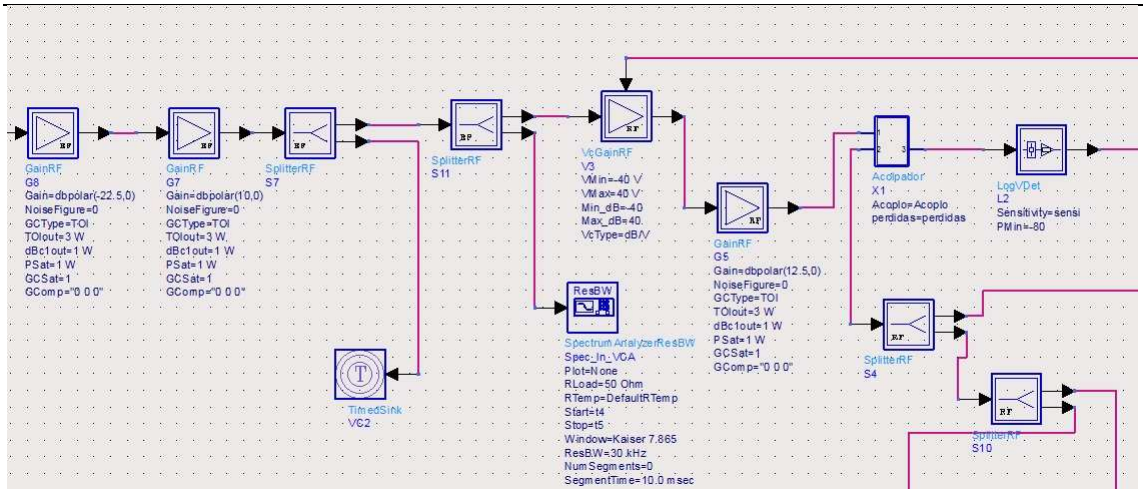

Figure 3-13: Detail of LTE scheme

After the power obtained from the LTE source is reduced by 22.5 dB three Amplifier are used. The first amplifier introduces 10 dB gain and then a VCA, controlled by the AGC loop, feeds the last Amplifier that introduces a 12.5 dB gain. This last amplifier works as a HPA that feds the antenna and the Logdetector using a coupler. The coupler has a 20 dB coupling factor and 1.5 dB losses in the direct branch to the antenna, a quite real data. The splitters shown in Figure 3-13 and Figure 3-11 are used to obtain measuring points in the simulations and introduce no losses or distortions.

3.4.1.3 Simulation Results

Following figures shows the simulation results obtained for BW=20 MHz, 15 MHz, 10 MHz and 5 MHz.

BW=20 MHz:

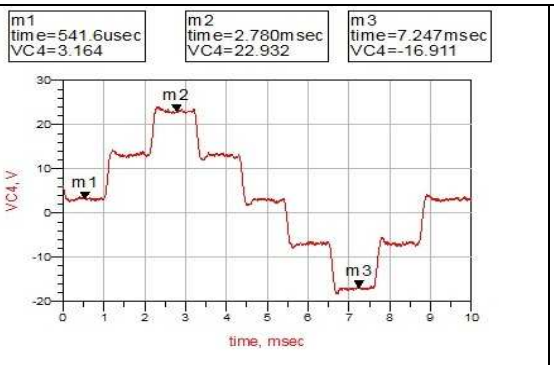

Figure 3-14: VCA control voltage

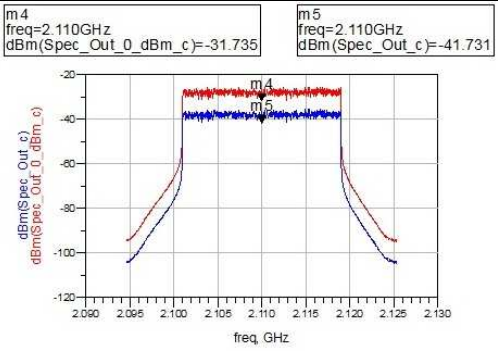

Figure 3-15: Output power for -10dBm

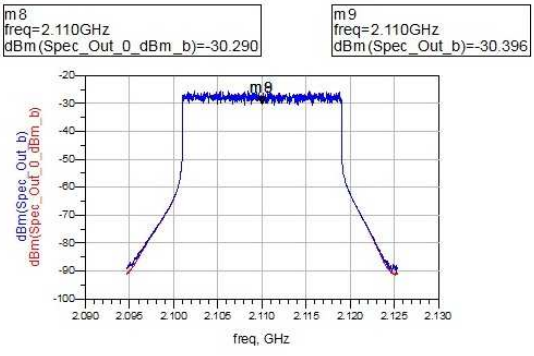

Figure 3-16: Output power for 0dBm

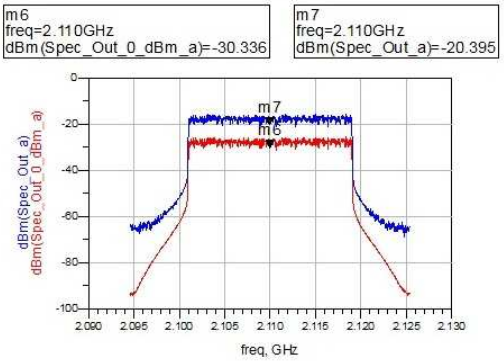

Figure 3-17: Output power for 10dBm

Figure 3-14 shows the output power of the AGC loop that feeds the control input of the VCA and changes in time to obtain different output power levels between -10dBm and 10 dBm (-10dBm, -5dBm, 0dBm, 5dBm and 10dBm). In Figure 3-15 to Figure 3-17 the blue lines are the output power that feed the antenna and red lines are the output power from the LTE source that has a 0dBm level.

Similar description is applied for following BW=15MHz, 10 MHz and 5MHz cases and shown in Figure 3-18 to Figure 3-29.

BW=15 MHz:

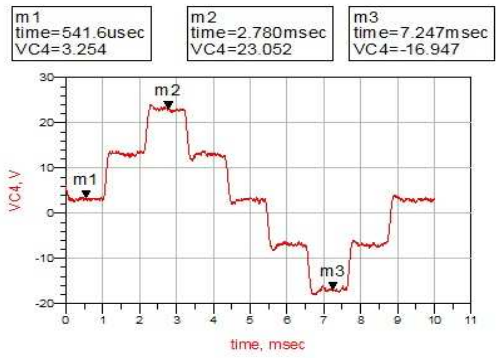

Figure 3-18: VCA control voltage

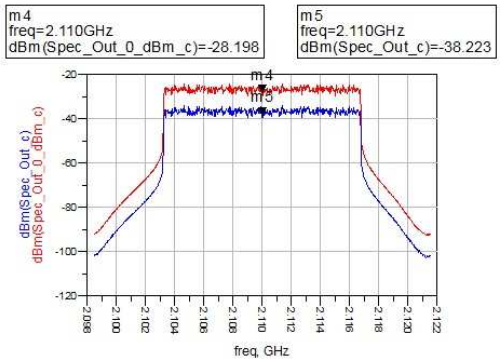

Figure 3-19: Output power for -10dBm

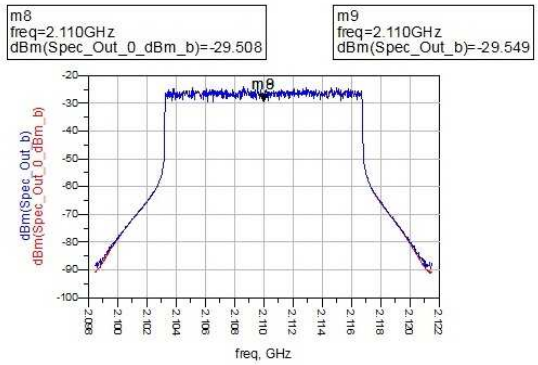

Figure 3-20: Output power for 0dBm

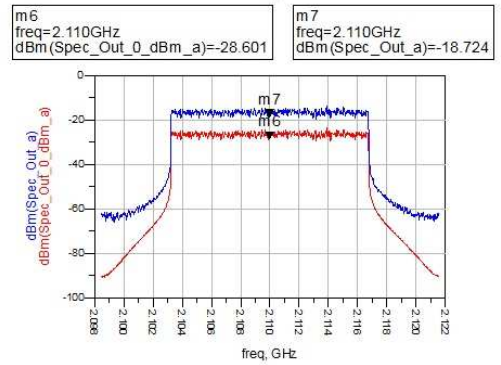

Figure 3-21: Output power for 10dBm

BW=10 MHz:

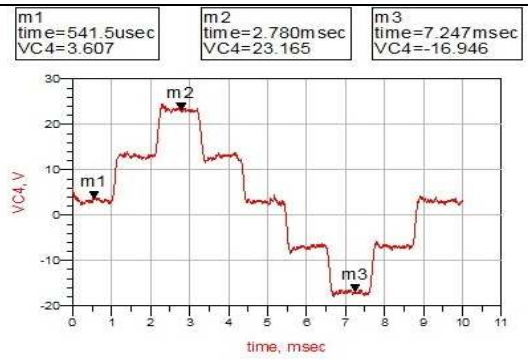

Figure 3-22: VCA control voltage

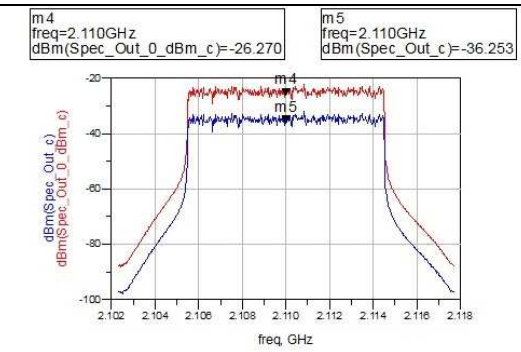

Figure 3-23: Output power for -10dBm

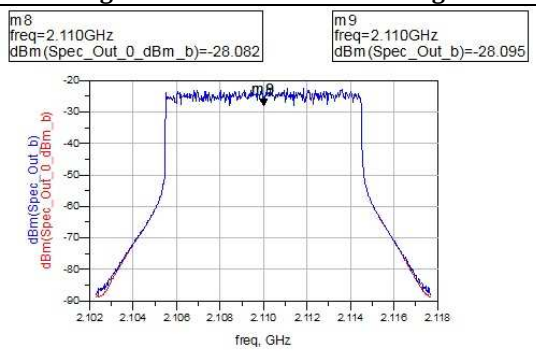

Figure 3-24: Output power for 0dBm

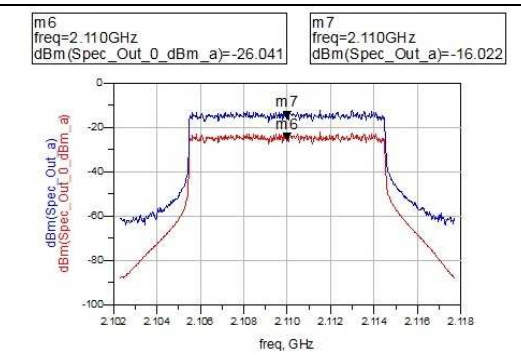

Figure 3-25: Output power for 10dBm

BW=5 MHz:

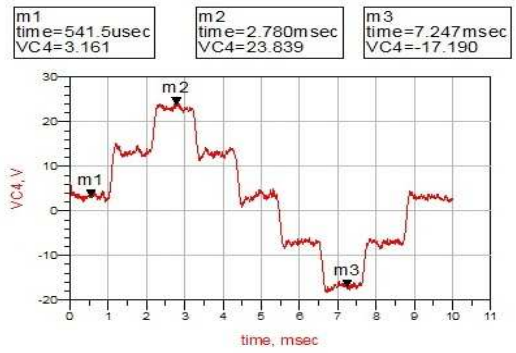

Figure 3-26: VCA control voltage

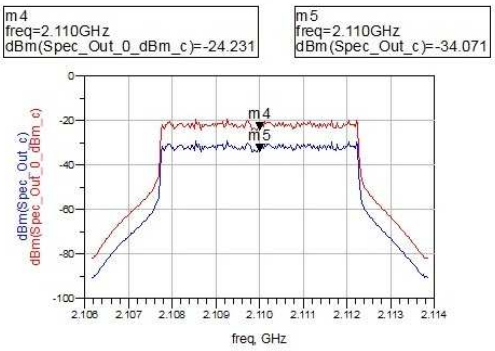

Figure 3-27: Output power for -10dBm

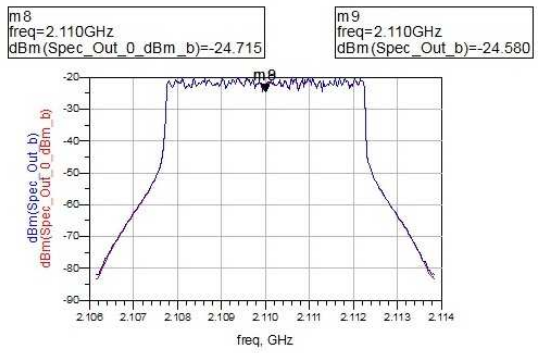

Figure 3-28: Output power for 0dBm

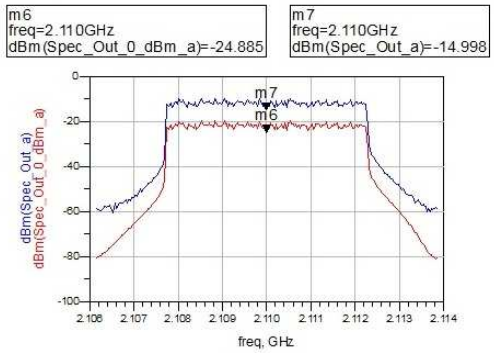

Figure 3-29: Output power for 10dBm

Table 3-1 shows the Error Vector Magnitude (EVM) error, described in [21], calculated over a frame (1msec) for different output power levels and BWs. For E-TM3.3 the limit is 17.5% (QPSK modulation), for E-TM3.2 the limit is 12.5% (16QAM modulation) and for E-TM3.1 the limit is 8% (64QAM modulation)

Table 3-1: EVM error.

	-10dBm	-5dBm	0dBm	5dBm	10dBm
	EVM% for BW=20 MHz				
E-TM3.1	0.762	1.027	1.048	1.035	1.170
E-TM3.2	0.903	1.319	1.335	1.332	1.499
E-TM3.3	1.048	1.729	1.724	1.733	1.998
	EVM% for BW=15 MHz				
E-TM3.1	1.317	1.313	1.318	1.325	1.410
E-TM3.2	1.894	1.893	1.859	1.852	2.005
E-TM3.3	2.077	2.077	2.069	2.088	2.323
	EVM% for BW=10 MHz				
E-TM3.1	2.364	2.365	2.364	2.372	2.413
E-TM3.2	2.290	2.279	2.270	2.298	2.140
E-TM3.3	2.918	2.918	2.926	2.935	3.071
	EVM% for BW=5 MHz				
E-TM3.1	3.582	3.574	3.602	3.567	3.596
E-TM3.2	3.333	3.332	3.339	3.350	3.360
E-TM3.3	6.098	6.095	6.160	6.084	6.111

Allowing the transitions between levels to take place at the end of frames and taking 10 frames (10 msec) the EVM stays in similar levels as described in Table 3-1, see Table 3-2

Table 3-2: EVM error

	20 MHz	15 MHz	10 MHz	5 MHz
E-TM3.1	1.048	1.325	2.367	3.602
E-TM3.2	1.329	1.897	2.274	3.347
E-TM3.3	1.727	2.091	2.953	6.15

Figure 3-30 to Figure 3-33 show the 64QAM, 16 QAM and QPSK constellations.

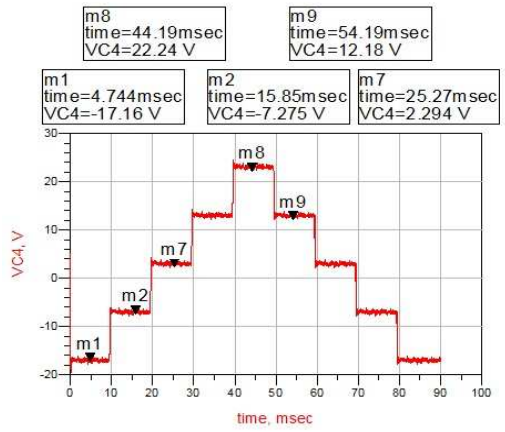

Figure 3-30: VCA control voltage

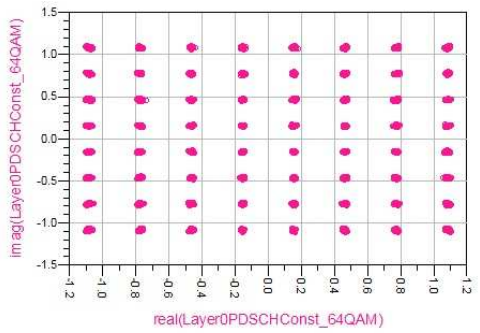

Figure 3-31: 64 QAM constellation

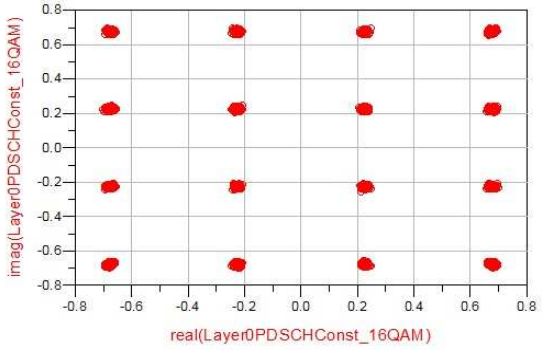

Figure 3-32: 16 QAM constellation

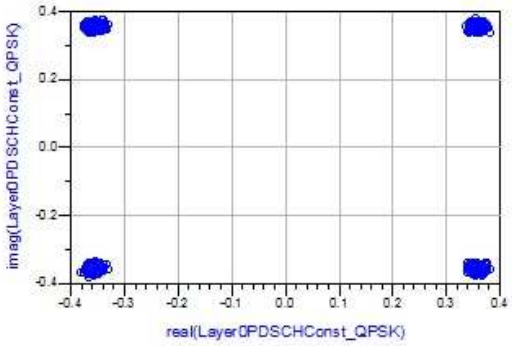

Figure 3-33: QPSK constellation

This type of power control loop also allows recovery from temporary failures of other RF chain components. Working in normal conditions is shown in Figure 3-34.

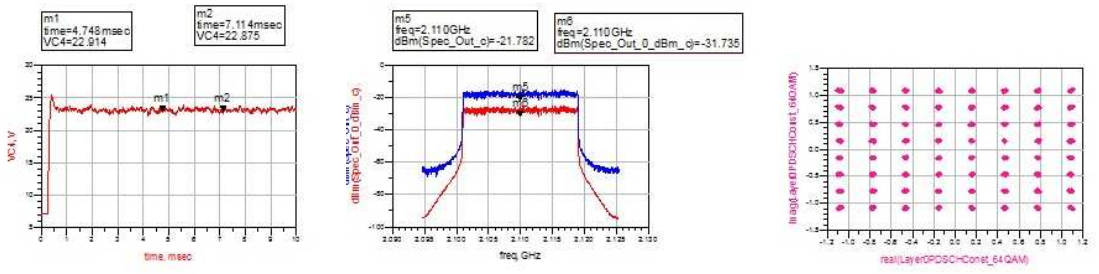

Figure 3-34: VCA voltage control, output power and 64QAM constellation in normal conditions.

Working with 2dB fail of one of the fixed amplifiers is shown in Figure 3-35. The VCA voltage produces a +4V signal to compensate the 2 dB losses fixed amplifier.

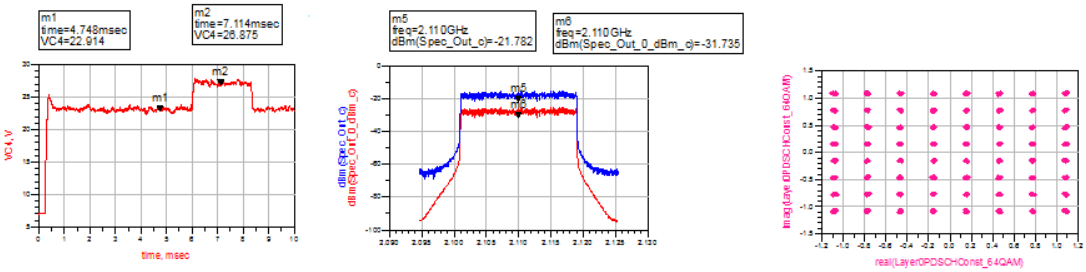

Figure 3-35: VCA voltage control, output power and 64QAM constellation in failure conditions.

3.4.1.4 Conclusions

The open-closed power loop block scheme presented in this section allows to follow changes of the desired transmitted power, that can be required for modifications in the output power level by SON algorithms. The spectrum of the output power signal is not significantly disturbed and errors shows by EVM are kept unther the maximum levels specified The simulations also show that this scheme recovers from possible power failures of other components in the RF transmitter chain.

3.4.2 Sniffing Capability

3.4.2.1 Sniffer Overview

The Sniffer Module is a real-time system that continuously captures/monitors data or signal passing through the network. It is also called Network Listen Module (NLM), Network Monitor Module (NMM), Radio Environment Measurement (REM) or "HeNB Sniffer" in [24] and [25]. With it, the HeNB incorporates functionalities of user receiver, that is, a downlink receiver with a special possibility of performing calculation of Reference Signal Received Power (RSRP), Reference Signal Received Quality (RSRQ) to obtain the power received from other femtocells and macrocells at FBS. With these measurements, a femtocell can calculate the best working point taking into account coverage and interference to both too close co-channel macrocell users (that they listen on their conventional UL receiver) and co-channel FBSs (monitored by the NLM). Other type of measurements described in [26] are performed in order to minimize interference to adjacent MUEs and macrocells, detection of victim UEs, and to obtain other cell IDs.

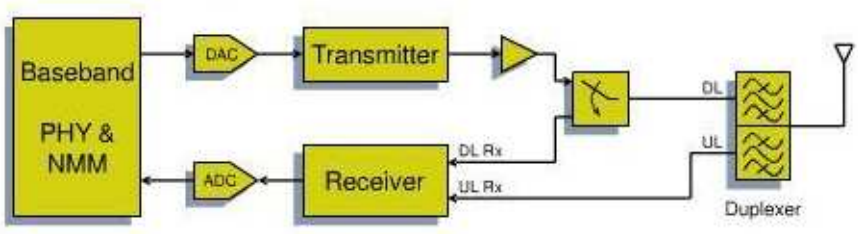

Figure 3-36: Sniffer Module.

Standalone femtocells can use the sniffer capabilities to obtain information about their environment and take decisions in accordance. Measurements performed by the sniffer module are also used by SON techniques implemented in Networked femtocell. To implement this sniffer capability, the femtocell needs to incorporate a DownLink receiver with UE receiver characteristic described in [89] if transmit and receive frequencies are different.

This sniffing capability is used in networked femtocells to minimize interferences between femtocells and macrocell deployments. For standalone femtocells it can also be useful to calculate interference from macrocell and to obtain input to optimize transmitting power to minimize interference to macrocell.

3.4.2.2 Conclusions

The sniffer block is a useful tool whose measurements can be used in SON techniques to adapt the transmitting power taking into account interferences to other users and systems. For FDD systems, a

receiver with full RF chain is needed to perform NLM measurements, that are in fact those defined for user equipments, viz. RSRP and RSRQ.

4. SON Algorithm Descriptions

This section is entirely dedicated to the various local, distributed and central SON algorithms. Again, for the sake of completeness not only novel contributions are documented but also prior SON algorithms, which are deemed to be promising, are dwelled on.

4.1 Local SON Algorithms

4.1.1 Automatic Coverage Control

Literature investigation provides different methods to have control over uplink and downlink coverage based on measurements of real deployments, with which automatic coverage estimation can be performed. This automatic estimation can mismatch from a desired coverage because it takes into account the presence of alien mobiles (FUEs from other femtocells and MUEs) and other events that produce interference and can reduce the coverage.

4.1.1.1 Downlink Coverage

Using the transmitter with fixed power is not an optimal solution when there are co-channel deployments in the neighbourhood. Three main methods based on the control of the transmitted power transmitted by the femtocell are presented, i.e. Network Listen, Mobile Assisted Range Tuning and Active Macro Mobile Protection.

- Network Listen (NL): This type of Downlink Tx power configuration is described in [19]. In this method, the femtocell's transmitted power is configured using the measurement of the received power from the macrocell and doing corrections. There must be constraints to set power to the femtocell transmitter that are Macro Mobile Protection Constraint and Home Mobile Coverage Constraint. The femtocell power is configured to produce a minimum received power for a potential user at a distance r placed between the macrocell and femtocell. This potential FUE will receive the transmitted power from the femtocell reduced by the propagation losses. The initial femtocell power, P_{femto} can be calculated in decibels as $P_{femto} = \min\left(\left(P_{rx\_from\_macro} + L_{femto}(r)\right), P_{femto\_Tx\_\max}\right)$, where $P_{rx\_from\_macro}$ is the power received by the femtocell from the macrocell, $P_{femto\_Tx\_\max}$ is the maximum power the femtocell can transmit and $L_{femto}(r)$ is the estimated path-loss from the femtocell to a FUE at the target femtocell radius *r modelled as* $L(d) = L1 + L2 \times 10\log_{10}(d)$ L1 and L2 depend on the propagation model used

- Mobile Assisted Range Tuning (MART): This method is described in [18] and gives a more accurate estimation of coverage radius and improved tx power adjustment. Moreover, this method achieves a balance between coverage and interference minimization.

  Adequate coverage for home users can be ensured by using channel quality reports from home mobiles. A femtocell can request a home mobile to periodically measure and report back DL channel quality metrics. By using these reports, the femtocell can estimate the path- loss between itself and a home mobile at different locations in the home, and also learn the macro signal. Unlike Network Listen, reports from home mobiles allow the femtocell to sample RF environment at different locations in the home. Thus, a femtocell can learn the desired coverage range and also handle the measurement mismatch issue that fills Network Listen. As a result, by combining information from alien user registration statistics and home mobile reports, a femtocell can determine the optimal power.

- Active Macro Mobile Protection (AMMP): MART method [18] helps to reduce femtocell interference to macro users, but it cannot completely eliminate this interference. For example, guest users visiting a femtocell home and receiving service from a macrocell can still face significant interference. AMMP method gives better results than always transmitting with low power because it only sacrifices femtocell coverage when a macro user is detected. An active macro mobile is in femtocell vicinity and therefore is being interfered on the DL by the femtocell (macro and femtocell are co-channel). The femtocell detects the presence of a macro user in its vicinity by continuously measuring out-of-cell interference on the Uplink channel. Out-of-cell interference level above a certain threshold serves as an indication of the presence of an active macro user in the femtocell vicinity. When out-of-cell interference greater than a certain threshold

is observed, the femtocell "throttles" its DL transmission, i.e., it reduces Tx power on its DL or completely shuts down DL temporarily to protect the active macro mobile. The new Tx power level can be determined as a function of the out-of-cell interference level. Normal DL transmission is resumed by discontinuing throttling after a time out or when the out-of-cell interference level falls below a certain threshold.

4.1.1.2 Uplink Coverage

The main problem that concerns the uplink operation is high level received signals. A FUE can get arbitrarily close to the femtocell and it cannot obey the power control (PC) down commands due to reaching its minimum transmit power capability because the dynamic range has a limit. Such transmitting higher than the required power may desensitize the femtocell receiver.

- Uplink Adaptive Attenuation (UAA): One simple solution to deal with the high input power problem is to raise the input threshold. A better solution is to desensitize the interference by attenuating the signal at the receiver. As a result, interference operation is more comparable to thermal noise. Another advantage is that the attenuation pulls nearby FUEs to a power controllable range and solves the saturation problem, using attenuation only when high out-of-cell interference or receiver desensitization is detected at the femtocell. The UL signal to be attenuated only when the total received signal level is saturating the receiver or the UL is being jammed by a nearby non-associated cell.

4.1.1.3 Simulation Results

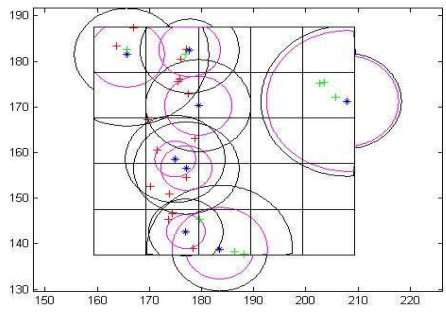

Figure 4-1: Example of coverage with P_{FBS}=10 dBm and interference from macrocells, other FBSs MUEs and other FUEs

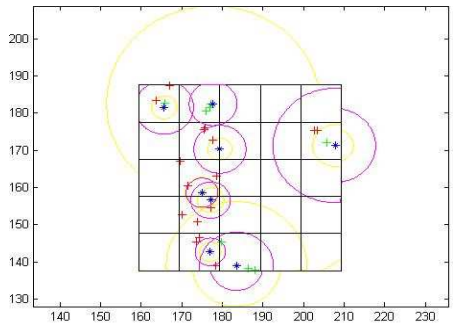

Figure 4-2: Example of coverage with P_{FBS}=opt dBm and interference from macrocells, other FBSs MUEs and other FUEs.

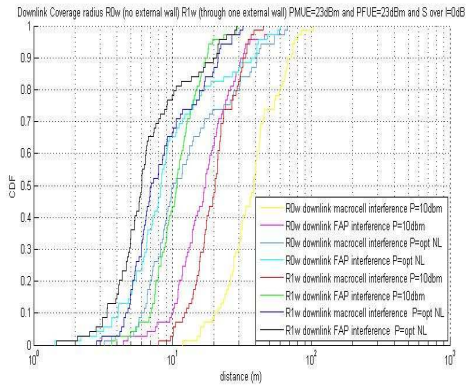

Figure 4-3: Downlink coverage radius.

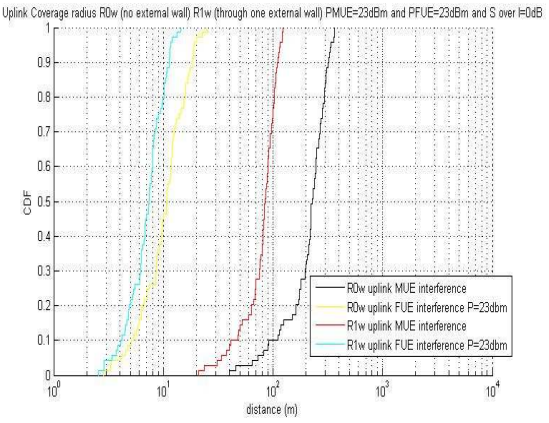

Figure 4-4: Uplink coverage radius.

In Figure 3-5.and Figure 3-6 an example of combination of downlink for NLM and uplink coverage is shown. In this case SINR is 0 dB. The blue stars represent the femto Base Station (FBS) active inside the apartment block and the crosses are FUEs. If the FUE receives signal from above SINR and its FBS also receives signal above SINR it is green cross. If in one or both cases received signal is not above SINR its colour is red. Downlink coverage with P_{FBS}=10 dBm are black lines in Figure 3-5. Downlink coverage with

P_{FBS} =Popt dBm from NL method are yellow lines in Figure 3-6. Uplink coverages in the two figures are represented by pink lines. Details of the particular setup and variables used are in BeFEMTO D4.2 [16].

In Figure 3-7, the CDF of the different coverage radius are shown for SINR=0 dB and all the FUE inside their apartments. In Figure 3-8, the CDF of the different coverage radius are shown for SINR=0 dB and all the FUE inside their apartments.

For the interested reader, there are more simulations results tabulated in BeFEMTO D4.2 [16].

4.1.1.4 Conclusions

Simulations implemented in Matlab for NL, MART, AMMP and UAA shown in this section can give rough coverage estimation like the 0-wall radius and 1-wall-radius before and after using the different coverage control methods. They are useful to a first contact to coverage control and coverage estimation. Losses have been calculated using general formulas and knowing distance between macrocells, FBSs and FUEs obtained from their location information. For the real world case, path losses can be calculated using measurements of received power and distance between the different macrocells, FBSs and users if the location info of each one is reliable or can be estimated with negligible error.

4.1.2 Self-Organizing Interference Management Techniques for Femtocell Networks

4.1.2.1 Problem statement

Driven by the massive data traffic increase, network densification and scarce frequency resources, efficient interference management techniques are needed, in which small cell base stations (pico-, femto-cells, relays) self-organize in a totally decentralized manner. For doing so, they rely on local information at cell level and no information exchange among femtocells; *only* a (possibly imperfect) feedback from the served FUEs is required. During their self-organization procedure, every femtocell needs to strike a balance between *exploitation* and *exploration*. While in the former femtocells exploit the accumulated knowledge over time when taking some strategies (i.e., power level on a given frequency band), in the latter femtocells explore new strategies which may yield higher performance. Our proposed self-organizing interference management algorithm is inspired from reinforcement learning (RL) and game theoretic tools which has received lots of attention in the literature ([27][28][29][30] to cite a very few). In a nutshell, femtocells simultaneously *estimate* their long-term utility metric (i.e., transmission rate) and *optimize* their transmission probability distribution. *Sufficient* conditions are given for the convergence of the RL algorithm to the *epsilon*-Nash equilibrium of the game, which constitutes a stable network operation point.

4.1.2.2 System Model

Let us assume one macrocell (denoted by subscript "0") operating over a set of S frequency bands, and underlaid with an arbitrary number of femtocells K. Let $\Gamma_0 = \left[\Gamma_0^1,...,\Gamma_0^S\right]$ denote the minimum SINR offered by a Macro Base Station (MBS) to its MUEs (1 MUE is scheduled per frequency band). Each femtocell can use any of the available frequency bands to serve its corresponding FUE as long as it does not induce a lower average SINR than the minimum required by the MUE Γ_0. At every time instant, a femtocell serves only one FUE. Let $p_0^{(s)}$ denote the transmit power of MBS on frequency band s,.and the S-dimensional vector $p_k(t) = \left(p_k^{(1)},..., p_k^{(S)}\right)$ denote the power allocation vector of FBS k at time t. Here $p_k^{(s)}(t)$ is the transmit power of femtocell k over frequency band s at time t. All FBSs are assumed to transmit over one frequency band only at each time t at a given power level not exceeding $p_{k,\max}$. Let $q_k^{(l,s)}$ denote the l-th transmit power level when used over channel s. Thus, the discrete action space of FBS k is given by: $A_k = \left\{q_k^{(l,s)} : (l,s) \in L_k \times S\right\}$. L_k is the set of power levels and S is the set of carriers.

Denoting by $|h_{i,j}^{(s)}|$ the channel gain from transmitter j to receiver i on frequency band s, the signal to interference plus noise ratio of MBS at MUE (denoted by subscript "0") is given as follows:

$$SINR_0^{(s)} = \frac{|h_{0,0}^{(s)}|^2 \; p_0^{(s)}}{\sigma_0^{(s)^2} + \sum_k |h_{0,k}^{(s)}|^2 \; p_k^{(s)}} \tag{4.1}$$

Likewise, the SINR of FUE is given as follows:

$$SINR_k^{(s)} = \frac{|h_{k,k}^{(s)}|^2 \; p_k^{(s)}}{\sigma_0^{(s)^2} + |h_{k,0}^{(s)}|^2 \; p_0^{(s)} + \sum_j |h_{k,j}^{(s)}|^2 \; p_j^{(s)}} \tag{4.2}$$

The femtocell utility metric considered is the transmission rate: $u_k(p_k, p_{-k}) = \sum_k \log\left(1 + SINR_k^{(s)}\right)$.

Note that the performance of femtocell k at time t depends not only on its own configuration $p_k(t)$ but also on the configuration $p_{-k}(t)$ adopted by all the other FBSs in the network.

4.1.2.2.1 Solution Overview

The proposed interference management solution is inspired from reinforcement learning. At every time instant t, every FBS k chooses its action from the finite set A_k following a probability distribution function $\pi_k(t) = \left(\pi_{k,q_k^{(1,s)}}(t), ..., \pi_{k,q_k^{(L,S)}}(t)\right)$ where $\pi_{k,q_k^{(l,s)}}$ is the probability that femtocell k plays action $q_k^{(l,s)}$ at time t, that is:

$$\pi_{k,q_k^{(l,s)}}(t) = \Pr\left(p_k(t) = q_k^{(l,s)}\right) \tag{4.3}$$

Then at time t, each FBS k observes a feedback in the form of:

$$\tilde{u}_k(t) = u_k(p_k(t), p_{-k}(t)) \tag{4.4}$$

In the proposed solution, femtocells jointly estimate their long-term utility metric and optimize their probability distribution of the taken strategies. Specifically, the estimated utility function of FBS k when playing action $q_k^{(l,s)}$ is written as:

$$\hat{u}_{k,q_k^{(l,s)}}(t) = \frac{1}{T_{k,q_k^{(l,s)}}(t)} \sum_{n=1}^{t} \tilde{u}_k(n) 1_{\{p_k(n) = q_k^{(l,s)}\}} \tag{4.5}$$

where $T_{k,q_k^{(l,s)}}(t) = \sum_{n=1}^{t} 1_{\{pk(n) = q_k^{(l,s)}\}}$. Once the estimation vector is obtained by every FBS k, $\hat{u}_k(t) = \left(\hat{u}_{k,q_k^{(1,1)}}(t), ..., \hat{u}_{k,q_k^{(L,S)}}(t)\right)$ is used to determine the optimal distribution probability. Now, since femto cells need to strike a balance between their exploration and exploitation procedure in which they should play at every time instant the strategy that yields the highest performance while leaving always non-zero probability for playing other actions, the following decision mapping function is given:

$$\beta_{k,q_k^{(l,s)}}(\tilde{u}_k(t)) = \frac{\exp\left(\frac{1}{\kappa} \tilde{u}_{k,q_k^{(l,s)}}(t)\right)}{\sum_{p_k} \exp\left(\frac{1}{\kappa} \tilde{u}_{k,p_k}(t)\right)} \tag{4.6}$$

where $\beta_{k,q_k^{(l,s)}}(\tilde{u}_k(t)) > 0$ with strict inequality regardless of the estimation vector. (4.6) is known in the game theory jargon as Boltzmann-Gibbs equation, which naturally arises when considering perturbed utility maximization. κ is the temperature parameter.

To summarize, the proposed interference management algorithm inspired from reinforcement learning is given as follows:

$$\begin{cases} \hat{u}_{k,q_k^{(l,s)}}(t) = \hat{u}_{k,q_k^{(l,s)}}(t-1) + \alpha(t)\dfrac{1_{\{pk(t)=q_k^{(l,s)}\}}}{\pi_{k,q_k^{(l,s)}}(t)}\left(\tilde{u}(t) - u_{k,q_k^{(l,s)}}(t-1)\right) \\ \pi_{k,q_k^{(l,s)}}(t) = \pi_{k,q_k^{(l,s)}}(t-1) + \lambda(t)\left(\beta_{k,q_k^{(l,s)}}(\tilde{u}_k(t)) - \pi_{k,q_k^{(l,s)}}(t-1)\right) \end{cases} \quad (4.7)$$

If $\lim_{t\to\infty}\frac{\lambda(t)}{\alpha(t)} = 0$, it can be shown that the proposed algorithm given in (4.7) converges to the so-called epsilon-Nash equilibrium. Furthermore, it is worth mentioning that several other algorithms can be derived from this framework, such as multi-armed bandit [31] etc.

4.1.2.3 Simulation Results

In order to substantiate our results, the proposed solution is verified in an LTE-A simulator. First, let us look at the convergence issues and gauge the impact of the temperature parameter κ given in (4.6). We consider 2 MUEs, 2 sub-carriers and 8 FBSs. Figure 4-5 depicts the convergence behavior of the proposed algorithm in addition to the benchmark comparison based on a genie (*semi-centralized* case) which knows all channels and strategies taken by various femtocells in the network. As can be seen, femtocells can self-organize in a totally decentralized manner while achieving a performance very close to the semi-centralized case. In addition, the smaller κ is, the less patient femtocells are, and thus lower performance is obtained. In contrast, when femtocells are patient enough (larger κ), the gap with the semi-centralized case is bridged. Let us now consider a denser network deployment featuring 6 MUEs, 60 FBSs, and 6 sub-carriers. Figure 4-6 illustrates the average femtocell spectral efficiency of the proposed SON-RL algorithm as a function of the femtocell density, in addition to its myopic version in which femtocells maximize their instantaneous utility metric. Clearly, the overall performance decreases as the network gets denser, however the proposed SON-RL decays at a much lower pace as compared to BRD. This is attributed to the fact that under SON-RL, femtocells are interesting in maximizing their long-term utility. Figure 4-7 depicts the impact of the number of available sub-carriers on the femtocell average spectral efficiency.

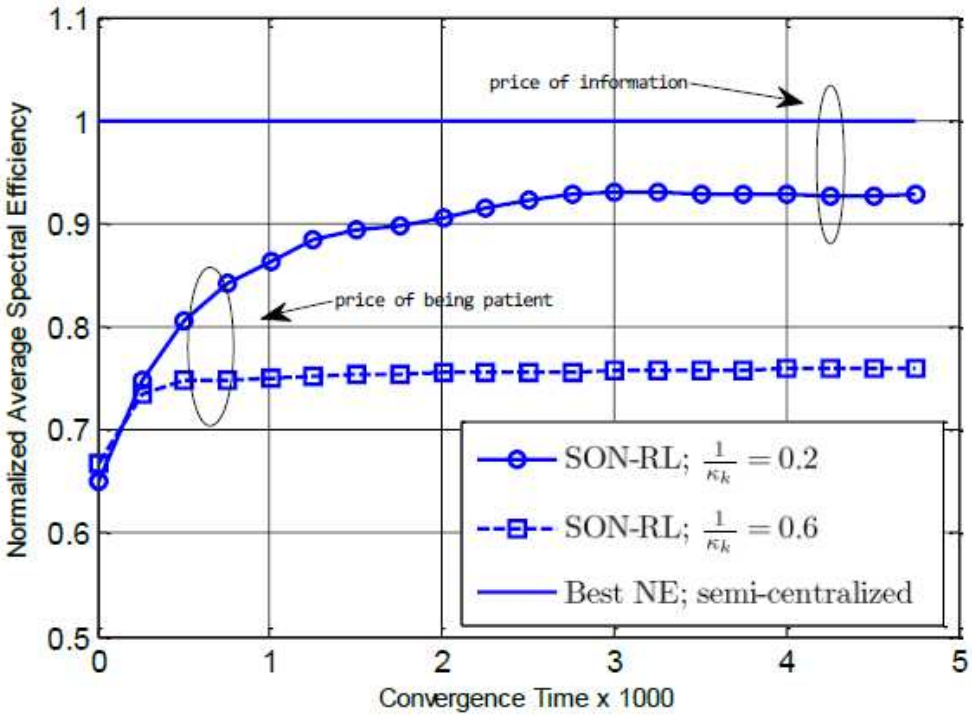

Figure 4-5: Convergence behaviour of the proposed algorithm (SON-RL) with respect to the best Nash equilibrium (semi-centralized case). The impact of the temperature parameter is also shown.

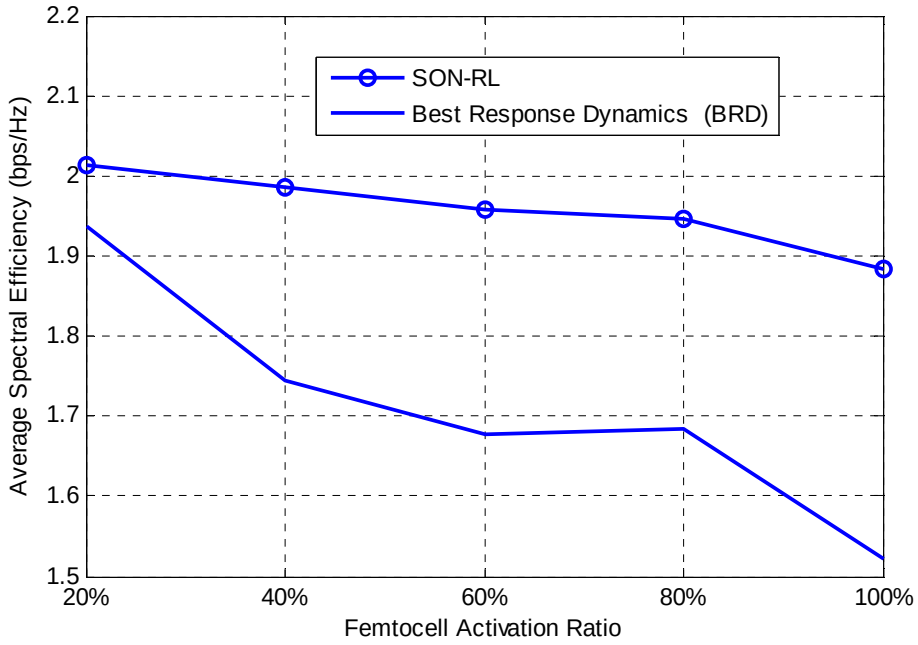

Figure 4-6: Average spectral efficiency as a function of the femtocell density. Here, SON-RL is compared with the best response dynamics in which femtocells maximize their instantaneous utility metric.

Due to the inherent feature of the proposed algorithm in which femtocells learn in the long-term, the larger the action space, the lower the performance, since as per (4.7) femtocells leave a non-zero probability for every given strategy.

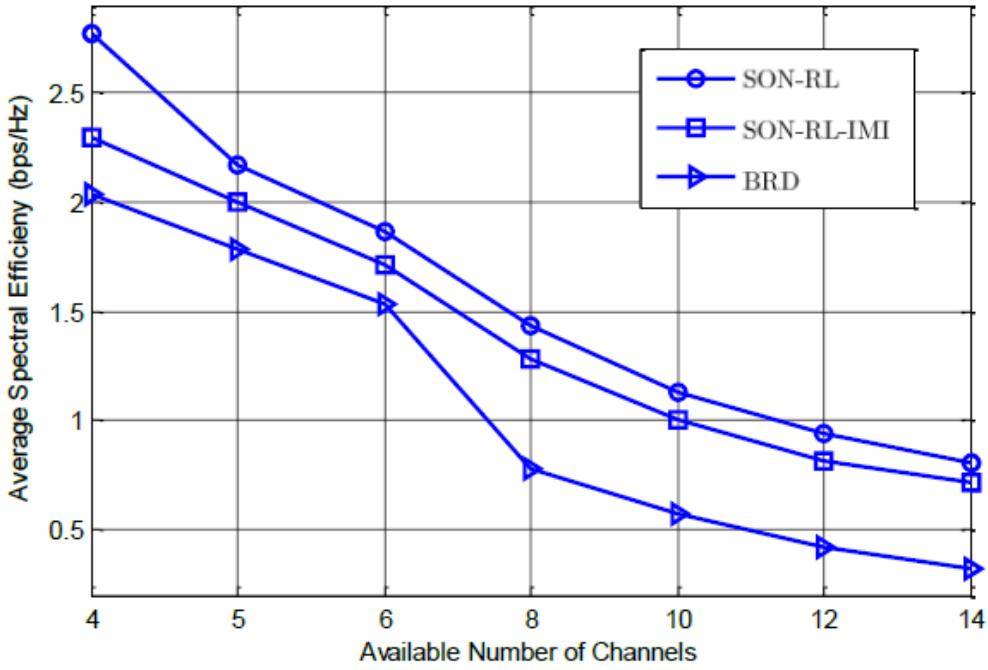

Figure 4-7: Impact of the number of channels on the various learning schemes. Here, SON-RL, SON-RL-IMI, and BRD are compared.

4.1.2.4 Conclusions

We have proposed a decentralized interference management inspired from reinforcement learning, in which femtocells self-organize so as to maximize their long-term utility. It was shown that femtocells face intricate trade-offs arising from the exploitation and exploration paradigm. In this work, femtocells were assumed to be totally selfish in the sense that no information exchange was allowed nor correlation among the strategies. This latter can indeed further improve the performance of the femtocells. Recent work [32] has shown that through coordination and other tools from reinforcement learning, femtocells can achieve performance close to when femtocells are cooperative.

4.2 Distributed SON Algorithms (global)

4.2.1 Spatial Domain based Interference Coordination

4.2.1.1 Description of the Scheme

Base Station Coordinated Beam Selection (BSCBS) has been introduced in [34]. The general idea of beamforming for transmitting data to mobile users in a wireless network with sectorized base station antennas is to radiate most of the power into the desired direction. A beam directed towards a cell-edge user may cause significant interference to a nearby user in an adjacent cell when both users are served at the same time-frequency resources. Performance gains can be expected when the selection of beams can be coordinated in neighbour cells in such a way that beam collisions between nearby cell-edge users can be avoided. An example situation is shown in Figure 4-8. Beam collisions can be avoided by coordinating the selection of precoding matrices in different cells. The coordination is based on feedback from UEs including not only CQI, Rank Indicator (RI) and Precoding Matrix Indicator (PMI), but also different types of additional messages to support the cooperation. For example, a RESTRICTION REQUEST (RR) feedback message from the UE contains information about unwanted precoding matrices. The users request in advance the restriction of the usage of certain precoding matrices in neighbour cells over the resources that could be used for data transmission at a later time instant. The coordination takes place between a victim cell and an aggressor cell. The UE sends the aforementioned air interface messages to its serving cell. In case that the UE is strongly interfered by an aggressor cell, then the serving cell (victim cell) forwards the air interface messages to the aggressor cell. More details of the message design and the coordination over X2 interface are provided in [34] and [35]. The process of SON-based establishment of an X2 interface between aggressor and victim cell has been investigated in [40].

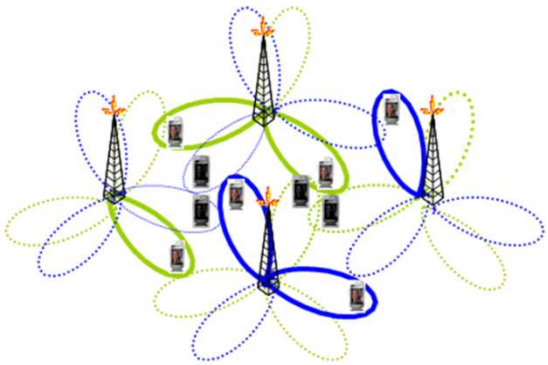

Figure 4-8: Avoidance of Beam Collisions

The overall goal of the coordination approach is then to maximize a network (cluster) wide utility metric over all the combinations of precoding matrices considering the restriction request received from users. This requires the exchange of messages between base stations over the X2 interface that logically connects base stations with each other in LTE. In order to keep the information exchange acceptable both in delay and complexity, a scheduling design was chosen that can be added on top of the Rel. 8 scheduling functionality. More details can be found in [34] and [35].

In the following we show simulation results for a 4x2 antenna configuration for a scenario with CSG femtos and macro cells. In such a scenario only the UEs belonging to the CSG of the femto cell can connect to it. UEs not belonging to the CSG cannot connect to the femto cell and must connect to a macro cell even if they are in the coverage area of the femto cell. Those macro UEs suffer from strong interference from the femto cell and can benefit from sending RR messages.

Detailed simulation assumptions can be found in [34]. In the simulations it is assumed that each RR message sent by the UE covers a frequency subband of 5 Physical Resource Blocks (PRBs) (called frequency validity of 5 PRBs in the following). Only macro UEs experiencing a geometry below -3 dB are allowed to send RR messages. Figure 4-9 shows the mean relative gain in throughput for the macro and femto UEs compared to the reference system without codebook restrictions when a different percentage of codebook entries is restricted. It is seen in Figure 4-9 that the macro UEs that are allowed to send RR messages benefit significantly from the reduction in interference by avoiding unfavourable beams in the femto cell. It is further seen that the gains become the larger the more codebook entries are restricted. Figure 4-9 shows that even macro UEs in better RF conditions (i.e. whose geometry is larger than -3 dB) benefit slightly from restricting beams in the femto cell. Gains are again largest, if the femto restricts all beams in the current subframe since then the femto does not generate interference at all.

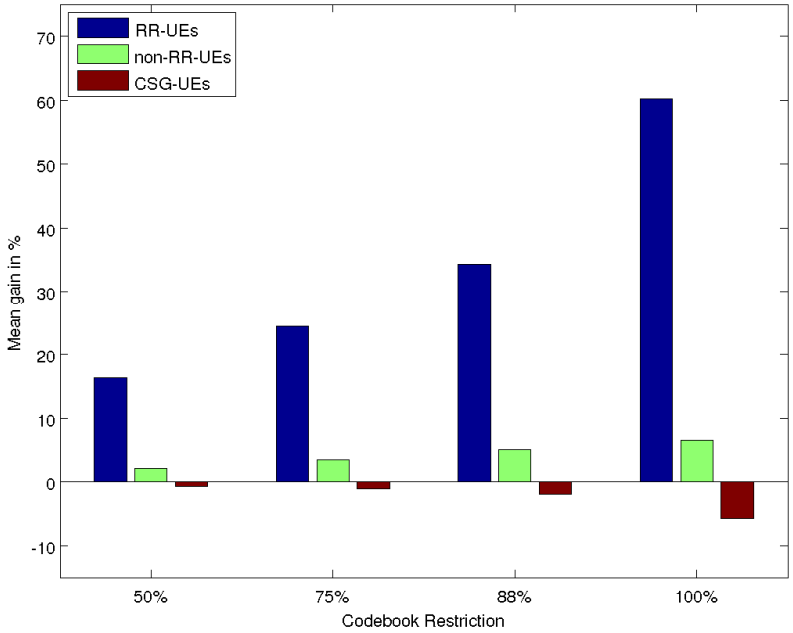

Figure 4-9: Relative Gain of Macro and Femto UEs

Figure 4-9 shows that in average 5% throughput reduction for femto users needs to be taken into account by improving the throughput for macro users that suffer from strong interference by the femto cell. However, this loss seems tolerable since the load in a femto cell is low and the user throughput in bps/Hz is very large.

4.2.1.2 Contribution to BeFEMTO System Concept and Objectives

BSCBS is an interference coordination scheme in spatial domain by restricting precoding matrices that aims to improve the user throughput of UEs in a victim cell suffering from strong interference by an aggressor cell and, therefore, fits to the BeFEMTO system concept and objectives. The largest gains are achieved if the entire codebook is restricted for a specific frequency subband. In this case the spatial domain coordination converges to a time domain interference management. In [34], it has been shown that BSCBS can then be seen as an extension of eICIC in LTE Rel-10 since it applies time-domain restrictions in a frequency-domain subband and not for the entire bandwidth as eICIC does.

4.2.2 Spectrum Leasing as an Incentive for Macro-Femtocell cooperation in the UL

4.2.2.1 Problem Statement

Cooperation in heterogeneous networks is a crucial paradigm in order to leverage on the existence of open access low-power nodes, and in which cell-edge MUEs can improve their uplink performance. In this section, FUEs act as relays for MUEs in a device-to-device communication fashion. In return, each cooperative macrocell user grants the FUE a fraction of its super-frame as a reward mechanism. The problem is looked at from a game theoretic perspective where a coalitional game is formulated whereby MUEs and FUEs are the decision makers (i.e., *players*), taking individual and distributed decisions on whether to cooperate or not. The considered utility metric captures cooperative gains, in terms of

throughput and delay. It is shown that the network can self-organize into a partition composed of disjoint coalitions/clusters which constitutes the recursive *core* of the game, being a key solution concept for coalition formation games in partition form.

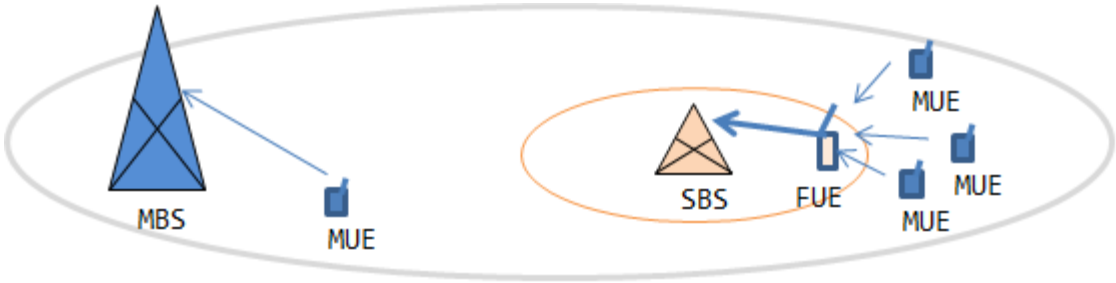

Figure 4-10: Illustration of the proposed solution. Here, an FUE is relaying the traffic of neighbouring cell-edge MUEs to its respective HeNB. As a result HeNB gets an extra resource for its own transmission, and as a by-product lower transmit power is required and the overall network performance is improved.

4.2.2.2 Proposed Solution

We formulate a coalitional game, whose solution is the concept of the *recursive core*. The aim of the proposed cooperative approach is to minimize the delay of the MUE transmissions through FUE assisted traffic relay, considering bandwidth exchange as a mechanism of reimbursement for the cooperating FUEs. The goals of the HeNBs and the MUEs are intertwined from different viewpoints. At the HeNB side, high interference level can be due to MUEs operating over the same sub-channel which consequently limits the achievable rates. At the MUE side, poor signal strength reception may result in a high number of retransmissions and higher delays. To overcome this, we propose that upon retransmissions, an MUE delivers its packets to the core network by means of FUE acting as relay terminal. We model each relay FUE as an M/D/1 queue and use the Kleinrock independence approximation. For the relaying FUE, cooperation incurs significant costs in terms of delay and spectral resources, since the FUE relays the combined traffic $\tilde{\lambda}_l$ over its originally assigned sub-channels. Therefore, it is reasonable to assume that FUEs will willingly bear the cooperation cost only upon a reimbursement from the serviced MUEs. We propose that, upon cooperation, the MUE autonomously delegates a fraction $0 < \alpha \leq 1$ of its own superframe to the serving FUE l. At the relay FUE l, the portion α is further decomposed into two subslots according to a parameter $0 < \beta_l \leq 1$. The first subslot $\alpha\beta$ is dedicated to relay MUE‘s traffic. The second subslot of duration $\alpha(1-\beta_l)$ represents a reward for the FUE granted by the serviced MUE, and it is used by the FUE for transmitting its own traffic. This method is known in the literature as spectrum leasing or bandwidth exchange and represents a natural choice for such kind of incentive mechanisms. Note that this concept solution allows to align and separate in time the transmissions allowing avoiding interference at the HeNB from the MUEs within the coalition. In order to do that, we assume that operations are synchronized. In order to increase their throughput and reduce MUE-to-HeNB interference, the FUEs have an incentive to cooperate and relay the MUE’s traffic. In this respect, FUEs may decide to service a group of MUEs, and thus form a coalition S_l in which transmissions from FUE l and MUEs within the same coalition are separated in time. In this work, we use a decode and forward relay scheme, assuming that a packet is successfully received.

4.2.2.3 Simulation Results

We consider a single hexagonal macrocell with a radius of 1 Km within which N HeNBs are underlaid with M MUEs. Each SBS N serves $L_n = 1$ FUE scheduled over orthogonal subchannel, adopting a closed access policy. We set the maximum transmit power at MUEs and FUEs to $P_{\max} = 20$ dBm, which includes both the power for the serviced MUE’s and its own transmissions. The considered macrocell has 500 available subcarriers, each one having a bandwidth of 180 KHz, and dedicates one OFDMA subchannel to femtocell transmissions. In Figure 4-11, we evaluate the performance of the proposed coalition formation game model by showing the average payoff achieved per MUE during the whole

transmission time scale as a function of the number of MUEs M. We compare the performance of the proposed algorithm to that of the non-cooperative case, for a network with 50, 100, 200 FAPs using a closed access policy. The curves are normalized to the performance of the non-cooperative solution. For small network sizes, MUEs do not cooperate with FUEs due to spatial separation. Thus, the proposed algorithm has a performance that is close to the non-cooperative case for M < 60. As the number of MUEs grows, the probability of being in proximity of an FUE gradually increases and forming coalitions becomes more desirable. Hence, the MUEs become connected to a nearby FUE which allows for a higher SINR, allowing for high values of payoff. For example, Figure 4-11 shows that cooperating MUE can gain up to 75% with respect to the non-cooperative case in a network with N = 200 HeNBs and M = 160 MUEs. In fact, Figure 4-11 clearly shows that the average payoff per MUE increases in the cooperative case as the number of femtocells is large. It is also demonstrated that the proposed coalitional game model has a significant advantage over the non-cooperative case, which increases with the probability of having FUEs and MUEs in proximity, and resulting in an improvement of up to 205% for M = 200 MUEs.

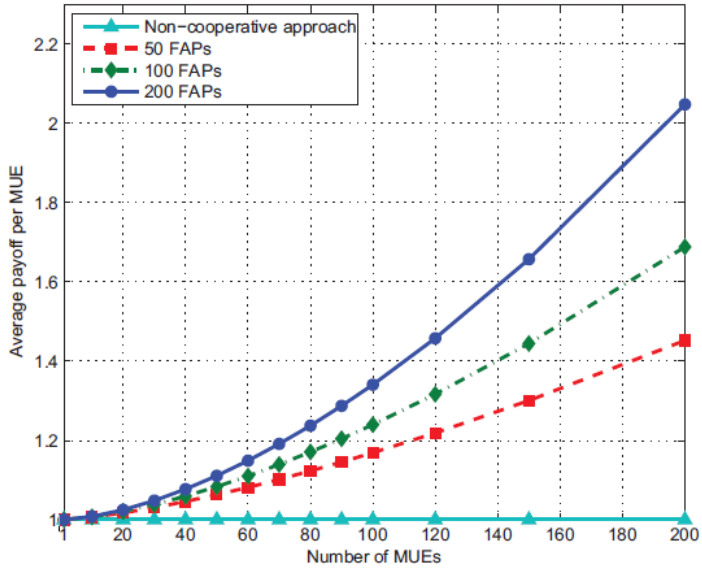

Figure 4-11: Average individual payoff per MUE, normalized to the average payoff in the non-cooperative approach, for a network having N = 50, 100, 200 FAPs, δ = 0.5, r = 20m.

4.2.2.4 Conclusions

We have introduced a novel framework of cooperation among FUEs and MUEs, which has a great potential for upgrading the performance of both classes of mobile users in next generation wireless femtocell systems. We formulated a coalitional game among the FUEs and MUEs in a network adopting a closed access policy at each femtocell. Further we have introduced a coalitional value function which accounts for the main utilities in a cellular network: transmission delay and achievable throughput. To form coalitions, we have proposed a distributed coalition formation algorithm that enables MUEs and FUEs to autonomously decide on whether to cooperate or not, based on the tradeoff between the cooperation gains, in form of increased throughput to delay ratio, and the costs in terms of leased spectrum and transmit power. We have shown that the proposed algorithm reaches a stable partition which lies in the recursive core of the studied game. Results have shown that the performance of MUEs and FUEs are respectively limited by delay and interference, therefore, the proposed cooperative strategy can provide significant gains, when compared to the non-cooperative case as well as to the closed access policy

4.2.3 Interference Control Based on Decentralized Online Learning

4.2.3.1 Problem Statement

In the situation where femtocells work in closed access and co-channel operation with the macrocell system, the interference management task becomes a challenging problem. Since femtocells are placed by end consumers, their number and position is unknown to the network operator, so that the interference cannot be handled by means of a centralized frequency planning. Therefore, in this section, femtocells are modelled as a decentralized system able to autonomously select their downlink transmission power per Resource Block (RB) in order to manage the aggregated interference they may generate at macro users. The

interpretation we give to autonomous decisions relies on the self-organization theory, where each femtocell is an agent able to evolve coherent behaviours in accordance with the environment [36]. When multi-agent systems have to deal with interdependent and dynamic problems, (i.e. agents cannot have an environment representation) the agents conforming the system are called reactive agents and have to act using stimulus-response type of behaviour [37]. As a form to implement reactive agents, Machine Learning (ML) introduces the concept of Reinforcement Learning (RL), which works based on learning from interactions with the environment, and on the observed consequences when a given action is executed. From the RL methods we focus on the Q-learning Time Difference (TD) algorithm, since in the considered problem, it is required an incremental learning method, able to adapt to the environment online and without environmental models [38].

4.2.3.2 Algorithm overview of Q-learning algorithm

It is assumed that the environment is a finite-state, discrete time stochastic dynamical system, as shown in Figure 4-12. The interactions between the multi-agent system and the environment at each time instant corresponding to RB *r* consist of the following sequence: 1) The agent *i* senses the state of the environment; 2) Based on the perceived state, agent *i* selects an action (i.e. a transmission power level); 3) As a result, the environment makes a transition to the new state; 4) The transition to the new state generates a return for agent *i*; 5) The return is fed back to the agent and the process is repeated. The objective of each agent is to find an optimal policy for each state, to maximize some cumulative measure of the return received over time.

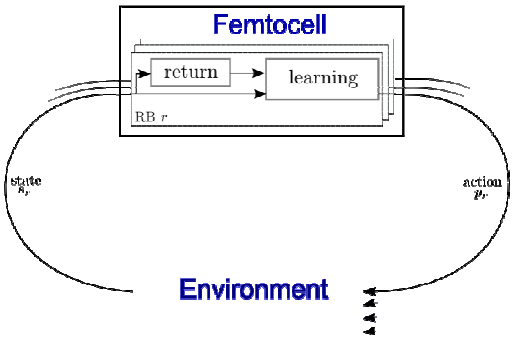

Figure 4-12. Learner-environment interaction.

In our system the multiple agents with learning capabilities are the femto Base Stations (BSs), so that for each RB they are in charge of identifying the current environment state, select the action based on the Q-learning methodology and execute it. The detailed explanation of this solution can be found in D 4.1 [34].

It has to be noted that the decentralized Q-learning algorithm, as any other learning scheme, needs a learning phase to learn the optimal decision policies. However, once completed the learning process and acquired the optimal policy, the multi-agent system takes only one iteration to reach the optimal power allocation configuration, when starting at any initial state $s \in S$.

4.2.3.3 Simulation Results

The scenario considered for validating the proposed approach is described in D2.1 [82] and is based on RAN4 3GPP documents. Simulation results are obtained for one macro cell of area *CA*, where different block of buildings are deployed, according to the dual stripe model proposed by 3GPP.

Figure 4-13 shows the probability that total transmission power of femtocell *i* exceeds the maximum power *PF* max. Simulations are run for a *PF* max = 10 dBm. It can be observed that the probability of $\sum_{r=1}^{RB} p_r^{i,F} > P_{\max}^F$ decreases with iterations reaching very low values, for low and high density of femtocells, and that when the probability of visiting random states ε is set to zero (at iteration 2000000), it decreases faster. Further results regarding this solution can be found in deliverable D2.1 [82].

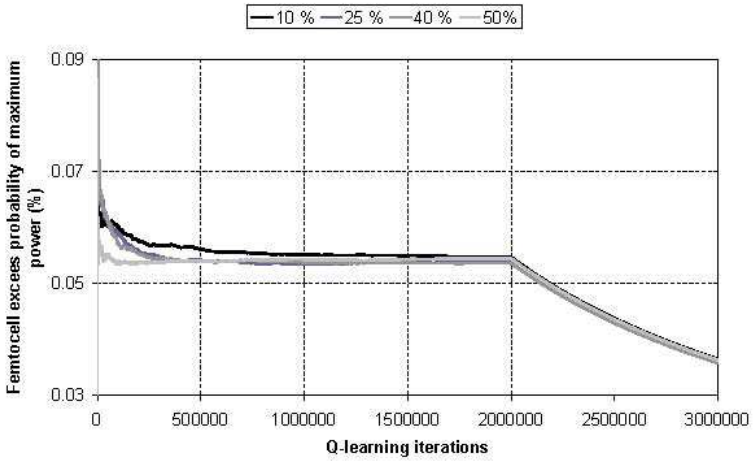

Figure 4-13: Maximum total transmission power exceed for a femtocell with different femtocell density

4.2.3.4 Docition Algorithm Overview

However, in the context of decentralized multiagent systems, the environment perceived by a given agent is no longer stationary, since it consists of other nodes who are similarly adapting. The dynamics of learning may thus be long and complex in terms of required operations and memory, with complexity increasing with an increasing observation space. A possible solution to mitigate this problem, to speed up the learning process and to create rules for unseen situations, is to facilitate expert knowledge exchange among learners. To this end, the novel concept referred to as docitive radio was introduced in [39]. Whilst the emphasis in cognitive radios is to learn ("cognoscere" in Latin), the focus of docitive radios is on teaching ("docere" in Latin). It capitalizes on the fact that some nodes have naturally acquired a more pertinent knowledge for solving a specific system problem and are thus able to teach other nodes on how to cope under the same or similar situations. The high-level cognitive radios operational cycle, consists in acquisition, decision and actuation processes. We extend this cycle by the introduction of the docitive functionalities, given by the docitive entity, as shown in Figure 4-14. The acquisition unit provides quintessential information of the surrounding environment. The core of a cognitive radio is without doubt the environmental state dependent intelligent decision engine, which typically learns from past experiences. With the decision taken, an important aspect of the cognitive radio is to ensure that the intelligent decisions are being carried out, which is handled by the action unit. The docition unit has two main tasks, the knowledge relation and the knowledge dissemination and propagation among agents. Those tasks have to be realized under the non-trivial aim of improving the own or other agent's learning process and performance. As shown in Figure 4-14, the docition unit is linked to the intelligent decision unit and communicates with the other agents' docition units. By these means, each docition unit builds its relationships with the other agents in the system and decides on the key docitive parameters.

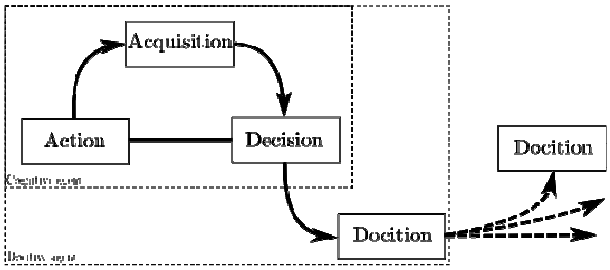

Figure 4-14. Docitive cycle which extends the cognitive cycle by cooperative teaching.

In our scenario, a femto BS which has recently been switched on can advantageously exchange information via a (backhaul) network, through a X2 interface between femtos, with other expert femto BSs in the neighbourhood, the so-called docitive femto-cells. The agents select the most appropriate femto BS from which to learn, based on the level of expertness and the similarity of the impact that their actions may have on the environment, as it was presented in D 4.3 [40].

4.2.3.5 Simulation Results

In the following, we compare the performance of 1) independent learning; 2) startup docition; and 3) IQ driven docition. Figure 4-15 shows performances in terms of precision, i.e., oscillations around the target SINR. In particular, it represents the complementary cumulative distribution function (CCDF) of the variance of the average SINR at the control point with respect to the set target of $SINR_{Th}$ = 20 dB. It can be observed that due to the distribution of intelligence among interactive learners the docition stabilizes the oscillations by reducing the variance of the SINR with respect to the specified target. More precisely, at a target outage of 1 %, we observe that the IQ driven docition outperforms the startup docition by a factor of two, and the independent learning algorithm by at about an order of magnitude

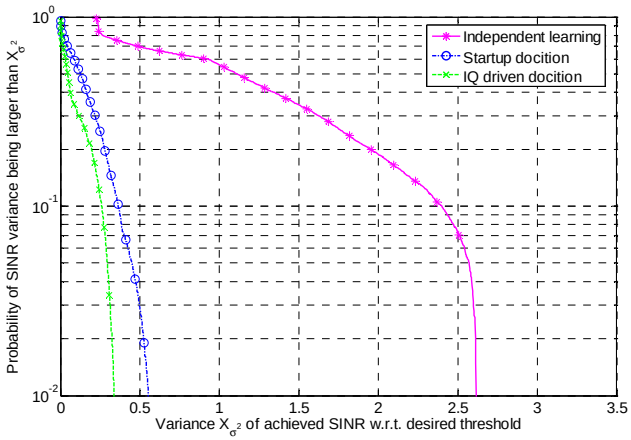

Figure 4-15. CCDF of the average SINR at macrouser.

4.2.3.6 Conclusions

We have presented a decentralized Q-learning approach for interference management in a macro-femto network to improve the systems' coexistence. However, the main drawback of the proposed scheme is the length of the learning process. As a result, we have focused on the novel paradigm of docition, with which a femto BS can learn the interference control policy already acquired by a neighbouring femtocell which has been active during a longer time, and thus saving significant energy during the startup and learning process. Notably, we have shown in a 3GPP compliant scenario that, with respect to decentralized Q-learning, docition applied at startup as well as continuously on the run yields significant gains in terms of convergence speed and precision. The proposed learning algorithm requires some information from the macrocell system regarding the macro user performance. This information is proposed to be conveyed through the X2' interface, introduced in deliverable D 2.2 [68]. These solutions are explained in more detail in deliverables D 4.1 [34] and D 4.3 [40], where further results can be found. Furthermore, in section 4.3.6 we present a solution which allows femtocells to learn in a completely autonomous fashion, i.e. without any communication with the macrocell.

4.2.4 Self-Optimization of Antenna Tilt (with fixed relays)

4.2.4.1 Problem Statement

The scope of this contribution is focused on Spectral Efficiency (SE) enhancement on the access link of Outdoor Fixed Relay femtocells (OFR) through Self-Organization (SO) of eNB antennas tilt.

OFR are different from conventional femtocells as, unlike femtocells, OFR generally have an over the air inband back haul link called access link, to relay the traffic data to and from their donor eNB. This access link requires radio resource partitioning between the eNB and OFR to avoid mutual interference. Such additional partitioning of resources is bound to have negative impact on the spectrum reuse efficiency of the system and hence capacity. Therefore, it is very desirable to optimise the spectral efficiency of the access link so that less fraction of radio resources have to be allocated to OFR access link and more resources can be used to provide service to users than back hauling. In this contribution we present a novel framework and the preliminary results of SE enhancement on the access link through SO of eNB antenna tilts.

The problem is then to optimize system wide antenna tilts to maximize the aggregate throughput at access link of all the OFRs. For detailed mathematical formulation and analysis, interested readers are referred to [40].

4.2.4.2 Design of SO Solution

The optimization problem as depicted above is a complex nonlinear multivariable optimization problem. Even if it could be solved easily, its solution would require global cooperation among all eNB's in the area and hence would not be scalable and agile, and therefore would lack SO.

In order to achieve a SO solution, the complexity of the problem needs to be reduced, such that its solution can be executed locally in a distributed manner. There are two main reasons of complexity in this problem; firstly the large scale vector optimization over vector θ_{tilt}^{N} that has as many components as number of sectors in the system i.e. $|N|$ which prevents scalability. Secondly the mutual coupling between these variables that require global cooperation is another reason of complexity of the problem. In order to disintegrate this complex global problem into simpler local problem, we propose to aim for sub optimal solution as suggested in [41].

By not aiming for optimal solution, the tilt optimization can be done locally. To enable this localisation, we propose the concept of *triplet*. The triplet is a fixed cluster of three adjacent and hence most interfering sectors. The original global optimization problem as discussed above can be solved within each triplet independently to determine the optimal tilt angle to be adapted and maintained by each triplet for given locations of OFR within that triplet.

The execution of this solution in each triplet independently, results in achievement of the system-wide objective, approximately. We call this framework TO-BSOF (Tilt Optimization through bio-mimetic SO Framework), as the basic idea of decomposing global objective into local objective is inspired from SO systems in nature. In next sub-section we present some numerical results to demonstrate the potential of TO-BSOF.

4.2.4.3 Simulation Results

In order to assess the potential gain TO-BSOF can yield, numerical results for two different set of location of OFRs in triplet are obtained, as shown in Figure 4-16

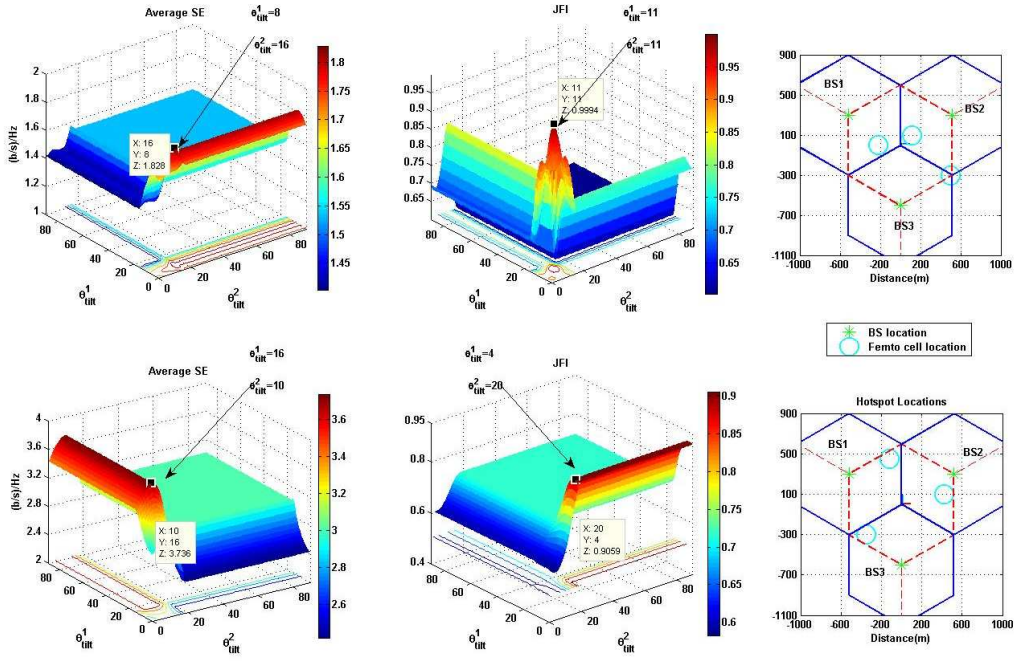

Figure 4-16: Average spectral efficiency per link and the Jain's fairness index among the access links within a triplet are plotted as function of tilt angle of two sectors while third is fixed at 13^0 degree.

It can be seen that depending on the location of OFRs, a gain in spectral efficiency from 1bps/Hz to 2bps/Hz can be achieved on average within each triplet, and hence system wide, through TO-BSOF. To investigate the impact of TO-BSOF on fairness, Jain's Fairness Index (JFI) is also plotted. It is interesting to note that optimal tilt angle for maximum fairness among access links throughput are different than the optimal tilt for maximum spectral efficiency. Nevertheless, it is anticipated that fairness among access link is not an important performance objective as long as significant gain in spectral efficiency can be achieved and TO-BSOF seems promising in this regard.

4.2.4.4 Practical Implementation of TO-BSOF

TO-BSOF is implementable in a distributed and self-organizing manner and performance close to optimal can be achieved. The main advantage of TO-BSOF is that it does not have heavy signalling overheads associated with it. A negligible amount of signalling among the sectors within triplet is required to determine the location of OFRs. This signalling can be done through X2 interface and needs to be done only when location of OFR is changed.

Another advantage of TO-BSOF that makes it pragmatic is that because of its highly localised nature it is very agile as it has no intrinsic delays caused by excessive global signalling or complex coordination. Therefore, TO-BSOF can be implemented in an online manner using event-based triggering mechanisms. The execution of TO-BSOF can also be periodic in an off-line manner. Such off-line execution will not require real time position information of OFR locations, rather it can rely on off-line information. In case of periodic execution the time period of re-execution can range from minutes to months and can be set based on the statistics of the long term variations of location of OFR in the area of interest.

4.2.5 Relay and Backhauling

4.2.5.1 Problem Statement

The proliferation of wireless services with stringent quality of service requirement is driving network operators to search for new solutions for wireless users and their serving stations to be closer to one another so as to enhance the coverage and capacity of next-generation wireless systems. In this respect, the deployment of small cells overlaid on existing cellular networks and serviced by low-cost, low-power, femtocell base stations (FBS) has emerged as a promising technique for improving the indoor wireless coverage, offloading data from the macro-cellular network, and enhancing the overall capacity. Cooperation has been identified as an important means to improve the overall network capacity, which materializes in different means (relaying, explicit coordination among tiers etc). However, allowing such cooperative techniques requires an efficient backhaul that connects the femtocell and macro-cell tiers. The nature and properties of this backhaul will strongly impact the overall network performance as well as the potential performance gains from cooperation. The backhaul takes central stage when dealing with macro-femto/picocell coordination and constitutes the objective of this work. In fact, the heterogeneous and unreliable nature of the femtocell backhaul leads to a fundamental question: should the femtocells use an over-the-air (in-band) backhaul which requires significant spectrum resources but can guarantee reasonable delays or should they use a wired backhaul which does not require any spectrum resources but could lead to significant traffic delays? The answer to this question is particularly important in order to enable advanced techniques such as femtocell relaying. In short, we propose a novel approach for interference management which leverages cooperation between the macro-cell and femtocell tiers while jointly optimizing the choice of an appropriate backhaul supporting this cooperation. In the proposed approach, macrocell users can seek the help of neighbouring open-access femtocells in order to improve their uplink data rate while taking into account the constraints introduced by an underlying heterogeneous backhaul.

4.2.5.2 Network Model

We consider an uplink macrocell transmission with F small cell base stations. Let N denote the set of sub-carriers. In the non-cooperative setting, there is no cooperation/coordination between the macrocell and femtocell tiers, and hence the achievable rates of MUE m and FUE k on subcarrier *n* are:

$$R_m^n = \log\left(1 + \frac{g_{m0}^n p_m^n}{N_0 + \sum_j g_{j0}^n p_j^n}\right) \tag{4.8}$$

$$R_k^n = \min\left\{\log\left(1+\frac{g_{kf}^n p_k^n}{N_0 + I_k}\right); C_f\right\} \quad (4.9)$$

where $I_k = g_{mf}^n p_m^n + \sum_{j\neq k} g_{jf}^n p_j^n$ is the aggregate interference experienced by the k-th FUE and C_f is the fixed backhaul capacity between the f-th FBS and the MBS. g_{ab}^n is the channel gain between nodes a and b on carrier n. p_a^n is the transmitted power of UE a on subcarrier n. The subscript "CLA" is used to denote the rates that are calculated for classical macro-femto deployment scenario.

In order to improve their transmission rates, the FUEs and MUEs can cooperate and coordinate their transmissions. However, one of the key challenges for deploying cooperation in femtocell networks is to design an adequate backhaul that can lead to an efficient communication between the macro and femtocell tiers. In fact, the reliability of the backhaul connection between FBSs and MBSs is instrumental in the optimal deployment of heterogeneous networks, hence requiring designs that jointly account for access and backhaul links. In practice, there are two possible types of backhaul networks: wired and wireless, which come with the cost and benefits. On one hand, a wired backhaul can provide a reliable platform for communication which does not require any spectral resources, but often leads to increased delays due to the presence of traffic from various sources. On the other hand, a wireless backhaul provides congestion-free communication but it requires additional spectrum resources and can lead to an increased interference in the network. To this end, before delving into the details of the proposed cooperative approach, we present the considered models for the two backhaul types.

- ***Wired backhaul****:* We consider that the packet generation process at the femtocells follows a Poisson distribution, and, thus, we model the entire backhaul of the system as an M/D/1 queue. Let C_f be the capacity of the f-th FBS- MBS link and, thus, the total wired backhaul capacity $\bar{C}$ could be given by: $\sum_f C_f \leq \bar{C}$.
- ***Wireless backhaul****:* In this scenario, we account for the increased interference over FBSs-MBS backhaul links due to femtocell transmissions over the backhaul with power p_f^n. Here, the rate of FBS f is given by: $R_{f0}^n = \log\left(1+\frac{g_{f0}^n p_f^n}{N_0 + \sum_{l\neq f} g_{l0}^n p_l^n}\right)$

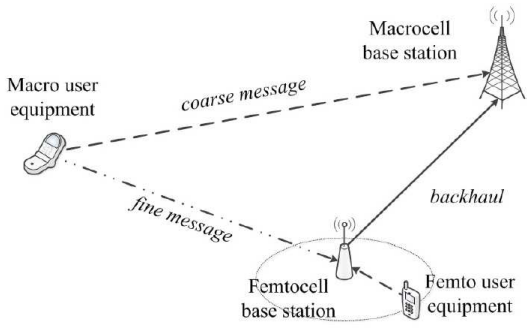

Figure 4-17: Illustration of the proposed relaying approach in which MUEs use rate splitting in their UL transmission.

4.2.5.3 Algorithm Overview: Cooperative relaying between the macro and femtocell tiers

To enable an efficient co-existence between the two network tiers, we propose a cooperative approach using whichever femtocells that can assist nearby MUEs in order to improve the overall data rates via the

concept of rate splitting. In this context, each MUE m builds a *coarse* $X_{m,C}^{n}$ and a *fine* message $X_{m,F}^{n}$ (direct signal and relayed signal, respectively) for each of its transmitted signals as illustrated in Figure 4-17. With these two messages, the source MUE superimposes two codewords thus, the transmission rates associated with these messages are such that the FBSs can reliably decode the fine message while the MBS decodes the coarse message. Mathematically, this can be expressed as follows: $X_{m}^{n} = X_{m,C}^{n} + X_{m,F}^{n}$. Moreover, the transmission power allocations of the MUE's coarse signal to the MBS and the fine signal for FBSs are $p_{m,C}^{n} = (1-\theta)p_{m.}^{n}$ and $p_{m,F}^{n} = \theta\, p_{m.}^{n}$ with $0 \le \theta < 1$. In this proposed scheme, a femtocell with both a good channel gain from a neighbouring MUE and a high backhaul capacity can assist the MUE by first decoding, and subsequently relaying its *fine* message to the MBS over the backhaul. Subsequently, the overall MUEs' transmission rates are improved. Here, we consider that, upon relaying MUE's *fine* messages, the FBSs can simultaneously service their own FUEs using successive interference cancellation (SIC).

4.2.5.3.1 Wireless over-the-air (OTA) backhaul:

We assume a half-duplex decode and forward (DF) uplink transmission in which both MUEs and FUEs transmit during the first time slot and FBSs relay both signals (over the backhaul) during the second time slot. The uplink rate of MUE m when transmitting its coarse message to its serving MBS over sub-channel n is given by:

$$R_{m,C}^{n} = \log\left(1 + \frac{g_{m0}^{n}(1-\theta)p_{m}^{n}}{N_0 + \sum_{j} g_{j0}^{n} p_{j}^{n}}\right) \tag{4.10}$$

where $(1-\theta)p_{m}^{n}$ is the MUE's transmission power allocated for the *coarse* message. Similarly, the rate of MUE m when transmitting its fine message to FBS f over sub-channel n is given by:

$$R_{mf,F}^{n} = \log\left(1 + \frac{g_{mf}^{n}(\theta)p_{m}^{n}}{N_0 + I_k}\right) \tag{4.11}$$

where the interference term is due to: *(i)*- the power used to transmit the *coarse* messages of other MUEs and *(ii)*- the transmissions from other interfering FUEs. The relayed FBS signal over the wireless backhaul includes the *fine* messages of both the MUEs and the FUEs in which a rate fraction of νR_{f0}^{n} is allocated for the MUE's *fine* message and $(1-\nu)R_{f0}^{n}$ to the FUE's signal, where $0 \le \nu < 1$ Since the uplink rate of the backhaul is interference-limited, the rate of the relayed signal using DF relaying is the minimum rate of the MUE-FBS link and FBS-MBS backhaul. Therefore, the total throughput of the m th MUE's *fine* message is:

$$R_{mf,F}^{n} = \frac{1}{2}\min\left\{R_{mf,F}^{n}, \nu R_{f0}^{n}\right\} \tag{4.12}$$

4.2.5.3.2 Wired backhaul:

In the wired backhaul scenario, the backhaul capacity which is constrained by nature influences the final rate of the relayed *fine* message. Moreover, the rates of the *coarse* and *fine* messages of MUE m are given by:

$$\left[R_{m,C}^{n}\right]_{WRD} = \log\left(1 + \frac{g_{m0}^{n}(1-\theta)p_{m}^{n}}{N_0 + \sum_{j} g_{j0}^{n} p_{j}^{n}}\right) \tag{4.13}$$

$$\left[R_{m,F}^{n}\right]_{WRD} = \frac{1}{2}\min\left\{\log\left(1 + \frac{g_{mf}^{n}(\theta)p_{m}^{n}}{N_0 + I_k - g_{mf}^{n} p_{m}^{n}}\right), \nu C_f\right\} \tag{4.14}$$

where the fraction of the capacity allocated for the MUE's fine messages is νC_f

4.2.5.4 Algorithm Description: Game theoretic approach for enabling cooperative relaying

In order to benefit from rate splitting and femtocell relaying, the MUEs must be able to appropriately choose their preferred FBS, given the channel conditions as well as the underlying backhaul constraints. In this regard, we formulate a non-cooperative game where the players are the MUEs, the action are the transmit power levels and selected femtocell, and finally the chosen utility metric captures the tradeoff between the achieved throughput from relaying and the expected delay due to the backhaul constraints. One suitable metric for capturing the tradeoff between throughput and delay is that of a *system power* which is defined as the ratio of some power of the throughput and the delay. Hence, using this metric, the utility function of any MUE m

$$u(a_m, a_{-m}) = \frac{R_m(a_m, a_{-m})^{\delta}}{D_m(a_m, a_{-m})^{1-\delta}} \quad (4.15)$$

where $R_m(a_m, a_{-m})^{\delta}$ is the total rate and $D_m(a_m, a_{-m})^{1-\delta}$ is the total delay experienced by MUE m.

In the proposed non-cooperative game, the choices of the MUEs are discrete and relate essentially to the choice of a serving FBS and the associated power level. This type of games is reminiscent of the framework of network formation games in which individuals interact in order to decide on the friendship relationships or links that they wish to form. The solution of a network formation game is essentially a Nash network, which is a Nash equilibrium of the game that constitutes a stable network in which individuals are interconnected through a graph with each link having an associated "strength" or intensity. Similarly, for the proposed MUEs game, the sought solution is essentially a stable Nash network in which no MUE can improve its utility by unilaterally changing neither its chosen FBS nor the associated power level. Finding analytical closed-form solutions on the existence and properties of a network formation game's equilibrium is known to be a challenging task, notably under generic utility functions such as the one proposed in this work [15]. However, to overcome this complexity, one can develop algorithmic approaches that can be adopted by the MUEs so as to reach the equilibrium of this game. In this respect, we propose a *myopic* algorithm, based on best response dynamics in which MUEs optimally learn their best relaying FBS. The proposed algorithm is composed of three main steps:

Step 1: Neighbouring Femtocell Discovery: Each MUE discovers prospective relaying FBSs by monitoring the received signal strength indicator (RSSI) over pilot channels.

Step 2: Iterative Network Formation Algorithm:

Following the discovery phase, each MUE chooses its best response which consists of optimizing its *current* utility by choosing the relaying FBS and the associated power level. Step 2 is repeated until convergence to the Nash solution of the game.

Step 3: Rate Splitting: Once the final network forms, the MUEs can perform the proposed rate-splitting technique in which the helping FBS simultaneously decodes the MUE's fine message and its own FUE using SIC. Subsequently, the helping FBS transmits both MUE and FUE signals over the heterogeneous backhaul.

4.2.5.5 Simulation Results

We consider a single macrocell with radius R_m = 400 m in which a number of MUEs and FBSs with radius R_f = 20 m are deployed. Each FBS serves a single FUE. The maximum transmission power is set to 20 dBm and the noise level is set to -130 dBm. We use the 3GPP specifications for path loss and shadowing in both indoor and outdoor links. The shadowing standard deviation is set to 10 dB while the wall penetration loss is set to 12 dB. Moreover, both MUEs and FUEs have packet generation process with rates $\lambda_m = \lambda_f$ 150 Kbps, respectively.

Figure 4-18 and **Figure** 4-19 show the average MUE payoff as a function of the number of FBSs and MUEs, respectively. These figures show that the proposed approach yields a significant improvement over the classical approach in which MUEs communicate directly with the macrocell base station, reaching up to 140% for F = 150 femtocells. Furthermore, it can be seen that, as the network becomes denser, the average MUE payoff decreases due to the lower rates, increased interference, and higher delays. Nonetheless, for dense networks, it is more likely to have MUEs and FBSs close to one another which enable the MUEs to achieve a higher payoff using the proposed approach as opposed to the classical method with no coordination. In addition, we can observe that the gaps between proposed scheme and classical case are increasing as the system gets denser, i.e., the drop of utility is low for the proposed schemes compared to the classical scheme. The utility figures describe the combined behavior of rates and delays separately; it is

interesting to observe the rate and the delay separately. Figure 4-18 and Figure 4-20 depict the average utility metric per MUE as a function of the number of femto base stations and number of MUE, for the classical approach, and proposed approach over both wired and wireless backhauls. In addition, the cumulative density functions (CDFs) of transmission delays and rates are presented in Figure 4-19 and Figure 4-21, respectively. In these two figures, we observe a reduction in the delays and an improvement in the data rates when using the proposed approaches (wired and OTA) as compared to the classical approach. This is due to the fact that the relaying path provides additional rate gains due to the higher capacity of the MUE-FBS link and the FBS-MBS backhaul (as opposed to direct transmission). In fact, it is shown that the proposed approach can reduce the delay by 5 times for the wired backhaul case and by 10 times for the OTA case. For transmission rates, both proposed wired and OTA schemes improve the average rate of classical approach by 125% and 150%, respectively.

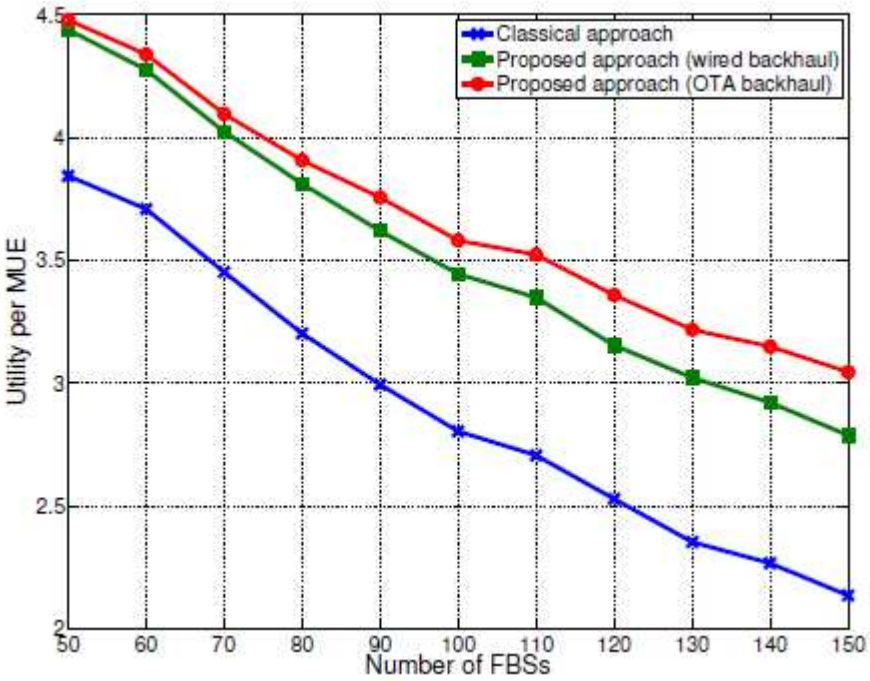

Figure 4-18: Utility per MUE as a function of the number of FBSs (M = 5, 37.5 Mbps wired backhaul and 32 OTA backhaul channels).

Figure 4-22 compares the achievable average utility per MUE for a system with M=5 MUEs and F = 80 FBSs under different backhaul constraints. As the capacity of wired backhaul and the number of channels in the wireless backhaul are increased, the average MUE utility is increased, in both cases. However, based on the capacity, a certain backhaul implementation (wired or OTA) may provide a higher average utility over the other. As an example, the wired backhaul with 45 Mbps capacity offers a higher average utility compared to the wireless backhaul with 8 (or less) channels while it is less compared to an OTA backhaul with 16 (or greater) channels. This tradeoff can be used to define the appropriate backhaul mechanism (wired or OTA) based on the resource availability for each.

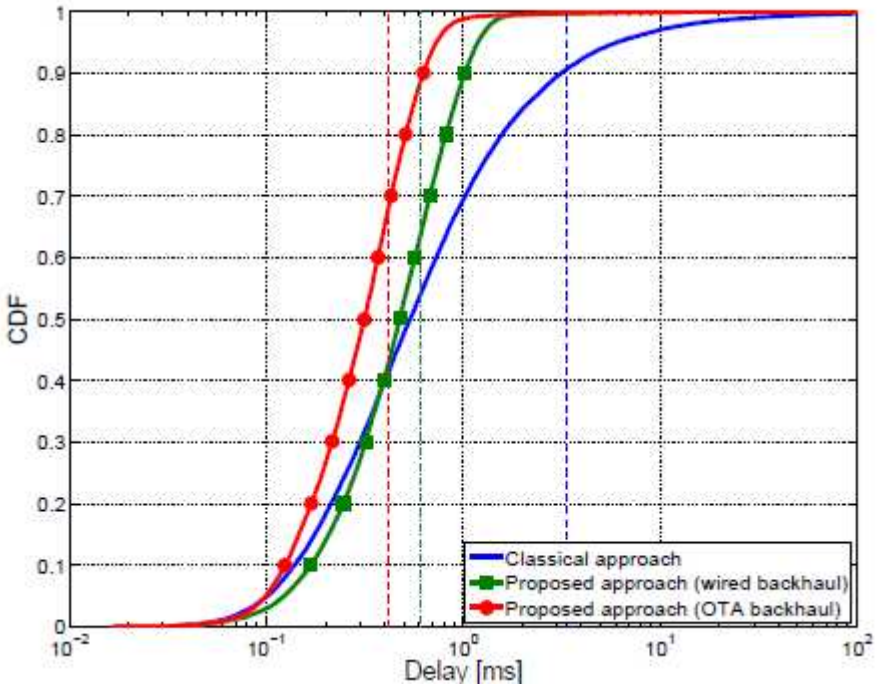

Figure 4-19: CDF of transmission delays.

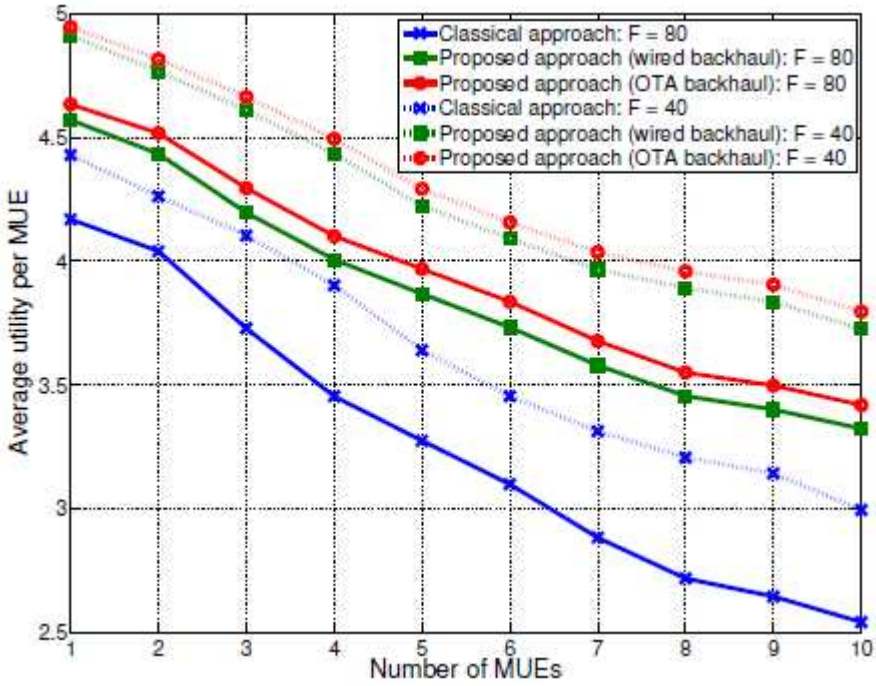

Figure 4-20: Average utility per MUE as a function of the number of MUEs (F =40, 80, 37.5 Mbps wired backhaul and 32 OTA backhaul channels).

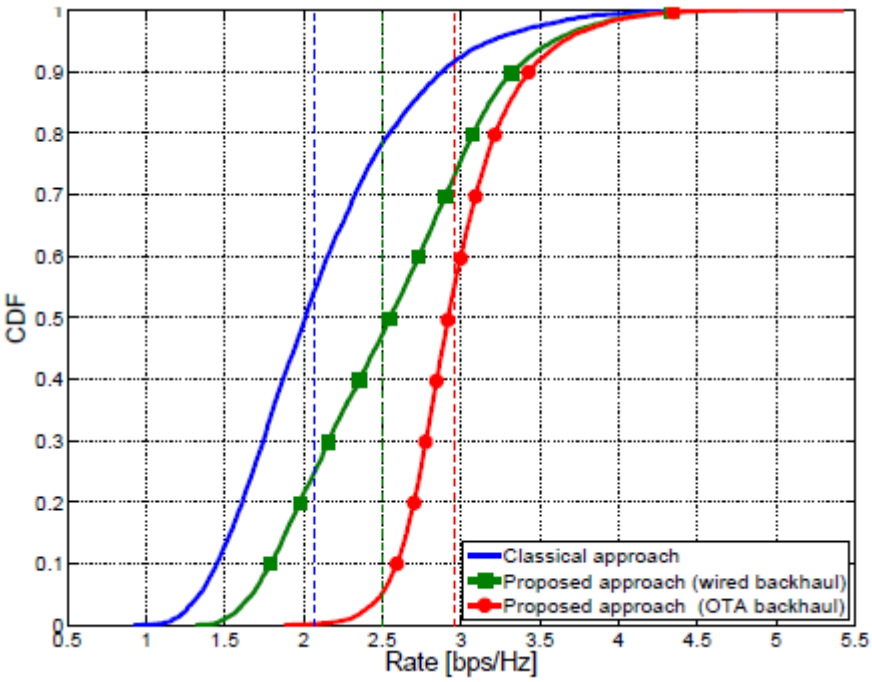

Figure 4-21: CDF of transmission rates.

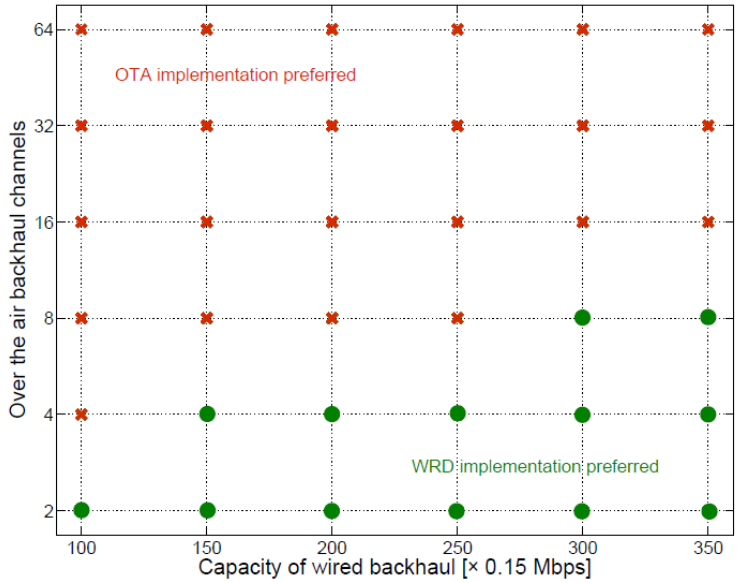

Figure 4-22: The impact of the backhaul capacity (wired) and number of channels (wireless) on the average achievable utility per MUE. The backhaul implementation which provides the best average utility is indicated at each point/combination (the above simulation is performed for a system M=5, F=80

4.2.5.6 Conclusions

We have proposed rate-splitting techniques so as to enhance the performance of MUEs with aid of open-access femtocells over a heterogeneous backhaul. The performance of MUEs is evaluated by a metric - system power - which captures both achieved throughput and the expected backhaul delay. Simulation results have shown that the proposed approach yields 50% of improvement in throughput and 10 times reduction in expected delays, compared to the system with no cross-tier cooperation is available. Furthermore, we have shown that the proposed approach can capture the tradeoff between two backhaul implementation techniques – wired and over-the-air - based on the achievable average utility. The proposed

scheme can thus be used to determine the appropriate backhaul implementation whenever the knowledge of resource availability for both wired and over-the-air backhauls is known a priori.

4.2.6 Mobile Relay Architecture

4.2.6.1 Problem Statement

After the introduction of relay functionality in Rel-10, as part of the 3GPP LTE advanced features set [75], [43], current standardization is focusing on the introduction of mobility function for relay nodes. The first relay feature is in fact focusing on fixed relays introduced mainly for coverage purposes, whereby the coverage of an eNB is extended by the introduction of a relay node, which consists in an eNB with wireless backhaul. Such a device supports a very basic form of mobility, whereby the relay can be turned off and reconnected in another location of the network (so called nomadic mobility). In this regard, procedures have been defined for the relay start-up to handle that with minimal operational costs [43], but no handover is possible for the relay backhaul link.

Afterwards, other scenarios in which relay could be used for coverage extensions have been considered, where also mobility of the relay node is playing a more significant role. The most relevant of such scenario, which gives good motivation for the introduction of mobility relay, is coverage extension to moving vehicles like high speed trains. In this case mobile relays can be installed on the train wagons to provide in-car coverage and this overcoming the high penetration loss an indoor UE would suffer otherwise.

According to what captured in [76], the high speed train scenario can be characterized by trains operating at very high speed (e.g. above 300 km/h) on a known trajectory (see Figure 4-23 from [76]). Typically such trains are sealed and show a high penetration loss of the radio signal through the shield carriages – as the users inside the trains are mainly stationary or move at pedestrian, providing coverage with a relay node is attractive.

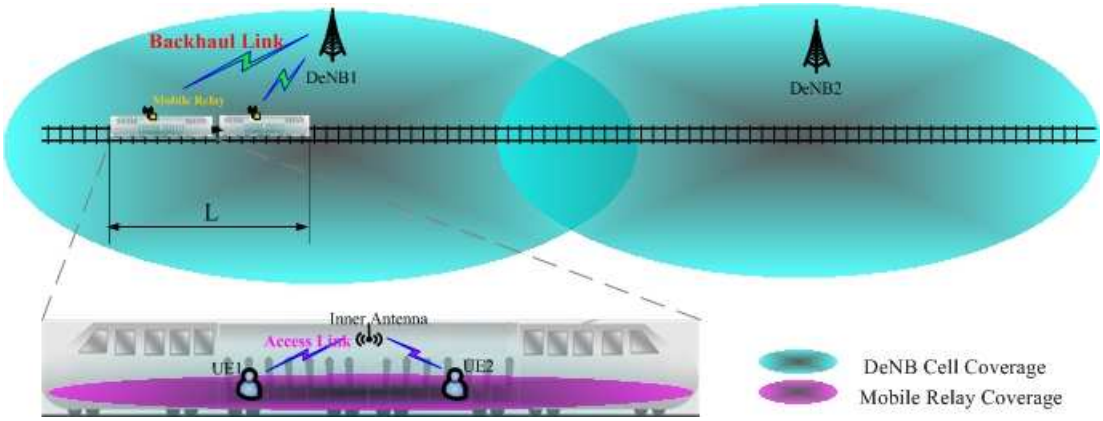

Figure 4-23: **A reference scenario for high speed train [76].**

Due to fast moving and shielded carriage, offering good wireless services to users travelling on a high speed trains from fixed eNBs faces severe challenges, like e.g. strong Doppler frequency shift, high penetration loss, reduced handover success rate and increased power consumption of UEs.

In this regard, mobile relays (when deployed) would be mounted on the high speed train and would communicate with donor eNBs placed along the railway by outdoor antenna installed on top of the train carriages, and serves UEs inside carriages by inner antenna installed inside the carriages. This way they can overcome high penetration losses and offer a stable handover execution, as well as reduce the user power consumption.

Other scenarios like relay-on-the-bus, increase backhaul robustness or temporary relay deployment have been also considered initially as candidate use cases for mobile relay in 3GPP. While they are surely possible cases for mobile relay, they do not seem to pose such a challenge that would justify the introduction of mobility functionality for relay nodes. In fact existing eNB and features for Rel-10 would be already sufficient to cover those cases.

4.2.6.2 Key Requirements

Different requirements have been derived for the mobile relay [76], here below the key ones are briefly summarized:

- The mobile relay study should focus on scenarios in which both backhaul link spectrum and access link spectrum belong to the same operator, but support for other models shall not be precluded (different operators for access and backhaul links).
- Both in-band (when applicable) and out-band mobile relay can be considered, as defined in [12].
- To limit the effort of optimizing the deployment for high speed train scenario when multiples RATs are used on the trains, multi-RAT support is considered for mobile relays, with LTE backhaul but different air interface technologies (e.g. LTE/3G/2G) on the access link

The mobile relay should fulfil these requirements, with clear benefits as compared to existing solution, to make the use case viable from a standard and deployment point of view. In particular dedicated macro eNBs deployments covering the rail tracks with directional antennas and introduction of radio repeaters which amplify the radio signal overcoming the carriage penetration loss should be considered in this regard. The comparison involves different aspects, among others spectral efficiency, signalling, handover success, coverage/capacity, complexity and battery consumption [76].

4.2.6.3 Mobile relay architectural aspects

One of the main aspects requiring careful selection is the architecture of the mobile relay. In rel-10 in fact the architecture was selected without considering mobility aspects and therefore may or may not be suitable when mobility function is introduced. In fact, the introduction of mobility may be not trivial when considering the rel-10 solution (see Figure 4-24), as the Donor eNB (DeNB) acts as a proxy for S1 and X2 signalling to and from the relay node and embeds the S-GW/P-GW functionalities needed for the relay operation (e.g. managing EPS bearers for the relay, mapping of signalling and data packets onto EPS bearers).

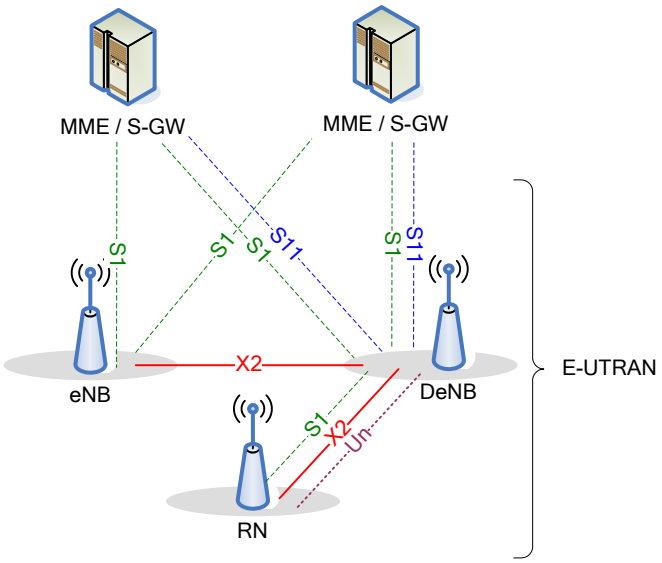

Figure 4-24 : Overall E-UTRAN Architecture supporting RNs [43]

One important principle for the architecture of the mobile relay is the selection of the mobility anchor point for the relay and for the UE [77].

4.2.6.3.1 Location of the mobility anchor for the Mobile Relay

In Rel-10, the Packet Data Network Gateway/ Serving Gateway (PGW/SGW) of the relay are co-located with the DeNB as described in [43]. To support relay mobility and trying to maximize the reuse of the existing core network design and procedures two possible options can be considered for the location of the GWs for the mobile relay, as illustrated in Figure 4-25:

1. The PGW/SGW are logically co-located with the DeNB as for Rel-10 relay architecture; or

2. The PGW/SGW are a logically separate function from the DeNB (reusing the S1 interface) as for Rel-8 UE architecture.

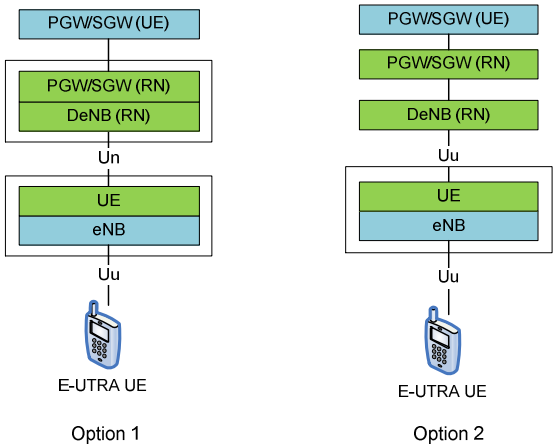

Figure 4-25: PGW/SGW locations for options 1 and 2 [77].

For option 1, in order to support mobility, either the PGW/SGW is moved to the new serving DeNB with each mobile relay handover (option 1A), or an interface from the PGW/SGW in the source DeNB to the target DeNB is defined (option 1B), as summarized in Figure 4-26

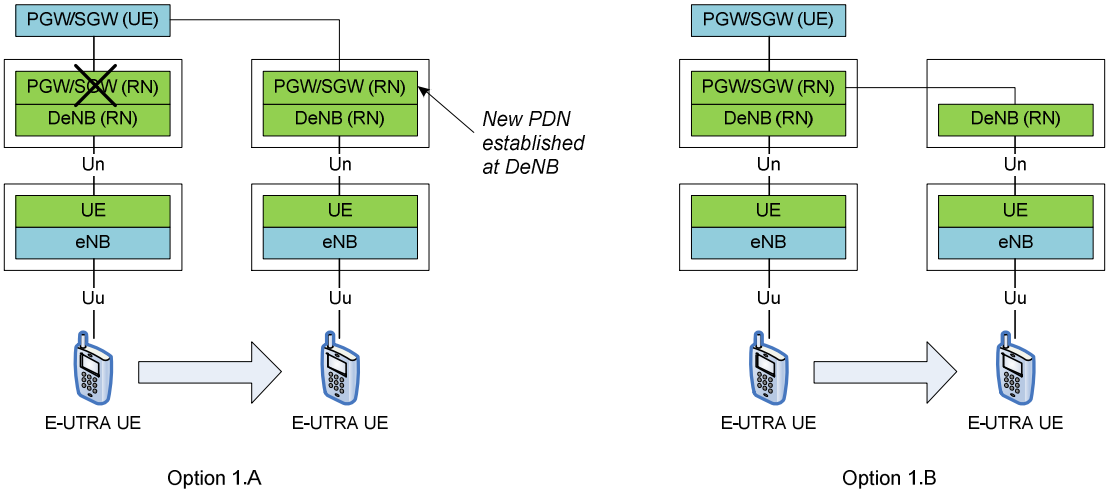

Figure 4-26: Support for options 1A and options 1B [77]

Among the cases, option 1A requires that either the mobile relay re-establishes the Packet Data Network (PDN) connection for handover (i.e., deactivate and reactive the PDN at each mobility event which is very disruptive to service since the IP address changes), or define a PGW relocation procedure which preserves the IP address of the mobile relay in order to minimize the service interruption, which incurs significant complexity to update network routing tables in real time.

It seems therefore wise to consider the PGW/SGW functions of the mobile relay as logically separated from the DeNB and reuse the S1 interface towards the DeNB (option 2, which is logically equivalent to option 1B).

This way the mobile relay SGW can serve as mobility anchor point for mobile relay inter-DeNB handovers [76]

4.2.6.3.2 Location of the mobility anchor for the UE

In case of the UE, the PGW/SGW reside in the core network and in order to optimize the traffic routing for UEs connected via mobile relays while supporting UE mobility, two possible options can be considered:

1. The PGW/SGW are located in the core network (as in Rel-8): full reuse of existing procedures but reduced routing efficiency as the UE traffic traverses two sets of GWs on the core network before arriving at the relay
2. The PGW/SGW are logically collocated with the mobile relay reusing the Rel-10 principles defined for Selected IP Traffic Offload/ Local IP Access (SIPTO/LIPA): maximum routing efficiency since the selection of the (relay) PGW/SGW can be optimized based on configuration and the expected route of the train, thus optimizing also routing for UE

In this regard, the first option could provide a baseline solution for mobility that reuse existing procedures and routing efficiency can be further optimized by adopting option 2 in addition.

4.2.6.3.3 Architecture alternatives

Based on the principles highlighted in sections 4.2.6.3.1 and 4.2.6.3.2, the relay-GW/PGW/SGW may be changed for routing optimization purpose, and this can be done independently of the relay mobility procedure (e.g. may be performed after completing handover). Different architectures can be considered for mobile relays under these principles [78].

Alt.1 (see e.g. [79])

This architecture is based on the Alt.1 architecture defined for fixed relay in [75], and shown in Figure 4-27. Both S1 user and control plane for the UE are terminated at relay and EPC and packets of a UE served by the mobile relay are transported by the relay user plane EPS bearers.

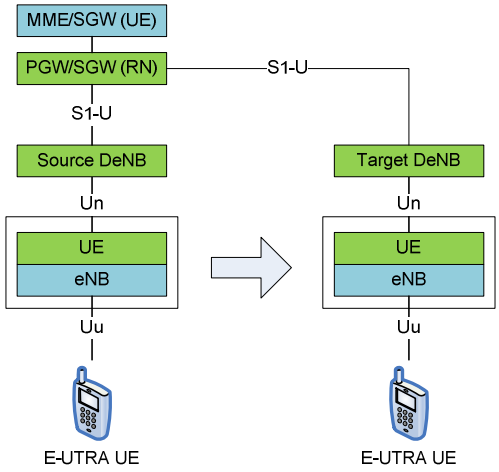

Figure 4-27: Alt. 1 relay architecture [78]

Existing handover procedures defined for UE can be reused for the relay itself with some enhancement/modification in case needed, and both UE and relay PDN connections are preserved during mobile relay handover. The mobility procedure (see Figure 4-28) is therefore identical to inter-eNB handover defined in [43], with no additional signalling for UE handovers, i.e. the relay handover is transparent to the UE in both radio access and core network.

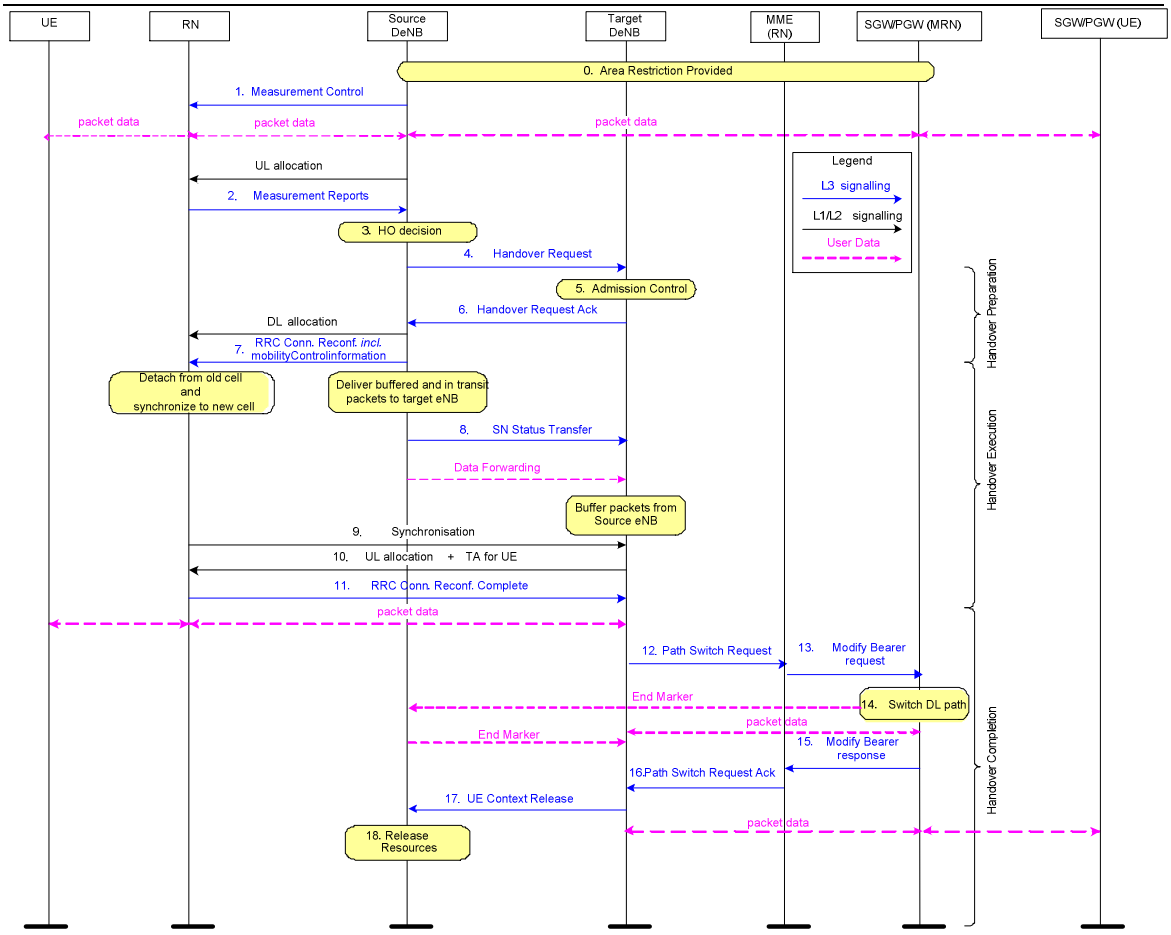

Figure 4-28: Alt. relay mobility procedure [78]

Alt.2 (see [78])

This architecture is based on the Alt.2 architecture defined for fixed relay in [75], and shown in Figure 4-29. In this case, the mobile relay GW/PGW/SGW are located in the initial DeNB where the mobile relay attaches for normal operation and kept upon handover. Both S1 user and control plane as well as packet transport now involves also the relay GW in the initial DeNB.

Existing handover procedures defined for UE can still be reused, and both UE and relay PDN connections are preserved during mobile relay handover. The mobility procedure is therefore identical to alt.1 case, except the relay PGW/SGW is always located in the initial DeNB, with no additional signalling for UE handovers, i.e. the relay handover is transparent to the UE in both radio access and core network.

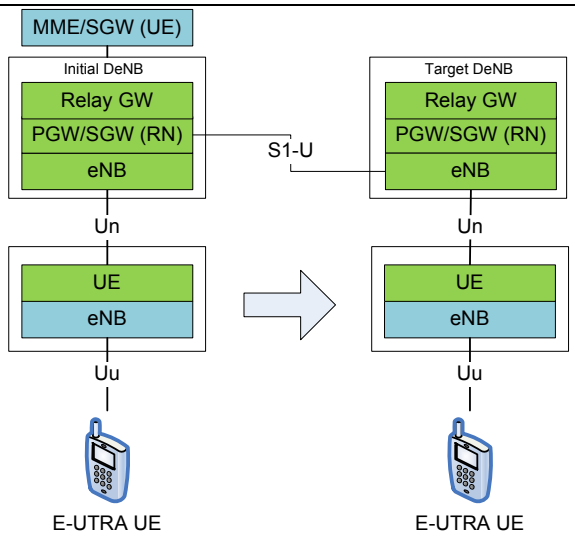

Figure 4-29: Alt. 2 relay architecture, with Relay GW and PGW/SGW co-located with initial DeNB [78].

Alt.2 variations and enhancements

While Alt. 1 calls for simplicity and good reuse of existing procedures to support mobile relays, Alt.2 was optimized for fixed relay and further enhancements may be necessary to deal with mobility.

One simple option, is to separate relay GW and PGW/SGW from initial DeNB and put them into a separate mobility anchor while still keeping the S1/X2 functionality, thus generalizing the alt. 2 as shown in Figure 4-30 (Alt.2 solution presented in section 0 can be seen as special case where selection was to the PGW/SGW at the initial DeNB). The mobility procedure is the same as alt.2, whereby the mobility anchor replaces the initial DeNB.

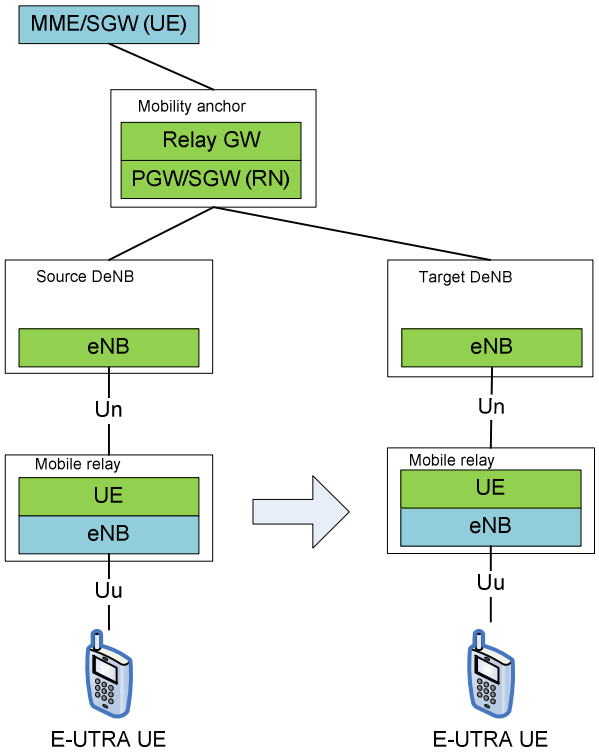

Figure 4-30: Alt. 2 relay architecture, with Relay GW and PGW/SGW separated from initial DeNB [78]

Another possible alternative proposed to enhance alt. 2, is to use two Rel-10 relays entities in the mobile relay device [78], as shown in Figure 4-31. These two entities act as two relays that attach to two neighbouring DeNBs, and can provide a similar function as RN handover: initially RN_UE1 connects to DeNB Cell1 and all the UEs in the train are served by RN Cell1. When the train moves into the coverage of DeNB2 Cell2, RN_UE2 attaches to DeNB2 Cell2, and activates RN_Cell2, so that the UEs under RN_Cell1 are handed over to RN_Cell2, via S1/X2 handover. When no more UEs are connected to RN_Cell1, RN_UE1 detaches from DeNB1 Cell1, and releases S1/X2 connections, being ready to attach to the next DeNB cell (e.g. DeNB3 Cell3). The relay handover is realized without a relay mobility procedure ands each UE performs the same inter-DeNB handover defined for fixed relays [75], [43]

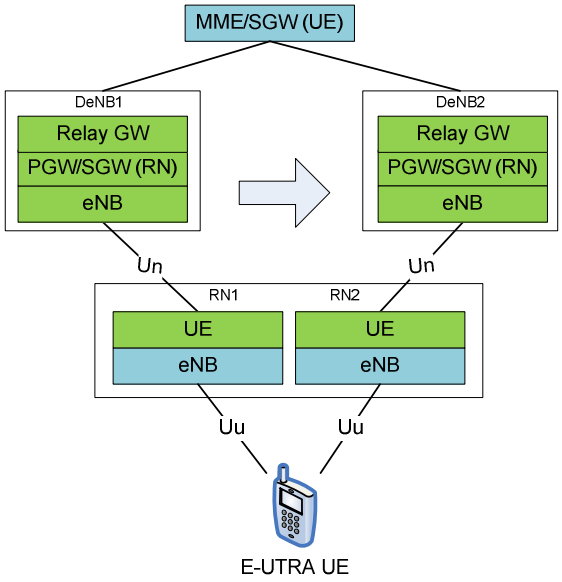

Figure 4-31: Alt. 2 architecture enhancement: dual relay entity [78]

Another possible enhancement to Alt. 2 is the addition of mobile IP (PMIP) function [78]. The basic idea of Alt2+PMIP is to integrate the functionality of Proxy MIP (PMIP) into DeNB of Alt2 so that the first DeNB to which a mobile relay attaches can function as the Local Mobility Anchor (LMA) for the relay. In the case of the relay's handover to a new DeNB, the new DeNB acts like a Mobile Access Gateway (MAG) to the relay. By taking advantage of PMIP-related signalling procedure, user plane transmission of a UE under the mobile relay can be accomplished via IP forwarding (in the form of PMIP tunnelling) from the LMA to the MAG directly, as illustrated in Figure 4-32. In this case the handover procedure is enhanced by PMIP operations, and path switch for UEs becomes unnecessary, since the LMA keeps the mobile relay's P-GW unchanged during mobility.

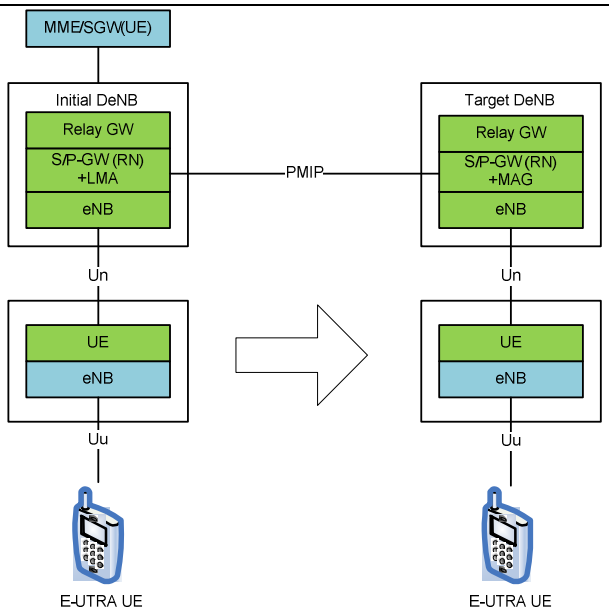

Figure 4-32: Alt. 2 architecture enhancement: mobile IP [78]

Alt.4 (see [78])

Alt 4 relay node architecture is shown in Figure 4-33and was also considered for fixed relay in [75], but eventually discarded. Like in alt. 2, both S1 user and control plane as well as packet transport now involves also the relay GW in the initial DeNB, with control plane packets of a UE served by mobile relay carried by SRB over Un interface and user plane bearers being one-to-one mapped to separate radio bearers on Un interface.

Existing handover procedures defined for UE can still be reused, but mobility procedure relies on DeNB awareness of every UE under the mobile relay, with stored information for each bearer of such UE and UE context transfer to the target DeNB during handover preparation phase (see [78] for details).

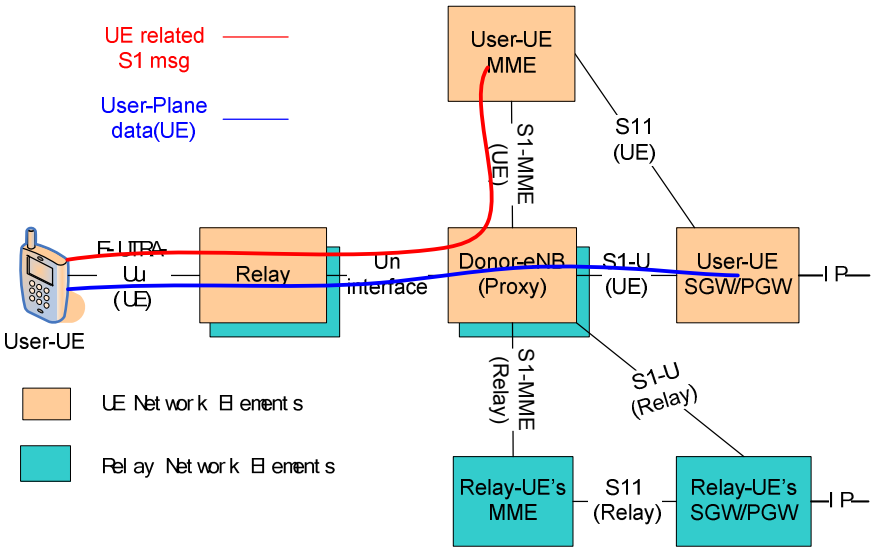

Figure 4-33: Alt. 4 relay architecture [78]

Observations on relay architectures

In Alt.1, the relay node SGW repoints the S1-U tunnel from the source DeNB to the target DeNB when the RN performs a handover to the target DeNB. As such, relay mobility can be supported reusing the existing Rel-8 handover principle and this is valid also in case the initial relay SGW selection was to a SGW that is collocated with the DeNB where the relay established the PDN.

In Alt. 2, in order to reuse the Rel-8 handover principle, the Mobility Management Entity (MME) needs to switch the S1-U path to the target DeNB for each inter-DeNB mobility event. As such, relay mobility can be supported reusing the existing Rel-8 handover principle. However the value of the relay GW, which was introduce to terminate the S1 and X2 interfaces thus making the relay to appear to the rest of the network as another cell of the source DeNB and to perform better QoS on the backhaul, seems vanishing when the relay moves far away.

While no strong differences can be identified between Alt. 1 and Alt.2 besides the relay GW role (see also [81]), in Alt. 4 no relay SGW is included for the mobile relay and therefore it seems drifting apart from the principles illustrated in section 4.2.6.3.1, where the SGW in the core network acts as mobility anchor for the relay.

4.2.6.4 Mobile relay interfaces and procedural aspects

In this section we analyze where the X2 and S1 interfaces for the mobile relay can terminate, for a maximized reuse of the existing design and procedures. Different alternatives options for where the X2 and S1 interfaces terminate for the Mobile Relay. In addition we consider the impact of the decision on how to support group mobility [80].

4.2.6.4.1 Mobile Relay interfaces to the RAN

While in Rel-10 the DeNB terminates the X2 interface of the relay and provides a proxy function to other RAN elements [43], it is worth revisiting this aspect and see what it provides when relay mobility is introduced.

Key scope of the X2 interface is to provide optimized mobility and to enable additional functionalities like support for SON and ICIC enhancements with neighbouring eNBs. These functions are beneficial in case of stable deployments, but as the mobile relay is expected to be fast moving on the high-speed train, it may not be able to benefit from X2 features as the neighbouring eNBs may be changing quite rapidly.

Given the additional complexity that may derives, it seems therefore more recommendable to not consider X2 interface for mobile relay and focus only on basic mobility provided by the S1 interface.

4.2.6.4.2 Mobile Relay interfaces to the Core Network

Similarly, in Rel-10, the DeNB terminates also the S1 interface of the relay. By applying the same rational of section 3.1, it is also worth revisiting this aspect. Two choices can be considered, with termination of the relay S1 interface at the DeNB as or with termination of the relay S1 interface directly at the MME (as done for regular eNBs).

As the relay moves and S1 interface is maintaining states as well, in order to terminate it at the DeNB upon relay mobility, the interface needs either to be moved as well to the new DeNB or to be reset at each relay handover. In both cases, there are complications and possibly even service disruption, so it is preferred to simply terminate the S1 interface directly at the MME, with the reuse of the S1 procedures.

4.2.6.4.3 Procedural aspects

A nice consequence of this is that, given the S1 interface is terminated at the MME, the mobile relay can be assigned a tracking area independent of the DeNB, so that relay mobility does not require the relay to change tracking area when moving, which makes the relay mobility transparent to UEs connected to the relay node. This way no further signalling is needed for relay handover events.

4.2.6.5 Access link options: LTE-only or multiple RATs access

The fixed relay introduced in Rel-10 is a LTE node, in which a regular eNB is connected to the network by means of a wireless backhaul, mainly for coverage extension purposes. Both access and backhaul links are LTE-based, and the backhaul is handled by a new interface called Un, which terminates at an upgraded eNB acting as donor for the relay (also named donor eNB - DeNB). However, in case of mobile relay, as the main scope is to provide realisable and high quality services on-board high-speed train carriages, 3GPP felt the need to not preclude support for additional or different RATs in the access link, like GSM or UMTS.

On one side there is in fact the wish to offer services on more than LTE radio access inside the train, in order to serve the needs of different operators – for example a train coverage could be deployed in strict collaboration with the railway company and operated to serve radio access of different kind and wireless operators, all from the same backhaul. By using LTE as sole backhaul, limits the standardization effort and ease the deployment and optimization effort for high-speed train coverage.

4.2.6.6 Conclusions

After the introduction of fixed relay nodes in Rel-10, 3GPP is investigating the possibility to also consider mobile relays from Rel-11, with main target high-speed train scenarios and related requirements, as alternative to existing specialized deployments such a dedicated macro coverage or radio repeaters, as illustrated in the initial part of this chapter. Different architectures have been presented, starting from what considered during the investigation of the fixed relay, and extending them to support mobility procedure for the backhaul link (i.e. mobile relay handover). Besides that, further procedural aspects and few considerations on access link options have been included.

4.2.7 Mobile Relays

4.2.7.1 Introduction

Mobile relays are currently a very hot topic in the 3GPP community in which low-power nodes are mounted on public transportation such as high-speed trains and ferries. These deployments pose many challenges which are unique in their nature and different from conventional fixed relays and Wi-Fi hotspots. Notably, mobile relays may operate in a closed or open subscriber group, and thus need to cope with a large number of onboard users. In addition, the high-speed aspect of these vehicles hinders conventional radio resource management techniques such as interference management and mobility management. As a result, there is a need for reliably ensuring high-data rates for onboard users through efficient and heterogeneous backhaul connections to donor eNodeBs. Besides, resources need to be shared in an efficient manner between onboard users and outdoor macrocell users. The focus of this section is on the backhaul, which is becoming a key element for guaranteeing the many-fold increase in data rates. Clearly, backhaul is one of the limiting factors of mobile femtocells, and hence, smart backhauling strategies are of utmost importance. Different heterogeneous backhauls are envisaged, such as wired, wireless and a combination thereof. The former is among mobile femtocells, whereas the latter is between one or multiple mobile femtocells and one or many donor eNodeBs. Coordinating these heterogeneous backhauls in an efficient manner in the case of load balancing, and mobility management is seen as instrumental. Furthermore, smarter duplexing methods to smartly carry out the joint access and backhaul design, and self-organization are seen as crucial.

4.2.7.2 Proposed Solution

In this section, we describe the proposed solution for mobile relays referred to as coordinated and cooperative relay system (CCRS) [40]. CCRS is made up of a group of mobile relays, each of which is responsible for a local cell (within a carriage) and which may have a backhaul link established with an eNodeB. The CCRS may be connected to multiple eNodeBs at any given time, as well as multiple parallel backhaul links to the same eNodeB. The donor cellular system may control and coordinate these mobile backhaul links, together with smart cooperation between the mobile relays inside the CCRS. A new interface is defined (crX2) interconnecting the mobile relays, used for cooperation in duplexing operation, load-balancing and capacity sharing amongst the MRs and the local cells thereof, and connection and mobility management. The crX2 interface may be wired or wireless, and if wireless preferably out of band to avoid interference to cellular users. Figure 4-34 depicts the considered network topology with two donor eNodeBs and a mobile femtocell train.

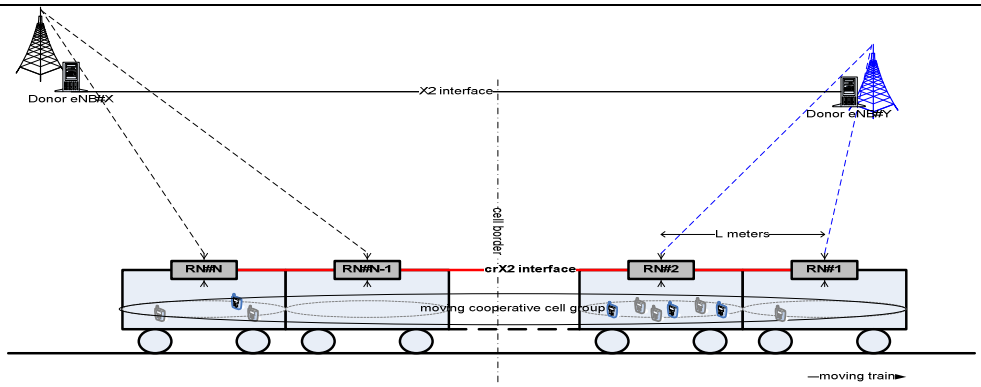

Figure 4-34: Simulation scenario.

4.2.7.3 Simulation Results

The primary assumption made for simulation of the CCRS is that the backhaul link (eNodeB to MR) is the capacity *bottleneck* of the whole system; therefore it is assumed that there is enough access link capacity for the moving relay nodes (MRNs) to share the backhaul capacity in an efficient manner amongst the served users within the train. The access link is not modeled in the simulator, and the throughput of train users when served by a MRN is calculated by simply dividing the backhaul throughput of the MRN by the number of users of the MRN. It is also assumed that the crX2 interface connecting the MRNs has zero latency, and unlimited capacity. Simulations are carried out for both full-duplex and half-duplex backhaul link operation. Currently handover is not supported in the simulator, so simulations are carried out with all users inside the train connected directly to an eNodeB or through a MRN. The simulator layout consists of 19 tri-sector eNodeBs, forming a 57 cell central layout. The 57 cells are then replicated around the edges of the central cell layout, to form the 399 cell wrap-around model shown in Figure 4-35. The wrap-around model is used so that there are equal levels of inter cell interference at all cells in the central layout. Macro UEs are evenly distributed throughout the 57 central cells (blue points). A train consisting of 8 carriages is dropped on the track (cyan) that runs through the cell layout with radius of 4 km (typical for high speed train lines), such that the whole of the train is always inside the central 57 cells. For each simulation carried out the train travels over the length of the track, moving 20m every drop. 20 users are evenly distributed throughout the 8 carriages, each served by the MRN in that carriage. A second train may also be dropped traveling in the opposite direction, however for the following simulations only one train was dropped in the layout. Each carriage has a MR (red points) at the center, and train UEs (green points) are evenly distributed throughout and inside the carriages (dark blue border). The trains UEs are paired with the MRNs on the carriage in which they are located, if they are connected to the MR, otherwise they are paired with the closest 57 cells as are the normal macro users.

All MRNs forming a train are independently assigned a serving eNodeB based on pathloss. MRNs are grouped based on their serving eNodeB, and of each of these groups only the MRN with the best link quality is assigned resources by the serving eNodeB, based on the assumption that the MRNs may cooperate to share the backhaul resources. In addition, the groups may also perform joint detection across all MRNs in the group. The large number of antennas, up to 64 in the case of the following simulations, and the large antenna spacing of 30m between clusters, provides a large diversity gain in this case. All links use the Urban Macro fast-fading model, and shadowing with distance dependent correlation. The path-loss model used for the normal macro users is also urban macro, macro users inside the train have and additional 20dB penetration loss. The path-loss model used for the backhaul link from eNodeB to MR is “Macro-to-relay” in [12].

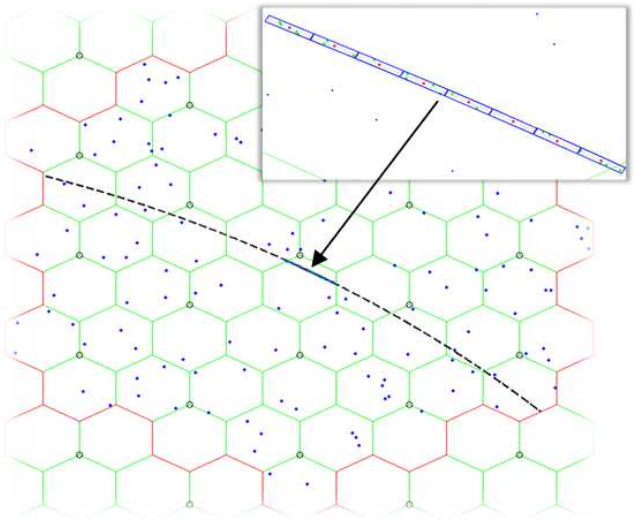

Figure 4-35: System layout generation highlighting the mobile femtocell's trajectory.

Since the focus is to investigate the backhaul capacity of MRNs, a full-buffer traffic model is applied to users inside the train. For normal macro users a rate constraint traffic model is applied using proportional fair scheduling, since the purpose of including macro users in the simulation is to create a realistic network load, and thus interference levels. Train users connected directly to an eNodeB are considered as normal macro users by the scheduler with no rate constraint. In the case of full-duplex MRN backhaul link operation, when MRNs are to be scheduled by an eNodeB, macro users are first scheduled, with a fair upper bound on the amount of resources to be assigned to them determined by the number of users the MRNs are serving, and the number of normal macro users. After assigning resources to macro users, the scheduler then schedules all remaining resources to the strongest MRN located in the sector. Scheduling is considered over a period of 4 TTIs, and in the case of half duplex operation the scheduler attempts to schedule all macro users during the time that the MRN backhaul link is inactive, in order to maximize the amount of resources available to for the MRN backhaul. In the case of half-duplex operation the upper-bound of resources available to normal macro users is therefore a minimum of 50%.

Table 4-1: Simulation assumptions.

System Bandwidth	10Mhz (50 PRB)
Propagation environment	Urban Macro
Base station sites	19 (57cells)
Base-station Tx Antennas	1
MRN Rx Antennas	8
UE Rx Antennas	2
MRN Rx Antenna height	5m
Train velocity	300Km/h
Train carriage length	30m
Train carriage penetration loss (eNodeB to UE)	20dB
Number of Macro users	570
Number of trains	1
Number of carriages per train (= Number of MRN)	8
Number of train users	20
Channel samples per drop	300 (1ms between samples = TTI)
Traffic Model	Full-Buffer

Two simulation scenarios are considered. In the first case all train users are directly connected to the macro eNodeB. In the second case all train users are connected to the network through a MRN, with simulations carried out for both half-duplex and full-duplex backhaul link operation. The average spectral efficiency and throughput are the performance metrics.

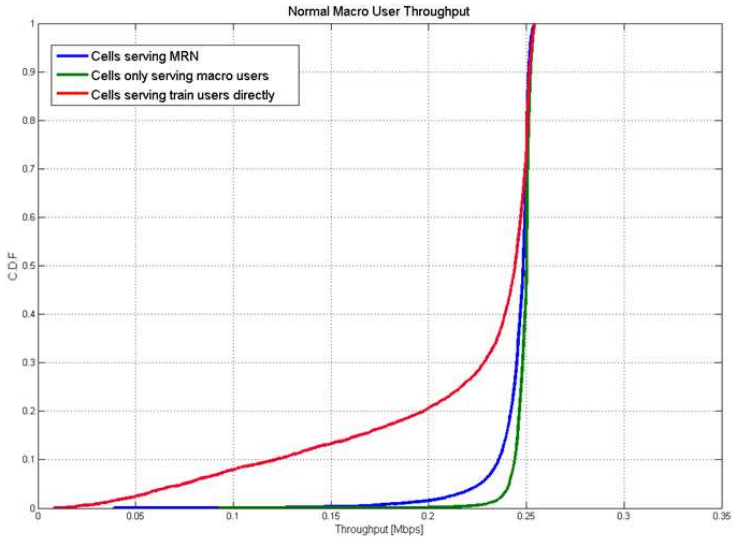

Figure 4-36: Cumulative distribution function (CDF) of the macrocell user throughput in cells serving MRNS, in cells serving train users, and in all other cells.

Figure 4-36 shows the cumulate distribution function (CDF) plot of user throughput for macro users located in cells serving MRNs, cells serving train users directly, and in all other cells. With the chosen simulation parameters, a small decrease in macro user throughput for cell edge users occurs in cells serving MRNs. When train users are served directly however a much larger decrease in macro user throughput occurs. This is a result of the fair upper bound set for allocating macro users resources in the case of MRN resource allocation. Figure 4-37 shows the throughput of train users when connected to MRNs with full duplex operation, MRNs with half-duplex operation, and the mean throughput of train users connected directly to an eNodeB. In the case of the chosen simulation parameters the use of half-duplex MRNs decreases the throughput of train users when compared to directly connecting to an eNodeB. The full-duplex case provides better throughput for more than half of the train users however in the Figure 4-37 shows the throughput of train users when connected to MRNs with full duplex operation, MRNs with half-duplex operation, and the mean throughput of train users connected directly to an eNodeB. In the case of the chosen simulation parameters the use of half-duplex MRNs decreases the throughput of train users when compared to directly connecting to an eNodeB. The full-duplex case provides better throughput for more than half of the train users however in the case of direct connection the peak throughput is higher, at the expense of normal macro user throughput as shown in Figure 4-36

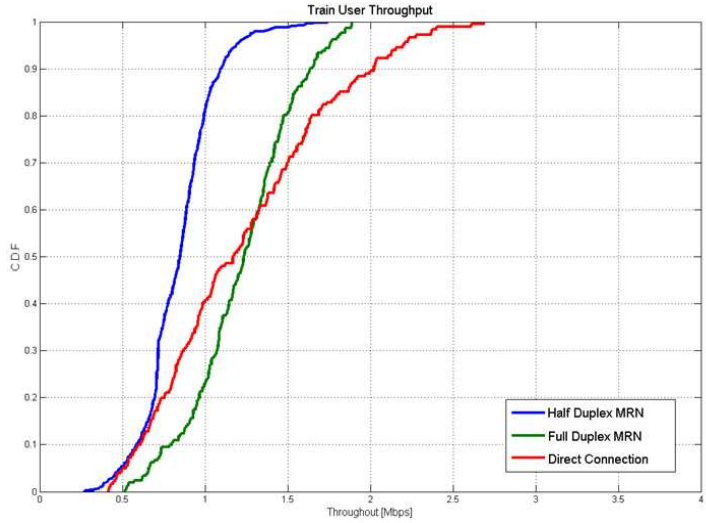

Figure 4-37 cumulative distribution function (CDF) of the train user throughputs.

4.2.7.4 Conclusions

The initial simulation results of the high speed train scenario show that in the case of the chosen simulation parameters, the CCRS does not improve the throughput of users aboard the train. However with cooperation, the CCRS does improve resource sharing at lower capacity for the train users, at the cost of the throughput of normal macro users in the cells the train is located in. Further research is needed to evaluate the potential system performance improvement provided by MRN concept. Another future research topic is related to the full duplex operation with MRN with the possibility of having some of the distributed antennas half-duplex whereas others are full duplex.

4.3 Distributed SON Algorithms (local)

4.3.1 Replication Dynamics, Fictitious Play and Classical Q-Learning

4.3.1.1 Problem Statement

When information exchange among femtocells is allowed, (either through an explicit OTA signalling or through the backhaul), the strategic coexistence among femtocells can be modelled using tools from Evolutionary Game Theory (EGT) which was explored as a means of mitigating interference towards the macrocell tier. EGT was shown to provide relatively high gains as compared to classical learning algorithms (Q-learning among others), by relying on a HeNB-GW, which acts as a semi-centralized entity through which femtocells exchange information in a two-way communication fashion (see [34] for more details).

4.3.1.2 Algorithm Description

The fictitious play (FP) goes beyond this which is yet another framework that can be defined as follows: let us first assume that femtocells have complete and perfect information, i.e., they know the structure of the game and observe at each time t the power allocation vector taken by all other femtocells. This perfect observation can be enabled through an exchange of information through the X2 interface. The FP game can be written in a strategic-form $g^{(FP)} = \left(K, \{A_k\}_{k\in K}, \{u_k\}_{k\in K}\right)$. Here, K denotes the set of players (i.e., FBSs). For every $k \in K$, the set of actions of FBS_k, is the set of power allocation vectors $A_k = \left\{q_k^{(l,n)} : l \in \{0,...,L\}, \quad n \in N\right\}$, where $L_k \in N$ is the number of discrete power levels of FBS_k. The power allocation vector when FBS_k transmits over sub-carrier n with power level l is given by:

$$q_k^{(l,n)} = \frac{l}{L} p_{k,\max} \tag{4.16}$$

Finally, $u_k(.)$ denotes the utility function of FBS_k. Each FBS assumes that all its counterparts play independent and stationary (time-invariant) mixed strategies $\pi_j, \forall j$, where $\pi_j = \left(\pi_{j,q_j^{(1,1)}},...,\pi_{j,q_j^{(L,N)}}\right)$ and $\pi_{j,q_j^{(l,n)}} = \Pr\left(p_j(t) = q_j^{(l,n)}\right)$. $p_j(t)$ is the transmit power of FBS j at time t. Under these conditions, femtocell k is able to build an empirical probability distribution over each action set A_j , for all j . Let $f_{k,p_k(t)} = \frac{1}{t}\sum_{s=1}^{t} 1_{\{p_k(s)=q_k^{(l,n)}\}}$ be the empirical probability with which player j observes that player k plays action $q_k^{(l,n)} \in A_k$. Hence, $\forall k$, $\forall p_k \in A_k$, the following recursive expression holds:

$$f_{k,p_k}(t+1) = f_{k,p_k}(t) + \frac{1}{t+1}\left(1_{\{p_k(t)=q_k^{(l,n)}\}} - f_{k,p_k}(t)\right) \tag{4.17}$$

Let $\bar{f}_{k,p_{-k}}(t) = \prod_{j\neq k} f_{j,p_j(t)}$ be the probability with which player k observes the action profile $p_{-k} \in A_{-k}$ at time t, for all k . Let the $|A_{-k}|$ dimensional vector $f_k(t) = \left(\bar{f}_{k,p_{-k}}\right)_{\forall p_{-k}\in A_{-k}}$ be the empirical probability distribution over the set A_{-k} observed by player k . In what follows, the vector $f_k(t)$ represents the belief

of player k over the strategies of all its corresponding counterparts. Hence, at each time t, and based on its own beliefs, $f_k(t)$, each FBS_k chooses its action $p_k(t) = q_k^{(l,n)}$, i.e.,

$$(l,n) \in \arg\max \bar{u}_k\left(p_k(t), f_k(t)\right) \tag{4.18}$$

where for all k, $\bar{u}_k(\pi) = E_\pi[u_k(p_k, p_{-k})]$ where $u_k(p_k, p_{-k})$ is the utility function of player k (transmission rate of the FBS conditioned by the MUE SINR being above a threshold). It can thus be implied that by playing FP, players become myopic, by building beliefs of strategies used by all other players, and at each time t, players choose the action that maximizes their instantaneous expected utility.

On the other hand, when information exchange among femtocells is no longer possible, different decentralized learning algorithms can be adopted by femtocells so as to mitigate their interference toward the macrocell tier. Among these learning algorithms is the classical Q-learning which was studied in greater details in the literature. In short, every FBS first carries out an exploration phase in which it learns by interacting with the environment in a trials-and-errors manner. After building its Q-table, and provided that the network does not dramatically change, each FBS picks the strategies that maximize the observed rewards over the interaction time of the players.

4.3.1.3 Simulation Results

In what follows, we compare performance results obtained through classical Q-learning and EGT, bearing in mind that contrarily to Q-Learning which is able to work in autonomous manner, or with limited feedback through the X2 interface, EGT requires a centralized controller (i.e., BeFEMTO gateway) to gather, process, and broadcast information about the agents.

We evaluate performances in a macrocell scenario with radius $R_m = 500$, underlaid with K femtocells of radius $R_f = 20$, transmitting over N = 8 sub-carriers. We assume that femtocells have L = 3 transmit power levels. The minimum SINR of the macrocell UEs is set to 3 dB for each sub-carrier. The macro BS transmission power is 43 dBm, and the maximum femto one is 10 dBm. The considered path-loss model is 3GPP compliant. We also assume fast fading and log-normal shadowing with standard deviation of 8 and 4 dBm for outdoor and indoor communications, respectively. The discount factor and exploration probability are set to 0.95 and, 0.5 respectively in the case of Q-learning formulation [16].

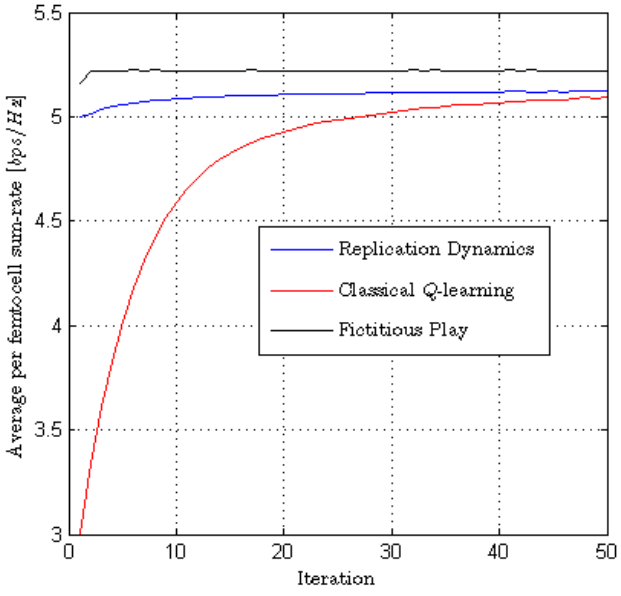

Figure 4-38: Convergence of the RL learning algorithms and their impact on the average femtocell sum-rate for K=50 femtocells and N=8 sub-carriers.

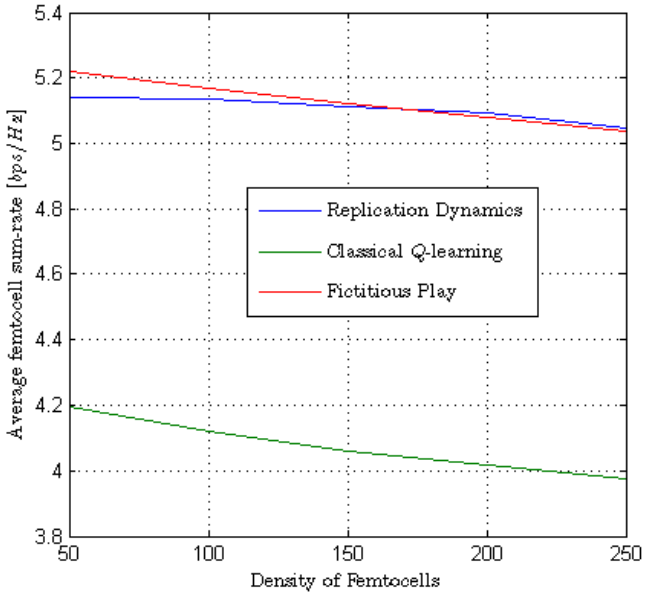

Figure 4-39: Effect of femtocell density on the average femtocell sum-rate, for different learning algorithms.

In Figure 4-38, we plot the average femtocell sum-rate for K=50 FBSs underlying one macrocell over N=8 sub-carriers, highlighting the convergence behaviour for different learning algorithms. It can be noticed that the replicator dynamics [16], fictitious play, Q-learning schemes eventually converge to some steady state. Moreover, the fictitious play showcases the highest sum-rate, whereas the classical Q-learning needs an exploration phase until convergence is eventually reached. On the other hand, Figure 4-39 plots the impact of the femtocell density on the average femtocell sum-rate for the different learning algorithms, for K= 50, 100, 150, 200, 250 femtocells. A general decline in performance is perceived as the number of femtocells increases, which reflects the interference-limited nature of the network. Nonetheless, and quite interestingly, we see that the rate of decrease in performance is not the same for all algorithms. In particular, for K=250, the femtocell average sum-rate of around 5 bps/Hz is obtained using replicator dynamics and fictitious play, whereas approximately 4 bps/Hz is obtained with Q-learning.

4.3.1.4 Conclusions

We have analysed one of the tradeoffs facing small cell networks, namely self-organization in a totally decentralized manner and get sub-optimal performance, or exchange information over the X2 interface or through the BeFEMTO local gateway and obtain better gains. In detail, the fictitious play formulation exhibits higher gains albeit more information exchange. In contrast, the classical Q-learning obtains slightly lower payoffs but requires long convergence time.

4.3.2 Decentralized Femto Base Station (HeNB) Coordination for Downlink Minimum Power Beamforming (TDD)

4.3.2.1 Problem Statement

A decentralized downlink beamformer design using coordinated HeNBs is proposed for minimizing the total transmitted power of coordinated HeNBs subject to fixed cross-tier interference constraints and femto-UE specific SINR constraints. The proposed minimum power beamformer design relies on limited backhaul information exchange between coordinated HeNBs. Instead of exchanging full channel state information between coordinated HeNBs, real valued HeNB specific co-tier interference terms are exchanged. Therefore, a centralized controlling unit is not required, and the minimum power beamformers are obtained locally at each HeNB. Coordination between HeNBs can be handled, for example, using X2 type of interface. Furthermore, setting up coordination can be part of the self-organization procedures of HeNBs. Our focus is on a co-channel deployment of macro and femtocell. In addition of handling co-tier interference, cross-tier interference constraints from HeNBs to Macro-UEs have to be taken into account. In other words, beamformers for femto-UEs have to be designed in a way that they cause minimum interference for Macro-UEs. To achieve this goal, an additional constraint is added to the optimization problem which limits the cross-tier interference power at a desired level. Note that eNB pays no attention for limiting the interference to femto-UEs when designing optimal minimum power beamformers for its

Macro-UEs. Consequently, coordination between macro and femtocells is highly limited. However, some limited amount of long-term coordination might be required in order to transfer the M-UE specific cross-tier interference constraint values from eNB to HeNBs.

Decentralized beamforming approach is proposed for TDD based system, and thus, it is fair to assume that each HeNB can measure at least the channels of all cell-edge users, independent of which HeNB they are connected to, for example, during the UL transmission phase of the TDD frame. Furthermore, it is assumed that the instantaneous interference from eNB to femto-UE is known at the HeNB in order to guarantee femto-UE specific SINR constraints. The interference knowledge can be achieved in two ways. First option is to measure femto-UE channel from uplink sounding signals at the eNB, and then forward it to the corresponding HeNB via backhaul. This option needs coordination between HeNB and eNB. The second option is to measure the interference at the femto-UE, and transmit it to the corresponding HeNB. In this case, the coordination between HeNB and eNB is not required. However, both these options might be impractical because of the high amount of information passing and signalling. Despite the fact that this assumption is somewhat impractical, we can obtain performance upper bounds for more practical cases where only partial interference knowledge is available at the HeNB. The proposed method can be deployed in open or closed access networks.

4.3.2.2 Decentralized approaches to CoMP

We derive a decentralized approach where the downlink beamformers are designed locally at each HeNB relying on the exchange of coupled real-valued co-tier interference terms between coordinated HeNBs. In order to turn the centralized problem into a decentralized one, the problem should be reformulated into a proper form for applying a dual decomposition method. The dual decomposition approach is appropriate when the optimization problem has a coupled constraint, and when relaxed the problem decouples into several sub-problems. Consequently, the original one level optimization problem can be divided into two levels of optimizations, i.e., a master dual problem and several sub-problems. Sub-problems are solved for fixed dual variables whereas the master problem is in charge of updating the dual variables. In other words, the amount of resources used in each sub-problem depends on the resources' prices set by the master problem.

4.3.2.3 Numerical results

A simplified simulation scenario with one eNB and 2 HeNBs is considered. Each HeNB serves a single cell-edge femto-UE. In addition, eNB serves a single Macro-UE. Each user is equipped with a single receive antenna. The number of transmit antennas at each HeNB/eNB is 4. The simulation scenario is depicted in Figure 4-40. We assume that both femto-UEs are located at the femtocell-edge having identical large scale fading coefficients $a_{b,k}$, i.e., $a_{1,1} = a_{2,2} = a$. Path gain to noise ratio is normalised to 1, i.e., $a^2/N_0 = 1$, for all users. We define a parameter α to denote the pathloss difference between the group of femto-UEs and the Macro-UE. By setting pathloss difference α to 0 dB we can model a scenario where all femto-UEs and Macro-UE are located exactly at the cell edge of macro- and femtocells. On the other hand, the cluster of 2 femtocells and the macrocell are totally isolated by setting $\alpha = \infty$.

Our focus is to study the required sum power of coordinating HeNBs for fulfilling the cross-tier interference constraints and the femto-UE specific SINR constraints in a block fading scenario. The elements of the channel vectors are modelled as i.i.d. Gaussian random variables. The following transmission schemes are compared by simulations:

1. Optimal decentralized coordinated beamforming (limited information exchange between HeNBs)
2. Decentralized coordinated beamforming with fixed co-tier interference (further reduced information exchange between HeNBs)
3. Decentralized Zero-Forcing beamforming (no information exchange between HeNBs)
4. Optimal decentralized coordinated beamforming without co-existence of Macro-UE (as a lower bound)

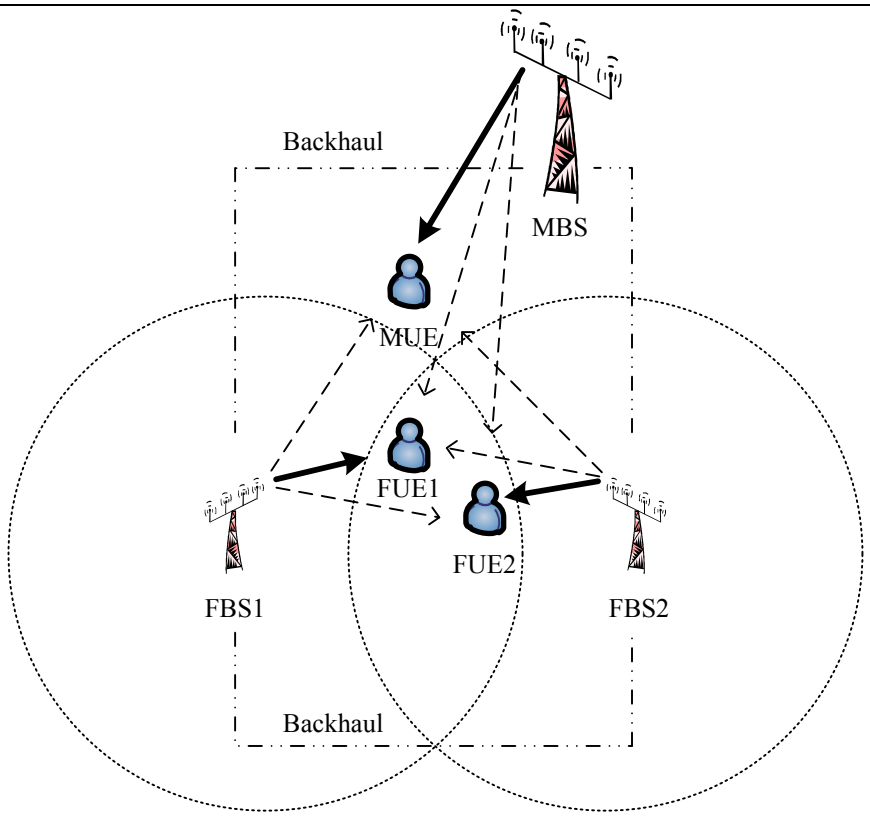

Figure 4-40: Simulation scenario

Figure 4-41 illustrates the average sum power of HeNBs as a function of pathloss difference α between Macro-UE and the group of cell-edge femto-UEs, to meet 0 dB SINR constraints for each user. Cross-tier interference constraint from HeNB to Macro-UE is set to 10 dB below the noise power level. Note that eNB employs optimal minimum power beamforming for serving its Macro-UE, and it is not concerned on the caused interference to femto-UEs. Therefore, the transmit power of eNB remains constant when pathloss difference α is varied. Consequently, eNB power is omitted from the simulation results. Low user specific SINR constraints can be interpreted as a user being far from its serving BS. Therefore, Figure 4-41 models a case where femtocells are located far from eNB. Results show that the proposed optimal decentralized coordinated beamforming can obtain significant performance gain over Zero-Forcing beamforming. Thus, it can be concluded that HeNB coordination is highly beneficial when the SINR constraints are low for Macro-UE and femto-UEs. Furthermore, it can be seen from the lower bound curve that non-controlled interference from eNB to femto-UEs causes significant performance loss for femtocells. Obviously, this is due to the fact that eNB pays no attention on the caused interference to femto-UEs.

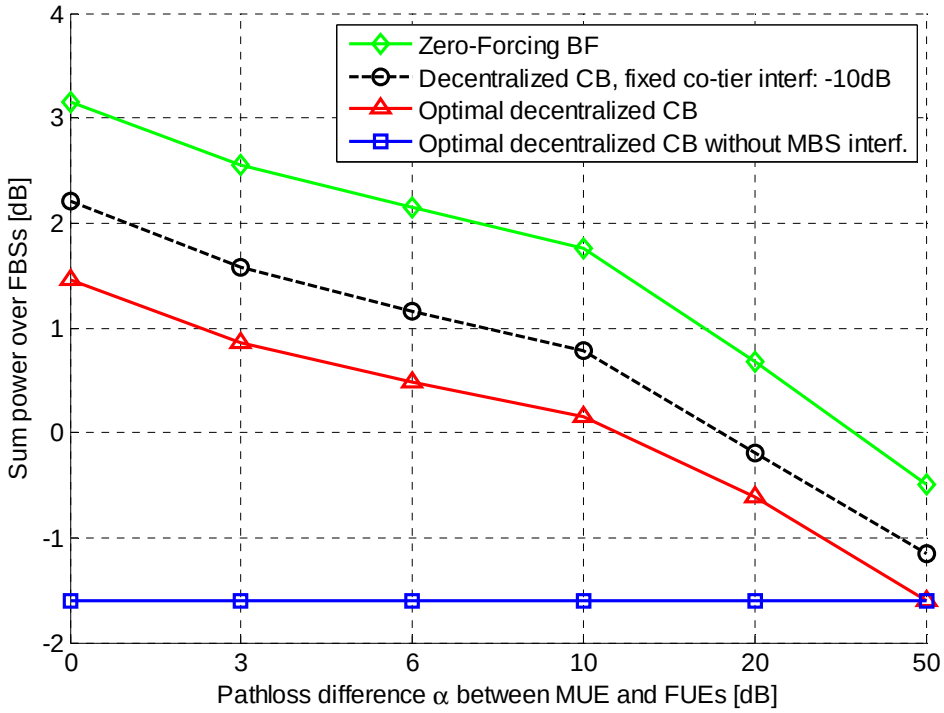

Figure 4-41: Average sum power of HeNBs for 0 dB femto-UE and 0 dB Macro-UE SINR targets.

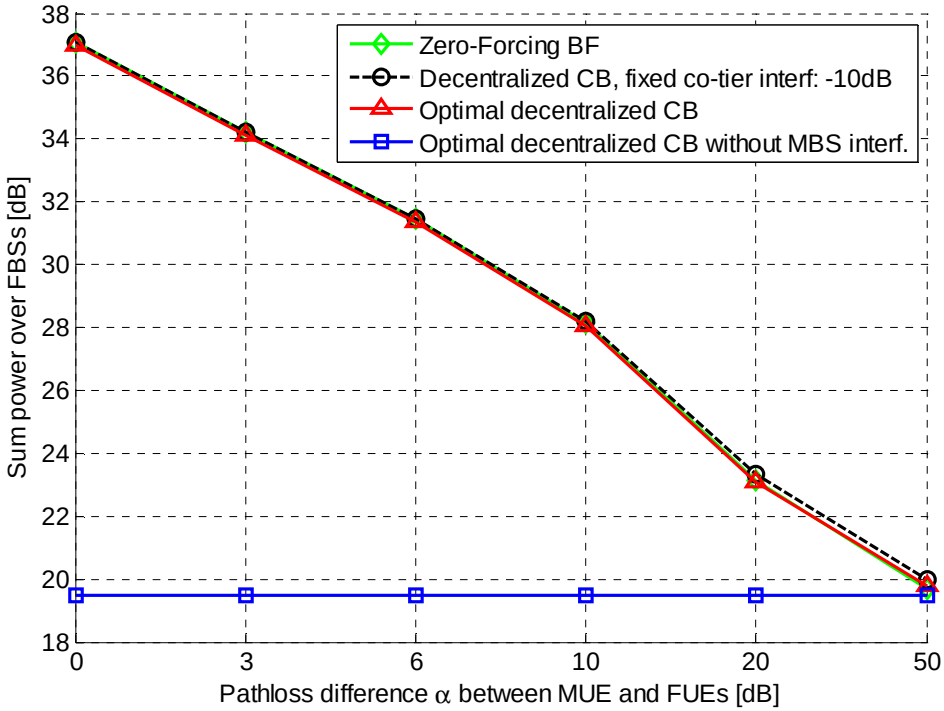

Figure 4-42: Average sum power of HeNBs for 20 dB femto-UE and 20 dB Macro-UE SINR targets.

Figure 4-42 illustrates the average sum power of HeNBs as a function of pathloss difference α between Macro-UE and femto-UEs, to meet 20 dB SINR constraints for each user. Again, cross-tier interference constraint is set to 10 dB below the noise power level. It can be seen that the proposed decentralized coordinated approach and Zero-Forcing beamforming scheme achieve similar performance in the case when both the femto-UEs and Macro-UE have high SINR targets. In this case, nearby eNB is causing tremendous interference to femto-UEs while HeNBs have to increase their power levels to guarantee femto-UEs' high SINR requirements. In addition, HeNBs have to generate almost zero interference to Macro-UE increasing the needed power levels even more. High SINR constraint implies that a user is near to its serving BS. Thus, the case where Macro-UE has high SINR constraint, and pathloss difference α is near 0 dB, models a scenario where femtocells are located relatively near to eNB. Results imply that in this kind

of scenarios HeNB coordination might not be beneficial and similar performance could be achieved with less complex transmission schemes.

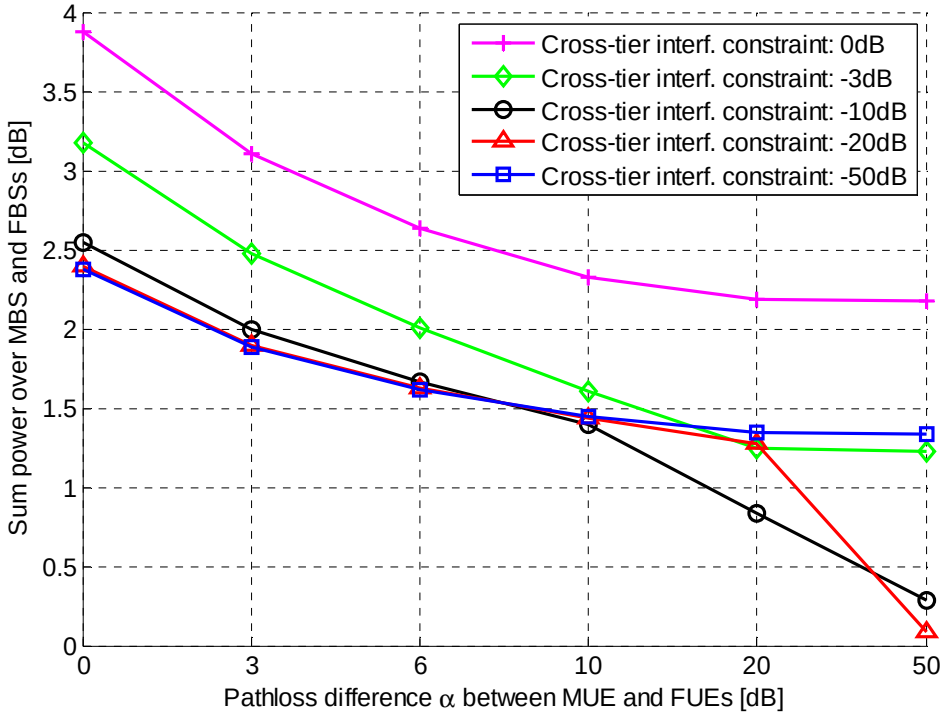

Figure 4-43: Average sum power of eNB and HeNBs for optimal decentralized coordinated beamforming scheme with varying cross-tier interference levels. SINR targets for femto-UEs and Macro-UE are set to 0 dB.

Figure 4-43 illustrates the average sum power of eNB and HeNBs as a function of pathloss difference α between Macro-UE and femto-UEs, to meet 0 dB SINR constraints when cross-tier interference power constraints are varied from -50 dB to noise power level, and optimal decentralized coordinated beamforming scheme is used. Simulation results show that the lowest sum power at the cell-edge is obtained when the cross-tier interference power constraints are -50 dB below the noise power level. Hence, it can be concluded that the cross-tier interference from HeNBs to Macro-UE should be kept as low as possible at the cell-edge scenario, and when the user specific SINR constraints are low. When Macro-UE is moving away from the femtocells the performance difference between the case with low cross-tier interference power and the cases with higher cross-tier interference powers, begins to decrease. When the pathloss difference α is over 10 dB, the lowest power is achieved if cross-tier interference power constraints are set to 10 dB below the noise level. This implies that, in some extent, the further away the Macro-UE is from the femtocell-edge the more cross-tier interference HeNBs can cause.

4.3.2.4 Conclusions

A decentralized minimum power beamforming design using HeNB coordination was proposed. The objective was to minimize the total transmitted power of coordinated HeNBs subject to fixed cross-layer interference constraints and femto-UE specific SINR constraints. The beamformers are obtained locally at each HeNB relying on limited information exchange on co-tier interference levels between coordinated HeNBs. The proposed approach allows for a number of special cases, where the signalling is reduced at the cost of somewhat sub-optimal performance. Numerical results showed that the proposed decentralized coordinated beamforming is highly beneficial over Zero-Forcing beamforming when the SINR constraints are low for femto-UEs and Macro-UE. However, when both the femto-UEs and Macro-UE have high SINR targets, HeNB coordination might not be beneficial and similar performance could be achieved with less complex transmission schemes. An interesting future work is to extend the decentralized beamformer design over coordinated HeNBs to other optimization criteria, and possibly study the performance in more realistic simulation scenarios.

4.3.3 Dynamic and Autonomous Subband Assignment

4.3.3.1 Problem Statement

In [34], we developed a central subband assignment method for femtocell networks called Graph-Based Dynamic Frequency Reuse (GB-DFR) where subbands are assigned to BSs by a central controller. In [51] we extended the GB-DFR for multi-user deployments and developed extended GB-DFR (eGB-DFR). In eGB-DFR, subbands are classified into two groups; primary subbands (PSs) and secondary subbands (SSs). PSs are assigned by a central controller and SSs are assigned by BSs autonomously. In this report we investigate a novel dynamic and autonomous subband assignment (DASA) method that is particularly well suited for decentralized wireless networks where subbands are assigned only by BSs in a distributed way. The proposed method is designed such that the interference protection does not coincide with an intolerable reduction in the attainable spatial reuse of radio resources.

4.3.3.2 System Model

Similar to the system models we used for GB-DFR and eGB-DFR, we consider the downlink of a LTE system where the system bandwidth consists of multiple subbands. Each subband consists of a fixed number of resource blocks (RBs) which are the most basic downlink resource allocation units for data transmission. A BS can allocate RBs of the same subband to multiple user equipments UEs; however, a RB can be allocated to only one UE in any given cell.

In LTE, UEs can differentiate between the received signals from various BSs in their vicinity with the help of cell-specific reference signals (CRSs). The received signal strength observed by UE_u from BS_n is determined by

$$R_{u,n} = T_{CRS}\, G_{u,n} \tag{4.19}$$

where T_{CRS} is the constant CRS transmit power and $G_{u;n}$ is the channel gain comprising the combined effect of path loss and shadowing between BS_n and UE_u. Each UE sends a measurement report to its serving BS including the cell identity with RSRP [26].

Furthermore, an LTE UE is also capable of calculating a SINR per subband by using the reference signals. It is clear that a UE reports high SINR if the reference signals sent by the serving BS do not face interference from other BSs. As will be explained later, such differences in SINR can be used for choosing the most suitable subbands. The signalling of SINR levels to a serving BS, in terms of suitable modulation and coding scheme, is achieved by using the channel quality indicator (CQI) [42].

Finally, in our system model, we assume that each BS sends an indicator to its neighbouring BSs which cause high interference. A BS is forbidden from using the subband if this subband has already been indicated as reserved by other BSs. Although such an indicator is not implicitly specified in the standards, it can be applied with minor changes on the signals already defined in standardization, such as the relative narrow-band transmit power (RNTP) [43] indicator.

4.3.3.3 DASA Algorithm Description

The main objective of DASA is that each BS in the network adapts its subband usage on-the-fly, so as to improve the capacity of cell-edge UEs, without causing a sharp decrease in the overall network capacity. In order to enable this, we define two classes of subbands depending on their foreseen usage: the primary subband (PS), and the secondary subband (SS). The PSs are reserved for cell-edge UEs facing high interference. A PS belonging to a particular BS cannot be used by neighbouring BSs which cause high interference to UEs of the BS in question. Such an arrangement helps to ensure that UEs allocated RBs from within the PSs experience low interference. A BS intending to use a particular subband as a PS needs to inform its interfering neighbours so that they do not use this subband. This is done via the transmission of a so-called PS indicator between BSs. When a BS receives such a message, it does not use the marked subband, thereby reducing the interference caused to its neighbouring cells. The subbands which remain unmarked, i.e., non-PS subbands, may be used by a BS as an SS depending on the prevailing interference conditions. However, SSs enjoy no privileges, these subbands cannot be blocked at interfering neighbouring BSs. RBs of SSs can therefore be allocated to cell-center UEs. The usage of the PS increases the cell-edge capacity, whereas, the SS increases the spatial reuse of resources. The classification of subbands is similar to eGB-DFR, however, in DASA, PSs are also assigned autonomously by BSs.

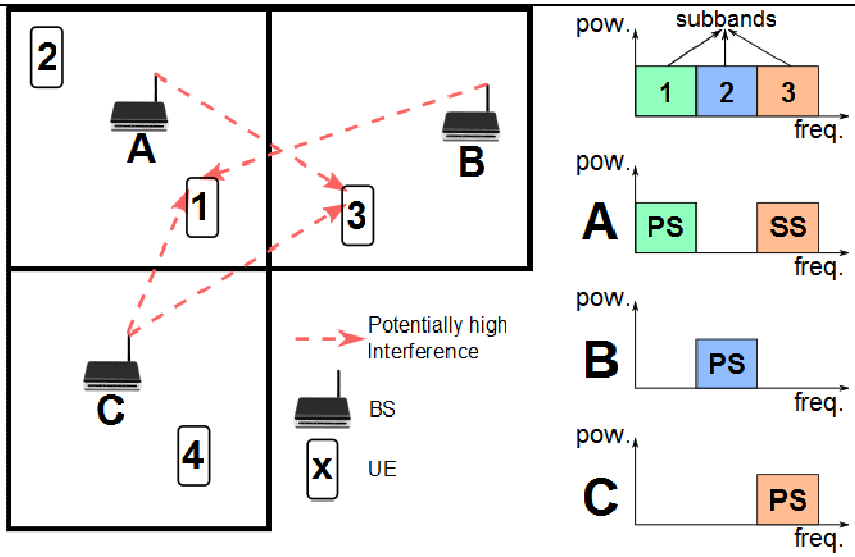

Figure 4-44 An example of subband assignment where the system bandwidth consists of 3 subbands.

To clarify the aim of the DASA, a toy example of the assignment of subbands by BSs is depicted in Figure 4-44. According to Figure 4-44, BS_C causes high interference to some UEs served by BS_A and BS_B. Since these UEs are allocated RBs from subbands 1 and 2, respectively, these subbands are blocked at BS_C. Likewise, BS_A cannot use subband 2 and BS_B cannot use 1. Therefore, subband 1 is declared the PS for cell A, subband 2 the PS for cell B and subband 3 for cell C. On the other hand, UE_2 served by BS_A does not face high interference from BS_B and BS_C, therefore BS_A may allocate subband 3 RBs to UE_2 without causing high interference to UE_4 served by BS_C.

A BS allocates RBs from PSs and SSs to UEs depending on the UEs' perceived interference conditions. Cell-edge UEs are prioritized for being allocated PS RBs, while the cell-centre UEs can be allocated RBs from SS. This results in a fair allocation of resources among UEs in the same cell. For instance, BS_A in Figure 4-44, serves UE_1 and UE_2 and can transmit data on subband 1 and subband 3 as PS and SS respectively. As UE_1 faces high interference from BS_C on the SS, only RBs from the PS can be allocated to it. On the other hand, RBs from both PS and SS can be allocated to UE_2. In such a situation, for the sake of fairness, UE_1 gets all resources from the PS and all resources from the SS are allocated to UE_2.

It is worth indicating that the subband assignment is done on an event triggered basis which means that subband *s* are updated only if there is a change in the interference environment. Additionally, all BSs are synchronized with a time duration equal to that of a so-called *time slot*. Between the starting instances of two time slots, the subband configuration remains undisturbed, *i.e.*, changes in the subband assignment are only made at the start of the time slots. Each BS computes the subband assignment for the next time slot, $t + 1$, based on the feedback received by it from its served UEs and neighbouring BSs regarding the previous time slot *t*. The duration of a time slot should be longer than the time required for receiving RSRP and PS-indicator feedback.

All the required signalling and subband selection processes are explained in the following subsections.

4.3.3.3.1 Identification of Interfering BSs

Owing to the uncoordinated deployment of BSs, it is impossible for a UE to identify the list of interfering BSs in advance. Instead, a global, pre-defined SINR threshold, γ_{th}, is defined which is the minimum desired SINR for each UE. As mentioned above, the RSRP reports from UEs are used for the identification of interfering neighbours. In every time slot, each UE sends RSRP reports of the BSs in its vicinity to its serving BS. Based on the received powers from the serving BS_b and from the set of all interfering BSs, I_u, a UE_u experiences a worst-case SINR of γ_u. If $\gamma_u < \gamma_{th}$, then from I_u, the largest interfering BS is removed and γ_u is recalculated. This process continues iteratively until

$$\gamma_u = \frac{R_{u,b}}{\sum_{i \in \bar{I}_u} R_{u,i} + \eta} \geq \gamma_{th} \qquad (4.20)$$

where η accounts for thermal noise and $\bar{I}_u$ is the set of tolerable interfering neighbours defined using set notation by:

$$\bar{I}_u = I_u - I_{u,\text{rem}} \quad (4.21)$$

where $I_{u,\text{rem}}$ is the set of removed interfering BSs. The set of BSs belonging to $I_{u,\text{rem}}$ must not use the same subband from which RBs are allocated to UE_u, so that UE_u may achieve an SINR of at least γ_{th} Having knowledge of the set $I_{u,\text{rem}}$, the serving BS_b of UE_u can inform the (potential) interfering BSs of UE_u via a PS indicator when it allocates RBs from the PS to UE_u. In this way, the serving BS prevents those interfering BSs from using its PS and the desired γ_{th} can be achieved at UE_u. If a BS serves multiple UEs, then it should perform the same process for all UEs since each UE has a distinct set of interfering BSs depending on its location as shown in Figure 4-44.

As a final remark, increasing γ_{th} increases the number of the interfering BSs in the set $I_{u,\text{rem}}$. This way, higher SINRs are achieved, but this is traded-off with a reduced spatial reuse of subbands.

4.3.3.3.2 Set of Available Subbands for Transmission

A BS needs to use a metric to choose the most efficient subband in terms of a desired performance criterion. For this purpose, a metric termed as subband availability is introduced. The availability of a subband indicates how many UEs experience an SINR higher than γ_{th} on that subband in a given cell. However, if a BS receives a PS indicator from its neighbour(s), the given BS cannot use that subband. Therefore, in this case, the availability of the subband becomes 0 independent of the SINR levels reported by UEs. The calculation of the availability of subband *s* in BS_b is as

$$A_{s,b} = \begin{cases} \sum_{u \in U_b} \iota(\gamma_u^s \geq \gamma_{th}) & \text{if } s \text{ is not blocked} \\ 0 & \text{if } s \text{ is blocked} \end{cases} \quad (4.22)$$

where ι is a conditional binary function whose output is 1 if its argument holds true and 0 otherwise. Here, γ_u^s is the SINR at subband s measured by UE_u and U_b is the set of all UEs served by BS_b.

4.3.3.3.3 Assignment of Idle Subbands

Since the subband assignment is determined by a BS based on UE feedback, which inherently induces latency, it is possible that multiple BSs access the same subband giving rise to destructive interference. The occurrence of such failed subband assignments decreases as BSs learn the nature of their environment and the network reaches a stable point where BSs no longer need to update their subband assignments. Moreover, frequent changes in subband assignments creates a cascading effect whereby neighbouring BSs are to update their subband selection, which increases the time required to reach a stable resource assignment. Therefore, we introduce a *p*-persistent slot allocation in SS assignment. In *p*-persistent slot allocation policy [49], when a channel is sensed idle by a transmitter, meaning no other transmitters send any packet, the transmitter sends the packet with a probability of *p*. In a similar manner, in DASA, an idle subband may be assigned with a certain probability depending on the subband's availability. For a given subband *s*, if a UE reports an SINR higher than γ_{th}, then BS_b assigns *s* with a probability of *p*. If multiple UEs experience an SINR higher than γ_{th}, which means availability of *s*, $A_{s,b}$, is greater than 1, then BS_b applies the *p*-persistent protocol $A_{s,b}$ times. The probability of the assigning *s* by BS_b for the next time slot *t+1* can be formulated as:

$$P_{s,b}(t+1) = 1 - (1-p)^{A_{s,b}} \quad (4.23)$$

A BS updates its subband assignment only if the probability condition in (4.23) holds, so that simultaneous assignment of the same subband by interfering BSs becomes less likely. The subband selection therefore converges quicker to a stable state. In (4.23), it is obvious that the probability of assigning a subband increases as subband's availability increases. This favours the selection of a subband that can be allocated to more users with high SINRs.

4.3.3.3.4 Primary Subband Assignment

Every BS may only assign one subband as a PS. The PS of a BS remains unchanged as long as another BS does not send a PS indicator pointing to the BS's current PS. In such a case, among the unblocked subbands, the subband having the highest availability is chosen. In order to decrease the collision and make

the system more stable, a BS updates its PS for the next time slot if the probability condition in (4.23) holds.

4.3.3.3.5 Secondary Subband Assignment

Similar to PSs, the same γ_{th} is set for SSs which means a BS can assign a subband as a SS if any of its served UEs experiences an SINR higher than γ_{th} on the given subband. However, the assigned subband should not interfere with the PSs of neighbouring BSs. Therefore, the SS selection algorithm first calculates the availability of all subbands using (4.22) Before adding any subband to SS set for time slot *t+1*, the BS updates its SS set used for time slot *t* by discarding the subbands having zero availability, because either these subbands are banned by the neighbouring BSs via a PS indicator or all UEs in the cell experience SINRs lower than γ_{th} over these subbands. Therefore, such subbands cannot be used for the next time slot *t+1*. Then, in the set of remaining subbands, the subbands having an availability higher than 0 are added to SS set with a probability that is calculated using (4.23).

4.3.3.4 Simulation Results

The simulated scenario consists of a single one-story building, modelled by a 5×5 grid, according to 3GPP specifications [50]. The 5×5 grid represents a square building consisting of 25 regularly arranged square-shaped apartments. Every apartment hosts a femto BS with a certain activation probability. If an apartment contains an active femto BS, it serves a certain number of UEs which are randomly distributed within the confines of the apartment. Full-buffer transmission is assumed such that every BSs assign all available resources from all available subbands to their served UEs. For the sake of simplicity, interference from the macrocell network is neglected, which may be accomplished by allocating different frequency bands to macro and femto BSs. The system parameters summarized in Table 4-2 are based on LTE specifications [50].

Table 4-2: Simulation Parameters

Parameter	Value
System bandwidth	20 MHz
Number of Subbands	4
Min. Sep. between UE and BS	20 cm
BS Antenna Gain	0 dBi
Antenna Pattern (Horizontal)	A(Θ) = 0 dB (omnidirectional)
Interior Path Loss	L=127 + 30log$_{10}$*d* [km] where *d* is the distance between UE and BS
Shadowing Std. Dev.	10 dB
Max BS Tx power	10 dBm
Thermal Noise Density	η = -174 dBm/Hz
UE Noise Figure	9 dB
Apartment Dimensions	10m x 10m
Number of UEs per Femto BS	4
Femto BS Activation Prob.	0.2
SINR Threshold	γ_{th} =5 dB
Prob. *p* in (4.23)	0.25

For throughput calculations, the attenuated and truncated Shannon bound is applied, which approximates the spectral efficiency of appropriately selected modulation and coding schemes subject to the achieved SINR. Detailed information on throughput calculations can be found in [34] and [40]. As a final remark, each snapshot of the simulator lasts for 10 time slots. During the snapshot, positions and shadowing values of BSs and UEs are assumed to remain unchanged. This is reasonable since indoors, the mobility of users is not as high as would be the case for outdoors. The statistics, such as SINR and capacity, are calculated at the end of the 10th time slot, *i.e.*, when a stable resource allocation is achieved.

The performance of DASA is compared to Fractional Frequency Reuse (FFR) where one BS is assigned one or two out of four available subbands. For DASA, in the first time slot, *i.e.*, at initialization, BSs randomly assign one subband as PS and subsequently update their primary and secondary subband assignment according the autonomous algorithm described in Section 4.3.3.3.5.

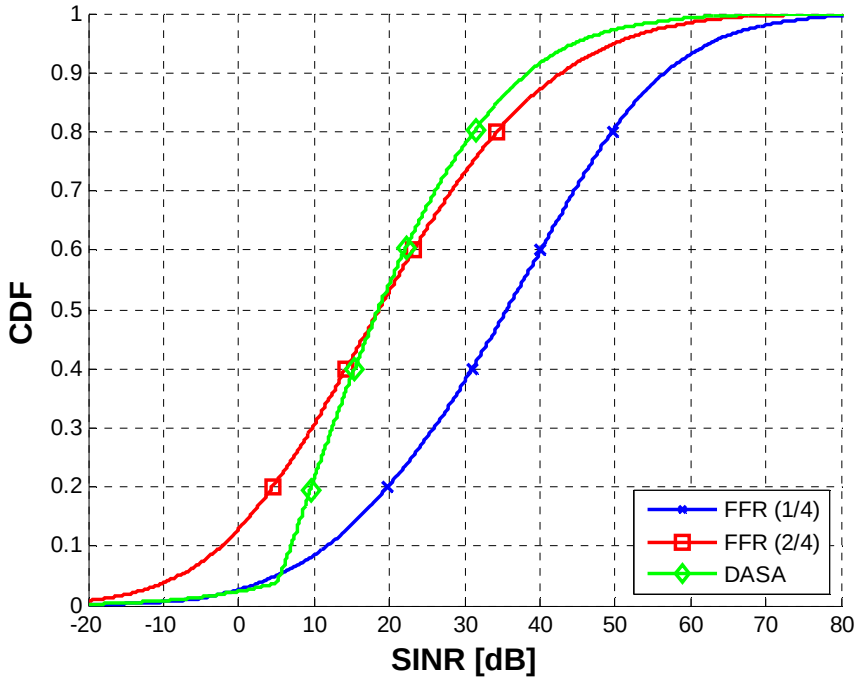

Figure 4-45: CDF of SINR

Figure 4-45 shows the CDF of the achieved SINR. With DASA, nearly all UEs achieve an SINR exceeding γ_{th} =5 dB. It is seen that the best SINR performance is achieved by the system where each femto BS only uses one out of four available subbands.

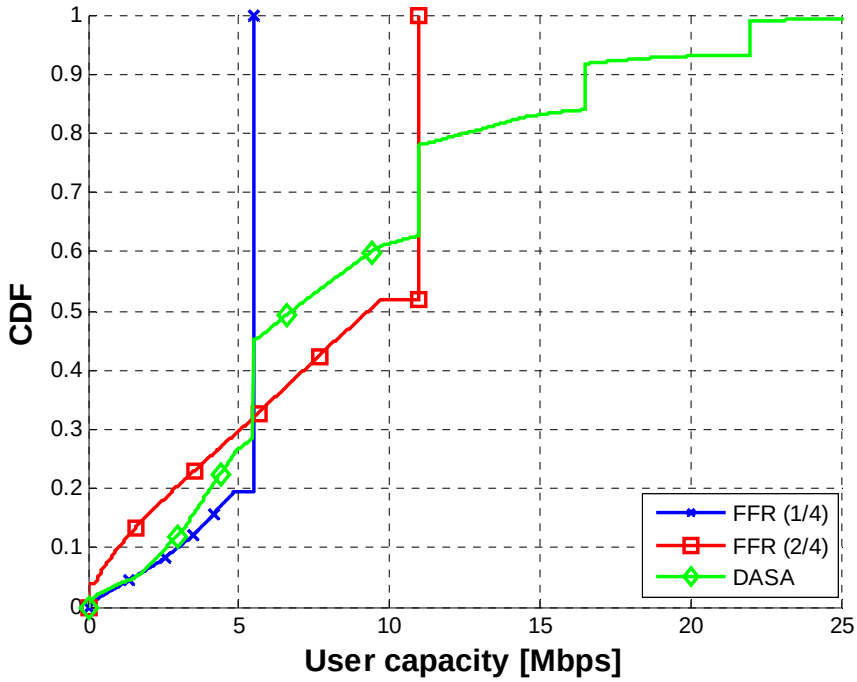

Figure 4-46: CDF of User Capacity

Figure 4-46 compares the CDFs of user capacity of the three methods. Due to the truncated Shannon bound, despite the encouraging SINR performance exhibited by the system employing FFR 1/4, the capacity saturates at a mere 6 Mbps, implying that a high proportion of resources remain unused. While the saturation capacity of FFR 1/4 is doubled over FFR 1/2, occasionally idle resources remain unused. Moreover, the cell-edge user throughput (given by the low percentiles of the user capacity CDF)

substantially degrades. DASA, like the FFR 1/4 system shows very good cell-edge performance (at the low capacity regime), but also shows very promising cell-center performance at the high capacity regime.

Table 4-3: **Performances of the Compared Methods**

Method	Cell-edge Capacity [Mbps]	Average Cell Capacity [Mbps]
FFR 1/4	1.54	19.83
FFR 2/4	0.32	30.14
DASA	1.60	35.26

The improvements in overall performance are summarized in Table 4-3, which compares the cell-edge capacity (defined as the 5% of the CDF of user capacity) and the average cell capacity. The results demonstrate that DASA significantly outperforms FFR in terms of cell-edge and average cell capacity. Since SSs are not blocked, more subbands are utilized with DASA, and hence, cell-center UEs can be allocated more resources. Therefore, DASA boosts cell-edge capacity without compromising the system capacity.

Figure 4-47 shows the percentage of allocated subbands as well as the percentage of the resources facing *collisions*, defined by an SINR below −10 dB, *i.e.* the spectral efficiency approaches 0 according to Shannon bound. Since each BS randomly assigns one PS in the first time slot, the percentage of the allocated subbands is always 25% at the beginning. Also, the random subband assignment increases the percentage of collisions at the start. Then based on the UE feedback, in the second time slot PSs and SSs are updated. Subband assignment exclusively relying on SINR measurements increases the subband usage and the collision probability to 70% and 6.7%, respectively, in Figure 4-47, because BSs do not know their neighbouring BSs yet. However, before the third time slot, BSs receive PS indicators, sent at the beginning of the second time slot. These PS indicators restrict interfering BSs from using their neighbours' PSs. Additionally, with the received SINR levels, BSs learn more about subbands used by their neighbours. Therefore, the percentage of the assigned resources and collisions both decrease at the third time slot. Subsequently, as BSs become more aware of their neighbours' decisions, the percentage of the assigned resources increases together with a decrease in the percentage of the collisions. After the fourth time slot, the proposed subband allocation reaches a stable state.

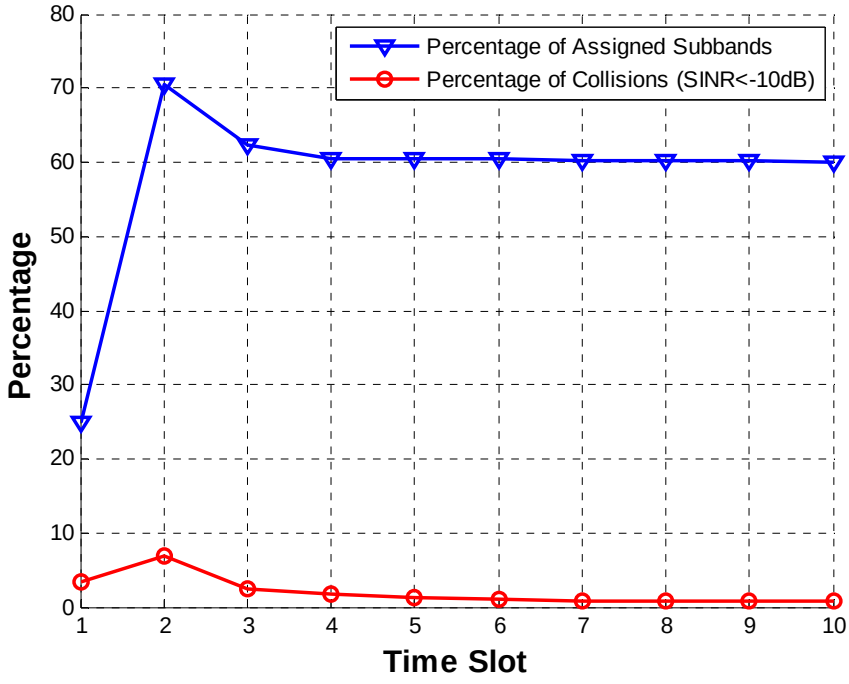

Figure 4-47: Percentage of the assigned subbands and the collisions measured at the end of each time slot.

4.3.3.5 Contribution to BeFEMTO System Concept and Objectives

The main contribution of this work is to autonomously assign resources in femtocell networks that are characterized by varying interference conditions. The method offers the BS an autonomous resource allocation limited by its interference environment. Additionally, the method has less signalling overhead as existing LTE signalling procedures are used and the system reaches the stable point after only a few iterations. Simulation results demonstrate that DASA attains a significant improvement for both cell-edge user as well as system capacities, compared to conventional centralized frequency reuse methods. As the method relies on the measurements of UEs, it is able to dynamically adapt to the interference conditions faced in random deployments, thus balancing high spatial reuse of radio resources with interference protection for cell-edge users. The average cell spectrum efficiency is around 1.75 bps/Hz for single antenna systems. By adapting the system parameters (such as SINR threshold) and using multi-antenna techniques, higher gains can be achieved.

4.3.4 UE Battery Power Requirements for SON Operations

4.3.4.1 Problem Statement

As a result of the dense femtocell deployments, one prime concern is the resulting substantial power usage in the small area. In the context of small cell scenarios from an energy perspective, only very few preliminary results on energy efficiency are available (e.g., see [61], [62] and references therein). For example, the opportunity of switching off some small cells during periods of low traffic intensity has been discussed in [61], [62]. This is in order to properly limit the power usage by the femtocell users. The limited power is crucial at each terminal. In the context of dense small cells, therefore, it will be very important to design the power resource usage of the dense femtocell deployments. So far, no concern was given to the effective battery power usage in the low-end device from the energy efficiency perspective. Thus, we must design effective battery power usage with respect to the energy efficiency between collaborative femtocell users.

In this work, we focus on a collaborative power usage that aims at enhancing the effective energy cost by the self-organization networking (SON) operation in the femtocell users. We elaborate the aggregate power usage of the OFDMA based femtocell by analyzing an effective battery power usage before the power amplifier by the users. Unlike conventional schemes, we take into account effective battery power usage for the channel information feedbacks as well as for the data transmission. Using this power usage, it is proposed to select the number of collaborative femtocell users and their power allocation level so that the energy efficiency is improved, as compared to the conventional case without the SON.

4.3.4.2 System Model

We consider *N* femtocell user equipments (FUEs) in networked femtocells, each FBS comprising of a FUE in a radius *r*. For the uplink, the femtocells cognitively share the radio spectrum with a known macro Base Station, and within the shared spectrum, the orthogonal channel deployment among the *N* femtocells is considered, which can be feasible by the use of X2 interface.

Suppose that the channels between FBSs and their own users experience Rayleigh flat fading and propagation losses, and the channels are known perfectly at the receiver. Here, the channel gain in the *i*-th FUE (FUE *i*) can be $h_i = \overline{\rho}\, x_i\, r^{-a}$ where x_i is the channel gain as a chi-squared distribution random variable, $\overline{\rho}$ denotes a log-normal shadowing, and r^{-a} is the path-loss with its exponent *a* at the distance *r*. The average power control ($P_o r^a$) is assumed to be adopted at the transmitter and compensates the propagation loss r^{-a}. The corresponding receiving SINR between FUE *i* and its FBS can be therefore given as

$$\rho = \overline{\rho}\,\frac{x_i P_o}{\sigma^2} \tag{4.24}$$

where σ^2 denotes, as the noise, the sum of the generic interference on average from the incumbent system and the variance of the complete valued zero mean additive white Gaussian noise (AWGN).

At each terminal side, notice that existing research in the context of the power control concerns only the power allocation level at the output of the power amplifier (PA) and takes into account homogeneous PA efficiency. In particular, notice that the above transmit power level $P_0\, r^a$ is the output power of the PA.

This reveals that the effective battery power usage before the PA can be written $P_e r^a = P_0 r^a \eta^{-1}$ where $\eta = P_e^{-1} P_0$ denotes the PA efficiency, as depicted in Figure-4-48.

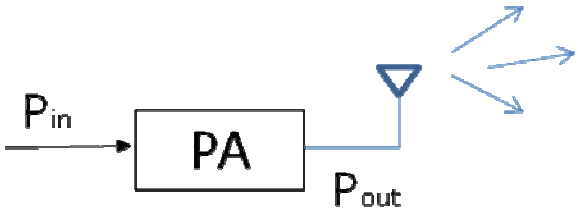

Figure-4-48: **The power amplifier at each terminal side**

Accordingly, the effective battery power usage related SINR from FUE *i* can be represented as

$$\rho_e = \bar{\rho} \frac{x_i \eta^{-1} P_e}{\sigma^2}. \tag{4.25}$$

4.3.4.3 Proposed SON Framework

We propose a framework, where the system power and channel resources are properly distributed to collaborative FUEs. For this, notice the fact that on every data transmission, there exist power usages at following three components: (i) self-organization of a set of collaborative FUEs; (ii) channel information feedbacks; (iii) data transmission.

As per the set of collaborative FUEs, first, we need to properly select the size of a subset of collaborative FUEs. In particular, for given *N* FUEs, only a subset of *n* random FUEs is proposed to be uniformly selected at every channel realization and this selection ensures that each entry in the subset is equally likely activated.

For the channel information feedbacks, then, within the activated subset, the corresponding *n* FUEs are exchanging the channel information feedbacks with their FBSs for the purpose of system power resource scheduling. Here for such feedbacks, let the above power allocation level of $P_o r^a$ be used by each FUE.

For the data transmission, once the channel information feedbacks from a random subset of *n* FUEs are available, the power allocation among them for the data can be done by applying, to the subset, the best channel gain scheduling scheme (which is well-known to be optimal in the sense of the maximum sum data rate of a fixed set of users.) That is, based on the channel information feedbacks, only the best among *n* FUE-FBS channels is allocated for the data transmission at every transmission. The selection criterion of the best is to select the FUE whose index is defined as $i^* := \arg\max_i x_i$. Therefore, the achievable system rate can be given with the use of P_e by

$$C = \log_2\left(1 + \bar{\rho}\alpha P_e \eta x_{i^*}\right) \tag{4.26}$$

where P_e, we recall, is equal to $P_o \eta^{-1}$, α is the given ratio of the desired power level for the channel feedbacks to that for the data transmission, and the unit noise variance is assumed for simplicity hereinafter. Notice that this rate is achieved effectively over the channel, scaled by the random product of the PA factors and fading channel coefficients.

4.3.4.4 Effective Power Usage Analysis

We now address how a joint design of *n* and P_e influences the power usage by the FUEs in the system. For this, notice the fact that at every data transmission, there exist power consumptions during all three components in the proposed framework. Particularly, as per the power usage model of the multi-user scenarios in [60], it can be obtained that for a given *N* collaborative FUEs, the aggregate power usage by the FUEs along with the best channel gain scheduling scheme consists of two terms of the power usage: the power usage for the channel information feedbacks and the power usage for the data transmission.

In this context, let all *N* FUEs be allocated to effective power level P_e for the channel feedbacks and the best among them for the data transmission is chosen. Then, the aggregate power usage among the *N* collaborative FUEs can be given as

$$P_T = \sum_{i=1}^{N} P_{e,i} r^a + \frac{\alpha}{N} P_{e,i} r^a \tag{4.27}$$

This expression represents the aggregate power usage by the *N* collaborative FUEs in the case when using no SON operation and is related to the battery power usage before the PA at each FUE. In this equation, the first and the second terms represent the power usage over the feedback and the data transmission, respectively. As shown in this expression, each FUE has equally likely been chosen for the data transmission (with the probability of 1/*N*).

Similarly, for the proposed SON case with the choice of *n* as being less than *N*, the uniformly distributed random selection of *n* collaborative FUEs ensures the equal probability that each FUE can access the channel for the collaboration. Therefore, P_T in this SON case can be statistically written with respect to *n* and *N* as

$$P_T^{SON} = \sum_{i=1}^{N} \left(\frac{n}{N} P_{e,i}^{'} r^a + \frac{\alpha}{N} P_{e,i}^{'} r^a \right) \tag{4.28}$$

where $P_{e,i}^{'}$ denotes $P_{e,i}$ at FUE *i* in the case with SON. In this equation, the first term represents the power usage by the self-organized collaborative FUEs, each having the probability of *n/N* to be involved as an entry in the subset of *n* collaborative FUEs, due to the proposed framework. Similarly, the second term denotes the power usage for the data transmission by the FUEs, each equally likely being as the best user with the probability of *1/N*.

4.3.4.5 Effective Power Requirement at the Terminal Side

To measure the battery requirement for the SON at the FUE side, firstly let us consider that P_T by all FUEs is limited to *P* which is assumed to be given such that the femto-macro interference is managed. Intuitively, for a known incumbent receiver (i.e., macro Base Station), the less the power usage by FUEs, the smaller the impact towards the macrocell Base Station is in terms of the interference level. Based on this, we consider the case when P_T^{SON} is limited to P_T (i.e., $P_T^{SON} \le P_T$).

For given P_T and *m*, then, we must have from above for $P_T^{SON} \le P_T$:

$$P_T^{SON} < P_T \Rightarrow P_{e,i}^{'} \le \frac{N}{n+\alpha} \frac{P_T}{\sum_m r^a} \tag{4.29}$$

As shown in this equation, $P_{e,i}^{'}$ is a decreasing function of *n* for given *N* and α. This reveals that while the effective power usage P_T^{SON} remains below or equal to P_T, the larger $n \le N$, the less $P_{e,i}^{'}$ must be allocated. The former results in increase in the collaboration gain while the latter does the loss of the individual channel equality.

Accordingly, when referring to both $P_{e,i}^{'}$ in the above equation and P_T^{SON} in (4.28), the effective battery power usage at the best channel for data transmission can be represented as

$$\alpha P_{e,i^*}^{'} r^a = \frac{\alpha P_T^{SON}}{n+\alpha}. \tag{4.30}$$

Using these power requirements, the system spectral efficiency can be obtained as follows. When having $P_T^{SON} = P_T$, it can be straightforwardly derived from the above power level for data transmission and the system rate in (4.26) that the corresponding system spectral efficiency (bits/Hz) along with the *n* collaborative FUEs is given as

$$C = \log_2\left(1 + \bar{\rho}\frac{\alpha P_T \eta}{(n+\alpha)r^a} x_{i^*}\right).$$

Based on this spectral efficiency (bits/Hz) as well as the effective power usage P_T^{SON} (W), the ratio between these can be defined as the energy efficiency (*EE*) in this work and it is measured easily by C/P_T (bits/Hz/W).

4.3.4.6 Numerical results

When using the proposed scheme, Figure 4-49 depicts the energy efficiency as an exponentially decreasing function of the spectral efficiency at various rates of the collaboration. For these curves, it is considered that there are 20 FUEs available. For comparison, this figure also illustrates the energy efficiency as well as the spectral efficiency in the case of using the conventional best channel gain scheduling scheme with no SON, which has 100 percent collaboration users. As per this figure, the trade-off between the energy efficiency and the spectral efficiency can be enhanced by a proper selection of the number of collaboration FUEs each satisfying the proposed battery power requirements.

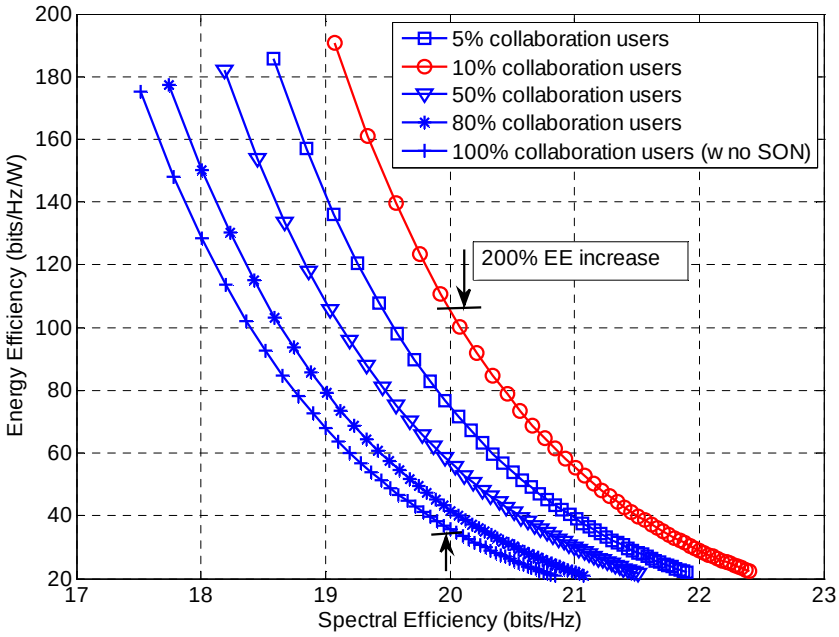

Figure 4-49: **The energy and spectral efficiencies of the collaborative power control among FUEs**

4.3.4.7 Conclusions

This section was focused on the SON power utilization by FUEs, where the impact of the PA efficiencies of FUEs on the overall power usage of the OFDMA femtocells has been addressed with respect to the power usages in the channel feedbacks, and the data transmission at each sub-channel. Particularly, we considered the case when the SON power allocation between FUEs each satisfying the proposed battery power requirements is used to enhance the energy and the spectral efficiencies along with the interference management. Via the numerical results, it has been confirmed that while controlling the size of collaboration users along with the battery power requirements, the proposed scheme is superior to the conventional case when using full collaboration FUEs with no SON power usage with respect to the trade-off between the energy efficiency (bits/Hz/W) and the spectral efficiency (bits/Hz).

For that end, we considered the orthogonal channel deployment between femtocells each having the X2 interface. Over the X2 interface, it was assumed that context information including, for example, the spectrum per FBS, the number of FUEs available, the presence of incumbent receiver and the sum power budget, has been exchanged one another.

4.3.5 Energy-Aware Self-Organized Networking Enabled Co-Channel Femtocell

In this section, we consider that a co-channel femto cell sharing the spectrum with the overlaid macrocell is randomly deployed within a service radius of the macrocell. We design a generic energy usage model in such a way that energy usage by femto cell users at both the signalling and the data phases is taken into consideration. Considering the worst-case scenario of interference when femto cell users are deployed in a corner of the femto cell nearest toward the macrocell, autonomously self-organizing techniques of the energy usage at the femto cell are proposed under realistic constraints.

4.3.5.1 System model and proposed algorithm

Consider a co-channel femto cell network that opportunistically operates over the same spectrum as the overlaid macrocell network. The serviced area by the co-channel FBS is assumed to be randomly deployed within the coverage of the macrocell network. We focus on the uplink of the co-channel femtocell network consisting of multiple FUEs. Each FUE has a single antenna and intends to communicate with the FBS having *d* receiving antennas via orthogonal channels in the frequency domain.

We propose the following distributed admission control and radio resource scheduling (RRS) scheme. To this end, it is worth pointing out the fact that in the context of resource scheduling, there exist two inherent phases: control signalling phase, and data phase:

i) Control signalling energy phase (denoted by Phase 0) in which signalling information is exchanged,

ii) Data-transmission energy phase (denoted by Phase 1) in which data transmission occurs.

Unlike conventional approaches emphasizing mainly the energy usage at Phase 1, we take into account the *sum energy usage by all FUEs* at both *control and data phases (i.e., Phase 0 and Phase 1).*

During the two phases, exchange of both signalling and data between the transmitters and the receivers occurs at every time slot. Particularly, we propose the following:

- Phase 0: By properly selecting a value for the size of admitted FUEs, the FBS randomly activates *n* among *N* FUEs at every time slot according to the Uniform distribution. This random selection at each time slot is used in order to achieve fairness among users in terms of equal probability of accessing the channel. Due to this random selection, also notice that the entries of the subset of active FUEs are random. Given a subset of *n* active FUEs, a subset of only *n*v* active sub-channels is self-organized, where *v* is the number of sub-channels per FUE. Here, notice that the corresponding entries of the subset are random according to the Uniform distribution such that all the sub-channels have equal likelihood of activation. Also, once active sub-channels are selected, the average power level for control signalling is selected for the mutual co-existence with the macrocell.

- Phase 1: In a given subset of active sub-channels from the control plane, opportunistic data transmission is performed [60]. That is, among the subset of active sub-channels, only the best is scheduled for data transmission at each time slot. The selection criterion for the best is to find the sub-channel whose SINR ρ^* is the best among others. As per this criterion, the resulting sum rate of the femtocell can be given by

$$C = \log\left(1+\rho^*\right) \tag{4.31}$$

In this work, we study a self-organizing problem such that in a given random deployment of the FBS the sum energy usage E by FUEs is maintained below the maximum allowance as well as the cross-interference I is less than the tolerance level by the MBS. It is investigated how to self-organize the sum energy usage among FUEs in order to enhance the sum capacity of a femto cell-of-interest. Toward this end, we take into account the following two constraints:

$$E \le E_o \qquad \text{and} \qquad I \le I_o \tag{4.32}$$

where E is the sum energy usage by all FUEs at both Phases 0 and 1, its maximum is limited by E_o. $I = \sum I_i$ denotes the sum of the interferences on average at the MBS from all FUEs, and its pre-defined maximum is I_o.

Inspired by the recent energy cost analysis for the available multi-user diversity in [60], our method firstly aims to identify the presence of the opportunity for controlling the inherent energy usage between both phases. Given a sum energy budget between Phases 0 and 1, for example, properly balancing the energy

usage between the phases can be taken into account with respect to the power allocation level per FUE and the number of active FUEs. This is due to the fact that the energy usage depends on the range of the active channels and the power allocation level per channel. As for the potential of this energy usage balance, it is referred to the details of the mathematical analysis available in [40]. Intuitively, given a sum energy usage, the more energy is used for the context exchanges via the signalling, the less the energy will be used for the data transmission. The former is related to the achievable gain of the radio resource scheduling, while the latter determines the link quality of the data transmission. Based on this intuition, a benefit-cost analysis of this energy usage balance has been further developed to enhance the opportunities for balancing between the ergodic sum rate and the interference. As for the impact of this energy usage balance on the system performance, it has been finally investigated how to properly select the number of active FUEs and the power allocation levels so that the system performance is enhanced.

4.3.5.2 Numerical results

When using the proposed energy-aware SON RRM scheme [64], Figure 4-50 depicts the achievable ergodic sum rate as a monotonically increasing function of the average SINR when there are 8 FUEs available. For comparison, this figure also illustrates the conventional greedy case when the best of all FUEs is allowed for the data at a given power allocation per FUE. As per this figure, the proposed scheme is superior to the conventional case with respect to the ergodic sum rate.

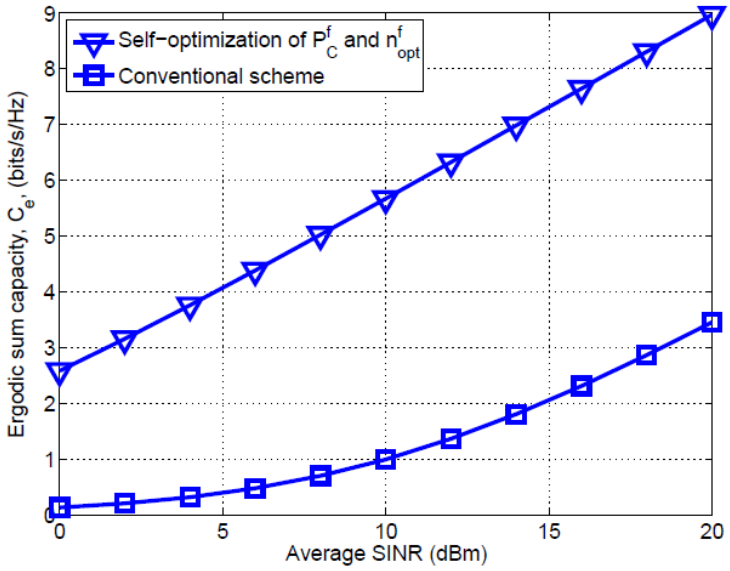

Figure 4-50: Comparison of the self-organizing cases to the conventional case has been depicted with respect to the ergodic sum capacity versus the average SINR.

4.3.5.3 Conclusions

We have presented a SON enabled admission control and scheduling scheme in a macro-femto network to improve the sum rate of the femto network. To co-exist with the macro, the sum energy usage by the femto should be limited, which degrades the sum rate of the femto network. To solve this problem, we have proposed the energy-aware SON RRM that maximizes the ergodic sum rate of the co-channel femto under the realistic constraints on the interference and the energy usage. For this end, we considered the orthogonal channel deployment between femtocells each having the X2 interface with neighbouring femtocells. Over the X2 interface, it was assumed that medium- or large-scale context information including, for example, the range of the spectrum per FBS, the number of FUEs available, and the sum energy budget, has been exchanged one another. It was shown that as per the ergodic sum rate, the proposed scheme outperforms the conventional greedy case which is optimal without the smart energy usage. These solutions are explained in [40], where further details and results can be found.

4.3.6 Managing Femto to Macro Interference without X2 Interface Support Through POMDP

4.3.6.1 Problem Statement

In the algorithms presented in Section 3.2.1.3, we assumed the existence of an X2' interface between macrocells and femtocells, which was introduced in deliverable D 2.2 [68], through which femtocells receive a bitmap feedback from near macrocells, equivalent to the Relative Narrowband Transmit Power (RNTP) indicator standardized in 3GPP LTE [42], about the interference perceived by the macro users. The assumption of the existence of the mentioned X2' is an important limitation since it has not been yet standardized in LTE Release 11 [43]. As a consequence of the lack of direct communication between macrocells and femtocells, the interference management task becomes even more challenging, since the femto network has to completely autonomously make decisions without any feedback about the impact it is having on the victim macro users. To solve this problem, we rely on the theory of Partially Observable Markov Decision Process (POMDP) [44], a suitable tool for decision making in scenarios with some degree of uncertainty. We assume here that femtocells communicate among each other some information, which is further specified below.

POMDP works by constructing a set of beliefs about the current state of the environment based on empirical observations. In our particular case, the beliefs depend on the service perception that femtocells estimate at the macro user receivers. We propose that femtocells, based on the SINR measured at their receivers, build a belief set through spatial interpolation techniques, such as ordinary Kriging [45]. In particular, these beliefs are built by first estimating the position of potential victim macro users and then by interpolating the SINR in those locations. The POMDP learning process is then executed based on this estimated information. We focus on networked femtocell systems for residential and corporative scenarios, where femtocells are able to exchange signalling information and interact among each other.

The advantage of the proposed solution is twofold. On the one hand, it allows femtocells to work in a completely autonomous fashion, which responds to the increasing need of self-organization of the overall network and to the possibility that the X2' interface will never be standardized. On the other hand, it avoids the signalling burden on the backhaul network introduced by the signalling overhead over the X2' interface required for the Q-learning implementation.

4.3.6.2 Algorithm Description

4.3.6.2.1 Proposed learning methodology for partially observable environments

In what follows, we propose a methodology consisting of four steps for the aggregated femto to macro interference management for femtocells autonomously operating. Notice that, the information gathered in Steps 1 and 2 of the proposed methodology is based on references that will be provided, whereas in this work we will focus on Steps 3 and 4, which are explained in detail in following sections.

> **Step 1. Femtocells location determination:** We assume femtocells to be able to evaluate their own position through femtocell positioning techniques e.g., as those proposed in deliverable D 4.1 [34]. In femtocells, all location determination algorithms are included in the HeNB Management System (HMS) [46].
>
> **Step 2. Estimation of macro users position:** Based on a Motorola's proposal discussed in a patent filed in February 2011 [47], we assume that every time a MUE is in the coverage area of a femtocell, it attempts an access to it, which may be either accepted, in case the macro user belongs to the closed subscriber group of the femtocell, or rejected in case the macro user does not belong to it. If the access is rejected, the femtocell is aware of the presence of a potential victim macro user. We also suppose that the macro user reports about the RB in which it is operating. When the macro user is in the coverage area of at least three femtocells, and has consequently attempted three accesses, we assume that by some positioning technique e.g., by triangulation, the networked femtocells are able to jointly estimate the position of the macro user. Notice that, differently from what happens in traditional cellular networks, the handover macro to femto in [47], is not started by the network, but a direct signalling message (supposed not to be power controlled) is sent from the macro user to the femtocell. This is shown in Figure 4-51, extracted from [47], which represents the exchanged messages between a macro user and a femtocell when the macro user attempts to access the femtocell.

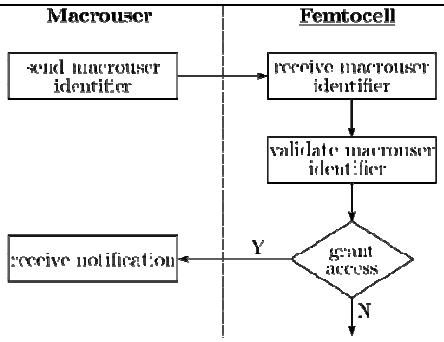

Figure 4-51: Messages exchanged when a macro user attempts to access a femtocell.

Step 3. SINR estimation at macro user: Once the femtocells have detected the presence of a victim macro user in the coverage area of the femtocell network, and have estimated its position, we propose that based on the SINR they measure, they perform a spatial interpolation to approximate the SINR at the victim macro user position. We perform the spatial interpolation through the ordinary Kriging interpolator algorithm [45]. The estimated SINR at victim macro users will be required in Step 4 as input to the learning process, as a macrocell system performance indicator.

Step 4. Learning in partially observable environments: With the approximated SINR estimated in Step 3, agents implemented in the femtocells have enough information to learn decision policies through the theory of POMDP. The estimated SINR is the POMDP's required observation, which provides information about the state of the environment.

4.3.6.2.2 Spatial characterization of interference in femtocell networks

In this section, we present the probabilistic analysis and modelling of the interference perceived at macro users. This interference modelling is based on the measurements of the SINR gathered by those femtocells which the user attempts an access to, as defined in Step 3 of the proposed methodology. Femtocells measurements are treated as a realization of a random field, assuming the SINR as a stationary stochastic process. Once measurements have been gathered, the random field fitting process is performed in two steps:

1. A structure analysis of the spatial continuity properties is performed, which consists of measuring the variability of the measured femtocells SINR, through a variogram model. Then, one of the available variogram models is selected and properly fitted.
2. The value at an unmeasured location is estimated through an interpolation process using variogram properties of neighbouring data.

We aim to estimate the aggregated interference generated at macro user receiver $\hat{Z}(x^*)$, whose location is estimated in position x^*. We consider as input the SINRs $Z(x_1),....,Z(x_n)$ perceived at n known locations $x_1,.....,x_n$, which are the locations of the n closest FUEs receivers. To evaluate the spatial behavior of the SINR over an area, a variogram analysis among the n known locations is required. The experimental variogram data are computed as the expected squared increment of the values between locations x_i and x_j, characterized as a sample of a random field, such as:

$$\gamma(x_i, x_j) = E\left[(Z(x_i) - Z(x_j))^2\right]$$

More in particular, for the case of a stationary field, it is possible to use an empirical variogram based on sample measurements at the n different locations $Z(x_1),.....,Z(x_n)$. First, the distance is divided in a set of lags with separation h, then distances between measurement sites $\left\|x_i - x_j\right\|, \quad \forall\, i, j$, with similar separation, are grouped into bins $N(h_i)$ centered in h_i. Finally, the empirical variogram is obtained through:

$$\gamma(h_i) = \frac{1}{N(h_i)} \sum_{i=1}^{N(h_i)} \left(Z(x_i) - Z(x_j)\right)^2$$

The empirical variogram cannot be used directly for the interpolation process because not all the distances are present in the sample data, so that a variogram model is required. Variogram models are mathematical

functions that describe the degree of spatial dependence of a spatial random field. There are infinitely possible variogram models, and the more commonly used are linear, exponential, gaussian and spherical. Variogram models are characterized by sill ρ_0^2, range a_0 and nugget c_0 parameters, as shown in Figure 4-52, whose values are computed through the fitting process.

- The sill, ρ_0^2, is the variogram model upper bound. It is equal to the total variance of the data set.
- The range, a_0, is the distance h where the fitted variogram model becomes constant with respect to the lag distance. For the particular case of exponential and gaussian models (see details of the models in the following) where the variogram model increases asymptotically toward its sill value, the term practical range is also used, and it is chosen so that the value of the resulting exponential or gaussian function evaluated at the practical range lag is 95% of the sill value.
- The nugget, c_0 is the value at which the variogram model intercepts the y-axis.

The following equations characterize the typical examples of variogram models and they are represented in Figure 4-52.

Linear model:

$$\gamma(h)=\begin{cases}\dfrac{\rho_0^2}{a_0}|h|, & 0<|h|\le a_0\\ \rho_0^2, & a_0<|h|\end{cases}$$

Spherical model:

$$\gamma(h)=\begin{cases}\rho_0^2\left[1.5\dfrac{|h|}{a_0}-0.5\left(\dfrac{|h|}{a_0}\right)^3\right], & 0<|h|\le a_0\\ \rho_0^2, & a_0<|h|\end{cases}$$

Exponential model:

$$\gamma(h)=\begin{cases}0, & h=0\\ \rho_0^2\left[1-\exp\left(-\dfrac{3|h|}{a_0}\right)\right], & h\neq 0\end{cases}$$

Gaussian model:

$$\gamma(h)=\begin{cases}0, & h=0\\ \rho_0^2\left[1-\exp\left(-\dfrac{|h|^2}{a_0}\right)\right], & h\neq 0\end{cases}$$

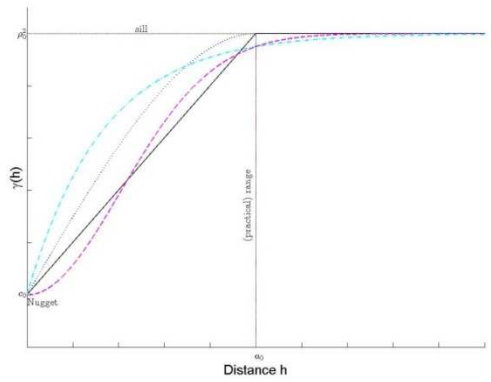

Figure 4-52: Generic variogram parameters.

The experimental variogram data are fitted to the variogram model by matching the shape of the curve of the experimental variogram data $\gamma(x_i, x_j)$, with the shape of the mathematical function $\gamma(h)$ by least-square regression. The variogram model parameters are then accordingly determined. The most appropriate variogram model is chosen by computing the error between experimental variogram data and the corresponding variogram model values in those points.

Once the variogram model is selected, the interpolation procedure can be performed. Interpolation allows the estimation of a variable at an unmeasured location based on the observed values at surrounding locations. We apply the ordinary Kriging [45] interpolation technique, whose main advantages are that it compensates the effects of data clustering (i.e. data within a cluster have less weight than isolated data points) and it provides estimation of errors, which allows to find the best unbiased estimation of the random field values between the measurement points. Assuming a stationary field, where the mean expected value $E\,Z(\hat{x}^*)=\mu$, is unknown but constant, and the variogram is known, the ordinary Kriging estimation is given by a linear combination such as:

$$Z(\hat{x}^*)=\sum_{j=1}^{n}\lambda_j Z(x_j)$$

where λ_j is the weight given to the observed value $Z(x_j)$. Weights should be chosen such that the variance $\sigma^2(x^*)=\mathrm{var}\left(\hat{Z}(x^*)-Z(x^*)\right)$ of the prediction error $\hat{Z}(x^*)-Z(x^*)$ is minimized, subject to the unbiased condition $E\left[\hat{Z}(x^*)-Z(x^*)\right]=0$. The weights are computed based on the ordinary Kriging equation system:

$$\begin{pmatrix}\lambda_1\\ \vdots\\ \lambda_q\\ \mu\end{pmatrix}=\begin{pmatrix}\gamma(x_1,x_1) & \dots & \gamma(x_1,x_n) & 1\\ \vdots & \ddots & \vdots & \vdots\\ \gamma(x_q,x_1) & \dots & \gamma(x_q,x_n) & 1\\ 1 & \cdots & 1 & 0\end{pmatrix}^{-1}\begin{pmatrix}\gamma(x_1,x^*)\\ \vdots\\ \gamma(x_q,x^*)\\ \mu\end{pmatrix}$$

where the additional parameter μ is a Lagrange multiplier used in the minimization of the variance $\sigma^2(x^*)$ to fulfill the unbiasedness condition $\sum_{j=1}^{n}\lambda_j = 1$.

4.3.6.2.3 Q-learning in partially observable environments

In many real world problems, it is not possible for the agent to have perfect and complete perception of the state of the environment. As a result, it makes sense to consider situations in which the agents make observations of the state of the environment, which may be noisy, or in general do not provide a complete picture of the state of the scenario. This is exactly the situation of a femtocell network autonomously making decisions without the assistance of the macro network through the X2' interface. The femtocells measure the SINR, and through this, they estimate the SINR at a given position where it has been estimated that a victim macro user is located. This information is only a partial and noisy representation of the reality, and is in general affected by error. The resulting formal model to operate in this kind of environments is called POMDP [44]. A POMDP is based on a State Estimator (SE), which computes the agent's *belief state* b, as a function of the old belief state, the last action and the current observation the agent makes of the environment o, as it is shown in Figure 4-53. In this context, a belief state is a probability distribution over states of the environment, indicating the likelihood that the environment is actually in each of those states given the agent's past experience. The SE can be constructed straightforwardly using the estimated world model and Bayes' rule [44]. So a POMDP consists of:

- a set of agents F.
- a set of states S.
- a set of actions A.
- a cost function. $C: S\times A\rightarrow R$
- a state transition function $P: S\times A\rightarrow \Pi(S)$
- a set of observations Ω.

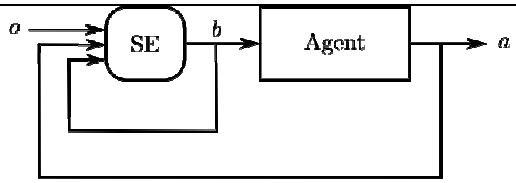

Figure 4-53: Basic structure of POMDP technique.

Similarly to the case of complete information, an optimal policy cannot be found. To implement a solution, we rely on the results in [44], where mechanisms to find reasonably good suboptimal policies are studied. In partially observable environments, the goal is to find a policy for selecting actions that minimize an infinite-horizon, discounted optimality criterion, based on the information available to the agents. The way to proceed is to maintain a probability distribution over the states of the underlying environment. We call this distribution *belief state*, $B=\{b(1),b(2),\cdots,b(k)\}$ and we use the notation $b(s)$ to indicate the agent's belief that it is in state s.
Based on the belief state, we can find an approximation of the Q-function, Q_b, as follows:

$$Q_b = \sum_s b(s)\,Q(s,a)$$

and we can use Q_b as a basis for action selection in the environment. Once the action a is selected and executed, the Q-learning update rule has to be generalized, so that the Q-value $Q(s,a)$ $Q(s,a)$, corresponding to state s and action a, is updated according to a weight, which is the belief that the agent is actually occupying the state s [44]:

$$Q(s,a) \leftarrow \{Q(s,a) + \Delta Q_b(s,a)\}$$

where $\Delta Q_b(s,a)$ is:

$$\Delta Q_b(s,a) = \alpha b(s)[c + \gamma \min_{a'} [Q(b',a)]]$$

where b' is the resulting belief state, after the execution of action a.
Now, to define the POMDP system, it is necessary to identify the system state, belief state, action, associated cost and the observations.

- **State:** The environment state is characterized as:

  $$s_r^f = \{Pow^f, \tilde{C}_r^m, C_r^f\}$$

  where Pow^f is the femtocell total transmission power over all RBs, C_r^f is the femtocell capacity and $\tilde{C}_r^m$ is the capacity of macrocell m in RB r estimated by the interpolation method defined in Step 3.
- **Action:** The set of possible actions are the l power levels. Here, the action selection procedure is performed based on the Q_b.
- **Belief state:** For each learning process, the femtocells have to build the belief state $B=\{b(H),b(L)\}$, defined by two components, i.e. $b(H)$ and $b(L)$, which represent the belief of the femtocell that the capacity at the macrouser is above or below the threshold, respectively. These beliefs are the result of the interpolation process.
- **Cost:** The cost equation is given by:

  $$c = \begin{cases} K & Pow^f > P_{\max}^F \quad or \quad \tilde{C}_r^m < C_{\min}^M \\ K\exp^{-C_r^f} & otherwise \end{cases}$$

  The rationale behind this cost function is that the total transmission power of each femtocell does not exceed the allowed $P_{\max}^F$, the capacity of the macrocell does not fall below a target $C_{\min}^M$, and the capacity of the femtocell is maximized.
- **Observations:** The set of observations Ω is characterized by all the estimations that the femtocell has to compute, as described in Steps 2 and 3 of the proposed methodology, which consist of

positioning of the macro user, and of the estimation of the aggregated interference at the macro user, based on the aggregated interference received by the networked femtocells.

4.3.6.3 Simulation results

The scenario considered for validating the proposed approach is described in deliverable D 2.1 [82] and is based on RAN4 3GPP documents. We present some significant simulation results regarding the implementation of ordinary Kriging spatial interpolator, the learning algorithms behaviour, and the femto and macro systems performance. We will refer to the Q-learning algorithm for completely observable environments as Q-learning, and to the Q-learning algorithm for partially observable environments as POMDP.

Results presented in this section were obtained for a $C_{\min}^{M}$ threshold equal to 1.2 Mbit/s per RB and R=4 RBs. Figure 4-54 represents the spherical model fitting curve for the sample variogram obtained for an occupation ratio of $p_{oc} = 60\%$. As it can be observed, the fitting curve reveals that the sample variogram can be correlated depending on the distance. In the given results we imposed the commonly used spherical variogram model, instead of selecting one from a set of models.

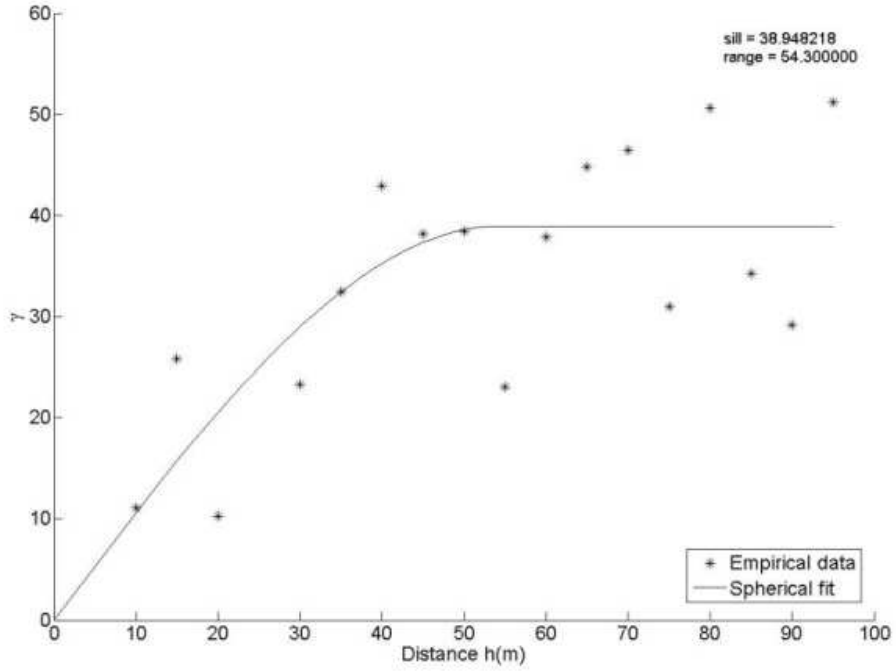

Figure 4-54: Variogram fit with spherical model for $p_{oc} = 60\%$.

In order to test the ordinary Kriging estimator performance, we compute an Interpolation Error (IE) in such a way that the error counter is incremented if the capacity estimated at femtocells is above the $C_{\min}^{M}$ threshold and the actual capacity perceived by macro user is below it and vice versa. Figure 4-55 represents the CCDF which indicates how often the IE is above a particular level. As it can be observed, the probability to obtain an IE higher than 6% is less than 8%. Therefore, we can affirm that, despite the complexity of the proposed methodology, errors resulting from the interpolation process can be tolerated. It is also worth mentioning that we are assuming hard constraints to measure the IE. This means that interpolated values that are very close to the actual values may still be counted as IEs if the actual and the interpolated values do not fall into the same side of the $C_{\min}^{M}$ threshold.

We now discuss the convergence capabilities of the proposed approach. We compare the Q-learning process for both cases of partially and completely observable environments. Figure 4-56 represents the probability of being out of capacity threshold as a function of the learning iterations, for a scenario with a femtocell occupation ratio of $p_{oc} = 45\%$. As it can be observed, in terms of interference, the femtocell applying the learning process with partially observable environment generates a more unstable performance

at macro user. This instability is associated to the inherent errors in the femtocells observations based on which they perform the action selection process.

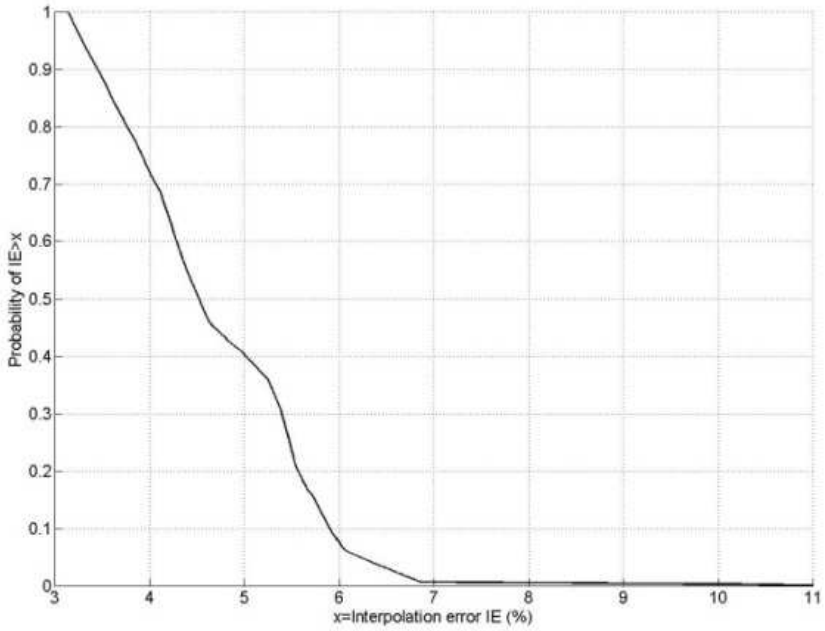

Figure 4-55: CCDF of the error of the SINR estimated by femto BS.

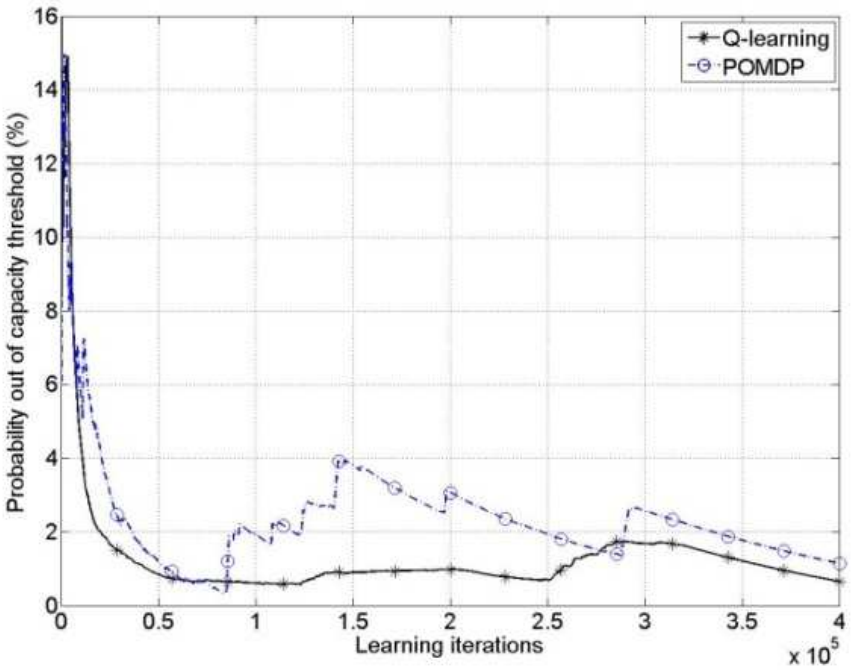

Figure 4-56: Probability of being out of capacity threshold as a function of the learning iterations.

Figure 4-57 presents the macrocell and femtocell average capacities for partially observable and completely observable environments. As can it be observed, both learning systems keep the macrocell capacity above the $C_{\min}^{M}$ threshold. As a result, it is demonstrated that through the proposed approach it is reasonable to operate without the support of X2' interface in partially observable environments. However, for the partially observable case, power levels are selected in a more conservative way with respect to the completely observable case, as a result of the errors in the observations. This results in higher macro capacities and lower femto capacities for the partially observable case with respect to the completely observable case. In

this sense, Q-learning with partial information achieves a poorer load balancing in the network, which is the price to pay for the unavailability of the X2' interface.

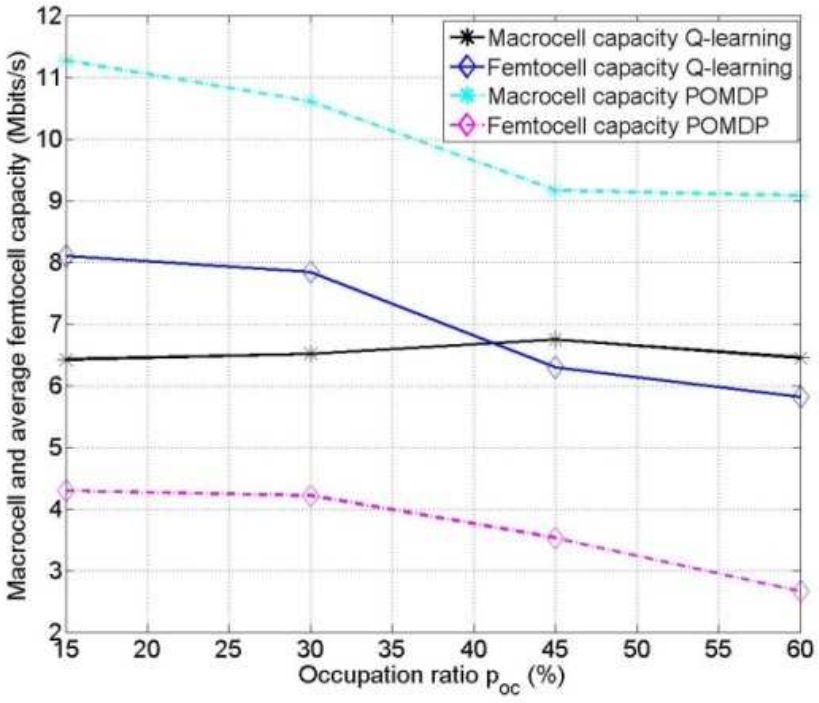

Figure 4-57: Macrocell and femtocell average capacity as a function of P_{oc}.

4.3.6.4 Conclusions

We have presented an autonomous learning algorithm for a heterogeneous network scenario, consisting of macrocells and femtocells working in co-channel operation, to solve the aggregated interference generated by the multiple femtocells at macrocell receivers. We consider 3GPP release 11 compliant architectural hypothesis, according to which the X2' interface from macrocells to femtocells is not available. The lack of feedback, which could be gathered through this X2' interface, makes the interference management problem even more challenging, since femtocells have to make decisions among themselves in an autonomous fashion. The resulting theoretical framework to model the interference management problem is a stochastic game with partial information, where the agents' decisions affect the perception of the environment of neighbour nodes, and where the environment is also affected by the typical dynamics of a wireless scenario. This game is proposed to be solved by means of the theory of POMDP, which works by constructing beliefs about the state of the environments. The belief set is built through the femtocells SINR measurements and by spatially interpolating them through the ordinary Kriging technique. Extensive simulation results have shown that POMDP algorithm is able to learn a sub-optimal solution, which guarantees to maintain the macrocell system performance above a desired threshold, allowing an autonomous femtocells deployment and avoiding the introduction of signalling overhead in the system.

4.4 Centralised SON Algorithms

4.4.1 Central Interference Mitigation between Femtocells

4.4.1.1 Description of the Scheme

Large-scale femtocell deployment comes with some challenges. Among these challenges, interference between BSs requires more attention, especially in networks where BSs are densely deployed, such as within enterprises or residential complexes. Frequency reuse, where interfering neighbours transmit data on different frequency resources (subbands), is used to enhance the throughput of cell edge users. Access to the remaining subbands is restricted, so as not to interfere with neighbouring BSs. Thus, UEs located in the vicinity of two or more BSs face less interference and enjoy better service quality. On the other hand, frequency reuse decreases the network's overall resource efficiency. Unlike macrocell networks, femtocells are installed by the end user, so that the operator cannot determine the locations of the neighbouring base

stations *a priori*. This may result in vast variations of the interference conditions experienced by BSs. This implies that BSs having a lower number of interfering neighbours can use more subbands than BSs that are in close vicinity to one another. Consequently, in order to increase the resource usage efficiency, BSs should use as many subbands as possible depending on their geographic distribution. In this work, a novel graph-based dynamic frequency reuse (GB-DFR) approach is presented. The main objective of GB-DFR is to dynamically assign subbands to BSs, so as to improve the throughput of cell-edge UEs, without causing a sharp decrease in the overall network throughput.

In GB-DFR, a central controller collects the cell identities of the interfering neighbours from all BSs and maps this information onto an interference graph. Interfering neighbours are identified based on a pre-defined SINR threshold, γ_{th}, which specifies the minimum desired SINR for each UE. Then, the central controller assigns subbands to BSs by applying a modified graph colouring algorithm that takes into account the usage efficiency of subbands. Conventional graph colouring algorithms, such as the one given in [34], colour the nodes of a graph with the minimum number of colours such that no two connected nodes have the same colour. By assuming that each colour represents a different subband, graph colouring facilitates subband assignment, where two BSs connected via an edge in the interference graph cannot use the same subband. The drawback of conventional graph colouring is the inefficient usage of the subbands since each BS is assigned only one subband. In order to increase the spatial reuse of subbands, a BS in a less interfering environment should be able to use more subbands without causing high interference to its neighbours. Shortcomings of conventional graph colouring are addressed with the proposed GB-DFR scheme, where the subbands are assigned to BSs in three steps and a cost function is introduced to maximize the spatial reuse of subbands. Additionally, in order to increase the fairness for situations where the number of subbands is high, a parameter s_{min} is introduced. It indicates the minimum number of subbands that should be assigned to each BS.

The novelty of GB-DFR comes from the flexibility in the number of assigned subbands which depends on the interference conditions of each BS. Those BSs facing low interference are assigned more subbands. Another advantage of GB-DFR is its low complexity and modest signalling overhead. The central controller only needs the cell-IDs of the interfering neighbours and determines the subband assignment by graph colouring and search algorithms which have low complexity. For more details, the reader may refer to [51] and [34]. However, GB-DFR is suitable only for single user deployments where each BS serves just one UE. As the BS serves more UEs, the utilization of subbands decreases. For this purpose, an extended GB-DFR (eGB-DFR) is investigated that is better suited to serve multi-user scenarios with the objective of increasing the cell-edge capacity whilst maintaining a high subband utilization. In order to enable this, we define two classes of subbands depending on their foreseen usage by a BS: primary subbands (PSs) and secondary subbands (SSs). The PSs are assigned by a central controller similar to GB-DFR [51] [34],, so as to protect cell-edge UEs facing high interference. The PSs belonging to a particular BS cannot be used by their interfering neighbouring BSs because such neighbours can cause high interference to UEs of the BS in question. In order to ban/block subbands at the interfering BSs, BSs send a PS indicator to their interfering neighbors. When a BS receives such an indicator, it cannot use the indicated subband and this way cell-edge UEs allocated resources from within the set of PSs experience low interference. Secondly, the SSs, belonging to the set of all unblocked (in other words, non-PS) subbands are assigned autonomously by BSs after PSs are assigned. SSs can be used by a BS depending on the prevailing interference conditions; but, enjoying no privileges, these subbands cannot be blocked at interfering neighbouring BSs. Resources of SSs can therefore be allocated to cell-centre UEs facing less interference as long as they do not cause high interference to neighbouring BSs. Consequently, the usage of the PSs boosts cell-edge capacity, whereas the SSs increases the spatial reuse of resources especially for multi-user deployments. This is therefore a hybrid method comprising a centralized and a decentralized component. The detailed explanation of the eGB-DFR can be found in [40].

4.4.1.2 Simulations

For simulations, a downlink transmission in a femtocell network based on 3GPP LTE is considered. The deployment of femtocells is modelled by a 5×5 grid, where a single floor building with 25 apartments is used. Every apartment hosts a femto BS with a certain activation probability. If an apartment contains an active femto BS, it serves a certain number of UEs which are randomly distributed within the confines of the apartment. Full-buffer transmission is assumed such that every BSs assign all available resources from all available subbands to their served UEs. For the sake of simplicity, interference from the macrocell network is neglected, which may be accomplished by allocating different frequency bands to macro and femto BSs. The system parameters are summarized in Table 4-4.

Table 4-4: Simulation Parameters

Parameter	Value
System bandwidth	20 MHz
Number of Subbands	4
Min. Sep. between UE and BS	20 cm
BS Antenna Gain	0 dBi
Antenna Pattern (Horizontal)	$A(\Theta) = 0$ dB (omnidirectional)
Interior Path Loss	$L=127 + 30\log_{10}d$ [km] where d is the distance between UE and BS
Shadowing Std. Dev.	10 dB
Max BS Tx power	10 dBm
Thermal Noise Density	η = -174 dBm/Hz
UE Noise Figure	9 dB
Apartment Dimensions	10m x 10m
Number of UEs per Femto BS	4
Femto BS Activation Prob.	0.2
SINR Threshold	γ_{th} =5 dB
Prob. p used for eGB-DFR	0.25

For throughput calculations, the attenuated and truncated Shannon bound is applied, which approximates the spectral efficiency of appropriately selected modulation and coding schemes subject to the achieved SINR. Detailed information on simulation environment and throughput calculations can be found in [51] and [34]. As a final remark, each snapshot of the simulator lasts for 10 time slots. During the snapshot, positions and shadowing values of BSs and UEs are assumed to remain unchanged. This is reasonable since indoors, the mobility of users is not as high as would be the case for outdoors. The statistics, such as SINR and capacity, are calculated at the end of the 10^{th} time slot, *i.e.*, when a stable resource allocation is achieved.

The performances of fractional frequency reuse, GB-DFR and eGB-DFR are compared. We use two FFR schemes: FFR 1/4 and FFR 2/4 where each BS is centrally assigned one and two subbands out of four available subbands respectively. For eGB-DFR, the number of PS per BS is set as 1.

Table 4-5: Performances of the Compared Methods

Method	Cell-edge Cap.	Average Cell Cap.
FFR 1/4	1.57 Mbps	19.82 Mbps
FFR 2/4	0.35 Mbps	30.23 Mbps
GB-DFR	1.90 Mbps	27.15 Mbps
eGB-DFR	1.96 Mbps	35.17 Mbps

The capacity performances of four methods are summarized in Table 4-5, which compares the cell-edge capacity (defined as the 5% of the CDF of user capacity) and the average cell capacity. eGB-DFR, like the FFR 1/4 system shows very good cell-edge performance, but also shows very promising overall cell capacity. Since SSs are not blocked, more subbands are utilized with eGB-DFR, and hence, cell-centre UEs can be allocated more resources. Therefore, eGB-DFR boosts cell-edge capacity without compromising the system capacity. The results demonstrate that eGB-DFR significantly outperforms FFR and GB-DFR in terms of cell-edge and average cell capacity.

4.4.1.3 Contribution to BeFEMTO System Concept and Objectives

The main contribution of this work is to assign resources in unplanned wireless networks that are characterized by varying interference conditions. The proposed eGB-DFR method takes the advantages of both central and autonomous resource assignment approaches. By assigning the PSs centrally, the system reaches a stable resource assignment in a short time and the cell-edge UEs are well-protected. Additionally, by assigning SSs autonomously, a BS gets more flexibility in choosing subbands available for transmission which increases the utilization of subbands. Simulation results demonstrate that eGB-DFR attains a significant improvement for both cell-edge as well as system capacities for multi-user deployments compared to conventional frequency reuse methods. The scheme depicted in this section also compatible

with the BeFEMTO system architecture. According to the given deployment parameters, the average spectral efficiency achieved is around 1.75 bps/Hz. However, these values are obtained by using single antenna transmission. By using the multi-antenna techniques, we can get higher spectral efficiencies.

4.4.2 Graph Colouring/Graph Partitioning

4.4.2.1 Problem Statement

One of the promising features of small cells is their high applicability in enterprise or domestic environments, considering buildings with numerous offices or small apartments. Inter-cell interference is an issue of major concern in such networks resulting from different origins, namely co-tier and cross-tier interference.

Three key points can distinguish interference management for small cell networks compared with macro-cell ones, thus making the inter-cell interference (ICI) management more challenging:

- **Unplanned nature:** The home eNodeBs (HeNBs) of small cells are deployed arbitrarily in local environments like houses or apartments. Hence, the co-existence of multiple randomly deployed HeNBs in a dense environment, operating at the same licensed spectrum, provides an additional burden to ICI mitigation.

- **Small Size:** In the small size of this type of cells, the traditional area-based flexible frequency reuse methods like Fractional and Soft Frequency Reuse are not applicable.

- **Level of Interference:** Another key challenge is the experienced level of interference in small networks. In the legacy ICI management methods, it is assumed that typically there are 1 or 2 dominant interferers causing ICI to the cell edge users. On the contrary, in small cell networks, we may have multiple strong interferers that cause problems to small cell users.

Considering the aforementioned challenges that small-cell deployments can face, we propose a novel dynamic graph-based solution that targets the ICI mitigation for small cell networks. Our proposed framework was inspired from [52] addressing the multi-cell OFDMA resource allocation problem in macro-cellular networks. Here, we come up with a framework adapted to the challenges of small-cell networks and therein we propose novel algorithms to efficiently solve the multi-cell OFDMA resource allocation problem.

4.4.2.2 System Model

The system is considered as a downlink multi-cell OFDMA cellular network that consists of a dense deployment of indoor small-cells. Each small cell is served by a single, randomly located, antenna denoted as HeNB. The entire network is regarded either way as an enterprise or domestic environment that comprises $\boldsymbol{L}$ HeNBs. Each HeNB serves $\boldsymbol{M_l}$ users and the total number of users in the system is the aggregation of the users of all $\boldsymbol{L}$ HeNBs, such that:

$$M_T = \bigcup_{l=1}^{L} M_l \tag{4.33}$$

This system also includes a locally central entity that acts as a control unit that resolves conflicts in the small cell network. Below in Figure 4-58, we illustrate an example deployment comprising a typical 3GPP LTE femtocell network which includes a LFGW. The LFGW is defined as an optional solution for management purposes mainly for enterprise small cell networks [53] and subsequently acts as a medium between small cells and the internet backhaul. Note that an interface, defined as X2, is also available between HeNBs for signalling exchange purposes.

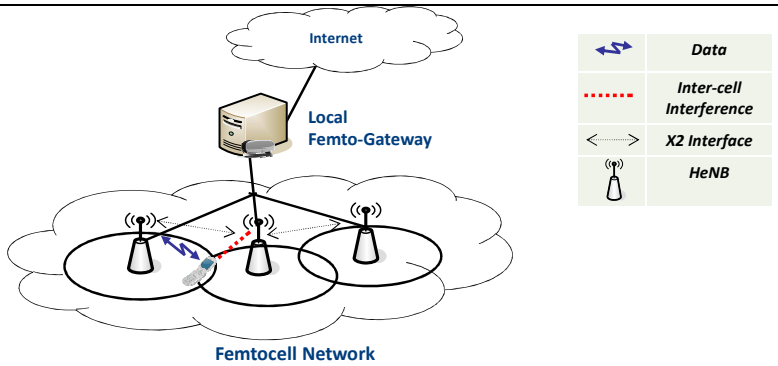

Figure 4-58: Femtocell Network Overview

Here, the resource allocation problem corresponds to the allocation of ***N*** sub-channels that can be reused throughout the network. However, due to intra-cell allocation policy in OFDMA systems, sub-channels are allocated orthogonally between users of the same cell.

It is assumed that when an HeNB powers on, it listens to the neighbouring control channel and reference signals and subsequently measures the path loss from them. Moreover, each HeNB receives the Signal-to-Interference and Noise Ratio (SINR) reports periodically from its corresponding UEs. Therefore, the HeNBs have the knowledge of channel state information. The corresponding SINR that UE *m* experiences at the channel n is derived by:

$$\Gamma(t) = \left\{ \gamma_{m,n}(t) \;\middle|\; \gamma_{m,n}(t) = \frac{P_l \, G_{l,m,n}(t)}{\sum_{i \neq l} P_i \, G_{i,m,n}(t) + \eta} \right\}_{MxN} \tag{4.34}$$

Where P_l accounts for the HeNB transmit power per sub-channel. The total transmit power of each HeNB is assumed to be fixed and remains the same for all HeNB in the network Transmit power is equally distributed among sub-channels. So, transmit power of HeNB *l* on sub- channel *n* depends on the number of sub-channels allocated to its users for a specific transmission time interval. Consequently, if an HeNB does not utilize all the available ***N*** sub-channels, the power transmitted per sub-channel is higher than nominal power per sub-channel in reuse-1.

Moreover, $G_{l,m,n}$ is the channel gain between HeNB *l* and UE *m* in the sub-channel *n* and η represents the thermal noise. Note that the channel gain is modelled as a function of path loss, lognormal shadowing and frequency selectivity. Downlink SINR is used to define the achievable user data rate on each sub-channel. This is highly dependent on the amount of inter-cell interference experienced by each user.

$$R_{m,n}(t) = \log_2(1 + \rho . \gamma_{m,n}(t)) \tag{4.35}$$

Here ρ is a constant related to the targeted Bit Error Rate (BER) via the function $\rho = -1.5 / \ln(5 \cdot BER)$ [54].

Each HeNB ***l*** forms a utility matrix consisting of the utilities of its users on different sub-channels. The network utility function is quite well known in literature as an indicator of user's "satisfaction", based on different factors including experienced delay, channel quality and QoS requirements [55]. A utility function is intuitively an increasing function of achievable rate on different resources. In our study, the utility function can be seen as a function of the user's data rate.

$$U_{m,n} = f\{R_{m,n}(t)\}, \forall m = 1,..,M, \forall n = 1,..,N, \forall t = 1,..,T \tag{4.36}$$

In this study, network utility is modelled based on long-term proportional fairness. Hence, the multi-cell OFDMA resource allocation problem can be formulated as a utility maximization problem stated below, where the individual utilities map the users' satisfaction rate to a real number.

$$\max \sum_{m=1}^{M_T} \sum_{n=1}^{N} U_{m,n} \cdot a_{m,n} \tag{4.37}$$

Here, $a_{m,n}$ is a binary variable corresponding to the allocation decision for the sub-channel *n* by user *m*, *i.e.* $a_{m,n} = 1$ if user *m* is allocated sub-channel *n*. This variable can generally be formulated as follows:

$$A(t) = \{a_{m,n}(t) \mid a_{m,n}(t) \in \{0,1\}\}_{M \times N} \tag{4.38}$$

The aforementioned optimization problem faces two challenges. Firstly, the utility function is related to the SINR of a user *m* at the sub-channel *n*. However, the SINR measurement cannot be known before the actual resource allocation as in a multi-cell environment the allocation of a sub-channel to a user might also affect the SINR of other users. Furthermore, the integer utility maximization problem as formulated above is NP-hard non-convex optimization problem [55]. These challenges can be seen as a burden to optimize resource allocation in multi-cell networks consisting of a multitude of small cells, in similar manner as macro-cell counterparts. For that reason, a solution framework is required that manages to solve this problem in a near-optimal way using heuristic methods.

4.4.2.3 Solution Framework

In the state-of-the-art literature, a graph-based solution framework was presented in [52] to deal with the multi-cell scheduling problem in OFDMA systems. In this study, we modify this framework for the small-cell network case. Subsequently, under this framework we propose novel adaptive algorithms that efficiently solve multi-cell resource allocation problem in a semi-centralized way. In this sub-section, the scope and the structure of the solution framework is briefly highlighted in three following subsections as depicted in Figure 4-59.

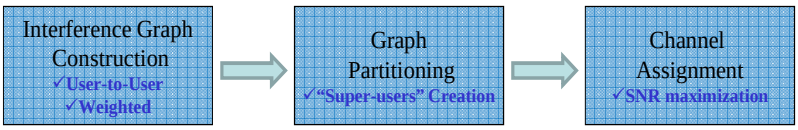

Figure 4-59: Solution framework

4.4.2.3.1 Interference Graph Construction:

The first part of the graph-based solution framework is the construction of the Interference graph:

- The interference graph *G (V, E)* consists of *V* vertices that correspond to users and *E* edges that show the downlink interference conditions between users.
- Edges are weighted via discrete costs. Weights are defined based on mutual interference conditions on users in close vicinity and can be classified as Intra-cell, Critical Inter-cell, and Potential Inter-cell and No-Interference cases.
- The aforementioned graph is fully meshed and un-directional, that means $E(u,v) = E(v,u), \forall u \neq v \in V$

The process of the creation of the interference graph can be distinguished by the way HeNBs and the LFGW coordinate. In our proposed scheme, we consider a centralized coordination that involves the control of a local gateway. In emerging wireless technologies the source of interference can be identified by each user. In LTE systems at maximum 6 interferers can be recognized by each user. In similar manner, in Wimax systems, the diversity set table keeps track of the serving BS and up to 3 interferers for each user [56].

Considering that the users are aware of the identities of the HeNBs causing high interference, their serving HeNB can convey this information to the local controller where the weighted graph is created. Therein, the LFGW has all the available information to identify the relationship between nodes in similar manner as the diversity set tables explained above but in much simpler way.

When a HeNB sends the information of its users, the LFGW records three key parameters in an interference table which are the: *Serving HeNB, Interfering HeNB, Interferer-link Channel Loss.* If this user suffers from many strong interferers, this results in many entries in the table. It is worth noting that as the position of users and the resulting interference condition change, the entries are updated in periodically

4.4.2.3.2 Graph partitioning:

Following the interference graph creation, the second step is the partitioning of the weighted graph in a way that vertices (users) connected through high cost edges are separated in different clusters. Consequently, a set of clusters is created to mitigate ICI by minimizing the intra-cluster sum. By this way, we ensure that highly interfering users do not co-exist at the same cluster.

The graph partitioning creates a notion of "super-users" per cluster enclosing a set of users with a low-level of interference between them. These "super-users" or clusters as defined in [52], utilize sub-channels as a single entity, thus mapping their enclosed users to each sub-channel. Hence, a sub-channel allocation to a super-user corresponds to the allocation to all the nodes that are included in that cluster. This is similar to Max-K-Cut problem [57]. The concept here provides the partitioning of the graph into K cuts in a way that no cut is smaller in size than any other cut. Notice that ***K*** is the number of clusters and the size of the cut is the intra-cluster sum weight of edges. In other words, the objective is to deliver clusters with lowest possible intra-cluster sum weight reflecting the best ICI isolation throughout the network.

In our proposed solution, initially the graph manipulation starts from a node that corresponds to the one with the best neighbourhood (minimum degree). The rationale of the choice of a node with the minimum degree as starting point is that our next-node search should start from a node that has the highest number of good solutions. Thereafter we traverse iteratively the graph by adding the node that minimizes the sum weight towards the already chosen nodes. As the first node is kept fixed, this choice might reflect to the construction of more efficient sub-graphs, i.e. graphs that have the highest number of nodes under a pre-defined sum-weight threshold. The constraint here is an upper bound targeting specific minimum QoS requirement, reflecting the tune-ability of this algorithm. When this bound is reached, a cluster is finalized and the algorithm continues to form another cluster, removing the traces of the pre-selected nodes. Here, the outcome number of clusters and the users therein is dynamic depending upon the QoS requirement.

The issue that might arise here is the uniqueness of outcome solution and the degree of sub-optimality compared to optimal solution. In particular, it is possible to have more than one candidate for both starting node and graph traversing where we face equal-weight solutions.

In order to achieve uniqueness, it is still possible to adopt an extra measure resulting into more efficient partitioning. Towards this objective, we introduce a Perturbation Matrix (PM) to be multiplied with the original graph. The matrix serves as a signature for each pair of nodes, considering the relative channel loss and previous allocation information for these users. The perturbation matrix enables transformation d graph into a graph with unique weights.

To form the PM, we need to adopt a metric. Here, the average channel loss encapsulating the Path Loss and Shadowing effect between the HeNB l to the UE u is defined as $Loss_{l,u}$. Notice that this metric is not dependent on the frequency selectivity effect and thus provides average information on the quality of the BS-to-user link. This parameter characterizes the Interference Metric λ_u for each user u that is exploited to create the PM.

$$\lambda_m = \frac{\sum_{i \neq l \in L} Loss_{i,m}}{Loss_{l,m}}, \forall\, m \in V \tag{4.39}$$

Therefore this interference metric shows for each user the total experienced interference by summing the path loss and shadowing of each individual interferer link over the total loss of the link between UE-serving HeNB. This metric can be seen as an Interference-to-Signal ratio (ISR) assuming a flat channel.

The next step is the inclusion of this parameters into the PM for each pair of users u, v. Here, the ratio of the ISRs for this pair of users determines the perturbation matrix. Note that the maximum ratio is taken into account to be consistent with graph creation strategy of worst case interference conditions. The PM is derived by the following equation.

$$PM_{u,v} = PM_{v,u} = 1 + \max\{\frac{\lambda_u}{\lambda_v}, \frac{\lambda_v}{\lambda_u}\}/100, \forall u \neq v \in V \tag{4.40}$$

The resulting edge matrix (EM) is the element product of the PM multiplied by the Edge Graph.

$$EM_{u,v} = PM_{u,v} \cdot E(u,v), \forall u \neq v \in V \tag{4.41}$$

The EM replaces the edge graph and the algorithm runs according to the new unique weights. This manipulation of the initial graph introduces an alternative version of the proposed Graph Partitioning algorithm to deal with the issues that arise in decision making.

4.4.2.3.3 Channel Assignment:

The partitioning of the graph leads to the creation of super-users as outlined above. The key task here is to assign the sub-channels to the super-users in near-optimal manner. This problem is essentially very similar to SNR maximization problem in single cell scenario. Here, our objective is to maximize the network utility; however instead of users, clusters of users (super-users) are engaged.

At first, the proposed algorithm iteratively assigns clusters to sub-channels to find the cluster with the maximum weighted sum-capacity per sub-channel. Note here that utility-maximization is used instead of capacity maximization to ensure proportional fairness between clusters of users.

However, an important issue arises regarding the power allocation. This originates from the fact that the proposed graph-partitioning algorithm creates a variable number of clusters assigning different amount of resources to them. The aforementioned challenge requires an adaptive power allocation algorithm on top of the channel assignment strategy. Here, we adopted an iterative near-optimal solution as in [58]. The concept in this algorithm is to iteratively adjust the power per resource for each HeNB based on the cluster channel assignments. Hence, for each iteration the transmit power per resource and consequently the utility functions per sub-channel are updated for all the users. The outcome utility values are extracted at the last iteration where all the sub-channels are allocated.

4.4.2.4 Numerical Results

One of the promising applications of small cells is their deployment in the enterprise domain or in a residential building consisting of several apartments. Therein, we introduce a LFGW that supports a number of HeNB in a number of small-cell blocks. The Small-cell deployment used in this study is a 3x3 grid of femtocells-apartments as can be seen in Figure 4-60. In this deployment, each HeNB and 4 users are randomly distributed in each apartment.

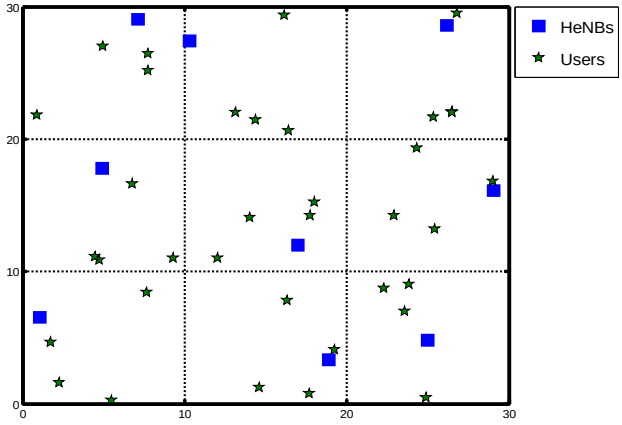

Figure 4-60: Random deployment of users, HeNBs in 3x3 grid

Therefore, a Matlab Monte Carlo simulation platform was developed with the following simulation parameters derived from the respective 3GPP standard as given in Table 4-6:

Table 4-6: Simulation Parameters

Cell Radius	7m
Snapshots	5000
HeNB transmission power	20dBm
UE Noise figure	10dB
HeNB/UE antenna gains	3dBi/0dBi

Number of Interfering HeNBs	8
Frequency Reuse Factor	1
Frequency Selectivity	Rayleigh Fading Channel (4-tap)
Sub-Channels	12 RBs
PF constant (Tc)	100
Path Loss Model	$PL(dB) = 127 + 30 \cdot \log_{10}(R/1000)$

Concerning the intra-cell scheduling, Proportional Fair (PF) Scheduling is used for a multi-channel system [43] in each Femtocell to exploit multi-user diversity and at the same time to have a fair allocation of resources between multiple users.

For evaluation purposes, our proposal is compared with two cases of Reuse-1 and Reuse-3 scenarios without any explicit inter-cell interference management. Furthermore, we evaluate also our proposal against the Dynamic Intercell Interference Control (ICIC) approach presented in [52]. To ensure a fair comparison between these two schemes, we assume that the demand factor for each user is extracted by the number of resources a user takes using our adaptive multi-cell scheduling algorithm in both cases.

Two modes of operation have been considered in implementing our proposal: *Strict bound*, where only connections with minimum interference are allowed to be included in each cluster. *Relaxed bound*, where besides the connections with minimum interference, we also allow a variable number of medium weighted edges (with potentially higher interference) to raise the number of nodes per clusters and thus to increase spectral efficiency

Figure 4-61 illustrates the CDF of users SINR for aforementioned schemes. Our proposal shows marginal differences considering the 2.2 dB as the threshold for the outage probability (0.6% using strict vs. 0.9 using relaxed bound). Reuse-3 with PF at intra-cell shows slightly higher outage (1.1%) whereas the scheme in [52] and Reuse-1 PF show much higher outages of 11% and 20%, respectively.

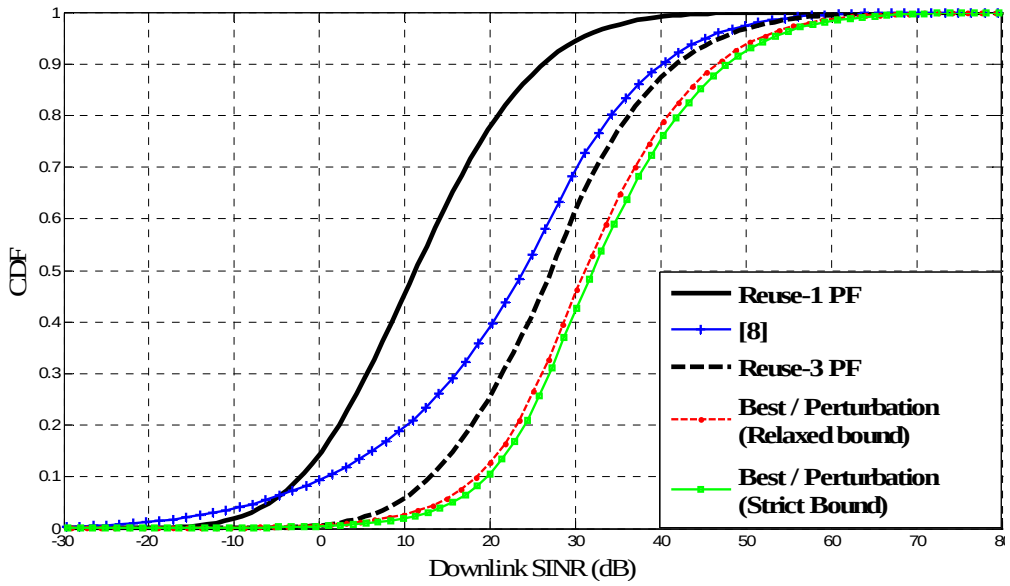

Figure 4-61: CDF of Downlink SINR comparison

Figure 4-62 presents the CDF of user throughput. Here, the improvement of our proposal is notable against the benchmarks. Targeting the 5th percentile of the CDF as QoS measure, our scheme (using Strict Bound) shows 11.5% enhancement over Relaxed Bound. Furthermore, up to 70% improvement is observable over the Reuse-3 PF and [52]. Additionally, our algorithm shows 91% enhancement over Reuse-1 PF.

At the 90th percentile, the improvement is also promising (26%, 40% and 63% over [52], Reuse-3 PF and Reuse-1 PF, respectively).

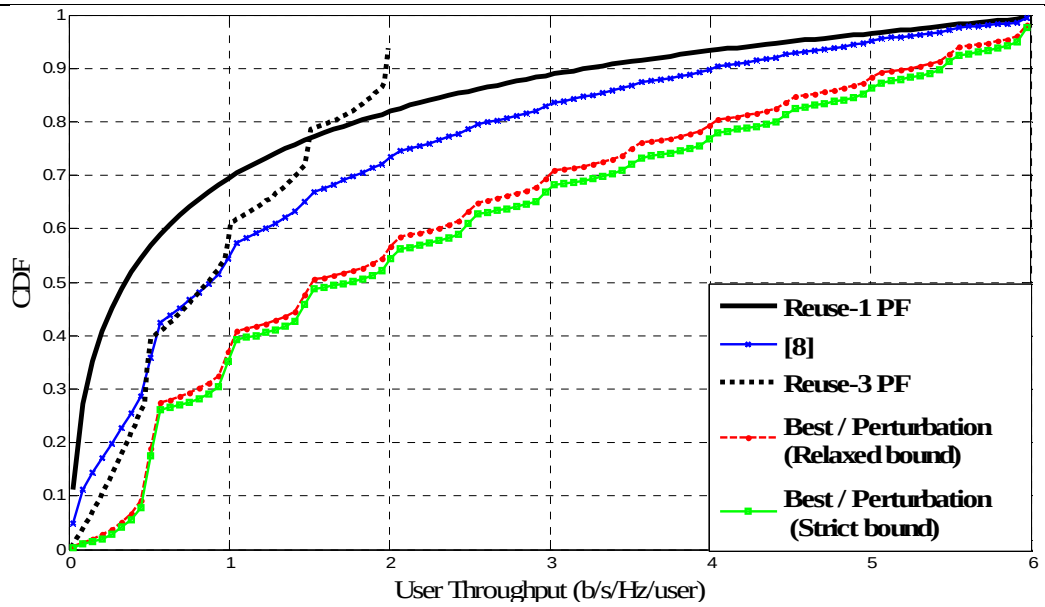

Figure 4-62: CDF of User Throughput comparison

Thereafter, the proposed scheme is compared with respect to spectral efficiency. Figure 4-63 shows the CDF of average cell throughput. Here, the proposed approach outperforms the Reuse-3 PF and [52] targeting the median of the CDF curves. Note that, Reuse-1 PF shows the best results regarding spectral efficiency due to full spectrum reuse at the cost of degrading experienced QoS per user in particular for highly interfered ones as depicted in previous results. In this case, the Relaxed Bound also shows an improvement over the Strict Bound mainly because the relaxation of the threshold allows more users per cluster resulting better spectrum utilization.

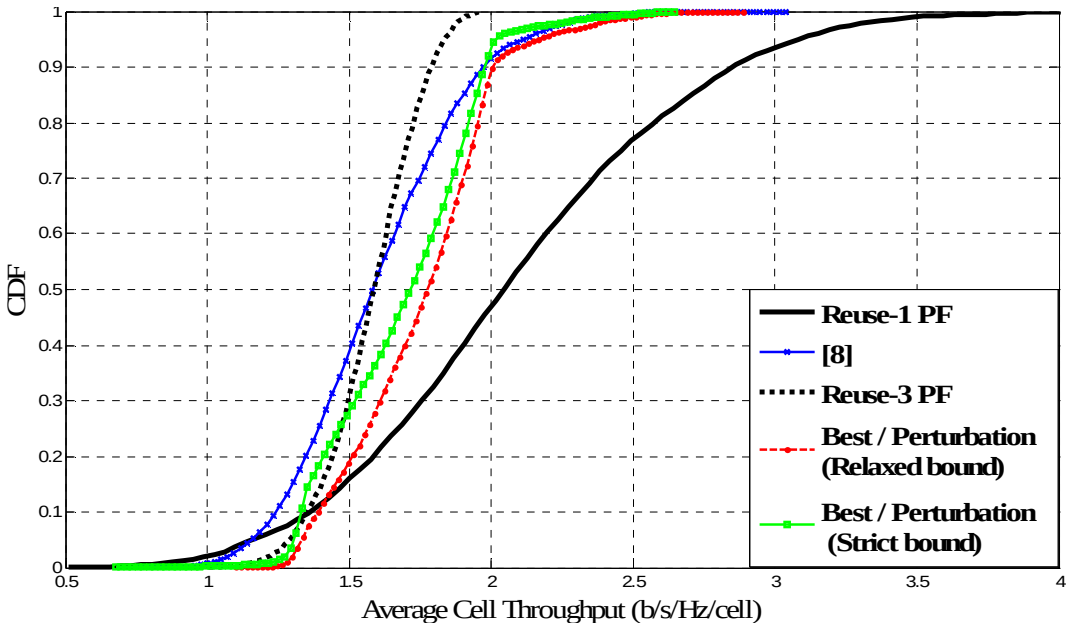

Figure 4-63: CDF of Average Femtocell Throughput comparison

4.4.2.5 Conclusions

This section proposed a “locally” centralized multi-cell scheduling algorithm to efficiently mitigate ICI in dense deployments of small cells. The outcome of this work shows promising results when tested in dense scenarios consisting of Femtocells. The outage factor as well as the user and Femtocell throughput shows a significant improvement over the benchmarks. Therefore, the proposed framework can mitigate the effect of inter-cell interference between dominant interferers, resulting in better performance in terms of outage and throughput representing a better overall spectral efficiency.

4.4.3 Comparing Distributed and Centralised Ghost Femtocell Algorithms

4.4.3.1 Problem statement

The femtocell deployment in 3GPP/LTE sets new challenges to energy efficiency and RRM. Traditional schemes are mainly designed for classical cellular networks while the ad hoc nature of femtocells notably limits the complexity of possible algorithms. Femtocells should self adapt their behaviour to the radio environment without rely on macrocell feedback. In fact, macro-femto coordination limits the system scalability and may result in excessive overhead. Thus, robust and scalable RRM schemes are essential for limiting the interference impact on end-user performance. The goal here is to achieve effective spectral reuse between neighbour cells and reduce the femtocell downlink power consumption while guaranteeing the QoS of users served by both macro and femto base stations.

4.4.3.2 Proposed Solution

The Ghost algorithm is a novel resource management scheme for OFDMA-based femtocell networks, which limits the overall interference per RB generated outside the coverage range of a femtocell while reducing the transmission power in each RB [40]. Ghost efficiently takes advantage of the unusual communication context of femtocells for which locally few UEs compete for a large amount of transmission resource. In order to strongly lower the HeNBs downlink transmission power; it trades off transmission energy for frequency resources.

Simulation results showed that Ghost significantly limits the impact of femto-to-femto interference and femto-to-macro interference in LTE downlink scenarios. The proposed algorithm results in enhanced communication reliability for user equipment associated with both the macro base station and femtocells. This method does not involve any message exchange between Femto and Macro BSs. However, a femtocell coordinator exploits the presence of the X2 interface to locally coordinate the access amongst neighbouring femtocell and limiting the spectrum reuse. This method is thus coined $Ghost_{NF,}$. where NF means Networked Femtocells. Each femto user overhears the broadcast channel (BCH) and estimates which neighbour HeNBs are currently strong interferers. Then, the cell-IDs of the HeNBs perceived as strong interferers are reported to the local coordinator. Therefore, resource scheduling is managed at the local controller that avoids allocating the same resource block to strong interfering cells. Accordingly, peaks of interference are limited and performance is improved, especially at neighbouring M-UEs.

Whenever the X2 interface is not available (i.e., in Stand-Alone Femtocells scenarios), an uncoordinated version of the Ghost can be implemented ($Ghost_{SAF}$), where each HeNB autonomously allocates available resource to its active users trying to maximize the spectrum reuse to limit the radiated transmission power.

In this chapter, we aim to compare these two approaches in order to understand in which scenarios cooperation is worthwhile from both energy and throughput perspectives.

RRM Ghost algorithms can potentially enable the coexistence of a high number of femtocells in the macrocell region. Moreover, the proposed $Ghost_{NF}$ exploits femtocell coordination to limit inter-cell frequency reuse and therefore reduce both cross-tier and co-tier interference. However, such a scheme results in higher overhead and complexity with respect to $Ghost_{SAF}$. The overhead is mainly due to the signaling exchange between HeNBs and the femtocell controller. Each scheduling period (i.e., N transmission time intervals, TTIs), first HeNBs report to the network controller the channel state information, then according to the RRM algorithm, the controller feedbacks the decided scheduling pattern to each HeNB. Furthermore, each M TTIs, HeNBs in the network transmit to their controller the ID of the neighbouring HeNBs, which are classified as strong interferers.

Interference relationships amongst neighbouring cells depend on both the users' mobility and HeNB activity status (on, off, sleep mode). These sets slowly change with time, therefore the frequency of related feedback is generally much lower than the scheduling period (i.e., M » N). For each femtocell network, such overhead can be expressed as follows

$$O_H = \frac{B\sum_{i\in F}|D_i| + \beta \cdot N_i \cdot N_{RB} \cdot (M+1)}{M \cdot T} \quad \left[\frac{bit}{s}\right] \tag{4.42}$$

where $M = \beta \cdot N$, B is the number of bytes used to represent the information, and T is the duration of one TTI. D_i is the number of strong interferers perceived at the femtocell $i \in F$. N_i and N_{RB} correspond to the number of active UEs in the cell i and the number of available resource blocks, respectively.

A further drawback of the centralized approach is its dependency on the controller reliability, which may result in low scalability in dense femtocell deployment. A distributed version of the discussed scheme, where signalling and computation costs are shared amongst neighbouring HeNBs, is feasible. However, this solution would result in higher overhead and latency. Due to the lack of inter-cell coordination, the proposed $Ghost_{SAF}$ is, on the contrary, characterized by limited overhead and complexity. Furthermore, it does not limit the spectrum reuse at HeNBs. However, it may result in harmful interference, especially in dense femtocell deployment scenarios. In the next section, we aim at evaluating the impact of this interference by investigating the impact of the proposed algorithm at both M-UEs and F-UEs.

4.4.3.3 Simulation Results

In this section, we compare the cooperative version of the Ghost algorithm ($Ghost_{NF}$) with the stand-alone scheme ($Ghost_{SAF}$) and a reference algorithm (RRM_{SOA}). Performance is measured at both macro and femto cells.

The main differences between these schemes are the following:

1) In both $Ghost_{SAF}$ and RRM_{SOA}, there is no coordination within the femtocell network. Hence, HeNBs are not aware of the presence and allocation strategy of neighbour HeNBs;
2) RRM_{SOA} aims at maximizing the spectral efficiency of femtocells while minimizing the probability that users that belong to different cells access to same RBs. Thus, the RRM_{SOA} attempts to limit the number of RBs allotted to each FUE;
3) RRM_{SOA} does not implement Modulation and Coding Scheme (MCS) and Power scaling (see [40] for more details).

It is important to mention that RRM_{SOA} is also used at the M-BS in each investigated scenario. We present simulation results for the system model and its parameters given in [50]. RRM algorithms are compared in terms of the following transmission cost metric, which measures the average amount of irradiated energy required to transmit a bit of information (for both macro/femto cells):

$$\Gamma^{F} = \frac{\sum_{k \in N_{Ch}} P_k^{RF}}{\sum_{k \in N_{Ch}} \sum_{j \in FUE} R_{k,j}} \quad \left[\frac{J}{bit}\right] \tag{4.43}$$

$$\Gamma^{M} = \frac{\sum_{k \in N_{Ch}} P_k^{RF}}{\sum_{k \in N_{Ch}} \sum_{j \in MUE} R_{k,j}} \quad \left[\frac{J}{bit}\right] \tag{4.44}$$

where Γ^{M} and Γ^{F} measure performance at the MBS and neighbouring HeNBs, N_{ch} is the set of available channels, MUE is the set of macro users, FUEi is the set of UEs served by the femtocell i. $R_{k,j}$ and P_k^{RF} respectively represent the rate associated to pair channel-user (k,j) and the irradiated power on the resource block k. Note that the introduced metric considers only irradiated energy, to better highlight the effect of the power control mechanism and co-channel interference.

Results are averaged over 50 independent runs. We simulate 10^3 independent TTIs during each run and update channel fading instances at each TTI. At the beginning of each run, we randomly place one block of apartments in which HeNBs, FUEs, and MUEs are randomly deployed. Moreover, in the presented simulations, we consider that all deployed HeNBs are active with four UEs per HeNB. Finally, indoor MUEs are randomly distributed in the apartments where HeNBs are not deployed.

In our simulations, solid, dashed, and dotted-dashed lines correspond to the performance of RRM_{SOA}, $Ghost_{SAF}$, and $Ghost_{NF}$ schemes, respectively.

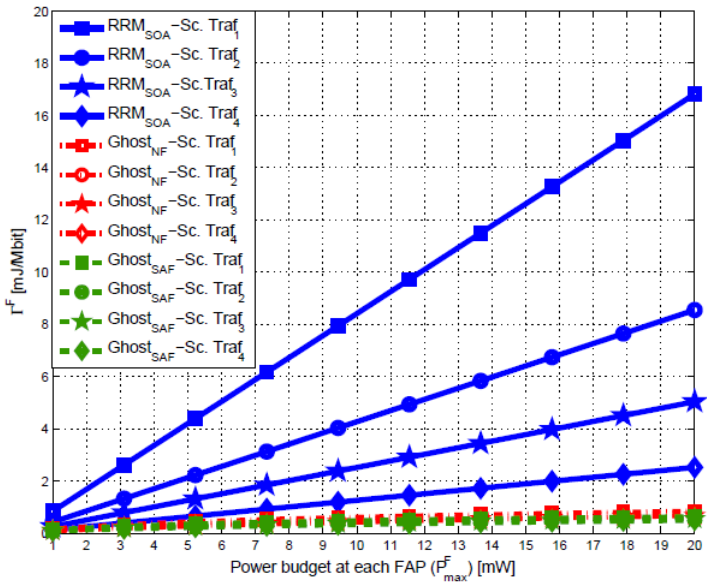

Figure 4-64: Average Γ^F as a function of the power budget P^F_{max} at each HeNB in different traffic scenarios.

Figure 4-64 shows the femtocell performance as ΓF versus the power budget P^F_{max} at each HeNB.

We have set the deployment ratio (ρ_d, see [3GPP]) equal to 0.3 and considered four different traffic scenarios:

1. Scenario Traf.1: F-UE throughput target T_{tg} = 300 kbit/s, square marked curves.
2. Scenario Traf.2: F-UE throughput target T_{tg} = 600 kbit/s, circle marked curves.
3. Scenario Traf.3: F-UE throughput target T_{tg} = 1 Mbit/s, star marked curves.
4. Scenario Traf.4: F-UE throughput target T_{tg} = 2 Mbit/s, diamond marked curves.

We can observe that both the proposed $Ghost_{NF}$ and $Ghost_{SAF}$ improve the femtocell performance with respect to RRM_{SOA}. For instance, considering a power budget equals to 10 mW, the proposed $Ghost_{NF}$ and $Ghost_{SAF}$ gain up to 95% with respect to RRM_{SOA} in Scenario Traf .1, up to 90% in Scenario Traf .2, up to 85% in Scenario Traf .3, and up to 75% in Scenario Traf .4.

Moreover, results outline that performance gain increases in lightly loaded scenarios (Scenario Tra f .1 and Scenario Traf .2) where our algorithms permit to strongly reduce the transmission power by lowering the selected MCS. In these cases, our schemes take advantage of the lower throughput targets to decrease the downlink irradiated power and spreading over RBs. On the contrary, in highly loaded scenarios the achieved gain is limited. This comes from some concurrent effects. With higher T_{tg}, a larger number of RBs and/or a higher MCS are needed for each user to meet QoS constraints. This translates in either larger interference generated to neighbouring cells on some RBs and/or a need to transmit on the same number of RBs, but with a higher order of MCS. Transmission is thus more sensitive to both noise and interference generated by close interferers. Finally, we can observe that $Ghost_{SAF}$ slightly improves the femtocell performance compared to $Ghost_{NF}$. Even though coordination between neighbour HeNBs permits to limit femto-to-femto interference, $Ghost_{SAF}$ increases the frequency reuse and exploits the available resources to further improve the energy saving at each cell. Furthermore, as discussed in the previous section, $Ghost_{NF}$ results in higher complexity and overhead due to signalling between HeNBs and the local controller. Therefore, we can conclude that the proposed $Ghost_{SAF}$ outperforms the $Ghost_{NF}$ from the femtocell perspective.

Figure 4-65 shows the improvement in MUE performance under $Ghost_{NF}$ and $Ghost_{SAF}$. In the co-channel femtocell deployment, indoor MUE performance is limited by femto-to-macro interference. In absence of coordination amongst the M-BS and the neighbouring HeNBs, the macrocell scheduler is not aware of the RBs exploited by the interfering HeNBs. When the MBS assigns to an indoor user a RB that is used by a nearby HeNB, this MUE can be exposed to a high level of interference. We aim to evaluate the effect of this interference at MUEs when femtocells use the reference RRM_{SOA} and the proposed $Ghost_{NF}$ and $Ghost_{SAF}$ schemes.

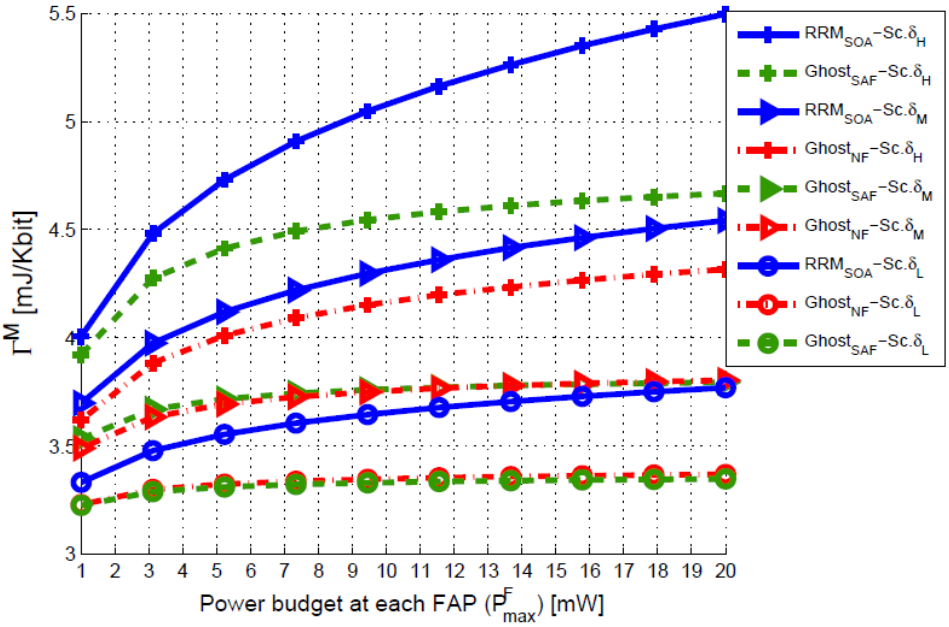

Figure 4-65 Average Γ^M measured at M-UEs as a function of the power budget at each FAP P^F_{max} in different traffic scenarios.

To compare these algorithms, we have set the MUE throughput target equals to 300 kbit/s, the FUE throughput target equals to 600 kbit/s, and considered three different femtocell deployment scenarios:

1. Scenario δL: low density—ρ_d = 0.3, circle marked curves.
2. Scenario δM: medium density—ρ_d = 0.5, triangle marked curves.
3. Scenario δH: high density—ρ_d = 0.8, plus marked curves.

On Figure 4-65, we show the macrocell performance as Γ^M versus the power budget P^F_{max} at each HeNB. Results indicate that $Ghost_{NF}$ and $Ghost_{SAF}$ permit to limit the impact of the femto-to-macro interference in all considered scenarios. This improvement only comes from the femtocell behaviour; in fact, the MBS uses a fixed RF power in each allotted RB. On the other side, MCS scaling, spreading, and power control mechanisms permit to reduce the HeNB downlink power transmission in each RB and mitigate interference. For instance, considering P^F_{max} equals to 20 mW, the proposed $Ghost_{SAF}$ gains up to 11%, 16%, and 15% with respect to RRM_{SOA} in Scenarios δ_L, δ_M, and δ_H. Moreover, the proposed $Ghost_{NF}$ gains up to 11%, 16%, and 22% with respect to RRM_{SOA} in Scenarios δ_L, δM, and δ_H. While in Scenario δ_L and Scenario δ_M the $Ghost_{SAF}$ slightly improves the performance achieved by the $Ghost_{NF}$, in Scenario δ_H the $Ghost_{NF}$ outperforms the $Ghost_{SAF}$. In fact, the probability that several neighbour HeNBs access to same RBs increases with the femtocell density, hence, in Scenario δ_H, MUEs may experience high peaks of cross-tier interference. In $Ghost_{NF}$, the local controller coordinates the access of neighbouring femtocells limiting the overall interference perceived at MUEs.

4.4.3.4 Conclusions

The future 3GPP/LTE femtocells deployment is expected to be dense: a large population of potential interferers will need to share scarce common frequency resources while indoor femtocell users will benefit of high quality links. Classical resource allocation and interference mitigation techniques cannot address the challenge of limiting interference between neighbouring femtocells and maintaining a high level of reliability for macro UE communications.

The femtocell deployment requires a new paradigm because of two main reasons. First, femtocell users can benefit from a high quality downlink signal enabled by short range communications characterizing femtocell deployments. Second, only few users locally compete for a large amount of frequency resources in a femtocell. Therefore, a femtocell benefits from a huge amount of spectral/power resources.

Such observations have led to the design of a novel transmission paradigm for femtocell networks, which trade-off irradiated power for frequency resources. Here we have compared two different schemes based on the Ghost paradigm, named as $Ghost_{SAF}$ and $Ghost_{NF}$, which can be implemented in stand-alone and networked femtocell scenarios, respectively. We have discussed the effectiveness of these algorithms in a

two-tier network in terms of complexity, overhead, and performance at both macro and femto cells. The proposed algorithms limit the undesired effects of interference by reducing the irradiated power per RB required at femtocells to meet target QoS constraints.

Simulation results have shown that the proposed schemes outperform the classic RRM strategies. Moreover, Ghost_{NF} can allow higher performance atUEs with respect the $\text{Ghost}_{\text{SAF}}$ by limiting spectrum reuse in dense femtocell deployment scenarios. However, such an improvement comes at the cost of higher complexity and overhead.

4.4.4 Power Control

4.4.4.1 Introduction

Heterogeneous Network (HetNet) co-channel deployment with femtocells in closed access urges the need of efficient interference mitigation mechanisms, especially when considering downlink. Indeed, the core network will deny the access to all users that do not belong to the femtocell CSG. Therefore, a User Equipment (UE) coming close to a femtocell but not listed in the femtocell CSG can be highly interfered and lose its network connection. Though frequency partitioning strategies could alleviate the interference affecting data channels in OFDMA-based systems like LTE (at the cost of the overall system throughput), control channels are more difficult to protect as they span over the whole bandwidth.

One simple way to minimise interference for both control and data channels is to rely on power setting. One classical approach is based on the femtocell capability to measure its environment thanks to an embedded NLM allowing it to perform the same measurements as a UE. Practically, the femtocell power is set according to the macrocell surrounding [65], [66] using:

$$P_t = \max\left(\min\left(\alpha P_r^{macro} + \beta, P_{\max}\right),\ P_{\min}\right) \tag{4.45}$$

where P_r^{macro} is the power received by the dominant MBS measured by the femtocell, $P_{\min}$ and $P_{\max}$ are the minimum and maximum femtocell transmission power respectively, and (α, β) are power setting parameters.

The main advantage of such fully distributed approach is the backward compatibility with the existing system architecture. Indeed, the transmission power is adjusted autonomously by the femtocell using its own NLM (ideal for standalone femtocell). However, one drawback is that the measurements are made at the femtocell location and not at the victim MUE position. To address this issue, some methods have been previously proposed which involve the feedback of some MUE measurements to the femtocell thus introducing new signalling and protected channels.

Another drawback is that this distributed power setting does not take into account the presence of other femtocells which may be in the vicinity nor their access policy. Thus it is not suitable for a cluster of femtocells covering a building of an enterprise for instance where all femtocells may broadcast the same CSG. A joint optimisation of the femtocell transmission powers in case of such deployment but with independent CSG per femtocell has been investigated in [67] where femtocell transmission powers are minimised in an effort to guarantee a given QoS to both macrocell and femtocell users. However, the solution requires the knowledge of the exact positions of all equipments as well as the availability of a second carrier.

In this section, we present a power setting algorithm for clusters of femtocells in a HetNet deployment which can be applied either in a centralised or in an iterative distributed way. In both cases, the algorithm exploits the BeFEMTO LFGW as a central unit which (temporally) coordinates one cluster of co-located femtocells through the Ps interface [68]. Using only measurements made by the femtocell NLMs, the femtocell transmission powers are jointly maximised under the constraint of ensuring a certain macrocell protection. The use of a linear programming framework ensures a computationally realistic solution. Femtocell transmission powers are then assigned following different strategies exploiting the femtocell access policy (independent or common CSG). Some strategies enable the switch-off of the most disrupting femtocells enabling an autonomous organisation of the cluster. Such approach leads to an overall enhanced HetNet performance as well as a massive energy saving in the case of a dense femtocell deployment.

4.4.4.2 System Model

A cluster of femtocell is made of N co-located Femtocell Base Stations (FBSs), all using the same carrier as the MBSs. An FBS n can adjust its transmission power P_t^n in the range $[P_{\min}^n, P_{\max}^n]$ and can broadcast

either an independent CSG or a common one within the cluster. The set of femtocells is connected to the BeFEMTO LFGW through the Ps interface [68] as shown in Figure 4-66.

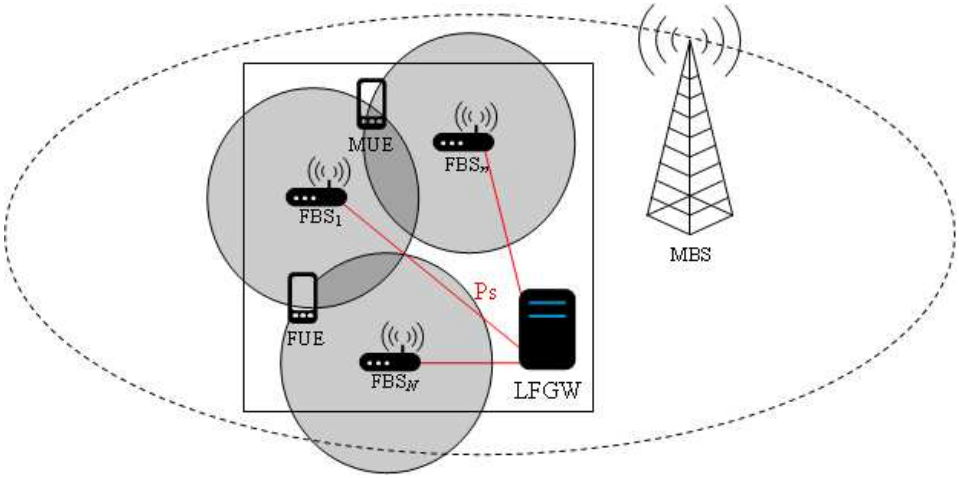

Figure 4-66: HetNet deployment

An MUE can only be served by a MBS while an FUE can be attached to either a FBS broadcasting a CSG identity (to whom the FUE belongs) or to a MBS based on the best received power. Let γ_{MUE} be the SINR experienced by the MUE in the vicinity of the femtocell network. It is given by:

$$\gamma_{\text{MUE}} = \frac{P_r^{macro}}{\sum_{n=1}^{N} P_r^n + \sigma^2_{\text{MUE}}}, \tag{4.46}$$

where P_r^{macro} is the power received from the MBS serving the MUE, P_r^n is the power received from the n^{th} interfering FBS and σ^2_{MUE} is the thermal noise power to which we add the received power coming from all the other interfering macrocells (excluding the serving one). The received power P_r^n can be expressed as $P_r^n = \alpha_n P_t^n$ with α_n the long-term channel attenuation between the n^{th} FBS and MUE which equals in dB to antenna gains minus the pathloss and the shadowing.

One way to protect the MUE is to ensure that its SINR is greater than a given target $\gamma_{\text{MUE}}^{\text{target}}$ (that can be associated to a QoS). This translates into a constraint on the FBS transmission powers $\left\{P_t^n\right\}_{1\le n\le N}$ such that:

$$\sum_{n=1}^{N} \alpha_n P_t^n \le \frac{P_r^{macro}}{\gamma_{\text{MUE}}^{\text{target}}} - \sigma^2_{\text{MUE}} \le \frac{P_r^{macro}}{\gamma_{\text{MUE}}^{\text{target}}}. \tag{4.47}$$

4.4.4.3 Algorithm Description

4.4.4.3.1 Power Setting Optimisation Problem

Our objective is to maximise the femtocell transmission powers $\left\{P_t^n\right\}_{1\le n\le N}$ while maintaining a given quality for the macrocell users. The MUE protection is given a special attention because any FUE has always the possibility to connect to the macrocell network if the femtocell network becomes too much constrained to satisfy the targeted macrocell protection.

To achieve a reasonable complexity in the resolution, we state our problem using a linear approach. Thus, we are going to maximise the following linear cost function:

$$\max_{P_t^n} \quad c = \sum_{n=1}^{N} c_n P_t^n, \tag{4.48}$$

where c_n are weighting factors allowing femtocell discrimination if necessary. Obviously, this cost function will carry the quality perceived by the FUEs. The maximisation is performed under constraints such that an MUE must experience an SINR greater than a predefined target. If we have a set of M MUEs in the vicinity of the femtocell network, then we can form the set of following constraints:

$$\forall m \in \{1, M\}, \sum_{n=1}^{N} \alpha_{m,n} P_t^n \leq \frac{P_r^{\mathrm{MUE}^m, macro}}{\gamma_{\mathrm{MUE}}^{\mathrm{target}}} - \sigma_m^2 \leq \frac{P_r^{\mathrm{MUE}^m, macro}}{\gamma_{\mathrm{MUE}}^{\mathrm{target}}}, \tag{4.49}$$

where $\alpha_{m,n}$ represents the long-term channel attenuation between the m^{th} MUE and the n^{th} FBS.

Maximising (4.48) subject to the set of constraints (4.49) with positive values to find (transmission powers) is an Optimisation Problem (OP) which can be easily solved using Linear Programming (LP) [68] in a centralised way. However, to apply LP to solve our OP, we need all MUEs to be able to feedback their measurements, namely the power they received from the macro network ($P_r^{\mathrm{MUE}^m, macro}$) and the long-term channel attenuation of all femtocell interfering links ($\alpha_{m,n}$) toward the central unit (here the LFGW) in case of a centralised resolution. This feedback may not be even possible over-the-air when the MUEs are in outage due to the femtocell presence.

To overcome this issue, we propose an approximation, by replacing the MUEs' measurements with the FBSs' ones. Indeed, a FBS usually embeds a NLM which gives the FBS the capability to perform the same measurements of its environment as does an UE, making it comparable to a Virtual MUE (VMUE). At the exact position of the femtocell n, we can rewrite (4.49) for the VMUE n as:

$$P_t^n + \sum_{m \neq n} \alpha_{n,m} P_t^m \leq \frac{P_r^{n,macro}}{\gamma_{\mathrm{MUE}}^{\mathrm{target}}} - \sigma_n^2 \leq \frac{P_r^{n,macro}}{\gamma_{\mathrm{MUE}}^{\mathrm{target}}}. \tag{4.50}$$

By moving a bit the VMUE from its initial position, it will receive less power from the femtocell n. Let ρ be this power attenuation. In the best case where the VMUE moves toward its dominant MBS, it will experience a gain in the received power, which we assumed to be $1/\rho$. To make the situation worst (thus strengthening our constraint), we also assume that the virtual MUE will move toward the $N-1$ other interfering femtocells as shown in Figure 4-67.

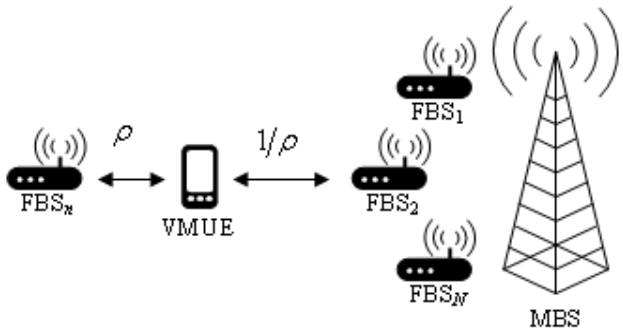

Figure 4-67: Virtual move, attenuation/gain repartition

Of course, if we had the exact topology, we could better estimate the worst case scenario. If we proceed in the same way for the N femtocells, then our OP becomes:

$$\begin{aligned} &\max_{P_t^n} \quad c = \sum_{n=1}^{N} c_n P_t^n \\ &\text{w.r.t} \quad \forall n \in \{1, N\}, P_t^n + \sum_{m \neq n} \frac{1}{\rho^2} \alpha_{n,m} P_t^m \leq \frac{1}{\rho^2} \frac{P_r^{n,macro}}{\gamma_{\mathrm{MUE}}^{\mathrm{target}}} - \sigma_n^2 \leq \frac{1}{\rho^2} \frac{P_r^{n,macro}}{\gamma_{\mathrm{MUE}}^{\mathrm{target}}}. \end{aligned} \tag{4.51}$$

We note $\mathbf{x} = [x_1, \ldots, x_N]^{\mathrm{T}}$ a column vector of length N and $y_{n,m}$ the n^{th} row m^{th} column element of the matrix $\mathbf{Y}$. With those following standard notations, we define:

$$p_n = P_t^n ; a_{n,n} = 1, a_{n,m} = \frac{1}{\rho^2}\alpha_{n,m} ; b_n = \frac{1}{\rho^2}\frac{P_r^{n,macro}}{\gamma_{\text{MUE}}^{\text{target}}}$$

We can thus rewrite (4.51) such that it becomes (by neglecting the term σ_n^2):

$$\begin{aligned} \max_{\mathbf{p}} \quad & c = \mathbf{c}^{\mathrm{T}}\mathbf{p} \\ \text{w.r.t} \quad & \mathbf{A}\mathbf{p} \le \mathbf{b} \\ & \mathbf{p} \ge 0 \end{aligned} \tag{4.52}$$

The OP is totally independent from the presence of one or several MUEs. We only need measurements (received powers, long-term channel attenuations) available at each FBS position. Those can be obtained through RSRP/RSSI measurements using temporally coordinated transmission and silent phases among the femtocells orchestrated by the LFGW.

Of course if we had all the adequate measurements coming from an MUE, we could create its constraint using (4.47) and integrate it to the set of the N previous constraints or replace the one coming from its most dominant femtocell interferer. With the latter approach, we have the advantage that we could adjust the femtocell transmission power only if MUEs are present, but the drawback is that a way must exist for them to report their measurements.

4.4.4.3.2 Centralised Solution

After temporally coordinating and gathering all the necessary FBSs' measurements to form (4.52) (or equivalently (4.51)), the LFGW can solve the OP using LP with the simplex algorithm [69] for instance. If a solution $\left\{\hat{P}_t^n\right\}_{1\le n\le N}$ is to be found, then we define three strategies for assigning by the LFGW the effective transmission power to each femtocell. $\forall n \in [1, N]$:

- Strategy 1: normal behaviour, similar to (4.45)

$$P_t^n = \max\left(\min\left(\hat{P}_t^n, P_{\max}\right), P_{\min}\right). \tag{4.53}$$

- Strategy 2: switch-off possible if zero power was assigned

$$P_t^n = \begin{cases} P_t^n = \max\left(\min\left(\hat{P}_t^n, P_{\max}\right), P_{\min}\right) & \text{if } \hat{P}_t^n > 0, \\ 0 & \text{otherwise.} \end{cases} \tag{4.54}$$

- Strategy 3: switch-off possible if a power below the minimum transmission power value was assigned

$$P_t^n = \begin{cases} P_t^n = \min\left(\hat{P}_t^n, P_{\max}\right) & \text{if } \hat{P}_t^n \ge P_{\min}, \\ 0 & \text{otherwise.} \end{cases} \tag{4.55}$$

In particular, the two last strategies allow a femtocell to be switched-off (either completely or its radio emission only), thus reducing the interference as well as the power consumption. They are well adapted to cluster of femtocells broadcasting the same CSG in a corporate environment for instance. Indeed, independent CSG per femtocell are usually assigned to residential femtocell and buying one femtocell to see it switched–off for the greatest good is not something a customer may accept. These strategies make more sense in a CSG per cluster context to still have a way to benefit from an HetNet deployment.

If no solution is found by the simplex (no strategy applicable), then all femtocells transmit with their maximum power:

$$\forall n \in [1, N], \quad P_t^n = P_{\max}. \tag{4.56}$$

Note that the solution of (4.52) is straightforward for $N = 1$ and similar to the distributed case (4.45) with:

$$\begin{cases} \alpha = 1 \\ \beta = -20\log_{10}(\rho) - \gamma_{\text{MUE}}^{\text{target}}\,(\text{dB}). \end{cases} \tag{4.57}$$

4.4.4.3.3 Iterative Distributed Solution

Iterative distributive resolutions are usually derived from centralised resolution. Indeed, from (4.52) one can search the set of femtocell transmission powers $\hat{\mathbf{p}}$ which fulfils the following linear system:

$$\mathbf{Ap} = \mathbf{b} \tag{4.58}$$

If a solution exists ($\hat{\mathbf{p}} = \mathbf{A}^{-1}\mathbf{b}$), this one can be either computed by a central unit which will then assign the resulting transmission power to the femtocells or achieved in an iterative distributed fashion using approaches such as the first-order Jacobian, Gauss-Seidel or Successive Over-Relaxation (SOR) [70]. This latter approach has the advantage that each femtocell will compute its new transmission power based on local information available thanks to its NLM, the central unit (LFGW) coordinating the iterations (and measurements phases).

Each femtocell n computes its new power at iteration i according to:

- Jacobian approach

$$\hat{P}_t^n(i) = b_n - \sum_{n \neq m} a_{n,m} P_t^m(i-1). \tag{4.59}$$

- Gauss-Seidel or SOR approach

$$\hat{P}_t^n(i) = (1-\omega)P_t^n(i) + \omega\left(b_n - \sum_{m<n} a_{n,m} P_t^m(i) - \sum_{n<m} a_{n,m} P_t^m(i-1) \right), \tag{4.60}$$

where $0 \leq \omega \leq 2$ is the over-relaxation parameter ($\omega = 1$ gives Gauss-Seidel resolution).

Previously defined strategies are also applied when going from the computed power $\hat{P}_t^n(i)$ to the actual transmitted one $P_t^n(i)$. SOR and Gauss-Seidel approaches include ordering in the way the femtocells update their power. Without loss of generality, we have assumed natural order but this topic may definitely need more investigation to speed up the convergence for instance. We initiate the femtocell transmission power ($i = 0$) with the ones resulting from the classical distributed power setting using (4.45).

4.4.4.4 System level simulation

In order to evaluate the power setting method described above, we rely on system-level simulations enabling its large-scale assessment within a classical HetNet deployment. Main assumptions for system-level simulations can be found in [71], [12], see also [72] for 2D correlated shadowing. We use a 3-sector hexagonal macrocell layout with 7 sites (21 cells, see Figure 4-68) to reduce the simulation complexity, with wrap-around to counter the edge effect.

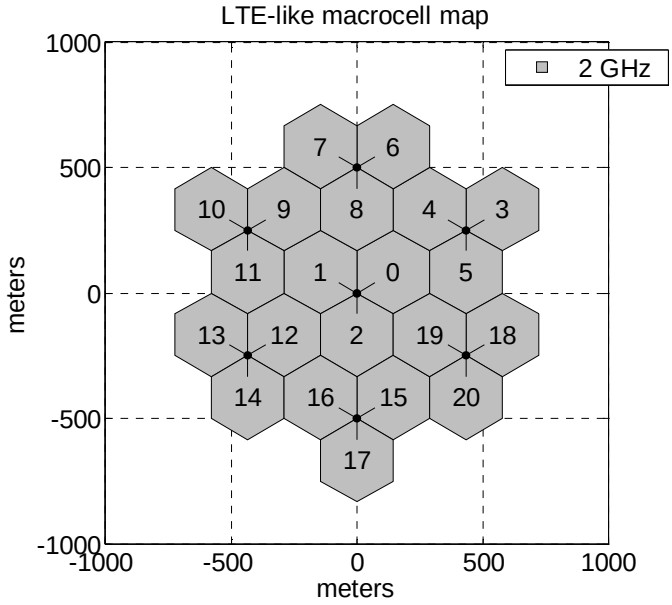

Figure 4-68: 7 tri-sector site macrocell layout

Aggressive 5x5 Grid urban model [73] has been used for femtocells. This model depicted in Figure 4-69 is made of 25 blocks (10m x 10m), each one being able to host a femtocell (2D uniform drop) according to a deployment probability. Unlike the Dual-Stripes urban model, internal walls are not explicitly modelled but have been taken into account thanks to comparatively higher shadowing standard deviation.

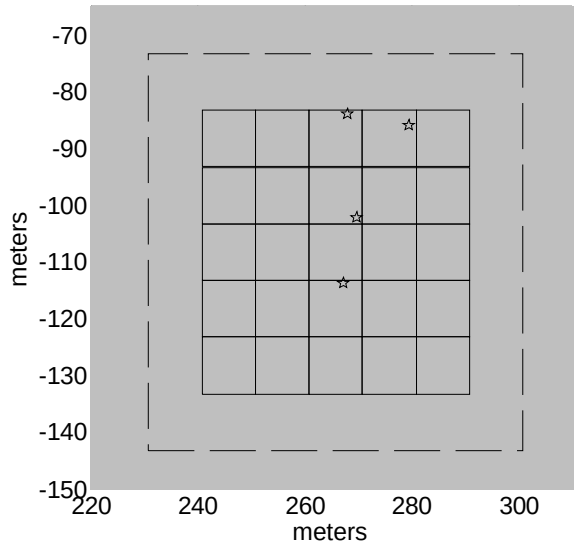

Figure 4-69: 5x5 grid model (random deployment)

Using a classical Monte-Carlo approach, one grid is uniformly dropped per sector during each run. All femtocells belonging to one grid form a femtocell cluster to which we apply our power setting. Regarding the CSG policy, we either envisage an independent CSG per femtocell or per cluster (i.e. all femtocells forming one cluster have the same CSG).

In each run, MUEs are dropped uniformly across the 2D plan until each macrocell has a given number of MUEs attached to it. This attachment is based on the best received power criterion. We also ensure that 35% of MUEs are dropped inside a grid. In each block containing a femtocell, a fixed number of FUEs, with the same CSG as the femtocell, is uniformly dropped. FUEs are attached to the best macrocell or to the best femtocell with which they share the same CSG. Table 4-7 summarizes the main simulation parameters.

Table 4-7: Main simulation parameters

Air interface		
Carrier		2GHz
Bandwidth		10MHz
Thermal noise density		-174dBm/Hz
MBS		
Inter-site distance		500m
Transmission power		46dBm
Antenna gain		14dBi
Antenna pattern		cf. [12], Table A.2.1.1.2-2
Pathloss		cf. [12], Table A.2.1.1.2-8
Shadowing standard deviation		8dB
Shadowing correlation	Intra-site	1
	Inter-site	0.5
Shadowing auto-correlation		50m

FBS	
Model	5x5 grid
Wall attenuation	20dB
Maximum transmission power P_{max}	20dBm
Minimum transmission power P_{min}	-10dBm
Antenna gain	0dBi (omni)
Pathloss	cf. [12], Table A.2.1.1.2-8
Shadowing standard deviation	10dB
Shadowing correlation	0
Shadowing auto-correlation	3m
UE	
Noise figure	9dB
Number of MUEs per macrocell	50
MUE indoor drop probability	0.35
Number FUEs per femtocell	4

4.4.4.5 Performance Evaluation

Our metric of interest is the SINR of each UE, which is equivalent to the Geometrical Factor (G-Factor) computed as:

$$\gamma_{\mathrm{UE}} = \frac{P_r(s)}{\sum_{i \neq s} P_r(i) + N_{th}}, \tag{4.61}$$

where $P_r(s)$ is the received power from the serving cell s, $P_r(i)$ is the received power from the interfering cell i and N_{th} is the thermal noise. We assume that if the SINR of one UE is below -6dB, then it is in outage.

4.4.4.5.1 Centralised Resolution (Classical Residential Deployment)

We consider a femtocell deployment of 15% and an independent CSG per femtocell (typical residential scenario). Figure 4-70 gives the cumulative density function (cdf) of the UE's SINR with the following Power Setting (PS) policies: none, distributed given by (4.45) and our proposed centralised power setting (resolution based on the simplex in the LFGW). To facilitate the comparison, we express the centralised parameters using (4.57) with $\gamma_{\mathrm{MUE}}^{\mathrm{target}} = 0\mathrm{dB}$ such that we could use the same β parameter ($\beta = 60\mathrm{dB}$).

Without power setting the average macrocell G-Factor is around -3.44dB while distributed and centralised power setting increase this value up to 1.94dB and 2.32dB respectively. There is also a visible difference for low SINR values in favour of our centralised PS which is reflected in the UE outage as seen in Table 4-8. Without PS, 29.79% of MUEs and 13.96% of FUEs are in outage leading to an unacceptable co-channel HetNet deployment. Distributed and centralised methods reduce those values below 10% for the MUEs and 4.5% for the FUEs respectively. Table 4-8 also shows that our centralised approach tends to reduce the average FBS transmit power consumption compared to the distributed one. With twice less transmitted power, we achieve better outage results.

Table 4-8: UE outage and FBS avg. Tx power comparison (15% deployment, independent CSG)

Average	No PS	Distributed PS	Centralised PS
MUE's outage	29.79%	9.36%	7.53%
FUE's outage	13.96%	4.35%	3.10%
FBS Tx power	20dBm	-0.76dBm	-3.44dBm

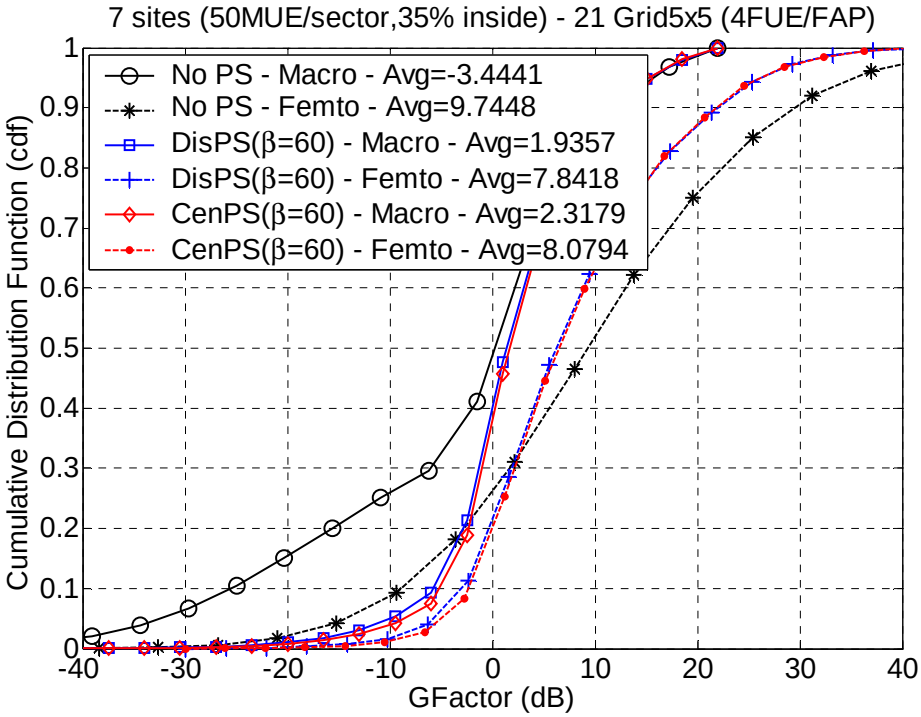

Figure 4-70: SINR comparison (15% deployment, independent CSG)

4.4.4.5.2 Impact of the Femtocell Deployment Ratio

Table 4-9 and Table 4-10 show the advantage of our centralised PS in terms of outage and transmitted power reduction which gets bigger as the FBS deployment ratio increases (while keeping an independent CSG per femtocell).

Table 4-9: UE outage and FBS avg. Tx power comparison (30% deployment, independent CSG)

Average	No PS	Distributed PS	Centralised PS
MUE's outage	36.03%	19.17%	12.87%
FUE's outage	24.29%	9.10%	5.74%
FBS Tx power	20dBm	-0.64dBm	-5.05dBm

Table 4-10: UE outage and FBS avg. Tx power comparison (60% deployment, independent CSG)

Average	No PS	Distributed PS	Centralised PS
MUE's outage	40.35%	37.01%	21.63%
FUE's outage	37.75%	18.08%	10.86%
FBS Tx power	20dBm	-0.99dBm	-6.81dBm

In a dense femtocell deployment ratio of 60%, almost 65% of the FBSs transmit at their minimum power (-10dBm) in the centralised case, whereas this number is around 15% in the distributed one. Clearly, the femto-femto interference plays a bigger role which is not captured by the traditional distributed PS, leading to high outage for MUEs but also FUEs.

4.4.4.5.3 Impact of the CSG (Corporate Deployment)

Table 4-11 shows the same system-level simulation results as Table 4-10 but considering a common CSG per cluster without any FBS switch-off (strategy 1). Such policy is usually applied in corporate deployment, where a set of femtocells will cover a building.

We obtain the same average FBS transmit powers as previously. However, the benefit of having a common CSG is straightforward for the FUEs which experiences really low outages, while the effect on the MUEs can also be appreciated. Indeed, some FUEs which were previously attached to one macrocell when their FBS was transmitting too low but still interfered by the other femtocells, have now the opportunity to stay

in the femtocell network due to the common CSG. Common CSG is a simple way to handle femto-femto interference, but macro-femto interference is still present.

Table 4-11: UE outage and FBS avg. Tx power comparison (60% deployment, common CSG)

Average	No PS	Distributed PS	Centralised PS
MUE's outage	37.53%	23.64%	12.51%
FUE's outage	0.18%	0.60%	0.39%
FBS Tx power	20dBm	-0.99dBm	-6.81dBm

4.4.4.5.4 Impact of the Transmission Strategy

To reduce macro-femto interference, we could also envisage applying strategy 2 or 3 of the proposed method. These strategies enable the automatic switch-off of the femtocells which do not (sufficiently) contribute to the maximisation of the femtocell performance cost function under the macrocell protection constraints paving the way to autonomous deployment of a set of femtocells. Such approach makes more sense in a CSG per cluster context where one femtocell subscriber has the opportunity to connect to any femtocells in its neighbourhood (e.g. corporate deployment) and not only to a dedicated one (residential).

In Table 4-12 and Table 4-13, transmission strategies 2 and 3 are applied to both PS solutions, respectively. In transmission strategy 2, one FBS will be switched-off if the PS affects a zero value to a femtocell, which is only possible for the centralised PS. In transmission mode 3, one FBS will be switched-off if the PS computes a value inferior to the minimum transmission power, which is possible for both PS solutions. We keep 60% as the femtocell deployment ratio but apply a common CSG for all femtocells within one cluster to simulate a corporate deployment scenario. Only active femtocells are considered when computing the average transmit power.

Table 4-12: UE outage and FBS avg. Tx power comparison (60% deployment, common CSG, strategy 2)

Average	No PS	Distributed PS	Centralised PS
MUE's outage	37.53%	23.64%	7.58%
FUE's outage	0.18%	0.60%	0.19%
FBS Tx power	20dBm	-0.99dBm	-4.32dBm
FBS switch-off ratio	0%	0%	43.50%

Table 4-13: UE outage and FBS avg. Tx power comparison (60% deployment, common CSG, strategy 3)

Average	No PS	Distributed PS	Centralised PS
MUE's outage	37.53%	19.14%	3.93%
FUE's outage	0.18%	0.53%	0.06%
FBS Tx power	20dBm	0.66dBm	-0.97dBm
FBS switch-off ratio	0%	15.67%	64.27%

Around 43% and 64% of FBSs are switched-off by our centralised PS in strategy 2 and strategy 3, respectively, which contribute to a significant power saving. Both strategies also significantly reduce the outage compared to the strategy 1 where no switch-off is possible (cf. Table 4-11). Indeed, the centralised PS with strategy 3 lowers the MUE outage below 4%, while the FUE outage does not exceed 0.06%. The classical distributed PS cannot compete with an MUE outage of 19.14%. This was expected since it only considers the macrocell and not the neighbouring femtocells contrary to our PS modelling. This centralised approach enables Self-Organising Network (SON) deployment. Indeed, FBSs could be deployed anywhere in a building and the ones degrading the overall macrocell network performance (according to our OP) would be automatically and dynamically switched-off.

4.4.4.5.5 Iterative Distributed Resolution

The drawback of the centralised PS relies in the central unit. If the computation itself is not demanding (simplex), the load on the network to feedback all the measurements (with their associated quantization) may be a bottleneck. Therefore, we also derive an iterative distributed resolution which does not involve any measurements exchange but only the iteration coordination by the LFGW.

We assume the same set-up as the one from Table 4-8, meaning FBS deployment ratio of 15%, independent CSG per femtocell and strategy 1 for transmission power allocation. Table 4-14 gives the average UE outage and FBS transmission power for the centralised PS and for the iterative distributed PS (Jacobian, Gauss-Seidel and SOR- $\omega = 0.5$) after 20 iterations. For Gauss-Seidel and SOR, we did not optimise the ordering of the FBS when doing the transmission power based on (4.60). We notice equivalent performance with a small advantage for the centralised version. If Gauss-Seidel and SOR resolutions exhibit similar results, Jacobian one is a little behind.

Table 4-14: Centralised vs. iterative distributed (15% deployment, independent CSG, strategy 1)

Average	Centralised	Jacobian	Gauss-Seidel	SOR (ω=0.5)
MUE's outage	7.53%	8.11%	8.09%	8.08%
FUE's outage	3.10%	3.40%	3.35%	3.35%
FBS Tx power	-3.44dBm	-3.02dBm	-3.13dBm	-3.13dBm

Figure 4-71 shows the convergence speed of the three resolution methods in terms of outage. Gauss-Seidel and SOR do converge toward their final value in less than 3 iterations. However, we notice an oscillation with the Jacobian method leading to an unstable situation. Due to the high shadowing standard deviation, the diagonal dominant condition for the matrix $\mathbf{A}$ ensuring a proper convergence of the method (see. [70]) is not always fulfilled. The main difference between Jacobian and Gauss-Seidel / SOR methods is in the ordering when computing the transmission power. Indeed, the update in the later methods takes into account the first FBS that have updated their power, which introduces a form of filtering limiting the oscillations.

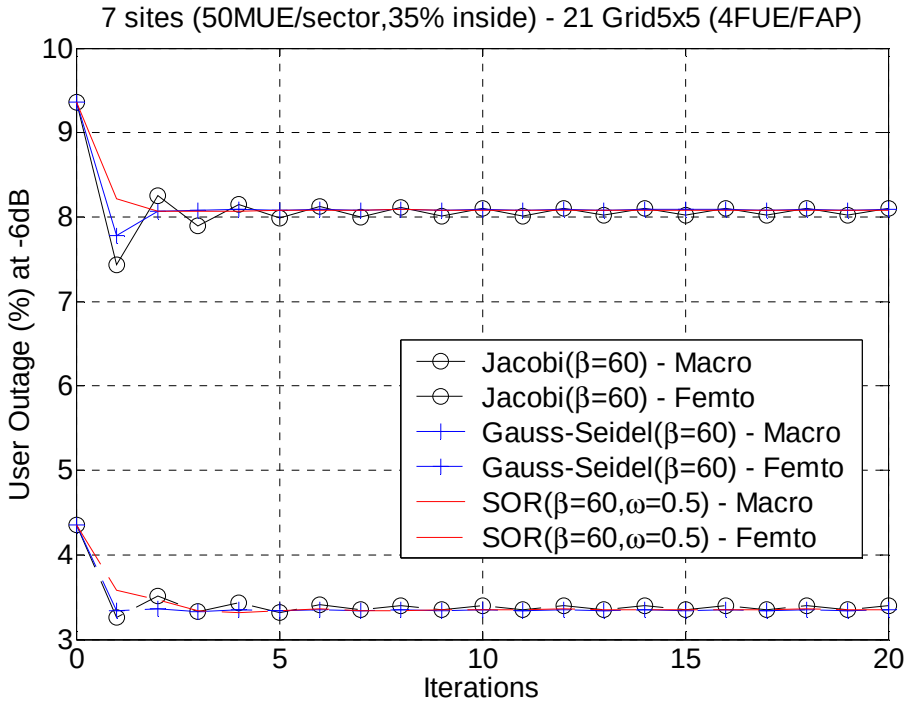

Figure 4-71: Convergence of iterative distributed (15% deployment, independent CSG, strategy 1)

We plot in Figure 4-72 and Figure 4-73 the same outage convergence curves in the heavy deployed scenario of 60% FBS deployment ratio, common CSG per cluster and transmission strategy 1 and 3, respectively. Contrary to the previous case, higher FBS deployment ratio causes stronger oscillations to the Jacobian method. In particular, the MUE outage ratio changes from 12.95% to 15.46% in strategy 1 while the gap gets bigger in strategy 3 with a jump from 3.59% to 12.94%. When considering the lower outage value, the Jacobian method significantly outperforms both Gauss-Seidel/SOR methods (especially in strategy 3) and gives equivalent results to the centralised approach (12.51% in strategy 1 and 3.93% in strategy 3).

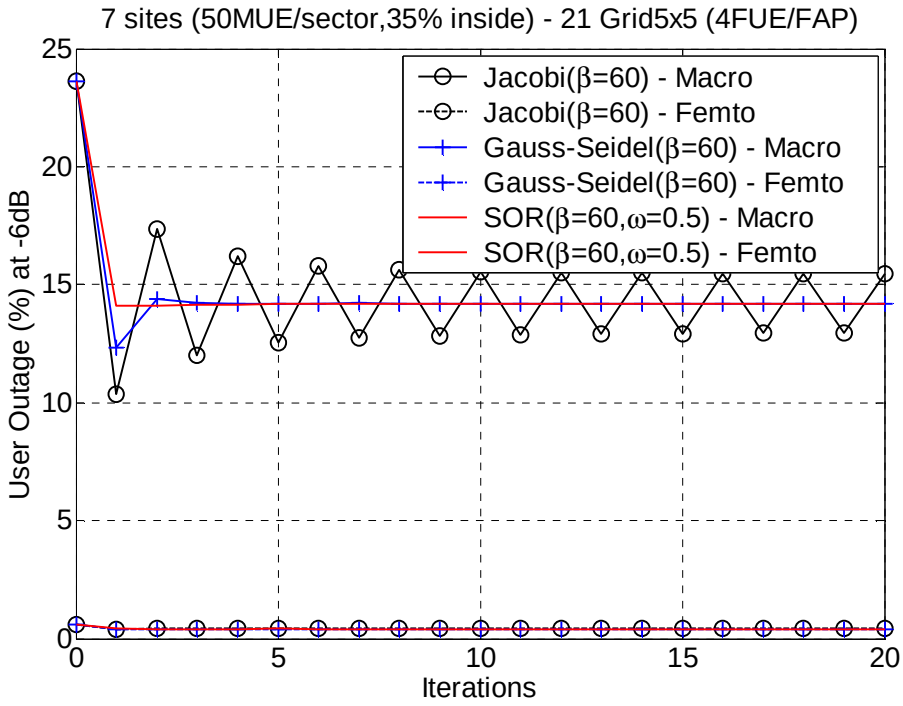

Figure 4-72: Convergence of iterative distributed (60% deployment, common CSG, strategy 1)

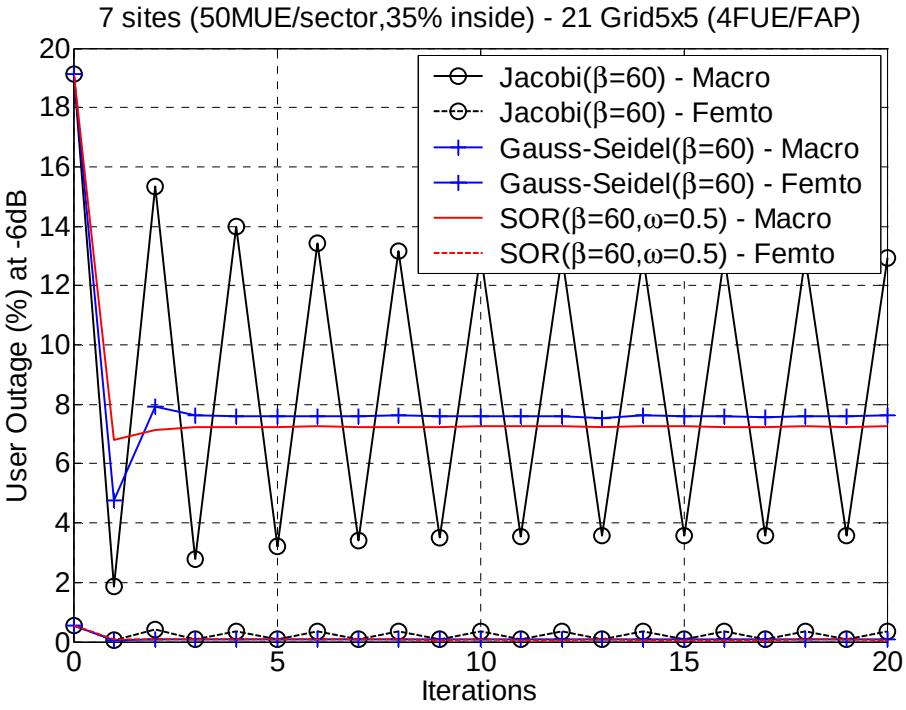

Figure 4-73: Convergence of iterative distributed (60% deployment, common CSG, strategy 3)

Note that we do also experience some oscillations for the FUEs, but in this common CSG context their outage stays below 0.5% in the worst case.

4.4.4.6 Conclusion

We have presented a HetNet-based power setting algorithm for femtocell clusters which makes use of a linear programming framework. The method is supported by the BeFEMTO architecture and especially the LFGW, which coordinates co-located femtocells. Compared to the traditional distributed approach, the centralised power setting algorithm allows significant macrocell and femtocell outage reductions which are

more pronounced in heavy femtocell deployments. The use of iterative distributed resolution methods, which brings similar results as the centralised one, tends to favour Gauss-Seidel/SOR method over the Jacobian one in low femtocell deployments, while the opposite occurs in high femtocell deployments (but a particular attention has to be paid due to oscillations). The algorithm in its centralised or iterative distributed implementation encompasses the possibility to switch-off the most disturbing femtocells in a pure SON fashion. Being able to have autonomous switch-off makes the deployment easier and the overall network performance better, since disruptive femtocells will be automatically removed from the network.

5. Conclusions

This document has exposed a large set of prior WP4 as well as new WP4 contributions to SON enablers and SON algorithms alike. To emphasis the correlation to 3GPP and NGMN work, contributions have been assembled following well established industry taxonomy of local, distributed and central SON approaches. How said list of introduced algorithms position w.r.t. said taxonomy had been summarised in Table 2-1. Furthermore, how it positions w.r.t. the NGMN use cases is clearly positioned in Table 2-2.

To conclude, the table below (from the DoW of BeFEMTO) summarizes the original challenges set out for WP4 at the beginning of BeFEMTO. The colour coding indicates if WP4 has achieved the challenge/innovation; notably, green means that the innovation has been accomplished, yellow means that it has not been applied directly but with some minor modification can be achieved; red means not achieved. Evidently, almost all of the challenges have been met. The only exceptions are cooperative multipoint transmission and cooperative positioning in the case of mobile femtocells which had finally been discarded due to technical complexity.

Table 5-1: WP4 challenges and innovations versus BeFEMTO themes; green = WP4 has addressed challenge; yellow = developed tools can be used to address challenge; red = not addressed.

Challenges / Innovations	Networked Femtocells	Fixed Relay Femtocells	Mobile Femtocells
Achieving 10 mW output power objective with same coverage & QoS	X		
Cooperative multipoint transmission	X	X	X
Integration between macro and relay femtocells		X	
Femto - macro co-existence: Interference characterisation, mitigation and coordination; centralized and de-centralized approaches	X	X	X
Capacity balancing between macro and femtocells	X		
Distributed resource management between macro and femtocells	X	X	X
Self-configuring & self-optimising femtocells	X	X	X
Scheduling for interference avoidance	X		
Interference mitigation through beamforming	X		
Decentralised resource allocation through game theoretic and learning approaches	X		
Range incorporated scheduling		X	X
Integrated femto hop selection and scheduling		X	X
Application of COMP technologies	X		
Resource-efficient and QoS-aware routing (including load balancing)	X		
Handover optimisations and efficient signalling			X
Handover in open access		X	X
Exchange of control information for radio resource management (may be a new X2 like interface)	X	X	
Cooperative positioning techniques	X		X
Automatic coverage estimation	X	X	X
Radio context aware learning mechanisms	X	X	X
Centralised versus distributed learning mechanisms	X	X	X
Dynamics and time scale for self- optimisation	X	X	X

All in all, BeFEMTO WP4 has had a significant and measureable impact onto the SON framework developments at European and international level, both in academic, industrial as well as standardisation circles.

6. References

[1] 3GPP TR 23.830, “Architecture aspects of Home Node B (HNB) / Home enhanced Node B (HeNB)”, v9.0.0

[2] 3GPP TS 32.500, “Telecommunication management; Self-Organizing Networks (SON); Concepts and requirements (Release 10),” v10.1.0, September 2010.

[3] D5.2, INFSO-ICT-248523 FP7-ICT BeFEMTO, “Femtocells access control, networking, mobility and management mechanisms”.

[4] 3GPP TS 32.541, “Telecommunication management; Self-Organizing Networks (SON); Self-healing concepts and requirements (Release 10)”, V10.0.0, March 2011.

[5] 3GPP TR 36.805, “Study on Minimization of drive-tests in Next Generation Networks; (Release 9)”, V9.0.0, December 2009.

[6] 3GPP TS 37.320, “Universal Terrestrial Radio Access (UTRA) and Evolved Universal Terrestrial Radio Access (E-UTRA); Radio measurement collection for Minimization of Drive Tests (MDT); Overall description; Stage 2 (Release 10)”, V10.3.0, September 2011.

[7] SOCRATES D5.9, “Final Report on Self-Organisation and its Implications in Wireless Access Networks”.

[8] 3GPP TS 36.401, “Evolved Universal Terrestrial Radio Access Network (E-UTRAN); Architecture Description (Release 9),” v9.2.0, June 2010.

[9] Femto Forum, “LTE MAC Scheduler Interface Specification v1.11,” Technical Paper, October 2010.

[10] *NGMN Recommendation on SON and O&M Requirements*, Version 1.23, Release Date: December 5th,. 2008.

[11] "*Top OPE recommendations*". *NGMN* Ltd. http://www.ngmn.org/uploads/media/NGMN_Top_OPE_Recommendations_1.0.pdf. Retrieved 16 June 2011.

[12] 3GPP TR 36.814, “Further Advancements for E-UTRA; Physical Layer Aspects,” V9.0.0, Mar. 2010.

[13] 3GPP TS 36.211, “Physical Channels and Modulations,” V10.2.0, Jun. 2011.

[14] “Guidelines for the evaluation of radio transmission technologies for IMT-2000,” Recommendation ITU-R M.1225, 1997

[15] 3GPP TS 36.133, “Evolved Universal Terrestrial Radio Access (EUTRA); Requirements for support of radio resource management (Release 9),” v9.3.0, Mar. 2010.

[16] D4.2, INFSO-ICT-248523 FP7-ICT BeFEMTO, “ SON Enabling Techniques”, Sept. 2011

[17] A. A. Sharov, E.A. Roberts, A. M. Liebhold, and F.W. Ravlin. 1995. Gypsy moth (Lepidoptera: Lymantriidae) spread in the Central Appalachians: Three methods for species boundary estimation. Environ. Entomol. 24: 1529-1538.

[18] Patel, et al., “Femtocell and Beacom Transmit Power Self-Calibration”, Qualcomm, Feb. 2010.

[19] Claussen, Ho, and Samuel, “Self-optimization of Coverage for Femtocell Deployments,” Wireless Telecommunications Symposium, Apr. 2008.

[20] Gustavson et al. , “Continuous alternating closed-open loop power control” , www.freepatentsonline.com/

[21] 3GPP TS 36.104 “Evolved Universal Terrestrial Radio Access (E-UTRA); Base station (BS) radio transmission and reception ”, V10.0.0, Dec. 2010

[22] Steve Egolf, “Intelligent Power Management: A Method to Improve 2G/3G Handset Talk Time”, Microwave Journal, vol.50 , no.7, July 2007

[23] Jackie Johnson, “How Mobile Devices Users are Impacting the Future of RF Front Ends”, Microwave Journal, vol. 53, no.11, Nov. 2010 supplement

[24] 3GPP TR 36.921, Home eNodeB (HeNB) Radio Frequency (RF) Requirements Analysis (FDD), 3rd Generation Partnership Project, March 2010.

[25] Patel et all, “Femtocell and Beacon Transmit Power Self-Calibration” www.qualcom.com

[26] 3GPP TS 36.214 “Evolved Universal Terrestrial Radio Access (E-UTRA); Physical layer; Measurements”, V10.0.0, Dec. 2010.

[27] A. Galindo-Serrano, L. Giupponi, M. Majoral, “On Implementation Requirements and Performances of Q-Learning for Self-Organized Femtocells,” in Proc. of the IEEE Global Communications Conference (IEEE Globecom 2011), second Workshop on Femtocell Networks (FEMnet), 5-9 December 2011, Houston, Texas, USA.

[28] L.G.U., Garcia, G.W.O. Costa, A.F. Cattoni, K.I. Pedersen, P.E. Mogensen, "Self-Organizing Coalitions for Conflict Evaluation and Resolution in Femtocells," *Global Telecommunications Conference (GLOBECOM 2010), 2010 IEEE* , vol., no., pp.1-6, 6-10 Dec. 2010

[29] L. Giupponi, A. Galindo-Serrano, P. Blasco, M. Dohler, “Docitive Networks - An Emerging Paradigm for Dynamic Spectrum Management,” IEEE Wireless Communications Magazine, Vol. 17, No. 4, pp. 47-54, August 2010.

[30] M. Bennis, S. Guruchurya, and D. Niyato, “Distributed Learning Strategies for Interference Mitigation in Femtocell Networks,” in proc. of IEEE GLOBECOM, Houston, USA.

[31] A. Feki, and V. Capdevielle, “Autonomous resource allocation for dense LTE networks: A Multi Armed Bandit formulation,” in proc. of IEEE PIMRC 2011, Toronto, Canada.

[32] M. Bennis, S.M. Perlaza, and M. Debbah “Learning Coarse-Correlated Equilibria in Two-Tier Networks,” in proc. of IEEE ICC 2012, Ottawa, Canada.

[33] M. Bennis, S.M. Perlaza, and M. Debbah “Decentralized Cross-Tier Interference Mitigation in Cognitive Femtocell Network,” in proc. of IEEE ICC 2011, Kyoto, Japan.

[34] D4.1, INFSO-ICT-248523 FP7-ICT BeFEMTO, “Preliminary SON enabling & multi-cell RRM techniques for networked femtocells”, Dec. 2010

[35] J. Giese, A. Amin, and S. Brueck, “Application of Coordinated Beam Selection in Heterogeneous LTE-Advanced Networks”, Proc. of the IEEE International Symposium on Wireless Communication Systems (ISWCS), Nov. 2011.

[36] C. Prehofer and C. Bettstetter, “Self-organization in communication networks: principles and design paradigms,” IEEE Communications Magazine, vol. 43, no. 7, pp. 78–85, July 2005

[37] K. P. Sycara, “Multiagent systems,” AI Magazine, vol. 19, no. 2, pp. 79–92, 1998.

[38] R. S. Sutton and A. G. Barto, Reinforcement Learning: An Introduction. The MIT Press, 1998.

[39] L. Giupponi, A. Galindo-Serrano, P. Blasco and M. Dohler, “Docitive Networks – An Emerging Paradigm for Dynamic Spectrum Management”, IEEE Wireless Communica- tions Magazine, vol. 17, no. 4, pp. 47 - 54, Aug. 2010.

[40] D4.3, INFSO-ICT-248523 FP7-ICT BeFEMTO, “Multi-cell RRM and self-optimisation for networked, fixed relay and mobile femtocells”, Dec. 2011

[41] C. Prehofer and C. Bettstetter, “Self-organization in communication networks: principles and design paradigms,” IEEE Communications Magazine, vol. 43, no. 7, pp. 78–85, 2005

[42] 3GPP TS 36.213 “Evolved Universal Terrestrial Radio Access (E-UTRA); Physical Layer Procedures (Release 8),”), V 8.8.0 Sep. 2009.

[43] 3GPP TS 36.300 “Evolved Universal Terrestrial Radio Access (E-UTRA); Overall description; Stage 2 (Release 11),” V11.1.0 March 2012.

[44] M. L. Littman, A. R. Cassandra, and L. P. Kaelbling, “Learning policies for partially observable environments: Scaling up,” Proceedings of the Twelfth International Conference on Machine Learning, pp. 362–370, 1995.

[45] G. Bohling, “Kriging,” C&PE 940, October 2005.

[46] 3GPP TS 25.467 UTRAN architecture for 3G home nodeB (stage 2.,) V8.1.0 Tech. Rep., March 2009.

[47] Y. Cai, X. C. P. Ding, X. Jin, and R. P. Moorut, “Mangement interference from femtocells,” U.S. Patent 12/536,125, Feb. 11, 2010.

[48] S. Samanrakoon, M. Bennis, W. Saad and M. Latva-aho, ”Enabling Relaying over Heteregenous Backhauls in Femtocell Networks,” IEEE WiOPT, 2012

[49] L. Kleinrock and F. Tobagi, “Packet Switching in Radio Channels: Part I–Carrier Sense Multiple-Access Modes and Their Throughput-Delay Characteristics,” *IEEE Transactions on Communications*, vol. 23, no. 12, pp. 1400–1416, Dec. 1975.

[50] 3GPP, “Simulation Assumptions and Parameters for FDD HeNB RF Requirements,” 3GPP TSG RAN WG4 R4-092042, May 2009 from www.3gpp.org/ftp/Specs/.

[51] S. Uygungelen, G. Auer, and Z. Bharucha, “Graph-Based Dynamic Frequency Reuse in Femtocell Networks,” *in Proc. of the 73rd IEEE Vehicular Technology Conference (VTC)*, Budapest, Hungary, May 15–18 2011.

[52] R. Y. Chang, T. Zhifeng, J. Zhang and C. C-J Kuo, "Multicell OFDMA Downlink Resource Allocation Using a Graphic Framework," Vehicular Technology, *IEEE Transactions on* , vol.58, no.7, pp.3494-3507, Sept. 2009.

[53] F.A. Zdarsky, A. Maeder, S. Al-Sabea and S. Schmid, "Localization of Data and Control Plane Traffic in Enterprise Femtocell Networks," *Vehicular Technology Conference (VTC Spring)*, 2011 IEEE 73rd , vol., no., pp.1-5, 15-18 May 2011.

[54] Q. Xiaoxin and K. Chawla, "On the performance of adaptive modulation in cellular systems," *Communications, IEEE Transactions on* , vol.47, no.6, pp.884-895, Jun 1999

[55] W-H Kuo and W. Liao, "Utility-Based Resource Allocation in Wireless Networks," Wireless Communications, IEEE Transactions on , vol.6, no.10, pp.3600-3606, October 2007

[56] Part 16: *Air Interface for Fixed and Mobile Broadband Wireless Access Systems*, IEEE Std. 802.16e-2005, 2006.

[57] S. Sahni and T. Gonzalez, "P-complete approximation problems", *J. Assoc. Comput. Mach.*, vol. 23, pp.555 1976.

[58] K. Kim; Y. Han and S-L. Kim, "Joint subcarrier and power allocation in uplink OFDMA systems,” *Communications Letters, IEEE* , vol.9, no.6, pp. 526- 528, Jun 2005.

[59] K. Hoon and H. Youngnam, "A proportional fair scheduling for multicarrier transmission systems," *Communications Letters, IEEE* , vol.9, no.3, pp. 210- 212, March 2005.

[60] Y. Ko, S. A. Vorobyov, and M. Ardakani, “How much multiuser diversity is required in energy limited multiuser systems?,” *IEEE Trans. Signal Processing*, vol. 58, no. 8, pp. 4367-4378, Aug. 2010

[61] I. Ashraf, L.T.W. Ho and H. Claussen, “Improving energy efficiency of femtocell architectures for green radio: Large versus small cell size deployment,” in Proc. IEEE Vehicular Technology Conference, Sep. 2009, pp.1-5.

[62] I. Asharf, F. Boccardi, and L. Ho, “SLEEP mode techniques for small cell deployments,” IEEE Commun. Mag., vol. 49, pp. 72-79, Aug. 2011.

[63] D. Tse and P. Viswanath, *Fundamentals of wireless communication*, 1st ed. Cambridge University Press, 2005.

[64] Y. Ko, A. Quddus, and R. Tafazolli, “On distributed optimum energy usage in a two–tier co-channel femtocells network,” *IEEE Trans. on Wireless Communications*, submitted Apr. 2012.

[65] 3GPP TR 25.967, “Home Node B (HNB) Radio Frequency (RF) requirements (FDD) (Release 10)”

[66] M. Yavuz, F. Meshkati, S. Nanda, A. Pokhariyal, N. Johnson, B. Raghothaman, and A. Richardson, “Interference management and performance analysis of UMTS/HSPA+ femtocells,” IEEE Communications Magazine, vol. 47, no. 9, pp. 102–109, Sept. 2009.

[67] Xiangfang Li, Lijun Qian, and D. Kataria, “Downlink power control in co-channel macrocell femtocell overlay,” in Proc. of IEEE 43rd Annual Conference on Information Sciences and Systems (CISS’09), pp. 383-388, Jun. 2009.

[68] D2.2, INFSO-ICT-248523 FP7-ICT BeFEMTO, BeFEMTO "The BeFEMTO system architecture,", Dec. 2011.

[69] G. B. Dantzig, Linear Programming and Extensions, Princeton University Press, 1963.

[70] D. Bertsekas and J. Tsitsiklis, Parallel and Distributed Computation: Numerical Methods, Prentice Hall, NJ, 1989.

[71] 3GPP TR 25.814, "Physical layer aspects for evolved Universal Terrestrial Radio Access (UTRA) (Release 7)," 3rd Generation Partnership Project.

[72] IEEE 802.16m, "IEEE 802.16m evaluation methodology document (EMD)", 2009.

[73] M. Maqbool, M. Lalam, and T. Lestable, "Comparison of femto cell deployment models for an interference avoidance technique," in Proc. of Future Network & Mobile Summit (FUNEMS'11), Jun. 2011

[74] D. Brélaz, "New Methods to Color the Vertices of A Graph," *Communications of the ACM*, vol. 22, no. 4, pp. 251–256, Apr. 1979

[75] 3GPP TR 36.806, "Relay architectures for EUTRA (LTE-Advanced)"

[76] 3GPP TR 36.416, "Mobile Relay for E-UTRA"

[77] R3-113020, "The location of the mobility anchor for Mobile Relays", Qualcomm Incorporated

[78] R3-120486, "Report email#10: Mobile architecture options", CATT (rapporteur)

[79] R3-120296, "Impact of mobility support for the candidate mobile relay architectures" , Qualcomm Incorporated

[80] R3-120297, "The termination of the X2 and S1 interfaces for Mobile Relays", Qualcomm Incorporated

[81] R3-120697, "Comparison between Alt 1 and Alt 2 - commonalities and differences", Qualcomm Incorporated

[82] D2.1 INFSO-ICT-248523 FP7-ICT BeFEMTO, "Description of baseline reference systems, use cases, requirements, evaluation and impact on business model" Dec 2010.

[83] SOCRATES, "Deliverable d2.1: use cases for self-organizing networks, eu strep socrates (infso-ict-216284)," Tech. Rep., March 2008.

[84] NGMN, "Use cases related to self-organizing networks, overall description."

[85] 3GPP R1-071956, Ericsson, (04-2007).

[86] H. Holma and A. Toskala, "*HSDPA / HSUPA for UMTS*", John Wiley & Sons, 2006.

[87] 3GPP TS 25.104 v8.5.0 Release 8 (12-2008).

[88] 3GPP TR 36.913 v8.0.0 Release 8 (06-2008).

[89] 3GPP TS 36.101, "Evolved universal terrestrial radio access network (E-UTRAN); User Equipment (UE) radio transmission and reception (release 10)", vol. 10.1.1., Jan. 2011.

[90] M. Jeruchim, P. Balaban and K. Shanmugan, "Simulation of Communication System," Plenum Press, New York and London, 1992.